TECHNICAL DIGEST

MPLP'2013

VI International Symposium

"MODERN PROBLEMS OF LASER PHYSICS"

Novosibirsk, Russia, August 25 – 31, 2013

mplp.laser.nsc.ru

Organized by:

Institute of Laser Physics, SB RAS, Novosibirsk, Russia

Novosibirsk State University, Novosibirsk, Russia

Institute of Spectroscopy, RAS, Troitsk, Russia

International Laser Center, M.V. Lomonosov Moscow State University, Russia

Sponsored by:

Siberian Branch of RAS

Russian Foundation for Basic Research

Ministry of Science and Education of the Novosibirsk Region

Non-profit Fund "Dynasty" (www.dynastyfdn.com)

OOO "Microsun company" (www.microsun.ru)

INTERNATIONAL ADVISORY COMMITTEE

Sergei Arakelian	*Vladimir State University, Vladimir, Russia*
Viktor Balykin	*Institute of Spectroscopy RAS, Troitsk, Russia*
Nicolo Beverini	*Dipartimento di Fisica, Universita' di Pisa, Italy*
Evgueni Dianov	*Fiber Optics Research Center at GPI RAS*
Martial Ducloy	*Laboratoire de Physique des Lasers, Universite Paris-Nord, France*
Elisabeth Giacobino	*Laboratoire Kastler Brossel, Université Paris 6, France*
Alexander Kaminskii	*A.V. Shubnikov Institute of Crystallography of RAS*
Hidetoshi Katori	*University of Tokyo, Science and Technology Agency, Japan*
Sergei Kilin	*B.I. Stepanov Institute of Physics NASB*
Vasiliy Klimov	*P.N. Lebedev Physics Institute RAS, Moscow, Russia*
Nikolai Kolachevsky	*P.N. Lebedev Physics Institute RAS, Moscow, Russia*
Leong Chuan Kwek	*Centre for Quantum Technologies, National University of Singapore*
Michele Leduc	*Laboratoire Kastler Brossel, Ecole Normale Supérieure, Paris*
Gerhard Leuchs	*Universität Erlangen-Nürnberg, Institut für Optik, Germany*
Filippo Levi	*INRIM, Optic Division, Torino, Italy*
Gerard Mourou	*Ecole Polytechnique, IZEST, France*
Hélèn Perrin	*Laboratoire de Physique des Lasers, Université Paris 13, France*
Fritz Riehle	*Physikalisch-Technische Bundesanstalt, Braunschweig, Germany*
Philip Russell	*Max Planck Institute for the Science of Light, Erlangen, Germany*
Aleksandr Sergeev	*Institute of Applied Physics of RAS, Nizhny Novgorod, Russia*
Vladimir Shalaev	*Purdue University, USA*
Anatoly Shalagin	*Institute of Automation and Electrometry SB RAS, Novosibirsk, Russia*
Feng Song	*School of Physics, Nankai University, Tianjin, China*
Aleksey Taichenachev	*Institute of Laser Physics SB RAS, Novosibirsk, Russia*
Sergei Turitsyn	*Aston University, Birmingham, UK*
Ken-ichi Ueda	*University of Electro-Communications, Tokyo, Japan*
Ernst Wintner	*Vienna University of Technology, Austria*
Jun Ye	*NIST, University of Colorado, Boulder, USA*
Viktor Zadkov	*M.V. Lomonosov Moscow State University, Russia*
Aleksey Zheltikov	*M.V. Lomonosov Moscow State University, Russia*

Symposium Chair: Prof. Sergei N. Bagayev, *Institute of Laser Physics, SB RAS*

Symposium Secretary: Dr. Denis V. Brazhnikov, *Institute of Laser Physics, SB RAS*

Table of Contents

Oral Presentations

(Presenting authors are listed in the alphabetical order within each chapter)

1. New trends in laser physics

2. High-resolution spectroscopy and fundamental metrology

3. Physics of ultracold atoms, ions, and molecules

4. Quantum optics and quantum information

5. Ultrahigh laser fields and attoscience

6. Nonlinear optics and novel phenomena

7. Nanophotonics, plasmonics, metamaterials and complex media

8. Fiber optics and fiber lasers

9. Applications of lasers

Round Table: "Optical Magnetometry"

Poster Sessions

Session A: *New trends in laser physics; High-resolution spectroscopy and fundamental metrology; Physics of ultracold atoms, ions, and molecules; Quantum optics and quantum information; Ultrahigh laser fields and attoscience; Applications of lasers*

Session B: *New trends in laser physics; Nonlinear optics and novel phenomena; Nanophotonics, plasmonics, metamaterials and complex media; Fiber optics and fiber lasers*

Ultra-precise optical clock of new generation: Leap into future

S.N. Bagayev, A.V. Taichenachev

Institute of Laser Physics SB RAS, pr. Ac. Lavrentyeva, 13/3, Novosibirsk, 630090 Russia
Novosibirsk State University, ul. Pirogova, 2, Novosibirsk, 630090, Russia
Novosibirsk State Technical University, pr. K. Marksa, 20, Novosibirsk, 630073, Russia
bagayev@laser.nsc.ru

Presently, laser spectroscopy and fundamental metrology are among the most important and actively developed directions in modern physics. Frequency and time are the most precisely measured physical quantities, which, apart from practical applications (in navigation and information systems), play critical roles in tests of fundamental physical theories (such as QED, QCD, unification theories, and cosmology) [1,2]. Now, laser metrology is confronting the challenging task of creating an optical clock with fractional inaccuracy and instability at the level of 10^{-17} to 10^{-18}. Indeed, considerable progress has already been achieved along this path for both ion-trap-based [3] and atomic-lattice-based [4,5] clocks.

Work in this direction has stimulated the development of novel spectroscopic methods such as spectroscopy using quantum logic [6], magnetically induced spectroscopy [7], Hyper-Ramsey spectroscopy [8], spectroscopy of "synthetic" frequency [9] and others. Part of these methods was developed in order to excite and detect strongly forbidden optical transitions. The other part fights with frequency shifts of various origins. In the present talk we will review both parts with special emphasis on methods developed and studied in Institute of Laser Physics SB RAS, Novosibirsk. The history and present status of experimental works devoted to optical frequency standards will be observed.

Our work is supported by the Ministry of Education and Science of the Russian Federation in the frame of the Program "Scientific and scientific-pedagogical personnel of innovative Russia" (Contract no. 16.740.11.0466 and Agreement no. 8387), by the Russian Foundation for Basic Research (grants nos. 12-02-00454, 12-02-00403, 11-02-00775, 11-02-01240), by the Russian Academy of Sciences and the Presidium of Siberian Branch of Russian Academy of Sciences, and the Russian Quantum Center.

References:

[1] S. N. Bagayev *et al.*, Appl. Phys. B **70**, 375 (2000).
[2] S. A. Diddams *et al.*, Science **306**, 1318 (2004).
[3] T. Rosenband *et al.*, Science **319**, 1808 (2008).
[4] T. Akatsuka,M. Takamoto, and H. Katori, Nature Physics **4**, 954 (2008).
[5] A. D. Ludlow *et al.*, Science **319**, 1805 (2008).
[6] P. O. Schmidt *et al.*, Science **309**, 749 (2005).
[7] A. V. Taichenachev *et al.*, Phys. Rev. Lett. **96**, 083001 (2006).
[8] V. I. Yudin *et al.*, Phys. Rev. A **82**, 011804(R) (2010).
[9] V. I. Yudin *et al.*, Phys. Rev. Lett. **107**, 030801 (2011).

Recent Advances in Plastic Electronics

W.Y. Lai[1], W. Huang[1,2]

[1] *Key Laboratory for Organic Electronics & Information Displays (KLOEID) and Institute of Advanced Materials (IAM), Nanjing University of Posts & Telecommunications, 9 Wenyuan Road, Nanjing 210046, China*
[2] *National Synergetic Innovation Center for Advanced Materials, Institute of Advanced Materials (IAM), Nanjing-Tech University, Nanjing 211816, China*
E-mail: iamwylai@njupt.edu.cn; iamwhuang@njut.edu.cn

Polymer semiconductors have been the subject of intensive research for a range of optoelectronic applications because they can realize most of the functions of silicon and other inorganic semiconductors. A key advantage of polymer materials is that they can be processed from solution for low-cost, large-area, and flexible optoelectronics. Because of these unique characteristics, polymer semiconductors are playing more and more important roles for applications in flat-panel displays, solid-state lighting, and solar energy, et al. Significant improvements in efficiency and stability have led to the realization of high-performance plastic electronic materials and optoelectronic devices, some of which have now approached/exceeded their inorganic counterparts. In this area, a world-wide challenge is to develop electrically pumped plastic lasers based on polymer semiconductors.

Our recent work is devoted to the development of high-performance polymer semiconductors for plastic electronics. We will present our recent advancement on rational molecular design of polymer semiconductors for plastic electronics, i.e. polymer electroluminescent devices, polymer electronic memory devices, and especially plastic lasers. We will focus on discussing our efforts in the field of plastic lasers with the following aspects: (1) the tunable optically pumped plastic lasers and the broadband optical amplifiers with gain up to 41dB; (2) the fabrication of low cost waveguide optical amplifier and switch; (3) the rational design of materials to achieve low lasing threshold; (4) the possible design strategy of device structure for electrically pumped plastic lasers, etc.

References

W. Huang, et al. *Prog. Polym. Sci.* **37**, 1192 (2012); *Adv. Mater.* 21, 355 (2009); *Adv. Mater.* **24**, 2901 (2012); *Adv. Funct. Mater.* **19**, 2844 (2009); *Adv. Funct. Mater.* **18**, 265 (2008); *J. Am. Chem. Soc.* **130**, 2120 (2008); *Adv. Funct. Mater.* 21, 979 (2011); *Polym. Chem.* **4**, 2540 (2013); *Adv. Funct. Mater.* **23**, 3268 (2013).

Nano spatially and femto temporally localized laser source

P.N. Melentiev, A.E. Afanasiev, V.I. Balykin

Institute for Spectroscopy RAS, Phizicheskaya str., 5, Troitsk. Moscow, 142190 Russia

The unique feature of femtosecond laser radiation is the time scale localization, which extends up to a single period of light. However, the spatial scale of localization is not better than the radiation wavelength, which is explained by the diffraction limitation. In the present work we state the problem for femtosecond laser radiation to reach the spatial localization of ~ 50 nm, which is of great fundamental and practical importance. Among of the important applied problems relevant to spatial localization of light we may recall the possibility to combine modern silicon electronics with optical components (known as 'silicon photonics') and to obtain short-wavelength laser radiation for optical lithography in a range 10 – 20 nm. One approach to nanometer-scale spatial localization of femtosecond laser radiation is employment of nonlinear processes occurring in metal nanostructures. Nonlinear photoprocesses in metal nanostructures are based on three principal factors: (1) concentration of electromagnetic energy in space with a characteristic nanometer-scale dimension by means of surface plasmons, (2) an ultrashort (in the range 0.1 – 10 fs) relaxation time in metals, and (3) availability of laser systems with ultrashort pulses.

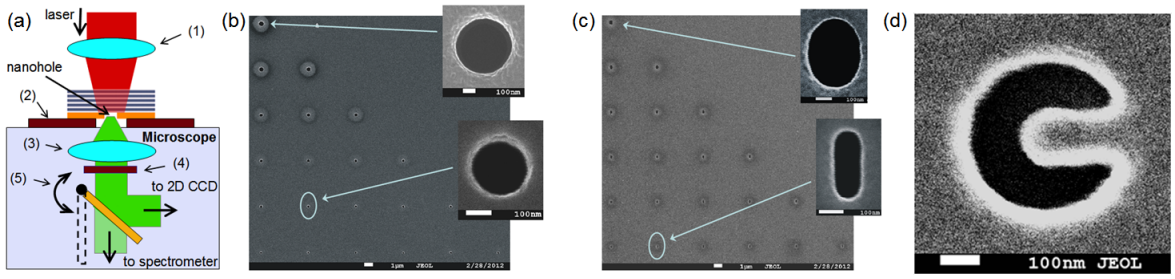

Fig.1. (a) Experimental setup: (1) 10x/0.25 objective that focuses excitation radiation, (2) 2D piezo stage with feedback sensors, (3) 100x/1.49 collecting objective, (4) interference filter to cut off the excitation radiation, and (5) flipping mirror. SEM images of a nanoopenings array made in an Au layer of a photonic crystal microcavity: (b) circular holes, (c) slit shaped holes, and (d) split-hole resonator. An enlarged images of nanoholes are shown in the insets.

Photo induced luminescence (PL) is an important physical processes occurring in the interaction of radiation with metals, and its physical nature is determined by interband and intraband transitions in a metal. Mooradian was the first who discovered interband transitions upon observation of the PL on the surface of Au; later, the PL phenomenon was actively investigated for different metals. The possibility of occurrence both of inter- and intraband transitions leads to an extremely broad spectrum of PL. One of the main physical reasons for interest in PL was and is the possibility to study the band structure of metals. The possibility of technological applicability of PL was considered to be unlikely because of an extremely low efficiency of PL: its quantum efficiency is on the order of 10^{-10}.

Presently, various nonlinear photoprocesses are investigated in metal nanostructures, such as multi photons PL, second harmonic generation, four-wave mixing on metal surfaces, ultrafast optical modulation based on third-order nonlinearity, and generation of higher harmonics. Unlike bulk media, harmonic generation in nanostructures does not necessitate the phase matching. Third harmonic generation (THG) is the simplest nonlinear effect allowed for nanostructures of arbitrary geometry, which is independent of their symmetry. It was theoretically shown that under the radiation intensity of ~10^{16} W cm^{-2}, the electric field amplitude of the third harmonic may be on the order of that of a fundamental-frequency radiation.

Here we present the study of PL and THG on individual nanometer - scale objects such as circular holes [1,2], slit shaped holes [3] and split-holes resonators [4] fabricated in gold and aluminum films (Fig.1). We have investigated the effect of film material and geometry on the efficiency of these processes and the dependence of this efficiency on the intensity of exciting laser radiation. The limitations were found on the utmost radiation intensity that does not yet melt the nanostructure. The possibility is revealed of creating the nanolocalized source of third-harmonic radiation free of the background of the laser radiation. Also the possibility of generating a wideband femtosecond radiation based on linear and multi photons metal PL is shown (Fig. 2).

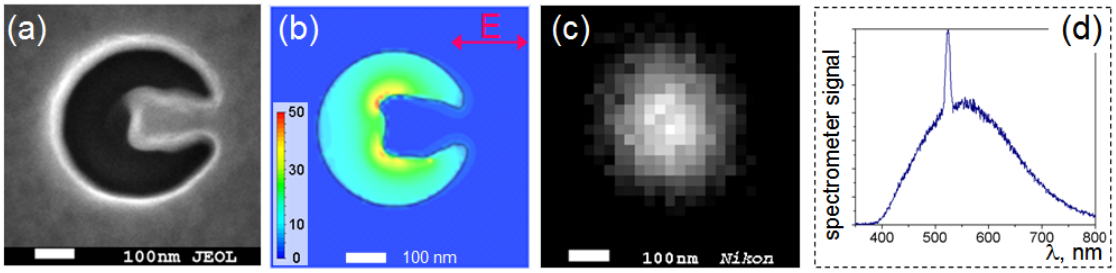

Fig.2. Broad – band nanolocalized light source based on use of a split – hole resonator: (a) an electron microscope image of the nanostructure, (b) calculated enhancement of the electric field amplitude inside the nanostructure upon irradiation of the nanostructure by a plane monochromatic wave with a wavelength of 1560 nm, (c) an optical image of the nanostructure upon its laser irradiation at a wavelength of 1560 nm and detection in the spectral range 400–800 nm, and (d) measured emission spectrum of multiphoton luminescence.

As a result of the research we show experimental demonstration of spatially localized femtosecond laser radiation to the size ~ 50 nm realized on two approaches: the employment of nonlinear optical processes in metal nanostructures for THG and the use of nonlinear processes in nano-objects for exciting PL. It was shown that the extremely high third-order optical susceptibility in metal nanostructures and strong plasmon resonances allow one to realize an efficient nanolocalized source of radiation at the third harmonic frequency and a wideband femtosecond radiation based on metal PL [5]. It was shown that a source of light realized on the split – hole resonator nanostructure allows a record efficiency of the THG. Besides, it makes it possible to realize a nanolocalized radiation source with a spatial localization of about $\lambda/15$ that posses strongly pronounced polarization characteristics and to realize all optical display [6].

References

1. P.N. Melentiev, N. A.E. Afanasiev, A.A. Kuzin, A.V. Zablotsky, A.S. Baturin, and V.I. Balykin, “Single nanohole and photonic crystal: wavelength selective enhanced transmission of light”, *Opt. Express* **19**, pp. 22743-22754 (2011).
2. P.N. Melentiev, T.V. Konstantinova, A.E. Afanasiev, A.A. Kuzin, A.S. Baturin, and V.I. Balykin, “Single nanohole and photoluminescence: nanolocalized and wavelength tunable light source”, *Opt. Express* **20,** 19474 (2012).
3. P.N. Melentiev, T.V. Konstantinova, A.E. Afanasiev, A.A. Kuzin, A.S. Baturin, and V.I. Balykin, “Single nano-hole as a new effective nonlinear element for third harmonic generation”, *Laser Phys. Lett.* **10**, 075901 (2013).
4. P.N. Melentiev, A.E. Afanasiev, A.A. Kuzin, A.S. Baturin, and V.I. Balykin, “Giant optical nonlinearity of a single plasmonic nanostructure”, *Optics Express* **21**, 13896-13905 (2013).
5. T.V. Konstantinova, P.N. Melentiev, A.E. Afanasiev, A.A. Kuzin, P.A. Starikov, A.S. Baturin, A.V. Tausenev, A.V. Konyaschenko, and V.I. Balykin, “Nanolocalized source of femtosecond radiation, *Quantum Electronics* **43**(4), 379-387 (2013).
6. P.N. Melentiev, A.E. Afanasiev, A.A. Kuzin, A.S. Baturin, and V.I. Balykin, “Sub-wavelength light localization based on optical nonlinearity and light polarization”, *Optics Letters* **38**, 2274 (2013).

Extreme Light
Laser ascent to subatomic physics

Gérard Mourou
IZEST, Ecole Polytechnique, Palaiseau, France

Fundamental High Energy Physics has been mainly driven by the high-energy fermionic colliding beam paradigm. Today the possibility to amplify laser to extreme energy and peak power offers, in addition to possibly more compact and cheaper way to help HEP, a complementary new alternative underpinned by single shot, large field laser pulse, that together we could call (Laser-based) High Field Fundamental Physics. The main mission of the International center on Zetta-Exawatt Science and Technology (IZEST) is to muster the scientific community behind this new concept. As an example, we project to use the laser field to probe the nonlinearity of vacuum We envision that seeking the non-collider paradigm without large luminosity substantially shorten our time-lien; We further accelerate the time-line of the research by adopting the existing large energy laser LIL. The accelerated research on the non-collider paradigm in TeV and beyond could, however, stimulate innovation in collider thinking such as lower luminosity paths, novel radiation cooling, and gamma-gamma colliders. The advancement of intense short-pulsed laser energy by 2-3 orders of magnitude empowers us a tremendous potential of unprecedented discoveries. These include: TeV physics, physics beyond TeV, new light-mass weak-coupling field discovery potential, nonlinear QED and QCD fields, radiation physics in the vicinity of the Schwinger field, and zeptosecond dynamical spectroscopy of vacuum.

On the application side, we will describe the program ICAN (International Coherent Amplification Network) dedicated to the generation of ultra high Intensity, high average power and efficiency based on a fiber-based revolutionary laser infrastructure. We see ICAN as the laser response to Grand Scientific and Societal Challenges like particle collider, Nuclear Transmutation, Proton Therapy.

Ceramic lasers and thermal-lens-free concept for coherent beam combining

Ken-ichi Ueda[1,2,3)]

Institute for Laser Science, University of Electro-Communications, Chofu, Tokyo 182-8585 Japan

[2] *Institute of Laser Engineering, Osaka University, 2-1 Yamada-ue, Suita, Osaka* 565-0871 *Japan*

[3] *Industries Development Laboratory, Hamamatsu Photonics K.K.,1820 Kurematsu, Hamamatsu, Sizuoka, 431-1202 Japan*

E-mail: ueda@ils.uec.ac.jp

We developed a new category of solid state lasers in this century. Ceramic lasers have a big potential because of their large size scaling and wide variation of new materials. Since 2000, we demonstrated high performance of ceramic lasers steadily. In 2004 we published a surprising result stating that the ceramic laser generated higher output and higher efficiency than the best quality of commercial single crystal YAG laser. In US, they carried out s systematic comparison between our ceramics (Konoshima Ceramics) and US single crystals intensively. After a year of survey, they accepted the ceramic YAG lasers are better than single crystal YAG laser in many points. They changed the funding policy of high power laser development from chemical lasers to electrical lasers. Electrical laser, it means ceramic laser pumped by lithium buttery driven laser diodes. Today maximum output power of ceramic lasers is more than 100 kW or more. Hiper project for inertial fusion energy development asks us to develop high quality and high power Yb:YAG ceramics. Ceramic laser demonstrate a highest performance for high power and high energy laser systems.

Today, we have another type of science front, high field science using ultrashort pulse lasers. In this region we need high peak power and high average power. In this case traditional scaling law, an aperture scaling is not available. We need new regime of scaling law, coherent beam combining. Coherent beam combining is quite attractive because it beam number scaling is limit-free in principle.

A paradigm shift in power scaling of solid state lasers is essential in the beam combining technique for post PW laser system. The aperture scaling has no power to develop high average and Exa- and Zeta-watt laser systems. Fiber laser arrays are proposed in ICAN program, because single-mode fiber lasers can generate plane wave output available in coherent beam combination. But Exa- and Zeta-watt output is very far from the view of present laser technologies. Of course a solid state laser including ceramic lasers can generate much more energy output than fiber lasers. Combination of high quality fiber laser in the front end and larger aperture solid state laser amplifier is an optimum design for our future. However, the beam quality of solid state lasers is poor because of the thermal-lens effect. Even thin disk laser technology could not solve the thermal lens effect. So, a thermal-lens-free solid state laser is a critical issue for our future.

A thermal-lens effect is a result of cooling of thermal conductive process. We need efficient cooling without thermal conductive cooling. Is it possible? I studied the cooling regime of gas, liquid and solid state lasers in the past. What is the most efficient way to avoid the wave front distortion in all kinds of lasers? It is simple. Removing the hot material from the laser volume. Fast gas and dye flow, and moving solid disk have been investigated last 50 years. I try to develop a new scaling covering gas, liquid, and solid state lasers.

Most efficient way to cool-down is exhaustion in gas lasers. Second efficient way is circulation for gas lasers and liquid lasers. It is a big advantage for gas and liquid, because they are fluid. Most of high power gas lasers, CO2 lasers and KrF excimer lasers, they use high speed gas flow and circulation cooling. Even in the fusion driver, ELECTRA of NRL, US, big circulation cooling is essential for 5 Hz operation.

Solid lasers have another advantage from Tabel 1. High density means high heat capacity. It means the capability of heat removal from lasing volume is larger than gas. When the moving speed is comparable, the removable heat is more than 1600 times larger. And optical quality is independent on the moving speed. This is another advantage.

I propose a couple of crazy ideas on the thermal-lens-free solid state laser herein. Until today, major mechanism of cooling of solid state lasers is conduction cooling. This is one of the reason why I developed ceramic laser. Ceramic YAG. this is a polycrystalline material has one order of magnitude larger thermal conductivity. High thermal conductivity has been really our future on solid state lasers.

1. Solid state laser vs Gas laser

	YAG		KrF	Ratio
density [g/cc]	4.55	>>	0.00498	914
Specific heat [J/g/K]	0.59	>	0.33	1.79
Specific heat [J/cc/K]	2.68	>>	0.00164	1634
Typical moving speed [m/s]	14 m/s for 3.5"" HD drive @7200 rpm	>	7.8 ms in ELECTRA @ 5 Hz operation	comparable

2. Solid state laser vs Liquid laser

	Rotation Disk		Liquid circulation
Optical distortion	no change	◎	$\Delta n \propto \Delta P$ (pressure drop)

Tabel 1 Heat removal potential of solid state lasers is best.

In Fig.1 I show a picture of typical hard disk (HD) drive. A HD is really popular device for us. The date is recorded on a platter surface. What is a platter. As shown in Fig. 1, today's platter is made of ceramic disk of 3.5 inches in diameter and 0.6 mm thickness. They have mirror-finished surfaces with a surface roughness of nm-scale. The rotation speed of a platter is 7200 rpm (120 Hz), but the power for rotation is only 2.4 W for constant speed.

Merging of electronics and laser technology should be our future. The cooling scaling is defined by the ratio of cooling ares/heating area. When we use a 5 mm beam size, the cooling power is calculated 1600 times larger than conventional conductive cooling.

We have a plan to introduce thermal barrier inside the disk. These ideas have never tried for solid state lasers until today. We need quite new ideas to realize a thermal-lens-free solid state laser for coherent beam combining.

Fig.1 HD technology

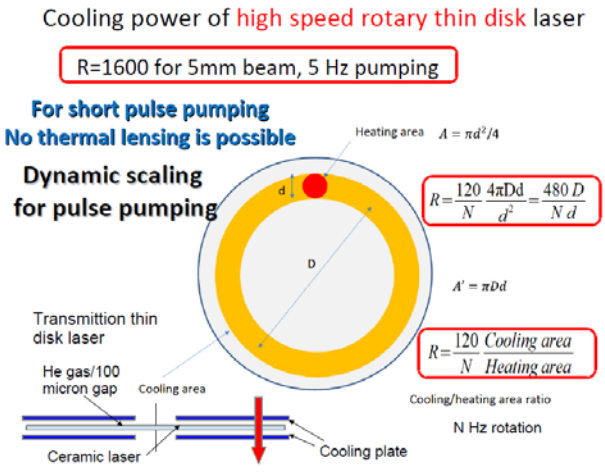

Fig. 2 Cooling scaling for hgh speed rotary thin disk

Mercury optical lattice clock at LNE-SYRTE

R. Tyumenev, Z. Xu, J. J. McFerran and S. Bize

LNE-SYRTE, Observatoire de Paris, CNRS UPMC, 61 Avenue de l'Observatoire, 75014 Paris, France
E-mail: rinat.tyumenev@obspm.fr

Highly accurate atomic frequency standards are an important and actively developing field. Today's primary frequency standards used for the realization of the SI second are based on microwave Cs fountain clocks and have accuracy near 10^{-16}, which is their limit. Optical clocks are a new generation of clocks, which will allow improving the uncertainty down to 10^{-18} or better. This trend is illustrated in Fig. 1. Several atomic species are used for development of optical clocks such as Sr, Yb, Ca, Mg, as well as ions Al^+, Yb^+, Sr^+.

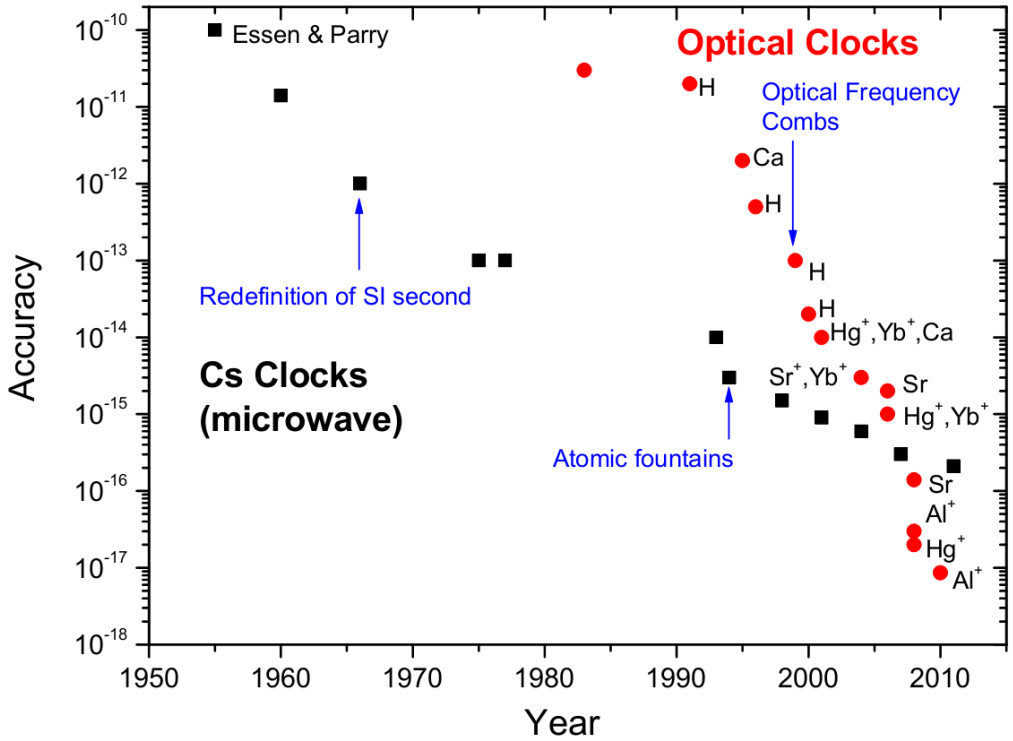

Fig. 1. Accuracy of microwave (black squares) and optical (red circles) clocks with respect to time.

Here we present the optical lattice clock based on neutral atoms of mercury that is developed at LNE-SYRTE. Hg is an interesting candidate for making an optical lattice clock, due to several favorable atomic properties. The $^1S_0$ – $^3P_0$ clock transition in Hg has a low blackbody radiation shift. The blackbody radiation sensitivity of Hg is a factor of 34 less than for Sr and a factor of 15 less than for Yb. Hg has 7 naturally occurring isotopes. Six of them have a natural abundance larger than 6%, among which 2 fermions and 4 bosons. It opens the possibility to study a large variety of effects, and all of them are interesting because mercury was almost not studied so in the laser-cooled regime. ^{199}Hg fermion has nuclear spin 1/2, which means absence of tensor light shift for the clock transition.

We laser-cool Hg atoms and trapped them in magneto-optical trap (MOT). The lowest temperature of atoms trapped in MOT is 30 μK for ^{201}Hg [1]. MOT atoms are loaded in the lattice trap, which operates at the magic wavelength [2]. Lattice trapped atoms enables the

Lamb-Dicke spectroscopy of the $^1S_0$ – $^3P_0$ clock transition at 265.6 nm, for which linewidth as low as of 11 Hz can be observed (Fig. 2). This corresponds to an atomic quality factor $Q=10^{14}$. Magic wavelength for Hg was experimentally measured with precision 10^{-3} nm [3]. When our probe laser is locked to the atomic transition, our clock shows fractional frequency instability of $5.4*10^{-15}$ at 1 second [4]. We performed a first study of systematic shifts and a series of absolute frequency measurements with an uncertainty of $5.7*10^{-15}$ [5]. Based on these measurements, ^{199}Hg entered the List of Recommended Transitions of the CIPM (Comité International des Poids et Mesures), following the recommendation of the 19th CCTF (Comité Consultatif du Temps et des Fréquences).

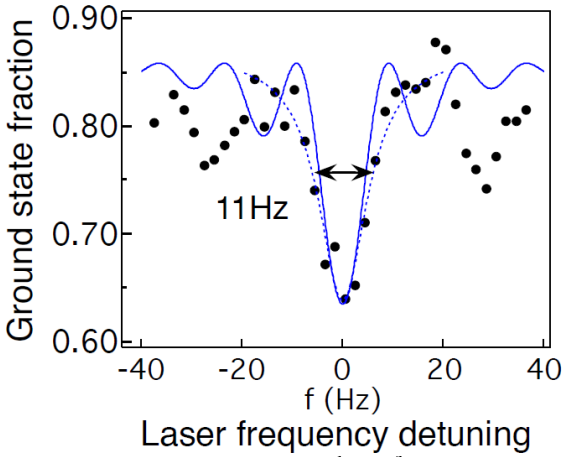

Fig. 2. Lamb-Dicke regime spectroscopy of $^1S_0$ – $^3P_0$ transition in ^{199}Hg atom.

Our recent work focused on improving key laser systems for the cooling light and for the lattice light. We implemented new lattice cavity mirrors, with which we can have 4 times deeper trap, which bring us close to a depth of 100 recoil energy. Also, we improved our cooling laser source to be more powerful and stable. Normally, this should allow us to increase the number of atoms trapped in MOT by a factor of 10. The number of atoms in the lattice should increase even more, thereby increasing the signal to noise ratio for the Lamb-Dicke spectroscopy. These improvements should yield stability below 10^{-15} at 1 second and enable an evaluation of uncertainties to better than 10^{-16} with our current ultra-stable laser source and probe laser system. Theoretical accuracy limit for the Hg lattice clock is below 1 part in 10^{18} at room temperature.

References

1. J. J. McFerran et al., Opt. Lett. 35, 3078 (2010)
2. H. Katori et al., Phys. Rev. Lett. 91, 173005 (2003)
3. L. Yi et al., Phys. Rev. Lett. 106, 073005 (2011)
4. J. J. McFerran et al., Opt. Lett. 37, 3477 (2012)
5. J. J. McFerran et al., Phys. Rev. Lett. 108, 183004 (2012)

LIFT: the Italian fiber network for time and frequency metrology

D. Calonico[1], F. Levi[1], C. Clivati[1,2], A. Mura[1], C. Calosso, E. Bertacco[1], M. Zucco[1],A. Godone[1], G.A. Costanzo[2], M. Prevedelli[3], G. M. Tino[4], D. A. Sutyrin[4], N. Poli[4].

[1]*INRIM, Istituto Nazionale Ricerca Metrologica, Strada delle Cacce 91, 10135, Torino, Italy*
[2]*Politecnico di Torino,Corso Duca degli Abruzzi24 , 10129, Torino, Italy*
[3]*Dipartimento di Fisica, Università di Bologna, Bologna, Italy*
[4]*Dip. Fisica e Astronomia,INFN and LENS,Università Firenze,Via Sansone 1, 50019 Sesto Fiorentino (FI), Italy*
E-mail: d.calonico@inrim.it

Optical frequency standards (OFS) are recommended by the BIPM for the secondary representation of the second in the International System of units, and are the most promising candidates for its future redefinition [1]. However, OFS remote comparison is still quite challenging, and only coherent optical fiber links are presently suited to this purpose [2,3], as their resolution outperforms the state-of-the-art satellite techniques by several orders of magnitude, provided the compensation of the phase noise due to the fiber mechanical and thermal stresses [4]. Frequency dissemination at the 10^{-18} level of stability [2,3] and time dissemination at the 20 ps level [5] over distances of 1000 km can be obtained.
The National Institute of Metrology (INRIM) is in charge in Italy for Time and Frequency (T&F) metrology, realizing the national timescale and disseminating accurate T&F signals. INRIM operates two Cs primary frequency standards (accuracy at the 10^{-16} level [6]), and is developing an OFS based on Yb atoms [7]. INRIM, Politecnico di Torino and University of Florence started the LIFT project (the Italian Link for Frequency and Time), to realize an optical link along a 650 km fiber backbone connecting Torino to Milano, Bologna, and Firenze (see Fig. 1). Present LIFT partnership includes also the National Institute of Nuclear Physics (INFN) and LENS, and the National Institute of Optics (INO) in Florence; the National Institute of Astrophysics (INAF) in Medicina (Bologna), and the National Council of Research (CNR) in Milano.

Fig. 1. Map of the 650 km optical link path from Turin to Florence.

LIFT targets to the distribution via optical fiber of the INRIM reference T&F signals with a relative instability $<10^{-13}$ at 1 s measurement time and 10^{-18} at one day, to a variety of scientific laboratories, representing national centers of excellence in their fields. This facility will further improve their scientific capabilities, allowing these laboratories to better exploit existing experiments and to establish new ones in the future.
INFN and CNR are involved in high resolution spectroscopic measurements, and will benefit from T&F dissemination via optical fiber. In particular, at LENS a Sr optical clock is operational and under metrological characterization [8], and its frequency comparison to the frequency standards of INRIM could allow a number of new fundamental physics experiments. INAF is involved in Very Long Baseline Interferometry (VLBI), needing ultrastable frequency references on long timescales.
A key point of the project is to use the same infrastructure to disseminate both time and frequency. For frequency dissemination, an ultrastable laser (1542 nm) is sent to the user, and

its frequency is simultaneously measured in the two laboratories, with two optical frequency combs. The frequency of the delivered laser is perturbed by environmental noise in the fiber; the noise cancellation technique requires a fully-optical backbone with no optical/electrical conversions, with perfect bi-directionality, quite a difference with respect to typical fiber transmission techniques. To disseminate time signals, a pseudorandom noise will be encoded on the optical carrier, similarly to what is done in two way satellite time and frequency transfer: instead of cancelling the phase noise of the carrier itself, the measured transmission delay will be calibrated and stabilized, with a resolution exceeding 100 ps.

The optical fiber used is a 650 km dedicated fiber, with a total optical losses of ~200 dB, partly compensated by 9 dedicated, fully bidirectional Erbium Doped Fiber Amplifiers along the path, that use the same active fiber in both directions [2-3]. Fig. 2 shows present power spectrum density of phase noise, with and without the noise compensation.

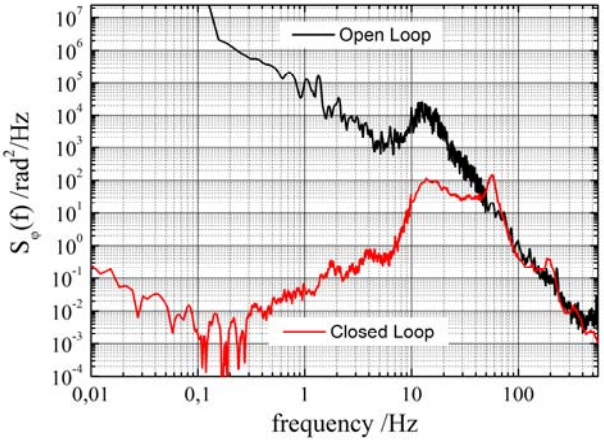

Fig. 2. Phase noise of the fiber link from INRIM to University of Florence, 650 km

At the conference, we will describe the experimental set-up and the preliminary characterization of the 650 km fiber link connecting Torino to Milano, Bologna and Firenze within the LIFT project. The amount of phase noise added by the optical fiber that cannot be compensated is not a limitation, and we estimated that frequency dissemination at the 10^{-16} level of stability in few minutes of averaging time can be obtained.

For funding, UNIFI, POLITO, INRIM acknowledge the Italian Ministry of University MIUR (PRIN09-2009ZJJBLX). INRIM acknowledges Compagnia di S. Paolo, the EMRP program (Project SIB02-NEAT-FT), and the MIUR (Progetti Premiali 2012). The EMRP is jointly funded by the EMRP participating countries within EURAMET and the European Union. INRIM acknowledges GARR for the technical help with the fiber.

References

1. C. W. Chou, et al., *Phys. Rev. Lett.* **104**, 070802 (2010).
2. O. Lopez, et al., *Opt. Expr*. **18**, 16849-16857 (2010).
3. K. Predehl, et al., *Science* **336**, 441-444 (2012).
4. W. Williams, W. C. Swann, and N. R. Newbury, *J. Opt. Soc. Am. B* **25**, 1284-1293 (2008).
5. O. Lopez, et al., , *Appl. Phys. B* **110**, 3–6 (2013).
6. F. Levi, et al., , *IEEE Trans. Ultrason. Ferroelectr. Freq. Contr*. **57**, 600-605, (2010)
7. M. Pizzocaro, et al., , *IEEE Trans. Ultrason. Ferroelectr. Freq. Contr*. **59**, 3, 426431 (2012).
8. N. Poli, M. G. Tarallo, M. Schioppo, C. W. Oates and G. M. Tino, Appl. Phys. B 97, 27-33 (2009).
9. L. Sliwczynski et al.,, IEEE Trans. Instrum. Meas. 62, 1, 2013.

Accuracy evaluation of IT CsF2

Filippo Levi[1], Giovanni A. Costanzo[2], Claudio E. Calosso[1], Davide Calonico[1]
[1]*Optic Division, INRIM, Torino, Italy*
[2]*Electronic Department, Politecnico di Torino, Torino, Italy*
Email: f.levi@inrim.it

At INRIM we have realized and characterized a nitrogen cooled Cs fountain, the new Italian primary frequency standard. Our fountain is the result of a fruitful collaboration with NIST Time and Frequency Division, where the physical package of two twin fountains NIST F2 and ITCsF2 was realized.

The fountain accuracy was evaluated with respect to the following frequency shift: atom density, blackbody radiation, Zeeman effect, gravitational potential, microwave leakage, distributed cavity phase and other minor effects. Thanks to nitrogen cooling, low atomic density and particular care in the physical structure design, we could reduce significantly important sources of uncertainty. The accuracy budget of IT CsF2 combine to a total type B uncertainty of 1.8×10^{-16}, and a similar statistical uncertainty over a twenty day measurement evaluation (density shift is accounted for in the type A uncertainty).

Laser spectroscopy of trapped thorium ions: Towards a nuclear optical clock.

M.V. Okhapkin, O.A. Herrera-Sancho, N. Nemitz, Chr. Tamm, E. Peik
Physikalisch-Technische Bundesanstalt, Bundesallee 100, 38116 Braunschweig, Germany

The possibility to realize a new generation of highly precise optical clocks based on laser excitation of the nuclear transition between the ground and isomeric states of ^{229}Th [1,2] has motivated experiments with thorium ions in traps. The application of precise methods of laser spectroscopy to a nuclear excitation promises to open a new field of research at the border between atomic and nuclear physics. To facilitate the search for the nuclear transition within the present wide uncertainty range of 7.8 ± 0.5 eV, we investigate two-photon excitation in the dense electronic level structure of Th^+, which enables the nuclear excitation via a resonantly enhanced electronic bridge process [3].

In our experiment, ^{232}Th ions are produced by laser ablation and are trapped in a linear Paul trap [4]. Argon buffer gas is used for collisional cooling of the trapped ions and for quenching of low-lying metastable states which are populated through spontaneous decay after laser excitation [5]. As the first excitation step, the Th^+ resonance line at 402 nm from the ($6d^27s$) J=3/2 ground state to the (6d7s7p) J=5/2 state is driven by pulses of an extended-cavity diode laser. Frequency-tripled pulses of a nanosecond Ti:Sa laser radiation in the 250 nm wavelength range are synchronized with the pulses from the diode laser and are used for the second step of a resonantly enhanced two-photon excitation. With this setup, we observe 44 energy levels within the energy range from 7.3 to 8.3 eV. Only one of those states was known previously. Excitation via a different intermediate state with J=1/2 allowes us to classify 16 of these levels as having J=3/2. The high density of electronic states indicates the possibility of obtaining a strongly enhanced electronic bridge excitation of the ^{229m}Th isomeric state that is expected in this energy range.

Using resonantly enhanced three-photon ionization of Th^+, the second ionization potential of thorium is determined for the first time. Moreover, we find that ultraviolet pulsed laser radiation in a wide wavelength range provides efficient photodissociation of molecular ions that are formed in reactions of Th^+ with the residual gas in the vacuum chamber and impurities in the buffer gas. This eliminates the dominant limitation of the storage time for thorium ions in our trap.

[1] E. Peik, Chr. Tamm, Europhys. Lett. 61, 181 (2003)
[2] C.J. Campbell, A.G. Radnaev, A. Kuzmich, V.A. Dzuba, V.V. Flambaum, A. Derevianko. Phys. Rev. Lett. 108, 120802 (2012)
[3] S.G. Porsev V.V. Flambaum, E. Peik, Chr. Tamm. Phys. Rev. Lett. 105, 182501 (2010)
[4] K. Zimmermann, M.V. Okhapkin, O.A. Herrera-Sancho, E.Peik. Appl. Phys. B 107, 883 (2012).
[5] O.A. Herrera-Sancho, M.V. Okhapkin, K. Zimmermann, Chr. Tamm, E.Peik, A.V. Taichenachev, V.I. Yudin, P. Glowacki. Phys. Rev. A 85, 033402 (2012).

Multipole, nonlinear and anharmonic uncertainties of Sr optical lattice clocks.

V.D. Ovsiannikov[1], V.G. Pal'chikov[2], A.V. Taichenachev[3], V.I.Yudin[3] and H. Katori[4]

[1] *Physics Department, Voronezh State University,Voronezh 394006, Russia*

[2] *Institute of Metrology for Time and Space at NationalResearch Institute for Physical--Technical and Radiotechnical Measurements, Mendeleevo, Moscow Region, 141579 Russia*

[3]*Institute of Laser Physics of SB RAS, Pr. Lavrentyeva 13/3, Novosibirsk, 630090 Russia*
Novosibirsk State University, ul. Pirogova, 2, Novosibirsk,630090, Russia
Novosibirsk State Technical University, pr. K. Marksa, 20, Novosibirsk, 630073, Russia

[4] *Department of Applied Physics, Graduate School of Engineering, The University of Tokyo, Bunkyo-ku,; Innovative Space-Time Project, ERATO, Japan; Science and Technology Agency, Bunkyo-ku, Tokyo 113-8656; Quantum Metrology Laboratory, RIKEN, Wako-shi, Saitama 351-0198, Japan*
E-mail: ovd@phys.vsu.ru

The basic idea of a magic wavelength (MWL) for high-precision clocks on atoms, confined to an optical lattice, is to equalize completely the lattice-induced Stark shifts in upper (excited) and lower (ground) clock states. To this end, the frequency-dependent electric dipole (E1) polarizabilities, determining the principal contributions to the Stark shifts, at the MWL should be equalized for the clock states to the highest possible precision. However, this equalization does not guarantee equal values of the multipole (M1 and E2) polarizability and higher-order dipole (hyperpolarizability) effects, which may introduce considerable uncertainties into the precision of the clock frequency.

In the field of a lattice standing wave of a frequency ω and wave vector $\mathbf{k} = k\mathbf{n}$, $k = \dfrac{\omega}{c}$,

$$\mathbf{E}(\mathbf{R},t) = 2\mathbf{E}_0 \cos(\mathbf{k}\cdot\mathbf{R})\cos(\omega t), \qquad (1)$$

where $\mathbf{R}$ is the position vector of atomic nucleus relative the standing-wave antinode, the spatial distribution of magnetic dipole (M1) and electric qudrupole (E2) interactions is a quarter of wavelength out of phase with electric dipole (E1) atom-lattice interaction. Therefore, the multipole terms do not influence on the depth of the Stark potential and contribute only to its position-dependent part, determining the frequency of vibrations $\Omega_{g(e)}$ for an atom in its ground (excited) state. Corresponding equation for the trapping potential of a 1D lattice ($\mathbf{k}\cdot\mathbf{R} = kX$), with account of harmonic ($\propto X^2$) and lowest-order anharmonic ($\propto X^4$) terms, may be presented, as follows

$$U^{latt}_{g(e)}(X) = -U^{(0)}_{g(e)} + U^{(2)}_{g(e)}X^2 - U^{(4)}_{g(e)}X^4, \qquad (2)$$

where $U^{(0)}_{g(e)} = \alpha^{E1}_{g(e)}(\omega)I + \beta^{E1}_{g(e)}(\omega)I^2$ is the depth of the Stark potential for atoms in their ground (excited) state, including linear and quadratic in the laser intensity I terms, determined by the electric-dipole dynamic polarizability $\alpha^{E1}_{g(e)}(\omega)$ and hyperpolarizability $\beta^{E1}_{g(e)}(\omega)$, respectively. The equality $U^{latt}_{g}(X) = U^{latt}_{e}(X)$ could eliminate completely the lattice-induced uncertainties of the clock-frequency measurements. But this equality assumes equal values of all coefficients in the lattice potential (2), which include different combinations of linear and quadratic in I terms, where $\alpha^{E1}_{g(e)}(\omega)$ appears in combination with multipole polarizability $\alpha^{qm}_{g(e)}(\omega) = \alpha^{E2}_{g(e)}(\omega) + \alpha^{M1}_{g(e)}(\omega)$. Equalization of linear in I terms and rigorous account for quadratic terms simultaneously requires high-precision control of the laser magic frequency and the laser intensity over all lattice sites. The principal contribution to all coefficients of potential (2) comes from the dipole polarizability. However, the trapping condition for an atom of the mass $\mathcal{M}$

$$U_{g(e)}^{(0)} >> \epsilon^{rec}, \qquad (3)$$

where $\epsilon^{rec} = k^2/2\mathcal{M}$ is the recoil energy transferred to atom from a scattered photon, requires sufficiently large laser intensity, for which the contribution of hyperpolarizability terms may influence considerably on the Stark-shift uncertainties.

The coefficient of the harmonic term, $U_{g(e)}^{(2)} = \left[\alpha_{g(e)}^{dqm}(\omega)I + 2\beta_{g(e)}^{E1}(\omega)I^2\right]k^2$, may be considered as the elastic force coefficient, $U_{g(e)}^{(2)} = \mathcal{M}\Omega_{g(e)}^2/2$. Thus the frequency of trapped atom vibrations in the well (2), $\Omega_{g(e)}$, determined mainly by the difference of dipole and multipole polarizabilities $\alpha_{g(e)}^{dqm}(\omega) = \alpha_{g(e)}^{E1}(\omega) - \alpha_{g(e)}^{qm}(\omega)$, is proportional to $I^{1/2}$.

The anharmonic term, with coefficient

$$U_{g(e)}^{(4)} = \left[\alpha_{g(e)}^{dqm}(\omega)I + 5\beta_{g(e)}^{E1}(\omega)I^2\right]\frac{k^4}{3} = \left[\frac{\mathcal{M}\Omega_{g(e)}^2}{6} + \beta_{g(e)}^{E1}(\omega)I^2\right]k^2$$

may be taken into account in the first-order perturbation theory. So, the energy of a bound state with the vibration quantum number n in a potential well (2) may be written as

$$E_{g(e)}^{vib}(I,n) = -U_{g(e)}^{(0)} + \Omega_{g(e)}(n+1/2) - \frac{\epsilon^{rec}}{2}\left[1 + \frac{3\beta_{g(e)}(\omega)I}{\alpha_{g(e)}^{E1}(\omega)}\right](n^2+n+1/2). \qquad (4)$$

For the laser intensity $I > 1$ kW/cm^2, sufficient to support inequality (3), the principal contribution to this energy gives the term of E1 polarizability, determining the depth of the potential well. The frequency of vibrations is on the order of $\sqrt{\epsilon^{rec}/U_{g(e)}^{(0)}} << 1$ in comparison with $U_{g(e)}^{(0)}$, and the third term is the contribution of anharmonic atom-lattice interaction, with the smallest absolute value (on the order of $\epsilon^{rec}/U_{g(e)}^{(0)}$). Both harmonic and anharmonic terms depend on the vibration state quantum number n, so the sideband cooling is required to minimize their contribution reducing oscillations to the ground state $n = 0$. It is evident from (4), the shift of the clock frequency may be presented in general, as

$$\Delta\nu_{cl}(I,n) = E_e^{vib} - E_g^{vib} = a_{1/2}I^{1/2} + a_1 I + a_{3/2}I^{3/2} + a_2 I^2, \qquad (5)$$

where the square-root and linear terms provide the main contribution. To achieve atomic-motion-independence for the clock frequency, means to tune the lattice laser to the magic frequency ω_m so as to eliminate or to minimize these terms. The condition $a_{1/2} = 0$ corresponds to equalization of combined polarizabilities for the ground and excited states, $\alpha_g^{dqm}(\omega_m) = \alpha_e^{dqm}(\omega_m) \equiv \alpha_m^{dqm}$. The remaining coefficients in (5) depend on the difference of multipole polarizabilities $\Delta\alpha^{qm} = \alpha_e^{qm} - \alpha_g^{qm}$ and hyperpolarizabilities $\Delta\beta = \beta_e - \beta_g$:

$$a_1 = -\Delta\alpha^{qm} - \frac{3\Delta\beta\epsilon^{rec}}{2\alpha_m^{dqm}}(n^2+n+1/2); \quad a_{3/2} = \Delta\beta\sqrt{\frac{\epsilon^{rec}}{\alpha_m^{dqm}}}(n+1/2); \quad a_2 = -\Delta\beta. \qquad (6)$$

Numerical calculations for a Sr red-detuned lattice with the MWL of 813.42727 nm [1] give for linear polarization of the lattice wave in the ground (n=0) vibrational state:
$a_1 = 6.82$ mHz/(kW/cm^2); $a_{3/2} = -0.192$ mHz/(kW/cm^2)$^{3/2}$; $a_2 = 1.66$ mHz/(kW/cm^2)^2.
An alternative definition of the MWL in a field of a traveling wave $\alpha_g^{\Sigma}(\omega_m) = \alpha_e^{\Sigma}(\omega_m) \equiv \alpha_m^{\Sigma}$, where $\alpha_{g(e)}^{\Sigma}(\omega) = \alpha_{g(e)}^{E1}(\omega) + \alpha_{g(e)}^{qm}(\omega)$, may be used. Then $a_{1/2} = -\Delta\alpha^{qm}\sqrt{\epsilon^{rec}/\alpha_m^{\Sigma}}(2n+1)$, the sign of the multipole polarizability α^{qm} should be reversed and α_m^{Σ} should substitute for α_m^{dqm} in the definition (6) of coefficients for the lattice-induced clock frequency shift (5).

1. P.G. Westergaard et al, Phys.Rev. Lett. **106**, 210801 (2011).

Optical lattice clocks with ^{87}Sr in a cryogenic environment

M. Takamoto[1,2], I. Ushijima[2,3], M. Das[1,2], T. Ohkubo[2,3], N. Nemitz[1,2], H. Katori[1,2,3]

[1] *Quantum Metrology Laboratory, RIKEN, Wako-shi, Saitama, Japan*
[2] *Innovative Space-Time Project, ERATO, JST, Bunkyo-ku, Tokyo, Japan*
[3] *Department of Applied Physics, Graduate School of Engineering, The University of Tokyo, Bunkyo-ku, Tokyo, Japan*
E-mail: takamoto@riken.jp

We have developed a cryogenic setup for Sr optical lattice clocks and directly measured the blackbody radiation shift of the clock transition. Such a development of temperature-controlled environment is an essential step towards the realization of a fractional frequency uncertainty of 10^{-18} with Sr optical lattice clocks.

Single-ion optical frequency standards based on $^{171}Yb^{+}$

Chr. Tamm, N. Huntemann, B. Lipphardt, Chr. Sanner, M.V. Okhapkin, E. Peik

Physikalisch-Technische Bundesanstalt, Bundesallee 100, 38116 Braunschweig, Germany

Optical frequency standards based on electric-dipole forbidden transitions in single ions or neutral atoms have the potential to reach systematic uncertainties in the 10^{-18} range. This accuracy provides the basis for a wide range of precision measurements and tests of fundamental physical theories. Among the ions investigated so far as optical frequency standards, Yb^{+} is unique because its energy level system includes states arising from excitation of the 4*f* electron shell. As a consequence, the lowest-lying excited state of Yb^{+}, the $4f^{13}6s^2\ ^2F_{7/2}$ state, is connected to the $^2S_{1/2}$ ground state by a highly forbidden electric-octupole (E3) transition which leads to a natural state lifetime in the range of five years [1].

For optical frequency standards based on $^{171}Yb^{+}$, both the E2 transition $^2S_{1/2}$ - $^2D_{3/2}$ at 436 nm and the E3 transition at 467 nm are being investigated. The E2 transition is recommended as a secondary realization of the SI second and a standard with a relative systematic uncertainty of $5\cdot10^{-16}$ has been demonstrated [2]. Spectroscopy of the E3 transition was pioneered at the NPL (Teddington, UK) [1]. This transition is attractive as a highly accurate optical standard because frequency shifts induced by static electric and magnetic fields are significantly smaller than in the E2 reference transitions of alkali-like ions [3]. The high optical power required for driving the E3 transition however leads to a large light shift.

We aim at realizing an optical frequency standard that takes advantage of the high accuracy and stability potential of the $^{171}Yb^{+}$ E3 transition. A probe laser system with low nonlinear frequency drift resolves the transition with a Fourier-limited minimum linewidth of 2.4 Hz. The laser frequency is locked to the line center of the E3 transition with quantum projection noise limited stability. Using a real-time extrapolation scheme to eliminate the light shift, the unperturbed transition frequency has been realized with an uncertainty of $7.1\cdot10^{-17}$ and the frequency measured as 642 121 496 772 645.15(52) Hz [3], with the uncertainty dominated by the caesium fountain reference. The result is in excellent agreement with a recent measurement conducted at the NPL [4].

Recently we have implemented the Hyper-Ramsey spectroscopy (HRS) scheme [5] for excitation of the Yb^{+} E3 transition. The HRS excitation uses a pulse sequence that is tailored to produce a resonance signal that is not affected by the the light shift induced by the probe laser. The experiments demonstrate a light shift suppression by four orders of magnitude and an immunity against its fluctuations [6]. The HRS scheme is also applied in frequency comparisons between the $^{171}Yb^{+}$ single-ion clock and the ^{87}Sr lattice clock of PTB and in a more precise measurement of the static quadratic Stark shift of the E3 transition. This will reduce the frequency uncertainty due to the blackbody shift and can improve the accuracy of the $^{171}Yb^{+}$ E3 clock further to the low 10^{-17} range.

References

1. M. Roberts, P. Taylor, G.P. Barwood, W.R.C. Rowley, P. Gill, Phys. Rev. A **62**, 020501(R) (2000).
2. Chr. Tamm, S. Weyers, B. Lipphardt, E. Peik, Phys. Rev. A **80**, 043403 (2009).
3. N. Huntemann, M. Okhapkin, B. Lipphardt, S. Weyers, Chr. Tamm, E. Peik, Phys. Rev. Lett. **108**, 090801 (2012).
4. S.A. King, R.M. Godun, S.A. Webster, H.S. Margolis, L.A.M. Johnson, K. Szymaniec, P.E.G. Baird, P.Gill, New J. Phys. **14**, 013045 (2012).
5. V.I. Yudin, A.V. Taichenachev, C.W. Oates, Z.W. Barber, N.D. Lemke, A.D. Ludlow, U. Sterr, C. Lisdat, F. Riehle, Phys. Rev. A **82**, 011804(R) (2010).
6. N. Huntemann, B. Lipphardt, M. Okhapkin, Chr. Tamm, E. Peik, Phys. Rev. Lett. **109**, 213002 (2012).

Active suppression of thermal noise in optical cavities

P. G. Westergaard[1], R. Martin[1], B. T. R. Christensen[1], J. Ye[2] and, J. W. Thomsen[1]

[1] *Niels Bohr Institute, Blegdamsvej 17, 2100 Copenhagen, Denmark*
[3] *JILA, Department of Physics, 440 UCB, Boulder, Colorado 80309, USA*
E-mail: jwt@fys.ku.dk

Optical atomic clocks based on two electron atoms have enjoyed tremendous progress over the past 10 years [1]. However, these clocks are limited by the frequency noise of the interrogation oscillator through the Dick effect.

To achieve the heralded ultimate stability, future optical frequency standards will need to produce light sources with frequency stability at the 10^{-17} fractional level or below at one second of integration time. Achieving this stability has so far been hampered by thermal noise in the reference cavity used for laser stabilization. These fluctuations are transferred to the laser frequency thereby limiting the practically achievable stability to the mid-10^{-16} level. By cooling the reference cavity and using an optimized material design the thermal noise limit can be reduced, and a stability at the 10^{-16} level was recently obtained this way [2]. However, this state-of-the-art stability still remains at least an order of magnitude too large for lattice clocks to reach their ultimate performance.

We propose a new strategy to overcome thermal noise by performing direct spectroscopy on atoms trapped inside a high Q cavity. Fully implemented, simulations show a shot noise limited operation corresponding to a one micro Hz line width [3].

Our system is schematically shown in figure 1 and consists of a cavity with atoms trapped inside in an optical lattice or provided by a cold atomic beam. The cavity will enhance atom-light interaction by an order of the finesse of the cavity and facilitate direct spectroscopy on the weakly allowed transitions of alkali-earth atoms. Even though such a system shows bi-stability it is possible to find a stable working regime at high input powers which enables laser stabilization [3]. By keeping the cavity on the atomic resonance and carefully choosing the parameters, the intra-cavity probe light will bleach the atomic transition in such a way that a narrow feature will arise within the atom/cavity resonance peak. Due to the presence of the atoms, this feature will remain unperturbed by thermal fluctuations of the cavity mirrors and can be used for stabilization of the laser.

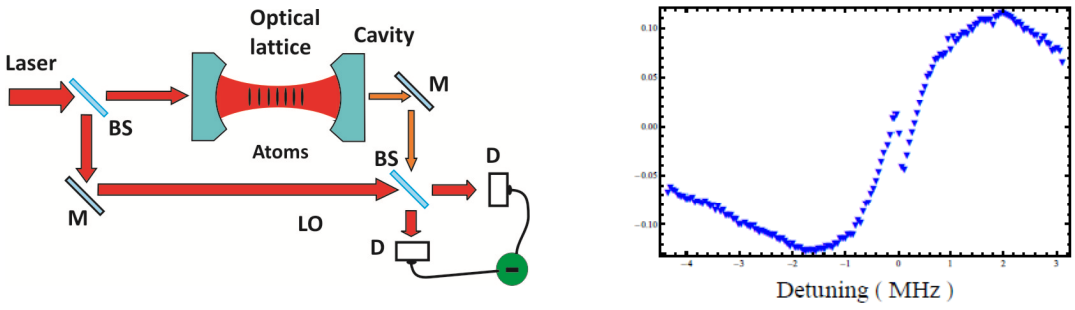

Fig. 1: (Left) The experimental setup for our proposal. (Right) Phase response of the atoms measured by direct cavity assisted spectroscopy on the ^{88}Sr $^1S_0 - {}^3P_1$ line in a MOT.

In a first phase we plan to demonstrate the locking signal by using atoms from a blue ^{88}Sr Magneto Optical Trap (MOT) and the intercombination line $^1S_0 - {}^3P_1$ as the probe. Figure 1 shows measurement of the phase induced by cold atoms in the MOT. The number of atoms contributing to the central s-shaped signal is about 10^6.

In a second phase we will employ an integrated monolithic design combining a high Q cavity with the optical lattice and use the narrow $^1S_0 - {}^3P_0$ clock transition which could ultimately provide a micro Hz line width.

At the conference we will also present our progress towards studying collective effects of the atoms in the cavity.

References

1. P.G. Westergaard et al., Phys. Rev. Lett. 106, 210801 (2011); M.D. Swallows et al., Science 331, 1043 (2011); S. Falke et al., Metrologia 48, 399 (2011); M. Takamoto et al., Nat. Photonics 5, 288 (2011), Y.Y. Jiang et al., Nature Photonics 5, 158–161 (2011); S. Mejri et al., Phys. Rev. A 84, 032507 (2011).
2. T. Kessler et al., J. Opt. Soc. Am. B 29, 178-184 (2012), T. Kessler et al., arXiv:1112.3854v1 (2011).
3. M.J. Martin et al., Phys. Rev. A 84, 063813 (2011).

Form plasmonics to cold atoms

Alexey Akimov[1,2,3], Jeff Thompson[2], Tobias Tiecke[2], J. Feist[2], D. Chang[2], C. Yu, N. De Leon[2], L. Liu[2], A. Zibrov[2], H. Park[2], V. Vuletić[4], M. Lukin[2]

[1]RQC,Skolkovo, Novaya str., 100, SKOLKOVO, Moscow region, 143025, Russia
[2]Harvard University, 17 Oxford str, Cambridge, MA 02138, USA
[3]P.N. Lebedev Institute RAS, 53 Leninsky prospect, Moscow, 119991, Russia
[4]MIT, 77 Massachusetts Ave.Cambridge, MA 02139, USA
E-mail: aa@rqc.ru

The interface between single atom like system and photons is an important part of any quantum communication network or computational scheme. Use of the plasmons in conducting nanowires enable's one to considerably improve single photon collection from nano scale solid state object, such as quantum dot or color center in diamond. Also, significant progress was achieved in this direction with photonic crystal cavities which have advantage over many other cavity QED systems due to their scalability. On another hand atoms are very natural candidates on qubits due to their long coherence time and narrow transitions. Extension of advanced of solid state techniques to the case of atom requires development of new trapping techniques, enabling sub wavelength localization of atoms near the surfaces. In this talk I will describe our efforts towards localizing atom near such a structure and building fiber interface for single atom.

Direct measurement of the van der Waals interaction between two Rydberg atoms

L. Béguin[1], A. Vernier[1], R. Chicireanu[2], T. Lahaye[1], A. Browaeys[1]

[1] *Laboratoire Charles Fabry, Institut d'Optique, CNRS, Univ Paris Sud, 2 avenue Augustin Fresnel, 91127 Palaiseau cedex, France*

[2] *Laboratoire de Physique des Lasers, Atomes et Molécules, Université Lille 1, CNRS, 59655 Villeneuve d'Ascq cedex, France*

E-mail: antoine.browaeys@institutoptique.fr

This talk will report on the direct measurement of the van der Waals interaction between two isolated, single Rydberg atoms separated by a controlled distance of a few micrometers.

By working in a regime where the single-atom Rabi frequency of the laser used for excitation to the Rydberg state is comparable to the interaction energy, we observe a partial Rydberg blockade, whereby the time-dependent populations of the various two-atom states exhibit coherent oscillations with several frequencies. A quantitative comparison of the data with a simple model based on the optical Bloch equations allows us to extract the van der Waals energy, and to observe its characteristic C_6/R^6 dependence, see Fig.1.

The magnitude of the measured C_6 coefficient agrees well with ab-initio calculations, and we observe its dramatic increase with the principal quantum number n of the Rydberg state. Our results demonstrate a good degree of experimental control, which opens interesting perspectives in quantum information processing and quantum simulation using long-range interactions between atoms [2].

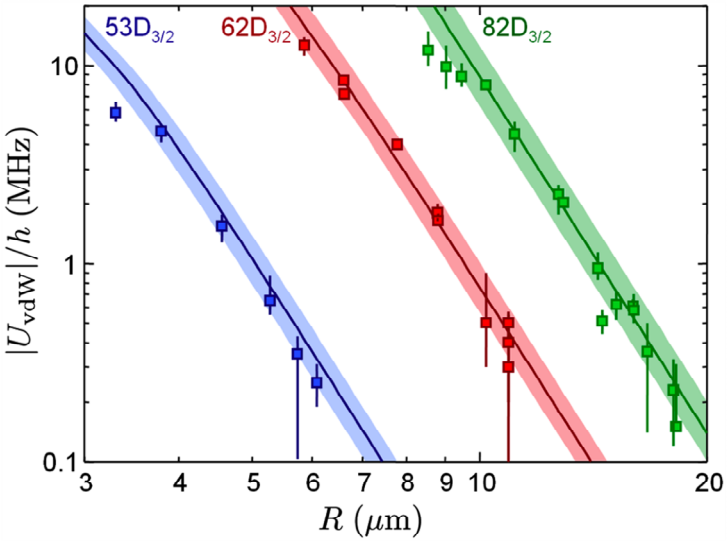

Fig.1. Measured interaction energy between two individual Rydberg atoms, as a function of the interparticle distance R, for three different Rydberg states $53d_{3/2}$, $62d_{3/2}$ and $82d_{3/2}$. The solid lines are the results of an ab-initio calculation.

1. L. Béguin, A. Vernier, R. Chicireanu, T. Lahaye, and A. Browaeys, *Phys. Rev. Lett.,* in press (2013).
2. M. Saffman, T.G. Walker, and K. Moelmer, *Rev. Mod. Phys*. **82**, 2313 (2010).

Ultra cold magnesium atoms for an optical frequency standard

A.N. Goncharov, A.E. Bonert, D.V. Brazhnikov, A.M. Shilov, A.V. Taichenachev, V.I. Yudin and S.N. Bagayev

Institute of Laser Physics SB RAS, pr. Lavrent'eva 13/3, 630090 Novosibirsk, Russia
Novosibirsk State University, st. Pirogova 2, 630090 Novosibirsk, Russia
Novosibirsk State Technical University, pr. Karla Marksa 20, 630092 Novosibirsk, Russia
gonchar@laser.nsc.ru

Frequency standards play an important role as powerful instruments for fundamental science and have numerous metrological and navigation applications. The relative uncertainty of a primary frequency standard based on a fountain of cold ^{133}Cs atoms most probably reaches the limit of 10^{-16}[1]. Further progress in accuracy is associated with frequency standards in the optical range. To take advantage of the optical range, the key problem is suppression of Doppler effects whose relative influence is independent of an absolute frequency - $\Delta\nu/\nu \sim v/c$. Spatial localization of single ion/atoms inside a trap with a size less than a wavelength, at least in the direction of observation, is needed to suppress Doppler and recoil effects. With this localization (the Lamb-Dicke regime) [2] the motional effects are strongly suppressed. Nowadays, the uncertainty of the most precise optical standard based on Al^+ ion goes down to 10^{-17}[3]. This is an order of magnitude less than the uncertainty of the most accurate microwave frequency standard. At present, optical frequency standards based on cooled and localized neutral Ca, Sr, Mg, Yb, and Hg atoms are less accurate. With experimental realization of cooling and trapping of 10^5 - 10^6 atoms inside a dipole optical trap (optical lattice) formed by a standing wave at the "magic" wavelength[4], the situation may change in favour of neutral atoms. An advantage is larger signal/noise ratio, which leads to higher frequency stability. Nowadays the Sr optical lattice frequency standard shows the best result: the uncertainty is 10^{-16}[5]. Magnesium atoms have some advantages over Sr atoms. Inner electronic shells of Mg atoms are completely filled, which simplifies calculations of the influence of various physical factors on the frequency shift of the clock transition. The black body radiation (BBR) shift of the Mg clock transition is one of the lowest among other alkaline-earth atoms [6]. The $^1S_0$ - $^3P_1$ transition with a natural width of 30 Hz and the ultra narrow $^1S_0$ - $^3P_2$ and $^1S_0$ - $^3P_0$ transitions (see Fig. 1) are of interest for the development of Mg frequency standard. In the case of the $^1S_0$ - $^3P_0$ transition, the use of the magneto-induced spectroscopy method [7] is promising. The greatest disadvantage of Mg is the problem of sub-Doppler cooling. Two-photon and quenching sub-Doppler cooling [8,9] was proposed and realized but these methods failed to cool Mg atoms to a temperature of ~10 μK that is necessary to load atoms into an optical lattice. Only recently magnesium atoms were cooled down to 5 μK and loaded into a dipole trap [10].

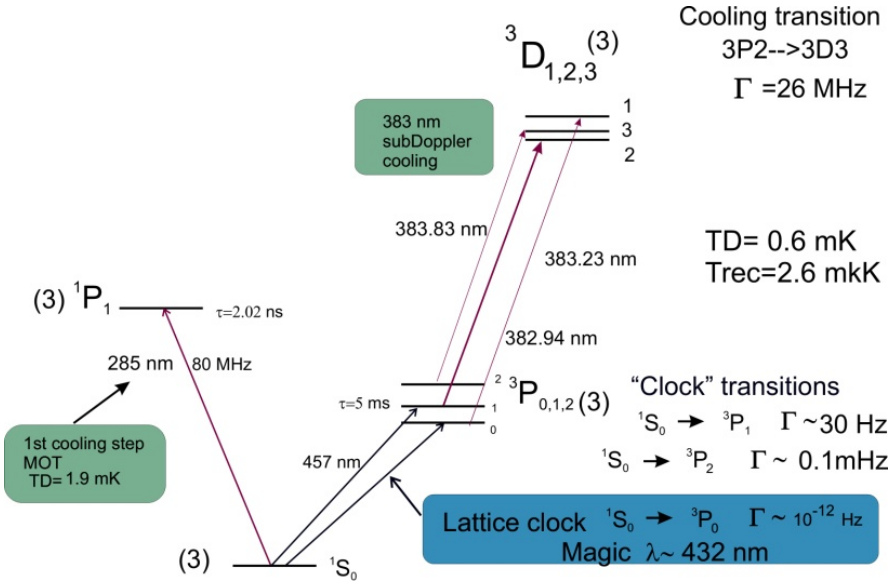

Fig.1 Level scheme of Mg atom.

The main purpose of our studies is to develop an optical frequency standard with ultracold Mg atoms [11]. At the first stage, we performed laser cooling and trapping of ^{24}Mg atoms into a MOT using the strong $^1S_0$ - $^1P_1$ transition. This "singlet MOT" with 10^6 -10^7 atoms at a temperature of ~3 mK was used for high-precision spectroscopy of the $^1S_0$ - $^3P_1$ clock transition. Fig. 2 shows our experimental setup for high-resolution spectroscopy of cooled Mg atoms. AOMs were used to form a four-pulse Ramsey-Bordé interferometer in the time domain [12] to probe the clock transition. Narrow resonances (Ramsey fringes) were detected in the luminescence signal of an atom cloud when interacting with probe laser pulses. Fig. 3 shows Ramsey fringes detected, with the three time delay values between pulses. The best spectral resolution of 2-3 KHz in this experiment was limited by the laser line width. An optical frequency standard at 655.7 THz with a relative uncertainty of 10^{-14} can be implemented by stabilizing laser frequency to the central Ramsey fringe. The main limitation of this stage is the residual Doppler and recoil effects of free atoms. For a further frequency uncertainty level of 10^{-16} we plan to implement a second cooling stage. Trapping of Mg atoms into 1D an optical lattice is the aim of our studies to reach this level of accuracy. Sub-Doppler cooling to ~10 μK is the necessary requirement for effective loading of an optical lattice. The $^3P_2$ -$^3D_3$ triplet transition will be used for sub-Doppler cooling of Mg atoms. The $^3P_2$ level of the transition is degenerate and sub-Doppler cooling by polarization gradients is possible [13]. In our case theoretical analysis of sub-Doppler 1D cooling [14] demonstrated that at a proper choice of laser radiation parameters a large part (up to 60%) of atoms will be cooled down to a temperature of ~10 μK. Now experimental realization of sub-Doppler cooling is in progress.

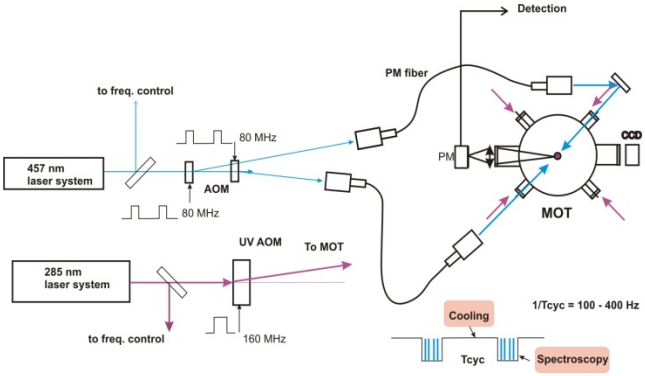

Fig. 2. Experimental setup for high-precision spectroscopy of Mg atoms in MOT.

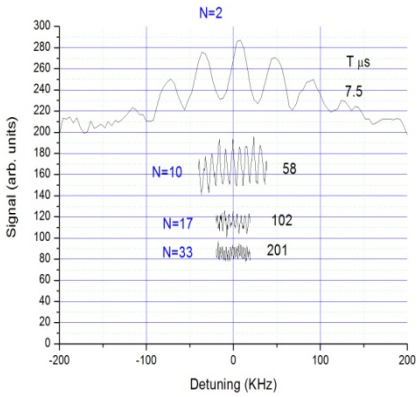

Fig.3. Ramsey fringes detected with a set of delay times T between pulses of duration τ=5 μs: T=7.5, 58, 102 and 201 μs. N is the number of Ramsey fringe periods between recoil components.

This work was supported by the Russian Foundation for Basic Research (grants nos. 12-02-00454, 12-02-00403, 11-02-00775, 11-02-01240), the Russian Academy of Sciences, the Presidium of Siberian Branch of the Russian Academy of Sciences, the Ministry of Education and Science of the Russian Federation within the framework of the Program "Scientific and Scientific-Pedagogical Personnel of Innovative Russia" (contract no. 16.740.11.0466 and agreement no. 8387), and the Russian Quantum Center. The work of young scientists D.V. Brazhnikov and A.M. Shilov was also supported by the Presidential Grant MK-3372.2912.2 and the RFBR Grant 12-02-31208-"mol_a".

[1] S. Bize *et al,* C. R. Phys. **5**, 829 (2004); T.E. Parker, Metrologia **47**, 1 (2010).
[2] R.H. Dicke, Phys. Rev. **89**, 472 (1953).
[3] T. Rosenband *et al, Science* **319,** 1808(2008).
[4] H. Katori et al, PRL**91**, 173005 (2003).
[5] St. Falke et al, Metrologia **48**, 399(2011); H. Katori, Nature Photonics **5**, 203 (2011); P. Lemonde, Eur.J. Special Topics **172**, 81(2009).
[6] S.G. Porsev et al, Phys. Rev. A **74**, 020502 (2006)
[7] A. V. Taichenachev et al, PRL**96**, 083001 (2006).
[8] T.E. Mehlstäubler et al,J. Opt. B: Quantum Semiclass. Opt. **5** (2003) S183(2003); T.E. Mehlstäubler et al, Phys. Rev. A **77**, 021402 (2008); N. Rehbein, Phys. Rev. A **76**, 043406(2007).
[9] W.C. Magno *et al.*, Phys. Rev. **A 67**, 043407 (2003).
[10] M. Riedmann et al, Phys. Rev. A **86**, 043416 (2012).
[11] A.N.Goncharov, Science First hand #**2(23),** 10(2009).
[12] F. Ruschewitz et al , PRL **80**, 3173(1998).
[13] J. Dalibard and C. Cohen-Tannoudji, J. Opt. Soc. Am. B **6**(11), 2023(1989).
[14] D.V. Brazhnikov et al., Vestnik NSU, Series "Physics", Vol. **7**, # 4, 6 (2012) [in Russian].

Collective modes of a two-dimensional quantum gas

K. Merloti[1], R. Dubessy[1], L. Longchambon[1], A. Perrin[1], T. Badr[1], P.-E. Pottie[2], V. Lorent[1] and H. Perrin[1]

[1] *Laboratoire de physique des lasers, Université Paris 13, UMR-CNRS 7538, Sorbonne Paris Cité, 99 avenue J.-B. Clément, F-93430 Villetaneuse, France*

[2] *LNE-SYRTE, Observatoire de Paris, UMR-CNRS 8630, 61 avenue de l'Observatoire, F-75014 Paris, France*
E-mail: helene.perrin@univ-paris13.fr

Quantum gases are fascinating systems for the investigation of the properties of quantum matter. They can be produced nowadays in a wide variety of geometries. Their properties, including volume, temperature and interactions between atoms, can be controlled with external optical, magnetic or radio-frequency fields. For the last ten years, dramatic progress has been made in the investigation of low dimensional quantum gases. When quantum gases are confined to one or two dimensions, the role of quantum correlations is strongly enhanced and the physics changes qualitatively[1]. Specifically, a homogeneous bosonic gas restricted to two dimensions undergoes a Berezinskii-Kosterlitz-Thouless (BKT) transition to a superfluid below a critical temperature.

The study of the excitation modes of a quantum gas is a way to characterise its dynamical properties. In particular, the low energy excitations of a quantum gas trapped in an harmonic potential are collective modes. They can be excited by inducing a sudden change in the trap parameters. In this conference, we will present results of the study of three collective modes of a two-dimensional bosonic quantum gas: the monopole mode (or breathing mode), the quadrupole mode and the scissors mode, see figure 1. In addition, we use the dipolar mode – which is not expected to be damped in an harmonic trap – to characterise the trap geometry and demonstrate its harmonic character and its smoothness.

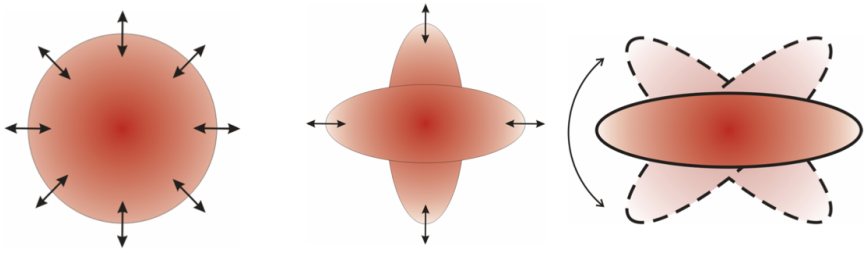

Fig.1. Three collective modes of a two-dimensional quantum gas: the monopole mode (left), the quadrupole mode (centre) and the scissors mode (right).

Our experiments are performed in a new kind of trap well suited to confine gases to two dimensions[2]. The trap relies on magnetic fields only, which results in a very smooth harmonic potential, ensuring a high quality factor of the dipolar oscillation and a controlled system for the study of the collective modes. A quadrupolar magnetic field with a gradient of above 400 G/cm is produced with a pair of coils with opposite currents. The atoms are dressed by a resonant radio-frequency (rf) field in the MHz range and confined in the resulting adiabatic potential[3,4], at the avoided crossing due to the rf dressing. The atoms are strongly confined to a given ellipsoidal isomagnetic surface of the quadrupolar field. Gravity ensures that the atoms gather at the bottom of the ellipsoid. This trap is naturally very anisotropic, with low pendulum frequencies (20 to 50 Hz) in the horizontal plane and a large transverse frequency reaching 2.3 kHz in the vertical direction. The in-plane trap anisotropy is controlled with the rf polarisation, and can be varied in time. The two-dimensional regime for the trapped gas is reached when all relevant energies – chemical potential and temperature – become lower than the transverse strong harmonic energy.

All trap frequencies can be controlled, including in a time-dependent way, with the values of the magnetic field gradient and the rf frequency and amplitude. We excite the various collective modes taking advantage of this feature. The dipolar oscillation of the whole gas is measured first to characterise the quality of the harmonic trap. Oscillations of the cloud can be observed for almost one second, without any observable damping, see figure 2. This remarkable feature makes the trap ideal for the study of collective modes.

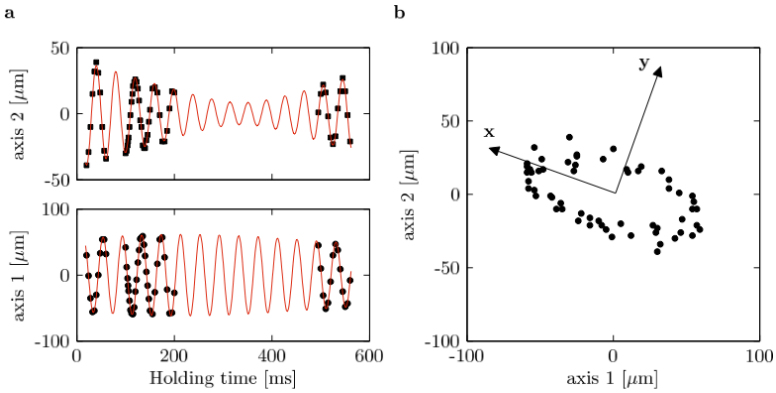

Fig.2. Observation of the undamped dipolar mode in the two-dimensional trap.

The measurement of the monopole mode frequency is of particular interest for a two-dimensional gas. Due to a scaling invariance, the frequency is expected to be independent of the amplitude and the oscillations should not present any damping[5]. Moreover, the monopole mode is well suited to study the equation of state of the quantum gas. For example, it could be used to evidence a quantum anomaly[6] in two dimensions through a very small frequency shift. Although the current experimental resolution doesn't allow for the detection of this anomaly, we do observe the Pitaevskii-Rosch symmetry, as no damping is observable in the monopole oscillation of the two-dimensional gas for several hundreds of milliseconds[2].

While the frequency of the monopole mode does not present a stepwise change when the temperature is lowered and the superfluid transition is met, the quadrupole mode presents different frequencies for a thermal gas in the collisionless regime, which is always the case in our experiment, and for a superfluid. The quadrupole mode consists in out-of-phase oscillations of the cloud radii along two orthogonal directions (see figure 1). This mode is excited by breaking the cylindrical symmetry of the trap and inducing an anisotropy in the trap potential. We observe indeed an oscillation at the expected frequency below the superfluid transition.

The ideal mode to study the superfluid nature of the gas is the scissors mode. Indeed, it relies on the irrotational character of the superfluid flow. This mode is excited by a sudden angular change in the eigenaxes of the trap, see figure 1. Above the superfluid transition, there is no collective mode corresponding to this excitation and the cloud oscillates with the frequencies of the trap. Below the critical temperature, however, the superfluid oscillates around a given axis. The study of this oscillation and its damping is highly relevant for the study of superfluidity in low dimensional quantum gases. We present very recent results of the scissors mode excited in two-dimensional gases above and below the critical temperature.

References

1. I. Bloch, J. Dalibard, and W. Zwerger, *Rev. Mod. Phys.* **80**, 885 (2008).
2. K. Merloti et al., *New J. Phys.***15**, 033007 (2013).
3. O. Zobay and B. M. Garraway, *Phys. Rev. Lett.* **86**, 1195 (2001).
4. Y. Colombe et al., *Europhys. Lett.* **67**, 593 (2004).
5. L. P. Pitaevskii and A. Rosch, *Phys. Rev. A* **55**, R853 (1997).
6. M. Olshanii, H. Perrin, and V. Lorent, *Phys. Rev. Lett.* **105**, 095302 (2010).

Photoassociation spectroscopy of cold ^{40}Ca near the $^3P_1 + {}^1S_0$ asymptote

F. Riehle[1], M. Kahmann[1], O. Appel[1], U. Sterr[1], E. Tiemann[2]

[1] *Physikalisch-Technische Bundesanstalt (PTB), Bundesallee 100, 38116 Braunschweig, Germany*
[2] *Institut für Quantenoptik, Leibniz Universität Hannover, Welfengarten 1, 30167 Hannover, Germany*

E-mail: fritz.riehle@ptb.de

The narrow $^1S_0$ - $^3P_1$ intercombination lines of the alkaline earth elements make them particularly attractive in various fields of basic research and applied technology, e.g. in optical atomic clocks[1,2], precision measurements[3], or the determination of molecular potentials with unprecedented accuracy[4]. In contrast to other alkaline earth elements and ytterbium a new regime is encountered where the long range potentials are dominated by the van der Waals (C_6) interaction. As has been pointed out[5] due to the similarly valued van der Waals coefficients in the involved ground and excited state potentials of Ca_2 the photoassociation (PA) is considerably different from other elements with stronger dipole (C_3) interaction. The small C_3 coefficient in Ca leads to two long range attractive potentials $^3\Pi_u$ and $^3\Sigma^+_u$ and therefore differs from all other so far investigated homonuclear PA studies. These similar potentials can effectively couple by spin-orbit and / or rotational interaction which both lead to a striking dependence of the molecular *g* factor on the molecular vibrational levels.

We trap and cool the ^{40}Ca atoms in two stages in magneto-optical traps at 423 nm and 657 nm, respectively[6], before we load them into a crossed dipole trap[7] at a temperature of about 12 µK. After further evaporation by lowering the dipole trap about N = 150 000 atoms are prepared at a temperature of $T \sim 1$ µK and a peak density of $\rho \sim 1.1 \times 10^{19}$ m^{-3}. The trap loss caused by photoassociation as a function of the laser frequency is observed from absorption images of the atomic cloud when irradiated by a 657 nm PA laser with a line width below 2 kHz. The frequency is referenced with respect to the atomic $^1S_0$ - $^3P_1$ transition.

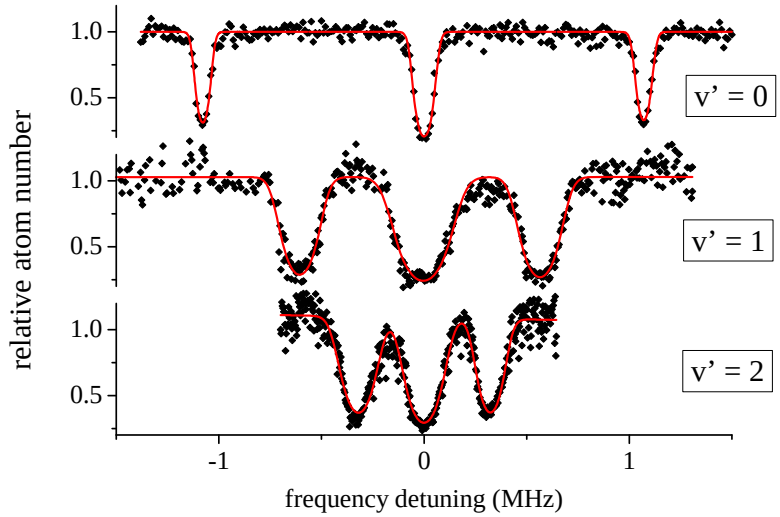

The figure shows the observed trap loss (diamonds) as function of frequency relative to the $m_J = 0$ component with the Zeeman triplet for the three weakest bound molecular states in the

c $^3\Pi_u$ ($\Omega=0^+_u$) potential for a magnetic field of B = 0.285(7) mT. The full lines are fitted solutions of two body loss differential equation removing a linear background drift.

From those curves the centers of the photoassociation lines of the three weakest bound vibration levels in the $^3\Pi_u$ ($\Omega = 0^+_u$) state and ($\Omega = 1_u$) of the coupled system $^3\Sigma^+_u$ / $^3\Pi_u$ were determined together with the molecular *g* factors. To derive the exact resonances we had to apply different corrections to the raw data e.g. shifts due to the finite temperature of the atoms, ac Stark shift resulting from both the dipole trap and the photoassociation laser, or the different recoil shifts when exciting the atoms or molecules.

In our experiment we observe states correlating to the $^3P_1 + ^1S_0$ asymptote which correspond to Hund's coupling (c) states c 0^+_u and (a, c) 1_u. In this approximation no Zeeman-splitting of the $\Omega = 0$ states would be expected. The fact that we observe Zeeman-splitting in all states requires a more sophisticated theoretical model:

We model the observed energy levels and low-field Zeeman splittings by a coupled channel calculation similarly to the one applied by Ciurylo et al.[5] Since the dipole-dipole term is small we keep the C_3 coefficient fixed and estimate it[5,8] from the lifetime of the state $^3P_1$ as τ = 0.48 ms and the transition frequency 15210.063 cm^{-1} of $^1S_0$ - $^3P_1$ to be C_3 = 9.504 cm^{-1} Å^3. The energies of the observed six photoassociation resonances and their molecular *g* factors were fitted simultaneously to obtain the coefficients C_6 and C_8. It turned out that the energies could be reproduced by different combinations of C_6 and C_8 equally well, but for a good fit of the *g* factors and the energies at the same time this ambiguity disappeared. We conclude therefore that for a consistent description of the long range interaction potential only the inclusion of both energies and Zeeman splittings provides experimentally determined accurate long range potential coefficients. The derived long range parameter C_6 and C_8 agree with the theoretical ones to about 2 % [5,9] and 10% [9], well within the estimated relative uncertainty of 5% and 20%, respectively.

Since the narrow line widths of the photoassociation lines make Ca an ideal candidate to tune the scattering length over a wide range we plan to use these findings in the future to investigate optical Feshbach resonances [10] with ^{40}Ca.

Acknowledgement

This work was supported by Deutsche Forschungsgemeinschaft (DFG) through the Center of Quantum Engineering and Space-Time Research (QUEST) of the Leibniz Universität Hannover and through the Research Training Group 1729 Fundamentals and Applications of ultracold Matter. The help of Stephan Schulz, Sebastian Kraft, and Evgenij Pachomow is gratefully acknowledged.

References

1. S. Falke et al, *Metrologia* **48**, 399 (2011).
2. N. D. Lemke et al, *Phys. Rev. Lett.* **103**, 063001 (2009).
3. S. Kotochigova, T. Zelevinsky, and J. Ye, *Phys. Rev. A* **79**, 012504 (2009).
4. K. M. Jones, E. Tiesinga, P. D. Lett, and P. S. Julienne, *Rev. Mod. Phys.* **78**, 483 (2006).
5. R. Ciurylo, E. Tiesinga, S. Kotochigova, and P. S. Julienne, *Phys. Rev. A* **70**, 062710 (2004).
6. C. Degenhardt et al *Phys. Rev. A* **72**, 062111 (2005).
7. S. Kraft, F. Vogt, O. Appel, F. Riehle, and U. Sterr, *Phys. Rev. Lett.* **103**, 130401 (2009).
8. There is an opposite sign definition in ref. 5 for the dipole-dipole term compared to the conventional usage which is applied here.
9. J. Mitroy and J.-Y. Zhang, J. Chem. Phys. 128, 134305 (2008).
10. P. O. Fedichev, M. W. Reynolds, and G. V. Shlyapnikov, Phys. Rev. Lett. 77, 2921 (1996

Spectroscopy of cold Rydberg atoms and their application in quantum information

I.I. Ryabtsev[1, 2, 5] *, I.I. Beterov[1, 2], D.B. Tretyakov[1], V.M. Entin[1], E.A. Yakshina[1, 2], V.P. Zhukov[4], M.P. Fedoruk[2, 4], M. Saffman[3], C.W. Mansell[6], C. MacCormick[6], S. Bergamini[6]

[1]*Rzhanov Institute of Semiconductor Physics SB RAS, 630090 Novosibirsk, Russia*
[2]*Novosibirsk State University, 630090 Novosibirsk, Russia*
[3]*Department of Physics, University of Wisconsin, Madison, Wisconsin, 53706, USA*
[4]*Institute of Computational Technologies SB RAS, 630090 Novosibirsk, Russia*
[5]*Russian Quantum Center, Skolkovo, Moscow Reg., 143025, Russia*
[6]*The Open University, Walton Hall, MK7 6AA, Milton Keynes, UK*
**E-mail: ryabtsev@isp.nsc.ru*

Highly excited Rydberg atoms have many unique properties compared to low-excited atoms: large electron orbit radius, large dipole moments of transitions between neighboring states, strong long-range interactions, long radiative lifetimes, huge polarizabilities, etc. Laser and microwave spectroscopy of Rydberg atoms reveals these properties by observing the quantum interference, dephasing, shifts or broadenings of various resonances in single Rydberg atoms. Control of long-range interactions between Rydberg atoms by laser and microwave radiations, as well as by external electric and magnetic fields, forms the basis for quantum information processing with neutral trapped atoms [1-3]. Experimental techniques of laser cooling and trapping of atoms and high precision spectroscopy allow confining and manipulating single atoms in optical dipole traps and optical lattices. Entangled states can be generated using a temporary excitation of ground-state atoms to a strongly interacting Rydberg state or using interaction-induced changes in the spectra of collective excitations of an ensemble of Rydberg atoms (dipole blockade effect [3]).

In this report we will review the recent experimental advances in quantum information processing with Rydberg atoms. We will also present our related experimental and theoretical results on laser and microwave spectroscopy cold Rb Rydberg atoms in a magneto-optical trap, on the excitation and detection statistics, and on dipole-dipole interaction between a few cold rubidium Rydberg atoms confined in a small laser excitation volume [3-7]. The new ideas on quantum gates with deterministic single-atom loading of optical lattices using dipole blockade with chirped laser pulses [8, 9] and on Doppler- and recoil-free laser excitation of Rydberg states via three-photon transitions [10] will be discussed in the context of quantum information processing with neutral atoms.

This work was supported by RFBR (Grant No. 13-02-00283), by the Russian Academy of Sciences, by the Presidential Grants No. MK-7060.2012.2, by the EU FP7 IRSES Project "COLIMA", by the Russian Quantum Center, EPSRC project 5EP/K022938/1, NSF, and AFOSR MURI program.

References

1. I.I. Ryabtsev et al., J. Phys. B **38**, S421 (2005).
2. M. Saffman et al., Rev. Mod. Phys. **82**, 2313 (2010).
3. D. Comparat et al., J. Opt. Soc. Am. B, **27**, p.A208, 2010.
4. I.I. Ryabtsev et al., Phys. Rev. Lett. **104**, 073003 (2010).
5. I.I. Ryabtsev et al., Phys. Rev. A **82**, 053409 (2010).
6. D.B. Tretyakov et al., JETP **114**, 14 (2012).
7. V.M. Entin et al., JETP (2013), in press.
8. I.I. Beterov et al., Phys. Rev. A **84**, 023413 (2011).
9. I.I. Beterov et al., arXiv:1212.1138 [quant-ph] (2013).
10. I.I. Ryabtsev et al., Phys. Rev. A **84**, 053409 (2011).

Two-dimensional Fermi and Bose gases with tunable interactions

Andrey Turlapov, Kirill Martiyanov, Vasiliy Makhalov

Institute of Applied Physics, Russian Academy of Sciences, ul. Ulyanova 46, Nizhniy Novgorod, 603000, Russia
E-mail: turlapov@appl.sci-nnov.ru

2D many-body quantum systems show interesting physics and are technologically important. In 2D the phenomena of superfluidity and Bose condensation become clearly separated [1]. High-temperature superconductivity is attributed to 2D structure of the materials [2]. Semiconductor and oxide interfaces containing 2D electron gas are important for modern and prospective electronics [3, 4].

We realize and study a general problem of quantum physics in reduced dimensions: quasi-2D Fermi gas with widely tunable s-wave interactions nearly in a ground state. An ultracold gas of fermionic atoms is used in experiment. Both in 3D and 2D, by gradually increasing pairwise interaction one may smoothly convert a gas of fermions into a gas of nearly point-like bosons, which are tightly bound pairs of the original fermions. The innumerable set of states corresponding to the respective values of the interaction is referred to as the "BCS-BEC crossover" [5] because the states on the fermionic asymptote are described within the Bardeen-Cooper-Schrieffer (BCS) theory of superfluidity/superconductivity while on the other asymptote, the bosons form a Bose-Einstein condensate (BEC), at least in a 3D system. Generally, the BCS-BEC crossover has been predicted for excitons in solids [6] and for quarks [7], however, the only system, where the collective state has been experimentally tuned between the Fermi and Bose asymptotes is a 3D gas of ultracold fermionic atoms [8]. Quantitative measurements on the ultracold gases have significantly stimulated development of many-body quantum theory [5], especially in the challenging regime of strong interactions which lies between the BCS and BEC asymptotes.

The reduction of spatial dimensionality from 3D to 2D changes the BCS-BEC crossover problem significantly. The difference is seen in the case of s-wave inter-actions considered here. From the perspective of two-body interactions, dimensionality two means that any purely attractive potential has a bound state. As a consequence, unlike in 3D, the necessary and sufficient condition of pairing in a zero-temperature many-body system is the existence of a two-body bound state in vacuum [9]. In regards to many-body properties, long-wavelength thermal fluctuations prohibit formation of a BEC in a uniform system [10]. Also mean-field description of many-body properties is limited. In 3D a mean-field approach qualitatively correctly models the BCS-BEC crossover (Fig. 5 of [5]), while in 2D similar model is qualitatively incorrect predicting interaction-independent equation of state at zero temperature [11]. The regime of strong s-wave interactions may be relevant to high-temperature superconductors. While the symmetry of the superconducting phase in the cuprates is d-wave [2], the s-wave symmetry has recently been detected in the pseudogap phase [12].

In experiment, the quasi-2D tunable Fermi system is a gas of lithium-6 atoms that is cooled and confined in a series of planar traps as shown in Fig. 1. Motion along one direction is "frozen" by tight confinement. The s-wave interactions between atoms in two different "spin" states are tuned by means of the Fano–Feshbach resonance. The experiment covers physically different regimes: weakly- and strongly-attractive Fermi gases and a Bose gas of tightly-bound

pairs of fermions. The system is characterized quantitatively by local in situ measurements of the pressure and density.

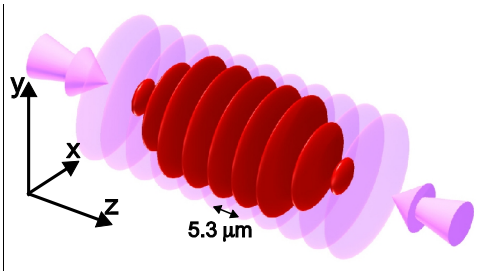

Fig. 1. Trapping ultracold atoms in antinodes of a standing optical wave. The isolated clouds of atoms shown in dark red, the standing-wave intensity shown in light purple.

In the Fermi regime of weak interactions, the pressure is systematically above a Fermi-liquid-theory prediction [13] probably due to mesoscopic effects. In the opposite Bose regime, the system is found to be a BEC of molecules despite low dimensionality. The pressure values agree with a mean-filed theory of point-like bosons in an unexpectedly wide range. In the strongly-interacting regime, the pressure is in some disagreement with the values obtained by Monte Carlo simulation within a strictly two-dimensional model [11]. It is possible that strong interactions break dimensionality two by populating excited states of motion along the tightly-confined direction. Interestingly, most of cuprate superconductors are not purely 2D systems either because some interlayer hopping of electrons is possible [2].

Generally, for a 2D Fermi system, calculations of thermodynamic quantities are more sensitive to the choice of model than those in 3D. Reported measurements, therefore, may serve for sensitive testing of theoretical methods applicable across different disciplines including nuclear and condensed matter physics as well as for finding out whether purely 2D models are applicable to strongly interacting systems.

References

1. V. L. Berezinskii, *Sov. Phys. JETP* **34**, 610 (1972).
2. V. M. Loktev, R. M. Quick, and S. G. Sharapov, *Phys. Rep.* **349**, 1 (2011).
3. T. Ando, A. B. Fowler, and F. Stern, *Rev. Mod. Phys.* **54**, 437 (1982).
4. J. Mannhart, D. H. A. Blank, H. Y. Hwang, A. J. Millis, and J.-M. Triscone, *MRS Bull.* **33**, 1027 (2008).
5. S. Giorgini, L. P. Pitaevskii, and S. Stringari, *Rev. Mod. Phys.* **80**, 1215 (2008).
6. L. V. Keldysh and A. N. Kozlov, *Sov. Phys. JETP* **27**, 521 (1968).
7. B. O. Kerbikov, *Phys. Atom. Nucl.* **65**, 1918 (2002); arXiv:hep-ph/0204209.
8. M. Bartenstein, A. Altmeyer, S. Riedl, S. Jochim, C. Chin, J. H. Denschlag, and R. Grimm, *Phys. Rev. Lett.* **92**, 120401 (2004).
9. M. Randeria, J.-M. Duan, and L.-Y. Shieh, *Phys. Rev. Lett.* **62**, 981 (1989).
10. I. Bloch, J. Dalibard, and W. Zwerger, *Rev. Mod. Phys.* **80**, 885 (2008).
11. G. Bertaina and S. Giorgini, *Phys. Rev. Lett.* **106**, 110403 (2011).
12. S. Sakai, S. Blanc, M. Civelli, Y. Gallais, M. Cazayous, M.-A. Measson, J. S.Wen, Z. J. Xu, G. D. Gu, G. Sangiovanni, Y. Motome, K. Held, A. Sacuto, A. Georges, and M. Imada, "Exploring the dark side of cuprate superconductors: s-wave symmetry of the pseudogap," arXiv:cond-mat/1207.5070 (2012).
13. P. Bloom, *Phys. Rev. B* **12**, 125 (1975).

Surface interactions in atom interferometry

T. Taillandier-Loize[1], M. Hamamda[1], G. Dutier[1], F. Perales[1], M.-P. Gorza[1], C. Mainos[1], J. Baudon[1], M. Boustimi[2], V. Bocvarski[3], M. Ducloy[1]

[1] *Laboratoire de Physique des Lasers, UMR 7538 du CNRS et de l'Université Paris 13, 99 Av. J.B. Clément, 93430 Villetaneuse, France*

[2] *Department of Physics, Umm Al-Qura University, Mekkah, Saudi Arabia*

[3] *Institute of Physics - Pregrevica 118, 11080-Belgrade, Serbia*
E-mail:martial.ducloy@univ-paris13.fr

We review the effects of surface interactions in matter-wave interferometry using material nano-gratings: influence of surface-induced van der Waals phase on the diffraction pattern, internal-state mixing by anisotropic (quadrupolar) van der Waals interaction with the correlated angular deviation of the atom wave. Recent advances using laser-cooled rare gas metastable beams will be described.

Single qubit single mode laser - an ultimate type of micro lasers

S.Ya. Kilin[1], A. B. Mikhalychev[1]

[1] *B.I. Stepanov Institute of Physics, National Academy of Sciences of Belarus, 220072, Nezavisimosti ave. 68, Minsk, Belarus*
E-mail: sergei_kilin@yahoo.com

The single-qubit-single-mode microlaser is of a great importance as a limiting case of lasers. This intrinsically quantum system with a number of properties strongly different from ordinary lasers requires specific cavity quantum electrodynamics methods for its description [1]. Rabi splitting [2], collapse-and-revival phenomenon [3] and photon blockade effect [4] are a few examples of quantum effects observed in the system.

Contrary to conventional lasers, microlasers (and especially single-qubit lasers) are known to be sources of non-classical light [5, 6]. It has already been shown, that single-atom laser, considered within the scope of strong-coupling $|2\rangle$ regime, can produce special kind of nonlinear coherent states (NCSs), namely Mittag-Leffler coherent states [7]. In the general case of arbitrary values of coupling strength and other system parameters, the stationary state of an incoherently pumped single-qubit laser is NCS, being the phase-averaged eigenstate of deformed annihilation operator of a specific form [8].

We consider the following model of a single-qubit laser. A 2-level system with the ground state $|1\rangle$ and excited state $|2\rangle$ interacts with a resonance field mode with coupling constant *g*. The qubit is pumped incoherently with mean rate R_{12}. Decay of the resonance field mode and decay and dephasing of the qubit with rates κ, R_{21} and Γ correspondingly are taken into account. The master equation for the density matrix, reduced over the states of the surrounding, in interaction representation has the form:

$$\dot{\rho} = -\frac{i}{\hbar}[H,\rho] + 2\kappa L_a\rho + R_{12}L_{\sigma_+}\rho + R_{21}L_{\sigma_-}\rho + \Gamma L_{\sigma_z}\rho,$$

where operators σ_+, σ_-, σ_z and $a^\dagger$, a describe dynamics of atom and field correspondingly, and relaxation is described by Lindblad operators: $2L_X\rho = 2X\rho X^\dagger - \rho X^\dagger X - X^\dagger X\rho$. The atom-field interaction is described by Jaynes-Cummings Hamiltonian $H = \hbar g(a\sigma_+ + a^\dagger\sigma_-)$.

The state of the system is completely characterized by operators $\rho_{11} = \langle 1|\rho|1\rangle$, $\rho_{22} = \langle 2|\rho|2\rangle$ and $u = i\langle 1|\rho a^\dagger|2\rangle$. In the stationary state the operators are diagonal in Fock states basis and can be expressed on the basis of eigenvalues of a deformed annihilation operators. For example, one can show that the conditional density matrix ρ_{11} satisfies the following equation: $A_{F_{11}}\rho_{11}A_{F_{11}}^\dagger = a_0^2\rho_{11}$, where $a_0^2 = R_{12}/(4\kappa)$ is normalized pump rate; $A_F = \sqrt{F(aa^\dagger)}\,a$ is deformed annihilation operator [12, 13] with the properties completely determined by discrete function *F*(*n*) (deformation function). For the ground-state conditional density operator this function equals $F_{11}(n) = (1/2) + \{(1/2) + (\nu_0/n)\}\{1 + d(n)\}$, where $\nu_0 = (R_{21} - 2\kappa)/(4\kappa)$ describes atomic loss excess over field loss and *d(n)* is a function, characterizing deviation of the density matrix from strong-coupling regime (see Ref.[8] for details). Eigenstates of deformed annihilation operators are known as nonlinear coherent states [9, 10] and represent a particular case of generalized coherent states (see e.g. [11]). In the special case $\nu_0 = 0$, $d(n) = 0$ eigenstates of operator *A* are ordinary coherent states. For $\nu_0 \neq 0$, $d(n) = 0$ (strong-coupling regime) the eigenstatates are Mittag-Leffler states [7]. In the general case the eigenstate has the following representation in terms of Fock states:

$$\left|a_0;F\right\rangle = const\cdot\sum_{n=0}^{\infty}\left|n\right\rangle\frac{a_0^n}{\sqrt{n!}}\prod_{m=1}^{n}\frac{1}{\sqrt{F(m)}}.$$

The process of reaching this stationary state can be investigated on the basis of *s*-parametrized phase space functions [12, 13] $P(\alpha; s)$. Being prepared in a coherent state $\left|\alpha_0\right\rangle$, the system passes the following regimes of dynamics: coherent, incoherent regimes and stationary state approaching (Fig.1 a,b,c). In the first two regimes analog of phase bistability, predicted for a single-qubit laser with coherent driving [14], manifests itself in presence of 2 distinct maxima in quasi-probability distribution (see Fig. 1 a,b).

Non-classical properties of the states, reached during the system evolution, can be characterized by non-classicality depth [15] – the minimal value s_0 for which the function $P(\alpha;s)$ becomes negative. Fig.1d shows that the state remains non-classical during all the stages of the evolution (s_0 for all $t>0$).

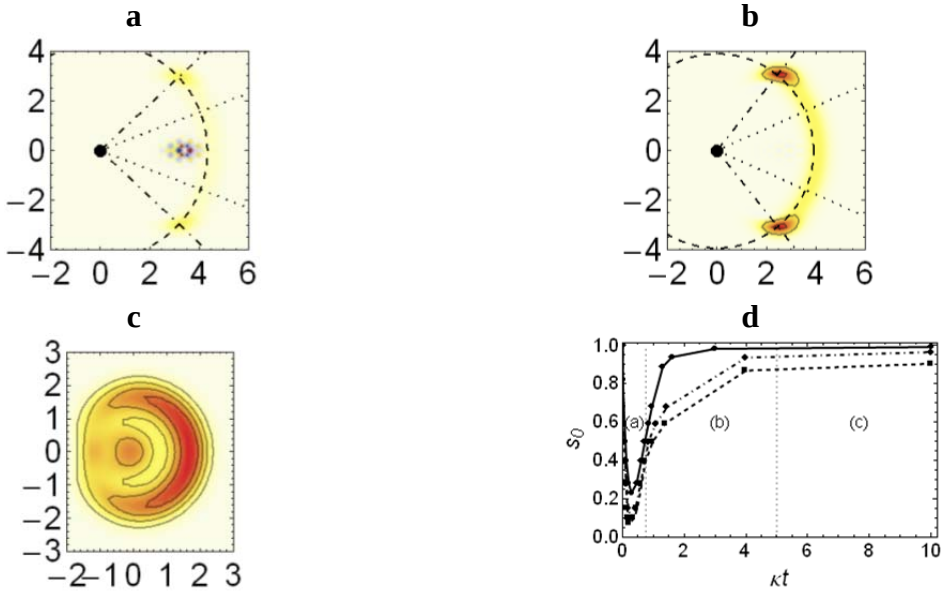

Fig.1. Dynamics of a single-qubit-single mode laser, initially prepared in a coherent state of the mode and the ground state of the qubit. **a, b, c** – conditional phase space quasi-distribution $P_{11}(\alpha;s)$, corresponding to the ground state of qubit, in coherent, incoherent stages of evolution and for approaching stationary state correspondingly. For coherent regime both bistability (presence of two maxima) and quantum interference (oscillations between the maxima) are present. For incoherent regime only bistability is preserved. **d** - Dynamics of non-classicality order: $a_0^2=1$, $\nu_0=1$ (solid line), $a_0^2=1$, $\nu_0=-0.3$ (dashed line), $a_0^2=0.1$, $\nu_0=-0.3$ (dot-dashed line). Regimes of dynamics: (a) – coherent, (b) – incoherent, (c) – approaching stationary state.

References

1. P. R. Berman, *Cavity Quantum Electrodynamics*, Academic Press, 1994.
2. R. J. Thompson, G. Rempe, and H. J. Kimble, *Phys. Rev. Lett.* **68**, 1132 (1992).
3. J. H. Eberly, N. B. Narozhny, and J. J. Sanchez-Mondragon, *Phys. Rev. Lett.* **44**, 1323 (1980).
4. K. M. Birnbaum, A. Boca, R. Miller, et al., *Nature* **436**, 87 (2005).
5. J. McKeever, A. Boca, A. D. Boozer, et al., *Science* **303**, 1992 (2004).
6. T. Wilk, S. C. Webster, A. Kuhn, et al., *Science* **317**, 488 (2007).
7. S.Ya. Kilin and T. B. Karlovich, *JETP* **95**, 805 (2002).
8. S. Ya. Kilin and A. B. Mikhalychev, *Phys. Rev. A* **85**, 063817 (2012).
9. R. L. de Matos Filho and W. Vogel, *Phys. Rev. A* **54**, 4560 (1996).
10. V. I. Man'ko, G. Marmo, E. C. G. Sudarshan, and F. Zaccaria, *Phys. Scr.* **55**, 528 (1997).
11. A. Perelomov, *Generalized Coherent States and their Applications,* Springer-Verlag, 1986.
12. K. E. Cahill and R. J. Glauber, *Phys. Rev.* **177**, 1857 (1969).
13. G.S. Agarwal and E. Wolf, *Phys. Lett. A* **26**, 485 (1968).
14. S.Kilin, T.Krinitskaya, *JOSA B* **8**, 2289 (1991).
15. N. Lutkenhaus and S. M. Barnett, *Phys. Rev. A* **51**, 3340 (1995).

Quantum logic for control and manipulation of molecular ions

D. N. Matsukevich

[1] *Centre of Quantum Technologies and Department of Physics, National University of Singapore, 3 Science Dr. 2, Singapore, 117543*
E-mail: phymd@nus.edu.sg

Due to their rich level structure, molecules are well-suited for probing time variation of fundamental constants, precisely measuring parity violation, and time-reversal non-invariance effects, studying quantum mechanical aspects of chemical reactions, and implementing scalable quantum information processing architectures [1, 2, 3]. Molecular ions are particularly attractive for these applications. Because of near-perfect isolation from the environment they have long storage and coherence times which are required to achieve high measurement precision and reduce systematic errors.

However, the control of molecular quantum states remains a challenge. Traditional methods of state detection for neutral atoms and atomic ions are difficult to apply in the case of molecules. It is hard to find a nearly closed cycling transition, which limits the applicability of standard fluorescence detection methods. Other methods such as resonance-enhanced multiphoton dissociation are destructive in nature.

Here, based on quantum logic technique [4], we propose a method for preparation, manipulation, and detection of quantum states of single molecular ions and discuss our progress towards its experimental implementation [5]. The proposed experimental setup is shown in Figure 1. We confine a diatomic molecular ion together with an atomic ion in a standard rf-Paul trap. Due to Coulomb interaction, the atomic and molecular ions share common modes of motion. The motional state of the ions can be coherently coupled to the internal state of atom or molecule by driving stimulated Raman transition between the states of atomic or molecular ions.

In order to drive Raman transition in our scheme, two laser beams generated by a modelocked pulsed laser with a repetition rate f_{rep} are offset by frequency ν_{AO} with acousto-optical modulators and focused on the ions from two different directions. To address two quantum states separated by energy difference $\Delta\omega$, the repetition rate f_{rep} and offset frequency ν_{AO} should satisfy the resonance condition $\Delta\omega = M f_{rep} \pm \nu_{AO}$, where the integer number M is the comb index. Adjustment of the repetition rate and offset frequency allows us to address any pair

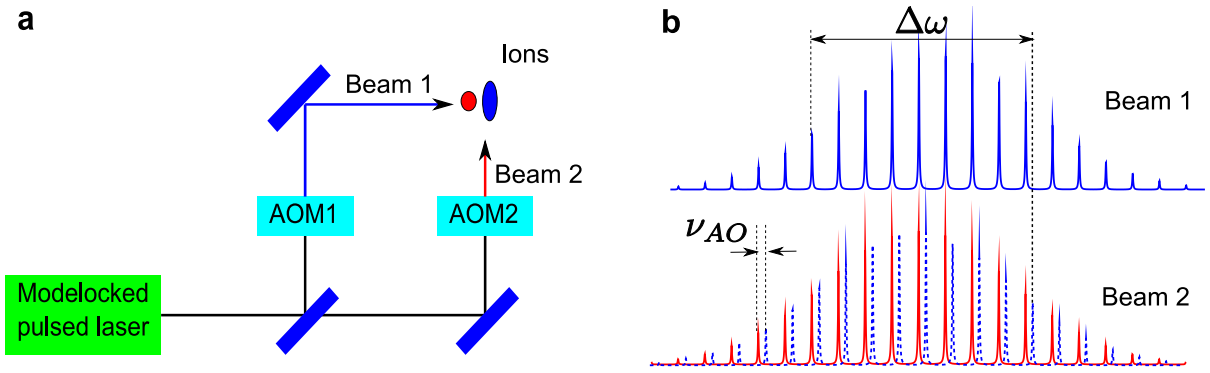

Fig. 1. The proposed experimental setup. (a) Light emitted by a modelocked pulsed laser with repetition rate f_{rep} is split into two beams, sent through acousto-optical modulators to offset the relative frequency between two beams by ν_{AO} and incident upon the atomic and molecular ions from two different directions. (b) Spectrum of the frequency combs. If resonance conditions are satisfied the setup can drive a stimulated Raman transition between a pair of energy levels $\Delta\omega$ apart.

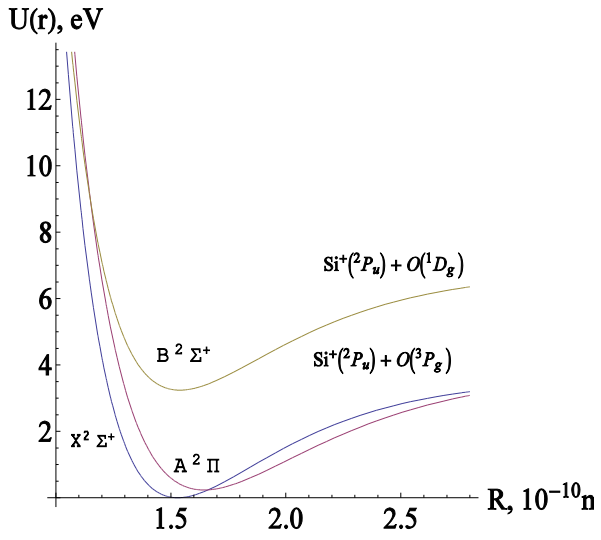

Fig. 2. Potential energy curves for low lying states of SiO^+ molecule

of energy levels within the bandwidth of the pulsed laser [6].

To manipulate the motion of the ions we detune the spectral beat note between the two laser beams from the two photon resonance between molecular states $|m_1\rangle$ and $|m_2\rangle$ by ω_t, the frequency of a common motional mode. The change in the molecular quantum state in this case is accompanied by a simultaneous change of the motional state of the ions.

If the atomic and molecular ions were initially in a ground state of motion, driving a Raman transition that couples the state of the molecular ion $|m_1\rangle$ to a collective motional mode of the ions generates a phonon if the molecular ion was in the state $|m_1\rangle$, and does not change the motion if the molecular ion was in any other state. The phonon can be detected later by coupling the motion of the ions to the spin of an atomic ion, followed by the atomic ion state detection using the standard fluorescence technique. Similar techniques can also be used to prepare the molecule in the lowest rotational states [5].

We are working on implementation of this scheme with the SiO^+ molecular ion and Yb^+ atomic ion. The spectral properties of SiO^+ are known [5]. The potential energy curves for the low lying energy levels of a SiO^+ are shown on Fig. 2. The wavelength for the $A^2\ \Pi\ (v=0) \rightarrow B^2\Sigma^+\ (v=0)$ transition is about 414 nm, and the $X^2\ \Sigma^+\ (v=0) \rightarrow B^2\Sigma^+\ (v=0)$ transition wavelength is near 383 nm, close to the 370 nm transition of atomic ion. Nearly diagonal Franck-Condon factors for the $X^2\ \Sigma^+ \rightarrow B^2\Sigma^+$ transition in SiO^+ maximize the two-photon Rabi frequency and minimize the leakage to the different vibration states due to off resonance excitation of the $B^2\Sigma^+$ state. The absence of hyperfine structure for the most abundant molecule $Si_{28}O_{16}$ simplifies the energy level structure.

The SiO^+ ions are produced in our setup using the laser ablation technique, from a silicon monooxide target and trapped in a standard rf-Paul trap with a radial trap frequency for Yb^+ ions about 1.2 MHz. The molecular ions are sympathetically cooled using co-trapped Yb^+ ions, and the presence of a molecular ion is confirmed by the trap frequency measurements. The state of Yb^+ ion is detected using the standard resonance fluorescence method with the fidelity greater than 98%. We are currently setting up a modelocked pulsed lasers to drive a Raman transitions, do a sideband cooling and optically pumping of SiO^+ rotational states [5].

The quantum logic scheme presented above is not limited to SiO^+ and can be applied to a wide range of molecular ions and can find its applications in precision measurements, quantum information, and quantum chemistry.

References

1. L. D. Carr. *et. al. New J. Phys.* **14**, 023028 (2012).
2. C. Chin, V.V. Flambaum, and M.G. Kozlov, *New J. Phys.* **11**, 055048 (2009).
3. S. Willitsch, M. T. Bell, A. D. Gingell, and T. P. Softley, *Phys. Chem. Chem. Phys.* 10, 7200 (2008).
4. P. O. Schmidt, *et. al,. Science* 309, 749-752 (2005).
5. S. Ding, and D. N. Matsukevich, *New J. Phys.* **14**, 023028 (2012).
6. D. Hayes*, et. al*, *Phys. Rev. Lett.* **104**, 140501 (2010).

Continuous Variable Entanglement at optical frequency by a type-II cw OPO: a survey on experimental characterization methods

D. Buono[1], G. Nocerino[2], S. Solimeno[2], and A. Porzio[3]

[2] *Dipartimento di Ingegneria Industriale, Università degli Studi di Salerno, Via Ponte don Melillo, I-84084 Fisciano (SA) Italy*

[2] *CNR –SPIN, Compl. Univ. Monte Sant'Angelo, via Cintia, 80126 Napoli, Italy*

[3] *Dipartimento di Fisica,Università "Federico II" di Napoli, Compl. Univ. Monte Sant'Angelo, via Cintia, 80126 Napoli, Italy*

E-mail: alberto.porzio@spin.cnr.it

The quantum characterization of an entangled quantum state has a fundamental interest on its own. Moreover, it is a basic tool for the design of realistic quantum information protocol. In particular, the full knowledge, at the quantum level, of optical quantum systems paves the way to the faithful description of real communication channels and to precise tests of the foundations of quantum mechanics [1–3]. Any quantum property, as *entanglement* [4-5], is very fragile and its survival over long distances and times is subtly interconnected to the amount of noise coupling into the physical system through its unavoidable interaction with the classical environment. The conceptual consequences of entanglement are somehow subtle yet deeply affect many aspects of modern physics as the interaction between reality and observer [6], the actual limit for defining metrology standards [7], and the limit to communication security [8]. The optical realization of such an intriguing quantum feature has gained, in the past decades, a central role for realizing complex quantum communication protocols [9].

Here we focus on the bipartite bright optical entangled states generated by parametric processes in a type-II optical parametric oscillators (OPOs) below threshold [10-15]. These are Gaussian states, *i.e.* their Wigner function is Gaussian and so are their field's quadrature marginal distributions. They play a crucial role in quantum information processing with continuous variables [16-19]. Indeed, using single- and two-mode Gaussian states, linear optical circuits, and Gaussian operations, like homodyne detection, several quantum information protocols have been implemented including teleportation, dense coding, and quantum cloning [9]. Being Gaussian these states are completely characterized by their covariance matrix (CM) in phase space [15,20].

Once the CM is experimentally accessed, one may retrieve all the relevant state properties, e.g., energy, purity, entropy, entanglement, and mutual information. Moreover, analysing the state in different *environmental* conditions represents a tool for analysing its behaviour under decoherence.

By interacting with the external world, a pure quantum state decoheres into a mixture [21] and its quantumness, if not completely death [22], needs to be restored or re-enhanced by suitable protocols [23]. The birth of an entangled state happens whenever a genuine quantum correlation, i.e., without a classical analogue, is set between two distinguishable quantum systems. This implies that the system wave function cannot factorize into the product of wave functions of the single subsystems. While this definition is almost unique, entanglement marks itself into different properties of the quantum state of the whole system and can be seen under different perspectives [24].

For this reason, since the first experimental demonstration of entanglement [25], several criteria and quantities have been introduced for analyzing *entanglement* [26,27]. Furthermore, the definition of an entangled state is conceptually connected to pure states [28]. At the same time, in the mixed state case the density matrix formalism is required and the quantum properties of the system are less immediate to find. For this reason, quantifying entanglement for mixed states is an issue still under discussion.

Moreover, the states we can prepare and manipulate in the laboratory are not pure but mixed, so that experimental entanglement tests are better described in terms of density matrices rather than wave functions. In optics the most common process leading to decoherence is the phase-insensitive loss of photons through diffusion and absorption mechanisms.

After giving a glance on some theoretical aspects we will introduce the experimental principle for a full characterization of such states and investigate the behaviour of the CV entangled system in the strong decoherence regime (up to 99% of loss). Specifically, we will discuss state purity, mutual information, quantum discord, and three different entanglement criteria: Peres-Horodechi-Simon [29,30], Duan [31], and EPR-Reid [26].

Interestingly, we found that some quantum features of these states survive and are still experimentally detectable even for very high loss (up to 99%) [32].

References

1. M. G. A. Paris and J. Řeháček, eds., *Quantum State Estimation*, Vol. 649 of Lecture Notes in Physics (Springer, 2004);
2. D.-G. Welsch, W. Vogle, and T. Opatrný, "Homodyne detection and quantum state reconstruction," in *Progress in Optics*, Vol. 39, E. Wolf, eds., pp. 63–211 (Elsevier, 1999);
3. A. I. Lvovsky and M. G. Raymer, Rev. Mod. Phys. **81**, 299 (2009);
4. E. Schrödinger, Proc. Cambridge Philos. Soc. **31**, 555 (1935);
5. A. Einstein, B. Podolsky, and N. Rosen, Phys. Rev. **47**, 777 (1935);
6. J. A. Wheeler, and W. H. Zurek, *Quantum Theory and Measurement* (Princeton University Press, Princeton, NJ, 1984); A. A. Clerk, M. H. Devoret, S. M. Girvin, F. Marquardt, and R. J. Schoelkopf, Rev. Mod. Phys. **82**, 1155 (2010);
7. V. Giovannetti, S. Lloyd, and L. Maccone, Phys. Rev. Lett. **96:**010401 (2006); Nat. Photonics **5**, 222 (2011);
8. V. Scarani, H. Bechmann-Pasquinucci, N. J. Cerf, M. Dušek, N. Lütkenhaus, and M. Peev, Rev. Mod. Phys. **81**, 1301 (2009);
9. S. L. Braunstein and P. van Loock, Rev. Mod. Phys. **77**, 513 (2005); C. H. Bennet and P. W. Shor, IEEE Trans. Inf. Theory **44**, 2724 (1998);
10. J. Laurat, G. Keller, J. A. Oliveira-Huguenin, C. Fabre, T. Coudreau, A. Serafini, G. Adesso, and F. Illuminati, J. Opt. B **7**, S577 (2005);
11. A. S. Villar, L. S. Cruz, K. N. Cassemiro, M. Martinelli, and P. Nussenzveig, Phys. Rev. Lett. **95**, 243603 (2005);
12. X. Su, A.g Tan, X. Jia, Q. Pan, C. Xie, and K. Peng, Opt. Lett. **31**, 1133 (2006);
13. J. Jing, S. Feng, R. Bloomer, and O. Pfister, Phys. Rev. A **74**, 041804(R) (2006);
14. G. Keller, V. D'Auria, N. Treps, T. Coudreau, J. Laurat, and C. Fabre, Opt. Express **16**, 9351 (2008);
15. V. D'Auria, S. Fornaro, A. Porzio, S. Solimeno, S. Olivares, and M. G. A. Paris, Phys. Rev. Lett. **102**, 020502 (2009); D. Buono, G. Nocerino, V. D'Auria, A. Porzio, S. Olivares, and M. G. A. Paris, J. Opt. Soc. Am. B **27**, A110 (2010);
16. J. Eisert and M. B. Plenio, Int. J. Quantum Inf. **1**, 479–506 (2003);
17. B.-G. Englert and K. Wodkiewicz, Int. J. Quantum Inf. **1**, 153–188 (2003);
18. A. Ferraro, S. Olivares, and M. G. A. Paris, *Gaussian States in Quantum Information* (Bibliopolis, 2005);
19. F. Dell'Anno, S. De Siena, and F. Illuminati, Phys. Rep. **428**, 53–168 (2006);
20. V. D'Auria, A. Porzio, S. Solimeno, S. Olivares, and M. G. A. Paris, J. Opt. B **7**, S750 (2005); A. Porzio, V. D'Auria, S. Solimeno, S. Olivares, and M. G. A. Paris, Int. J. Quantum Inf. **5**, 63 (2007);
21. A. Serafini, F. Illuminati, M. G. A. Paris, and S. De Siena, Phys. Rev. A **69**, 022318 (2004); A. Serafini, M. G. A. Paris, F. Illuminati, and S. De Siena, J. Opt. B **7**, R19 (2005);
22. T. Yu and J. H. Eberly, Science **323**, 598 (2009);
23. P. W. Shor, Phys. Rev. A **52**, 2493 (1995);
24. H. M.Wiseman, S. J. Jones, and A. C. Doherty, Phys. Rev. Lett. **98**, 140402 (2007);
25. A. Aspect, P. Grangier, and G. Roger, Phys. Rev. Lett. **47**, 460 (1981);
26. M. D. Reid, Phys. Rev. A **40**, 913 (1989);
27. E. G. Cavalcanti, S. J. Jones, H. M. Wiseman, and M. D. Reid, Phys. Rev. A **80**, 032112 (2009);
28. D. Cavalcanti, F. G. S. L. Brandão, and M. O. Terra Cunha, Phys. Rev. A **72**, 040303(R) (2005);
29. A. Peres, Phys. Rev. Lett. **77**, 1413 (1996); P. Horodecki, Phys. Lett. A **232**, 333 (1997);
30. R. Simon, Phys. Rev. Lett. **84**, 2726 (2000);
31. L.-M. Duan, G. Giedke, J. I. Cirac, and P. Zoller, Phys. Rev. Lett. **84**, 2722 (2000);
32. D. Buono, G. Nocerino, A. Porzio, and S. Solimeno, Phys. Rev. A **86**, 042308 (2012); G Nocerino, D Buono, A Porzio, and S Solimeno, Phys. Scr. **T153** 014049 (2013).

Exploring collective effects for precision measurement

J.G. Bohnet, Z. Chen, J.M. Weiner, K.C. Cox, M.A. Norcia, D. Meiser,

M.J. Holland, J.K. Thompson

JILA and Department of Physics, University of Colorado at Boulder, and
National Institute of Standards and Technology, 440 UCB, Boulder, CO 80309, U.S.A.
E-mail: jkt@jila.colorado.edu

A paradigm of precision measurements is to utilize many independent atoms to enhance measurement precision. Cooling and trapping techniques in atomic physics enable the generation of large ensembles of atoms with rich applications for studying correlated many-body physics. Is it also possible to exploit atom-atom correlations and entanglement to advance the field of precision measurement beyond the independent-atom paradigm? We have explored this question along two fronts using 87Rb atoms trapped inside of a low finesse F=700 optical cavity.

We have demonstrated a superradiant or maser oscillator in which the atoms collectively store the coherence of the oscillator, such that lasing is observed even when the average number of photons inside the laser cavity is < 1 [1]. This physics test-bed system may point the way to ultra-stable optical lasers with linewidths below 1 mHz [2], and may circumvent the problem of thermal and technical mirror vibrations that limit state-of-the-art laser linewidths [1,2]. Other work in this area includes the demonstration of a hybrid magnetometer that can be switched on-demand between active and passive sensing modes [3], connecting the Schawlow-Townes laser linewidth to the knowledge gained about the atoms inside the laser [4], and exploring the amplitude stability of the laser [5].

Secondly, we have created spin-squeezed states of nearly one million atoms using collective quantum non-demolition measurements (QND) [6]. These entangled states surpass the standard quantum limit on phase estimation uncertainty that sets a fundamental limit on the the precision of almost all measurements in atomic systems. The essence of the QND approach is to measure the quantum noise in the number of atoms in the quantum states spin up and spin down and then simply subtract the measured value from later measurements [6-10], for instance at the end of a Ramsey measurement. The optical QND approach we employ prepares a squeezed state in ~100 microseconds, after which the atoms can evolve without perturbations from the interaction used to generate the squeezing. Similar techniques may be applied in the future to optical lattice clocks to enhance their fundamental precision, bandwidth, and/or accuracy [11].

References

1. J. G. Bohnet et al, *Nature* **484**, 78-81 (2012).
2. D. Meiser et al, *Physical Review Letters*, **102**, 063601 (2009).
3. J. M. Weiner et al, *Applied Physics Letters* **101**, 261107 (2012).
4. J. G. Bohnet et al, arxiv:1208.1710v2 .
5. J. G. Bohnet et al, *Physical Review Letters* **109**, 253602 (2012).
6. Z. Chen et al, *Physical Review Letters* **106**, 133601 (2011).
7. Z. Chen et al, arxiv:1211.0723 .
8. J. Appel et al, *Proc. Natl. Acad. Sci. U.S.A*, **106**, 10960 (2009).
9. M.H. Schleier-Smith, I.D. Leroux, V. Vuletic, *Physical Review Letters* **104**, 073604 (2010).
10. R.J. Sewell et al, *Physical Review Letters* **109**, 253605 (2012).
11. J. Lodewyck, P.G. Westergaard, P. Lemonde, *Physical Review A* **79**, 061401R (2009).

Quantum optics of atoms near plasmonic nanostructures

V.N. Zadkov

M.V. Lomonosov Moscow State University, Moscow, Russia

High-power MHz femtosecond laser sources coming soon

A. Apolonski

Max-Planck-Institut für Quantenoptik, Hans-Kopfermann-Str. 1, D-85748 Garching, Germany
Ludwig-Maximilians-Universität München, Fakultät für Physik, Am Coulombwall 1,
D-85748 Garching, Germany
Institute of Automation and Electrometry, Siberian Branch of Academy of Sciences, 630090 Novosibirsk, Russia
E-mail: apolonskiy@lmu.de

High-power MHz femtosecond laser sources are of great interest to many groups who use femtosecond pulses for science and technology and why there is a tendency to push further the average power of femtosecond laser oscillators? The answer is pragmatic aiming to overcome two difficulties: a) any kind of nonlinear experiment with lasers has rather low yield leading to long acquisition time (days to weeks in case of coincidence spectroscopy). Current femtosecond lasers, especially lasers with the controlled carrier-envelope phase, can't be stable enough for such a long period of time. b) In supecontinuum generation, the initial power concentrated in a relatively narrow spectral interval of the laser radiation spreads up to several octaves drastically reducing thus the power per frequency comb teeth below the useful limit. In order to increase the experiment yield and energy per comb teeth, one can push either the pulse energy (i.e. number of photons per pulse) or the average power (number of photons per second). The former will unavoidably lead to the material damage under study. The latter will lead to higher yield provided that thermal effects are suppressed (or manageable).

In the presentation, 2 approaches of power- and energy-scalable femtosecond lasers will be discussed: thin-disk laser systems (oscillators and amplifiers) and femtosecond enhancement cavities. The latter is an empty resonant cavity pumped by a femtosecond laser. When all the necessary matching conditions are fulfilled, the pulse energy and average power inside such a cavity grow via a coherent build-up process and can be up to a factor of 10^3 higher than that of the pump laser. Regenerative amplifiers allow generating pulses at any repetition rates including the range not accessible for the laser oscillators, namely between kHz and MHz. These approaches demonstrate the average power of a femtosecond pulse train between 10 W (laser oscillator) and 100 kW (enhancement cavity). The question will be addressed whether the MW-level average power looks feasible in a short perspective.

Another important laser parameter is its central wavelength. By using multichannel difference generation and optical parametric amplification schemes, in combination with nonlinear processes in gases (generation of high harmonics, filamentation etc.), one can cover the whole range between xuv and midIR with the laser sources described above.

In general, one can formulate the vision of the universal laser source coming soon: a 100-W-level 100 MHz-to-100 kHz repetition rate system allowing to generate on demand femtosecond or even sub-fs pulses in the whole xuv-UV-vis-IR-midIR range.

Optical parametric amplification at critical wavelength degeneracy - a possible solution for multi-PW laser systems

Razvan Dabu

National Institute for Laser, Plasma and Radiation Physics,
Laser Department, Atomistilor Str. 409, PO Box MG-36, Bucharest 077125, Romania
Tel/Fax: 004021-4575066
E-mail: razvan.dabu@inflpr.ro

Optical parametric chirped pulse amplification (OPCPA) is one of the most powerful techniques for generating high-energy femtosecond laser pulses. Many efforts were devoted to get spectral-band amplification able to support sub-10-fs pulses. In the optical parametric amplification (OPA), broad gain bandwidths can be obtained if the wave-vectors mismatch, Δk, slowly increases when the signal frequency varies around the phase-matching (PM) condition. The wave-vectors mismatch is given by a Taylor series expansion

$$\Delta k = k_p(\omega_p) - k_s(\omega_{s0}) - k_i(\omega_{i0}) - \left(\frac{\partial k_s}{\partial \omega_s} - \frac{\partial k_i}{\partial \omega_i}\right)\Delta\omega - \frac{1}{2!}\left(\frac{\partial^2 k_s}{\partial \omega_s^2} + \frac{\partial^2 k_i}{\partial \omega_i^2}\right)(\Delta\omega)^2 -$$

$$-\frac{1}{3!}\left(\frac{\partial^3 k_s}{\partial \omega_s^3} - \frac{\partial^3 k_i}{\partial \omega_i^3}\right)(\Delta\omega)^3 - \frac{1}{4!}\left(\frac{\partial^4 k_s}{\partial \omega_s^4} + \frac{\partial^4 k_i}{\partial \omega_i^4}\right)(\Delta\omega)^4 \ldots = \Delta k^{(0)} + \Delta k^{(1)} + \Delta k^{(2)} + \Delta k^{(3)} + .\Delta k^{(4)} + \ldots$$

where k_p, k_s, k_i are the pump, signal, and idler wave-vectors, ω_p, ω_s, ω_i are the pump, signal, and idler frequencies, respectively; the PM condition is fulfilled at ω_{s0}, ω_{i0} signal and idler frequencies where zero-order term $\Delta k^{(0)} = 0$.

For a given pump wavelength, if both first and second order wave-vectors mismatch terms are simultaneously canceled, broad bandwidth (BB), in the range of one hundred nm, can be obtained by non-collinear optical parametric amplification (NOPA). Ultra-broad gain bandwidth, significantly broader compared to BB-NOPA, can be obtained around a central signal wavelength if, besides $\Delta k^{(1)}$and $\Delta k^{(2)}$, the $\Delta k^{(3)}$ term of Taylor series is canceled too. By solving the six-equations system comprising the energy conservation and all these PM conditions, the six variables involved in the OPA process (three wave frequencies and three internal angles) were determined: ω_p, ω_{s0}, ω_{i0}, θ – pump wave vector-optical axis angle, α – signal-pump wave vectors angle, β – signal-idler wave vectors angle. The equations system solution consists in a collinear phase matching ($\alpha = \beta = 0$) at degeneracy ($\omega_{s0} = \omega_{i0} = \omega_p/2$) at the critical wavelength (CWL), where the group velocity dispersion of the signal/idler is canceled [1].

By use of Sellmeier equations for refractive indexes of nonlinear crystals, under the approximation of plane waves, monochromatic pump wave, flat-top temporal pump profile, and negligible pump depletion, gain bandwidth (GB) calculations for type I OPA processes were performed. For all considered crystals (BBO, LBO, DKDP), the calculated GBs at CWL degeneracy (CWLD) were significantly larger than in case of optimized BB-NOPA. For high power OPCPA at CWLD, nonlinear crystals with the critical wavelength fitted to the emission wavelength of available high-energy green pump lasers (e.g., frequency doubled Nd:YAG at 532 nm, Nd:glass at 527 nm, Yb:YAG at 515 nm) would be of practical interest. For CWLD-OPCPA, when pumping by 515 nm and 527 nm wavelength lasers, very broad-bandwidth signal waves with ~ 1 μm central wavelength and nonlinear crystals with critical wavelengths of 1030 nm and 1054 nm are necessary. Very broad-bandwidth signal pulses can be obtained by spectral broadening techniques, for example, by ultra-broad band light generation in gas filled hollow

fibers [2] or in bulk crystals [3]. Large aperture KDP and DKDP crystals are considered like most appropriate media for generating fs multi-PW laser pulses by OPCPA. Refractive indexes of partially deuterated KDP (P-DKDP) crystals depend on the deuteration level [4]. In order to fit the CWL of P-DKDP crystals to SH wavelengths of Yb:YAG and Nd:glass pump lasers, deuteration levels of 40% and 58%, respectively, are required [1]. More than 500 nm gain bandwidths can be obtained by CWLD-OPCPA in P-DKDP crystals (figure 1), broad enough to amplify chirped pulses compressible to few-cycle pulse duration.

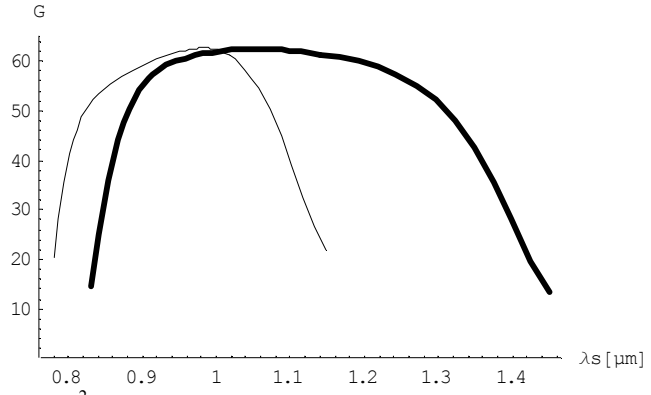

Fig. 1. Gain spectra for 64 GW/cm^2 pump intensity at 527 nm pump wavelength. Thick line, collinear CWLD-OPCPA in 58% P-DKDP crystal, 5-mm length. Thin line, optimized BB-NOPA in a similar length DKDP crystal.

The quasi-collinear pump-signal geometry can be used for signal-idler beams separation [5]. About 540 nm signal gain bandwidth was calculated for a quasi-collinear OPCPA process, phase-matched near CWLD in a 58% P-DKDP crystal (figure 2). Small modifications of the quasi-collinear interaction geometry allow the broadening of the signal wave gain bandwidth.

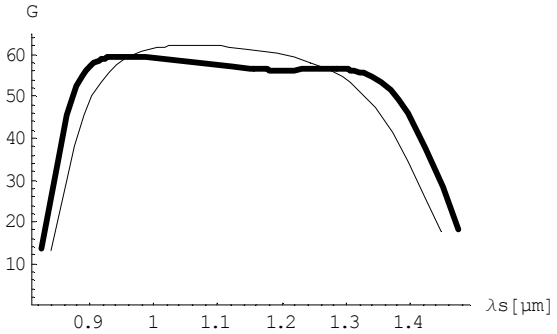

Fig. 2. Signal gain spectra for quasi-collinear OPA near CWD in a 58% P-DKDP crystal, 5-mm length, 64 GW/cm^2 pump intensity at 527 nm pump wavelength. Thin line, quasi-collinear phase-matching: θ = 673.6 mrad, α = 6.0 mrad, β = 11.8 mrad, external angle between signal and idler beams ~ 17 mrad. Thick line, quasi-collinear interaction with improved gain bandwidth: θ = 674 mrad, α = 5.4 mrad, β = 10.1 mrad, external angle between signal and idler beams ~ 15 mrad.

Ultra-broad bandwidth OPCPA (~ 440 nm) in 40% P-DKDP crystals, pumped by Yb:YAG ceramic lasers at 515 nm, was considered for the conceptual design of a Sub-Exa-Watts femtosecond laser system, Gekko EXA, Institute of Laser Engineering, Osaka, Japan [3].

References

1. R. Dabu, *Opt. Express* **18**, 11689 (2010).
2. I. Ahmad et al., *Appl. Phys. B*, **97** (3), 529 (2009).
3. J. Kawanaka and Gekko EXA design team, ICUIL Conference, Mamaia, Romania, September 17-21, 2012.
4. V.V. Lozhkarev et al., *Laser Physics* **15**, 1319 (2005).
5. R. Dabu, "Experimental Programme at ELI-NP" Workshop, Bucharest, October 3-5, 2012.

Ultrarelativistic physics with new generation of extreme light sources

A.V.Bashinov[1], A.A.Gonoskov [1,2], A.V.Kim [1,3], G.Mourou [3,4], A.M.Sergeev [1,3]

[1] *Institute of Applied Physics of Russian Academy of Sciences, 603950 Nizhny Novgorod, Russia*
[2] *Umea University, SE-90187 Umea, Sweden*
[3] *University of Nizhny Novgorod, 603950 Nizhny Novgorod, Russia*
[4] *IZEST, Ecole Polytechnique, 91120 Palaiseau, France*

The subexawatt laser facility announced in the mega-science research infrastructure XCELS [1] will open up unique opportunities for studying new phenomena at the interface of high-field and high-energy physics. In this report we will discussed, specifically, how new regimes of ultrarelativistic interactions can be used to produce extra-brilliant directed gamma ray bursts and to create attosecond light probes for studying nonlinear properties of vacuum.

Efficient conversion of the laser pulse energy to the energy of high brightness gamma rays at optical field interaction with electrons can be achieved at intensities exceeding 10^{24} W/cm^2. There are different approaches to the problem, and we will present two of the possible strategies. In the first case, a plasma layer is irradiated by two counter-propagating laser pulses with the co-rotating circular polarization of optical fields. Under the pondermotive pressure the electron distribution is compressed to an ultrathin sheet with a high density. Electrons in the sheet rotate at the frequency of the laser field, the angle between the velocity vector and the vector of the electric field being the same for all particles. As a result, the radiation of all electrons in the gamma range is synchronized and represents a type of a narrow light-house beam spinning in the plain of the compressed electron sheet. In the second case [2,3], synchronization of the electron motion can be due to effect of the radiation friction itself. If the radiation friction force becomes larger than the ponderomotive force in a standing electromagnetic wave, there appears a new attractor in the trajectory space of electrons and a regime of anomalous radiation trapping takes place. Electrons are trapped in the antinodes of the vector potential profile where the energy conversion from optics to gamma rays is maximal. This regime can be implemented in the converging dipole wave of 10+ PW total power, that grabs electrons to the focal area and drives them providing a narrow gamma ray beam in the axis direction of the dipole configuration.

Achieving extreme intensities in the XCELS project will provide optical field magnitude in excess of 10^{16} V/m, which is a few percent of the Sauter-Schwinger limit. In these conditions we can expect the appearance of a direct field-induced ionization of vacuum with production of electron-positron pairs in the geometry of the dipole focusing [4]. However, this fundamental effect of the nonlinear QED can be hidden by development of cascades with the participation of high-energy photons emitted by the particles born. To investigate the spatio-temporal properties of the vacuum in the "pure" form, a concept of superluminal attosecond probe has been formulated [5]. It involves a highly efficient conversion of femtosecond pulses of XCELS laser channels in attosecond pulses at a target with a special geometry, which provides energy concentration in a moving spot with dimensions of the order of 10 nm, i.e. an ideal probe to study nonlinear properties of vacuum.

The authors acknowledges the support of RAS under the program “Extreme light fields” and the Ministry of Education and Science (Agreement No. 11.G34.31.0011).

1. www.xcels.iapras.ru
2. A.V.Bashinov et al. Quantum Electronics 43(4),291 (2013)
3. A.Gonoskov et al. PRL (accepted)
4. A.Gonoskov et al. arXiv: 1302.4653 [hep-ph]
5. A.A.Gonoskov et al. Phys.Rev. E **84**, 046403 (2011)

Superintense femtosecond multichannel laser system with coherent beam combining

S.N. Bagayev, V.I. Trunov, E.V. Pestryakov, S.A. Frolov
V.E. Leschenko, A.E. Kokh, V.A. Vasiliev

Institute of Laser Physics SB RAS, Ac. Lavrentyev's prosp., 13/3,Novosibirsk, 630090, Russia
e-mail: trunov@laser.nsc.ru

At present time the various methods of realization the superpower laser beams operating at the single-shot [1] and repetition modes [2] are actively discussed. This article reviews the basic principles of creation of superintense laser developed by us, which can be formulated as follows:

- Multi channel few-cycle femtosecond pulses system (parametric amplification);
- Coherent combining of fields of channels;
- Phase-controlled generation and amplification of few-cycle pulses locked to reference standard (optical clock);
- Parametric amplification with picosecond pumping (high repetition rate of pulses);
- Precise time synchronization, based on reference standard (optical clock) between the picosecond and femtosecond oscillators.

Compared to laser amplifiers, parametric ones have an important advantage of almost complete absence of phase distortion caused by the thermal effects, if appropriate nonlinear optical crystals with low absorption coefficients for all of the interacting waves are chosen. Moreover, as the analysis shows [2], the parametric chirped pulse amplification does not introduce significant additional phase distortion associated with the processes of gain saturation. For these reasons, parametric amplifiers are the most promising candidates for the realization of ultra-high intensity laser systems based on coherent summation of a number of amplifier channels radiation.

The ability of the ultra-relativistic intensity laser system to operate at high repetition rate (up to 1 kHz) is important for a set of applications in the high-field physics, which can be realized only with parametric amplification with picosecond duration pump pulses [2].

The design of multichannel laser system with coherent beam combining being developed in ILP SB RAS is discussed. It is based on non-collinear chirped-pulse parametric amplification of few-cycle Ti:Sa femtosecond pulses up to the 10 petawatt level in LBO and BBO crystals with picosecond pump pulses. It is shown that the large-size BBO and LBO crystals open possibility of scaling of the amplification cascades up to multipetawatt level and at the same time provide the spectral amplification bandwidth, sufficient to maintain the amplification of pulses with duration up to 5-10 fs with pulse repetition rate up to 1 kHz [2]. The influence of the instability of parameters of individual beams of radiation on coherent combining efficiency is analyzed, and requirements of their values for realization of high efficiency coherent combining are determined.

We present experimental results demonstrating for the first time the principal possibility of coherent addition of parametrically amplified pulses in a dual-channel femtosecond laser system. The analysis and experimental results confirm the absence of fundamental restrictions on the intensity scaling by coherent combining of a powerful laser system, developed in the ILP SB RAS.

This work was performed in part under the support of Government Program “Extreme light fields” and by The Ministry of education and science of the Russian Federation, project 8387.

1. G.A. Mourou, N.J. Fisch, V.M. Malkin , Z. Toroker, E.A. Khazanov, A.M. Sergeev, T. Tajima, B. Le Garrec, “Exawatt-Zettawatt pulse generation and applications,” Optics Communications **285**, 720–724 (2012).
2. Bagaev S.N., Peastryakov E.V., Trunov V.I., “Exawatt laser systems - a new stage in the development of laser physics”, Atmospheric and Oceanic Optics **23**, 845-853 (2010).

The interaction of terawatt femtosecond radiation with atmospheric media

G.G. Matvienko, A.A. Zemlyanov

V.E. Zuev Institute of Atmospheric Optics SB RAS, 1 Academician Zuev Square, Tomsk, 634021 Russia
E-mail: mgg@iao.ru

We present analysis and generalization of the experimental and theoretical results of interaction between high-power ultrashort laser pulses with atmospheric matter. It was considered such interaction effects as laser beam self-focusing and filamentation, generation of supercontinuum emission, droplet destruction, and inelastic light scattering by liquid-drop aerosol particles. The results of laboratory and field experiments on propagation of high-power ultrashort laser pulses in the air and droplet media are given, as well as the theoretical models compared with the interpretation of the empirical results.

The new concept of light self-focusing in the regime of single filamentation was developed. It was supposed earlier that filament propagation is propagation of a light beam through a medium without diffraction. Our concept states that after nonlinear focus formation in the beam, the latter is split to two coaxial sub-beams; one of them, internal, compresses with formation of a filament, i.e., plasma channel, inside itself, while another sub-beam, external, firstly focuses and then defocuses. These sub-beams are connected with each other by the forces of diffraction interaction in the self-focusing medium. Thus filament is an area inside the laser beam, where the light energy dissipates in plasma. It is recorded visually as plasma emission.

We studied air-propagation of the sharply focused light pulses of Ti:Sapphire-laser of gigawatt power at the main and second harmonics (800 and 400 nm) theoretically and under laboratory conditions. A new regularity was qualitatively found out, that is invariance of the observed length of beam filamentation area with respect to variation of its diameter subject to equality of the initial intensities. The regime of single filamentation of a collimated high-power ultrashort pulse in the atmospheric air was studied and the effect of the initial size of the light beam on the main characteristics of the filaments generated, namely the coordinate of filamentation start, its length and continuity, was analyzed.

The field experiments on lidar remote sensing of an artificial aerosol cloud at an atmospheric path were carried out. We obtained the backscattered signals from the aerosol irradiated by supercontinual emission from the laser beam filamentation area. It was established that the result of remote sensing by supercontinuum can be described by the linear equation for sensing with the technique developed for multifrequency lidar sounding.

Numerical simulation of air-propagation of terawatt picosecond pulses of CO_2-laser with the central wavelength of 10.6 μm has shown that this process occurs under the condition of strong nonlinearity of the medium resulting in radiation self-focusing and filamentation with generation of the plasma areas in the beam channel. In contrast to filamentation in near-IR range (800 nm), the peculiarity of self-action of long wavelength radiation consists of generation of anomalously lengthy (in diffraction lengths of the initial beam) and wide in diameter intensive light channel (tens of TW/cm^2) accompanied by a homogeneous plasma column. The cause of this effect is the fact that the character of medium ionization varies in the radiation field of picosecond CO_2-laser pulses.

The determined regularities of self-action of the high-power ultrashort pulses of CO_2-laser allow to draw a conclusion on prospectivity of using radiation of ten-micrometer range of wavelength at the kilometer-range atmospheric paths for high-density light energy delivery and generation of the lengthy electroconductive channels.

Evolution of tracks induced by laser filaments in transparent media

E.F.Martynovich[1,2], V.P.Dresviansky[1], A.V.Kuznetsov[1], A.S.Kuzakov[1], A.A.Popov[1], S.V.Alekseev[3], V.F.Losev[3], A.N.Ratakhin[3], S.N.Bagayev[4]

[1]Irkutsk Branch of Institute of Laser Physics SB RAS,
130a Lermontov Str., Irkutsk, 664033 Russia,
[2]Irkutsk State University, 20, Gagarin Blvd, Irkutsk, 664003 Russia,
[3]Institute of High Current Electronics SB RAS, 2/3 Akademichesky Avenue, Tomsk, 634055 Russia
[4]Institute of Laser Physics SB RAS, 13/3 Acad. Lavrentyev Prosp., Novosibirsk, 630090 Russia
filial@ilph.irk.ru

Filamentation of laser pulses in optical media rather intensively investigated. However, due to the complexity of simultaneously occurring during filamentation phenomena, this research topic remains relevant [1].

The interaction of intense femtosecond laser pulses with transparent solid medium has been investigated in this work. Studies were performed with highly nonlinear photosensitive storage media [2-6]. Luminescence centers are formed in these media when interacting with laser radiation. This made it possible to apply highly sensitive luminescence methods for the study of the spatial distribution of the products of photochemical reactions in the interaction of light and matter. Ti: sapphire laser was used in the experiments to irradiate samples. Its pulse duration was 50 fs. Two harmonic of laser radiation used for exposure. The first had a central wavelength of 950 nm and a its pulse energy varied from zero to 8 mJ. The pulse energy of the second harmonic (475 nm) varied from zero to 0.4 mJ. Besides the laser intensity was varied by collimation. Luminescence spectra and kinetics were studied to determine the nature of the luminescence centers formed by laser radiation. Some experimental data are shown below in Fig. 1 - 4.

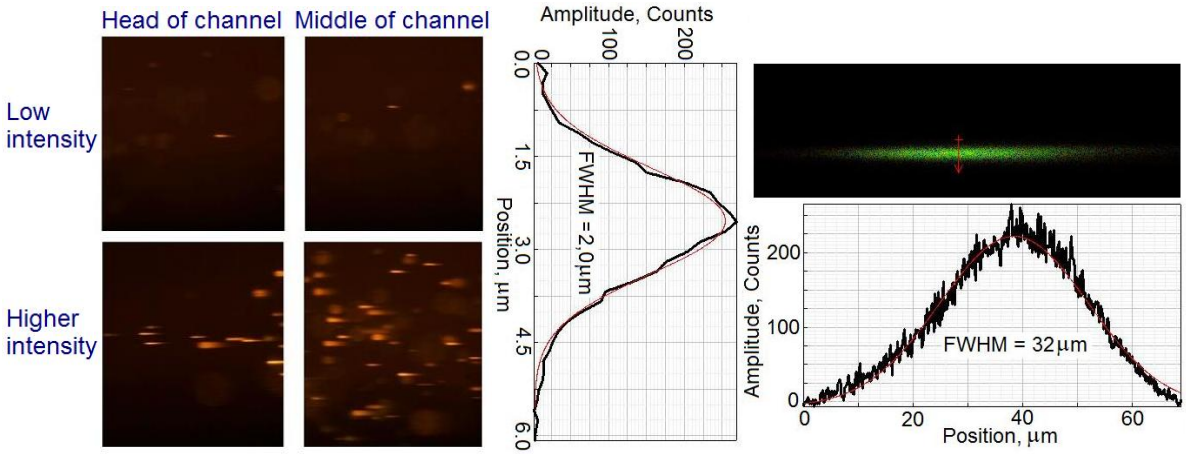

Fig. 1. Photoluminescent images of traces induced by a single femtosecond pulse. On the left - photo obtained by a simple fluorescence microscope Olimpus IX 71 (direction of the laser beam from left to right). Right - a photo of the single trace and the longitudinal and transverse distribution of light intensity in the the track obtained by confocal scanning microscope MicroTime 200.

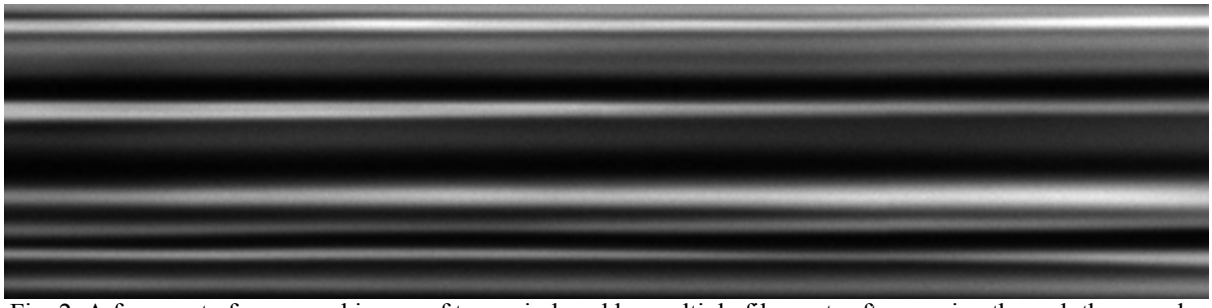

Fig. 2. A fragment of a scanned image of traces induced by multiple filaments after passing through the sample, 1,350 pulses (475 nm, 0.4 mJ). Image height 80 mm, length 280 mm. Microscope MicroTime 200.

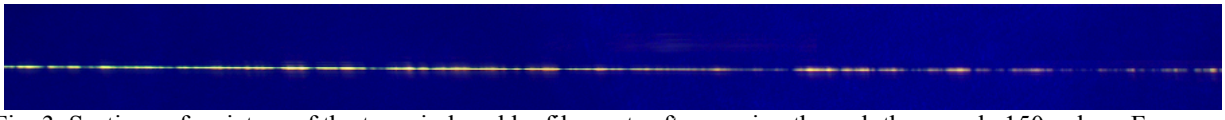

Fig. 3. Sections of a picture of the trace induced by filaments after passing through the sample 150 pulses. Fragment length of 5 mm. Microscope Olimpus IX 71

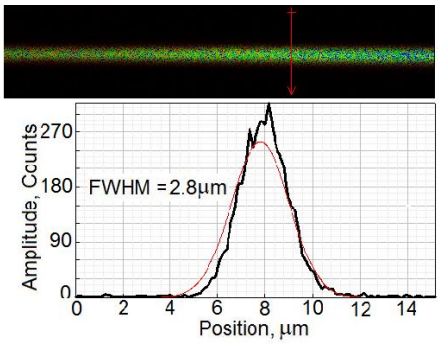

Fig. 4. Scanning of the cross section of the trace shown in Fig. 3.
Microscope MicroTime 200.

Based on the results of the experiments are analyzed models of the filamentation of femtosecond laser pulses in transparent dielectric media, as well as mechanisms for the formation of luminescent centers by laser radiation.

The research was supported by the Presidium of RAS (Programme No. 13, project № 4.12) and by the Siberian Branch of RAS (Programme No. II.8.1, project № 6).

References

1. S.V Chekalin, V.P Kandidov. From self-focusing light beams to femtosecond laser pulse filamentation. Physics-Uspekhi, 2013, V. 56, № 2, pp. 123-140.
2. E.F.Martynovich, A.V.Kuznetsov, A.V.Kirpichnikov, E.V.Pestryakov, S.N.Bagayev. Formation of luminescent emitters by intense laser radiation in transparent media. Quantum Electronics, 2013, 43 (5) 463 – 466.
3. E.F. Martynovich, D.S. Glazunov, A.V. Kuznetsov, E.V. Pestriakov, A.V. Kirpichnikov and S.N. Bagayev. 3D Fluorescent Imaging with Highly Nonlinear Photosensitive Materials. Optical Sensors, Optical Society of America, 2011, paper SWD6.
4. D.S.Glazunov, V.P.Dresvyanskiy, N.S.Bobina, V.F.Ivashechkin, A.I.Nepomnyashchikh, A.V.Kirpichnikov, A.V.Kuznetsov, E.V.Pestriakov, B.Chadraa, O.Bukhtsooj, E.F.Martynovich. Thermostimulated luminescence of LiF:Mg,Ti, irradiated with femtosecond laser pulses in filamentation mode. Russian Physics Journal, 2012, 55, № 11/3, p.47-49.
5. E.F. Martynovich, A.V.Kuznetsov, D.V.Baliunov, S.N.Bagayev. Optical storage media. Patent RU 85027 U1, 24.11.2008 (in Russian).
6. E.F. Martynovich. Color centers in laser crystals. Irkutsk: Irkutsk State University Publishing. 2004, 227 p.

Coherent four wave mixing with chirped pulses

A.A. Lanin[1,2], I.V. Fedotov[1,2], A.B.Fedotov[1,2], D.A.Sidorov-Biryukov[1,2], A.M.Zheltikov[1,2,3]

[1] *International Laser Center, Physics Department M.V. Lomonosov MSU, Moscow, 119991 Russia*
[2] *Russian Quantum Center, Skolkovo, Moscow Region, Novaya 100, 143025 Russia*
[3] *Department of Physics and Astronomy, Texas A&M University, College Station TX, 77843-4242 USA*
E-mail: dima-sidorov@mail.ru

Coherent Anti-Stokes Raman Scattering (CARS) became one of the most widely used methods of nonlinear spectroscopy which combines high selectivity, sensitivity, temporal, space, and spectral resolution [1, 2]. Femtosecond CARS spectroscopy [3] makes it possible to study fast processes and dynamics of oscillatory wave packets in molecular systems in gas, liquid, and solid phases. In contrast to the spontaneous regime of Raman scattering, where the phase of scattered field is random, effects related to the phase of the scattered signal are of paramount importance. The phase of the nonlinear Raman signal manifests itself in spectral line shapes of coherent Raman scattering and enters as an important parameter in nonlinear dynamics of ultrashort optical waveforms and pulse shape optimization for enhanced signal-to-background ratio in nonlinear Raman imaging and spectroscopy. The phase effects in coherent Raman scattering enable coherent Raman ellipsometery, optical heterodyne detection, and signal-to-background enhancement. Optimally shaped field waveforms, chirped light pulses and time-ordered pulse sequences have been intensively used in ultrafast Raman photonic technologies.

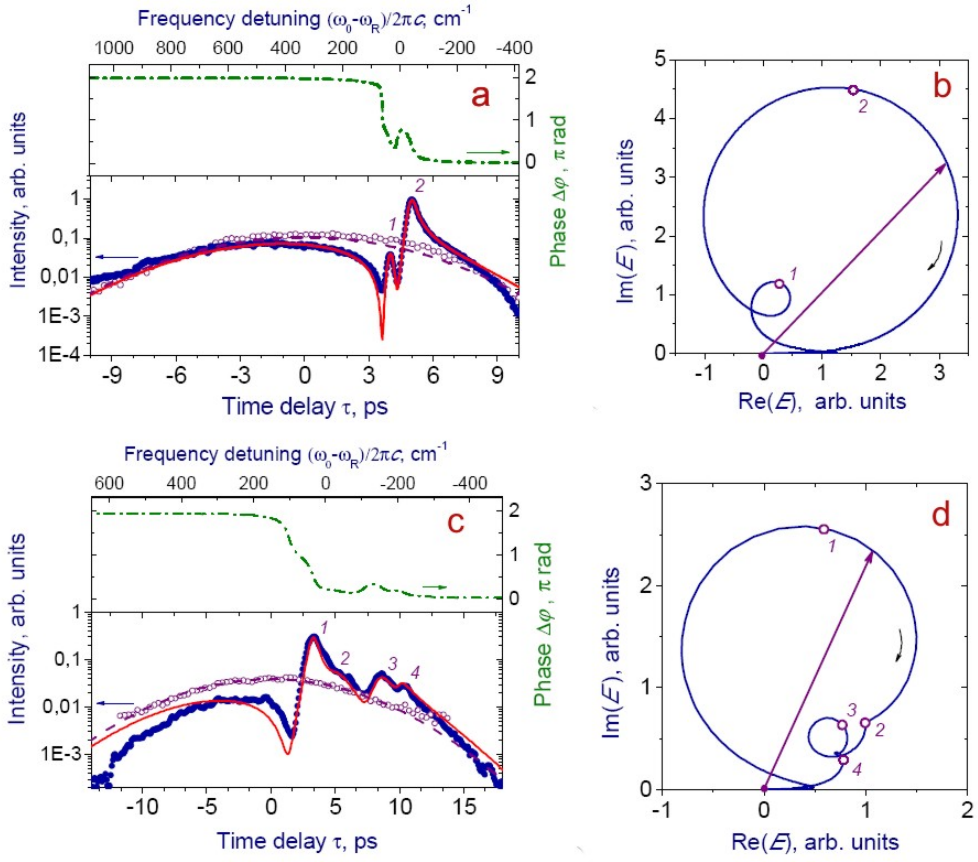

Fig. 1. Phase-controlled coherent Raman scattering in acetonitrile (a, b) and polysterene (c, d). (a, c) Intensity of the overall coherent signal measured (filled circles) and calculated (solid line) as a function of the delay time, cross-correlation trace of the laser pulses (open circles) and the intensity of the nonresonant component of the coherent response (dashed line) and the phase shift of the coherent Raman signal relative to the nonresonant background. (b, d) Trajectories traced by the complex amplitude of the overall coherent field in the plane where the abscissa and ordinate axes are chosen in such a way as to represent the real and imaginary parts of the overall signal. Direction of increasing delay time is shown by an arrow.

Tailored optical driver fields enabled a smooth tuning of the phase of the coherent Raman response, giving rise to a reach variety of interference effects, which can dramatically modify the nonlinear dynamics of ultrashort pulses and offer attractive solutions to long-standing issues in Raman imaging and spectroscopy. The nonlinear response measured as a function of the delay time between the chirp pulses forming an optical driver in our experiments is shown to feature a Fano-type profile with a well-resolved destructive interference deep on the dark side of the Raman peak visualizing a phase-controlled interference of the coherent Raman signal and the field-generated through four-wave mixing [4].

This work was supported in part by the Russian Foundation for Basic Research, project no. 12-02-12095-офи_м.

References

1. G. L. Eesley, *Coherent Raman Spectroscopy, Pergamon, Oxford (1981).*
2. A. M. Zheltikov and N. I. Koroteev, *Phys. Uspekhi* ***42****, 321 (1999).*
3. A.M. Zheltikov, *J. Raman Spectrosc.* ***31****, 653 (2000)*
4. A.A. Lanin, et. al, *Sci. Rep.* ***3****, 1842, DOI:10.1038/srep01842 (2013)*

Novel High-Efficiency Thin-Disk Lasers Based on Tm:$KLu(WO_4)_2$/$KLu(WO_4)_2$ Epitaxy

S. Vatnik[1], I. Vedin[1], X. Mateos[2], M. C. Pujol[2], F. Díaz[2], V. Petrov[3], Uwe Griebner[3]

[1] *Institute of Laser Physics, av Lavrentjeva 13/3, Novosibirsk 630090 Russia,*
[2] *Física i Cristal·lografia de Materials i Nanomaterials (FiCMA-FiCNA), Universitat Rovira i Virgili (URV), Campus Sescelades, c/ Marcel.lí Domingo, s/n, 43007-Tarragona, Spain,*
[3] *Max-Born-Institute for Nonlinear Optics and Ultrafast Spectroscopy, 2A Max-Born-Street, D-12489 Berlin, Germany.*
E-mail: vatnik@laser.nsc.ru

Monoclinic double tungstate (DT) crystals, due to their maximum absorption and emission cross sections and minimum concentration quenching, seem ideal as hosts for thin-disk lasers with simplified geometry (number of pump passes). The first diode-pumped thulium thin-disk laser based on Tm:$KY(WO_4)_2$ generated CW output power of 4.9 W at 1950 nm using 4 pump passes [1]. The power handling capability of the thin-disk concept scales inversely proportional to the thickness and the high absorption of the monoclinic DTs reveals another important advantage of these anisotropic materials - enormous scaling potential, which, however, could be technically exploited by only relying on doped epitaxial layers. Recently, employing Tm-doped epitaxial layers grown on un-doped $KLu(WO_4)_2$ (KLuW) and 4 pump passes, we achieved 47% slope efficiency and CW output power of 5.9 W [2]. Here, we study the power scaling potential of this laser in the quasi-CW (QCW) mode.

An epitaxial structure of 5 at. % Tm-doped KLuW layer grown on un-doped KLuW was used to prepare an active thin-disk element with dimensions 3.5×4×2.5 mm^3 where 2.5 mm is the thickness of substrate plus layer. The final layer thickness after polishing was 250 μm. A dielectric coating, highly reflecting (>99.9%) both at 1940 and 808 nm was deposited on the epitaxial side of the active element and then a metallic coating was added for soldering it to the copper heat sink. The substrate side was antireflection coated (<0.1%) at 1940 and 808 nm. The laser experiments were performed using only 2 passes of the pump through the Tm-doped epitaxial layer (i.e. no retroreflection of the pump beam at all) with nearly circular pump spot of ~0.95 mm diameter on the sample (50% larger spot area compared to [2]). The shaped pump beam from the laser diode was polarized along the N_m principal optical axis of KLuW for maximum absorption. The physical length of the two mirror cavity was 20 mm. The epitaxy served as a plane rear reflector while the concave output mirror had a radius of curvature of -40 mm and transmission ~7% at 1850 nm. The epitaxial Tm:KLuW/KLuW laser output was polarized, parallel to the N_m principal optical axis, as could be expected from the much higher gain in comparison to polarization along N_g for an N_p(***b***)-cut sample. Figure 1a shows the input-output characteristics of the laser in QCW regime with a duty cycle of 18% at ~20 Hz. The obtained slope efficiency (45.2%), optical efficiency (39.5%), and threshold, at increased output coupling, are very close to those in [2], but at larger spot sizes and higher pump level, the up-scaled output power (Fig. 1a) exceeds the results in [2] by 75%. The structured output spectrum extends from ~1838 to 1853 nm (Fig. 1b). The dependence on the heat sink temperature is shown in Fig. 1c.

The measured M^2 factors of the output beam at maximum power amounted to 7.2 (along N_m) and 9.2 (along N_g) as shown in Fig.2. No damage occurred with this epitaxial sample in QCW regime. In our opinion, rather poor M^2 factors are due to the short laser cavity (20 mm)

compared to the pump waist (0.95 mm), and laser beam profiles are obviously far from Gaussian's, see Fig.2 (b).

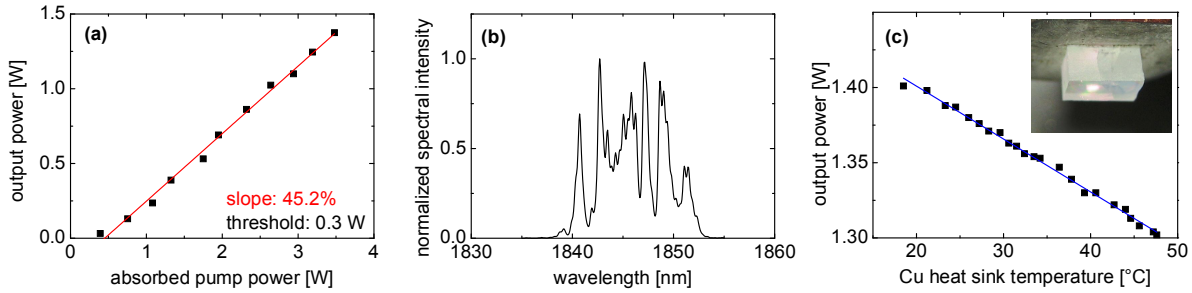

Fig. 1 (a) Input–output characteristics of the epitaxial Tm-laser pumped at 805 nm in terms of average power in QCW regime, (b) output spectrum, (c) temperature dependence. The inset in (c) shows a photograph of the Tm:KLuW/KLuW epitaxial disk element under QCW pump.

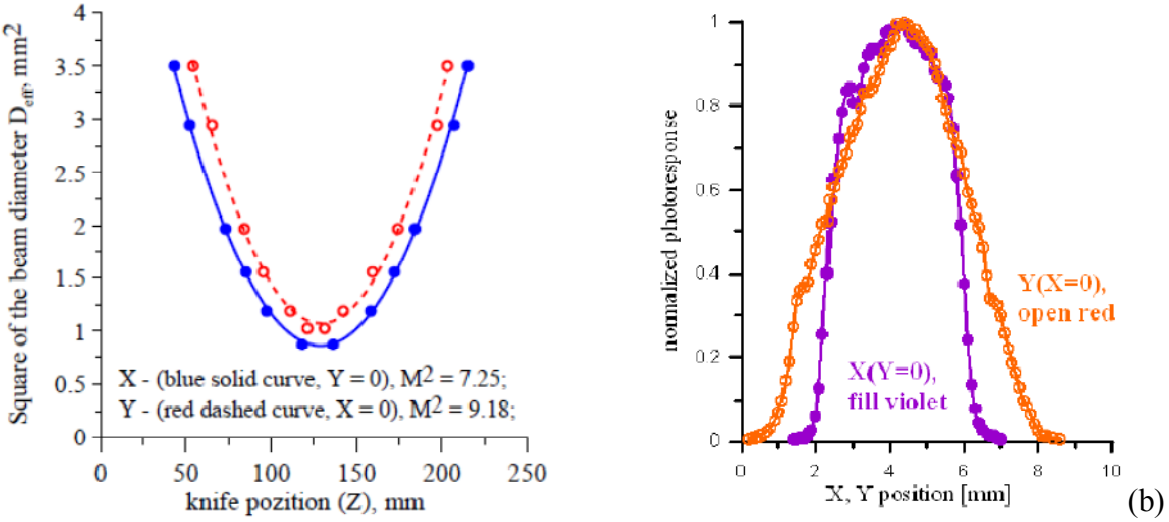

Fig. 2 (a) M^2 measurements by the knife-edge technique, (b) far-field X,Y beam's profiles.

To conclude, Tm-doped monoclinic DTs are very promising for use as epitaxial layers in thin-disk lasers to simplify drastically the pump geometry to a simple reflection at the highly reflecting epitaxial surface at a layer thickness that ensures efficient heat dissipation, essential for materials exhibiting modest thermal conductivity. Power up-scaling in the QCW regime has been demonstrated and true CW experiments are in progress.

References

1. S. M. Vatnik, I. A.Vedin, and A. A. Pavljuk, "Diode-pumped thin disk 15%Tm:KYW laser," Proc. SPIE **6731**, 673103 (2007).
2. S. Vatnik, I. Vedin, M. Segura, X. Mateos, M. C. Pujol, J. J. Carvajal, M. Aguiló, F. Díaz, V. Petrov, U. Griebner, "Efficient thin-disk Tm-laser operation based on Tm:$KLu(WO_4)_2$/$KLu(WO_4)_2$ epitaxies," Opt. Lett. **37**, 356 (2012).

Laser-induced nanostructured cluster materials: functional capability for experimental verification of macroscopic quantum phenomena

A. Antipov, S. Arakelian, S. Kutrovskaya, A. Kucherik, V. Prokoshev

Department of Physics and Applied Mathematics, Stoletov's Vladimir State University,
Gorky st. 87, Vladimir, 600000 Russia
Phone: +7(4922) 479847
Fax: +7(4922) 333369
E-mail: arak@vlsu.ru

1. The main goal of our work is the fabrication of nanostructured materials including the nano- and microclusters for control of electrical, optical and other properties of obtained structures.

2. First, we studied a possibility of both geometrical control by process of laser propagation and plasma propagation control in external fields. We showed an opportunity to select of particles in the sizes and weights and also in topology distribution for some materials (carbon, Ni, PbTe, etc.).

Second, for deposited extended array of nanoparticles we used method of laser deposition metal (and/or oxide) nanoparticles from colloidal systems (LDPCS) to obtain the multilayered nanostructures with controlled topology including the fractal cluster structures (for Ni, PbTe et all) – see the AFM-image figures.

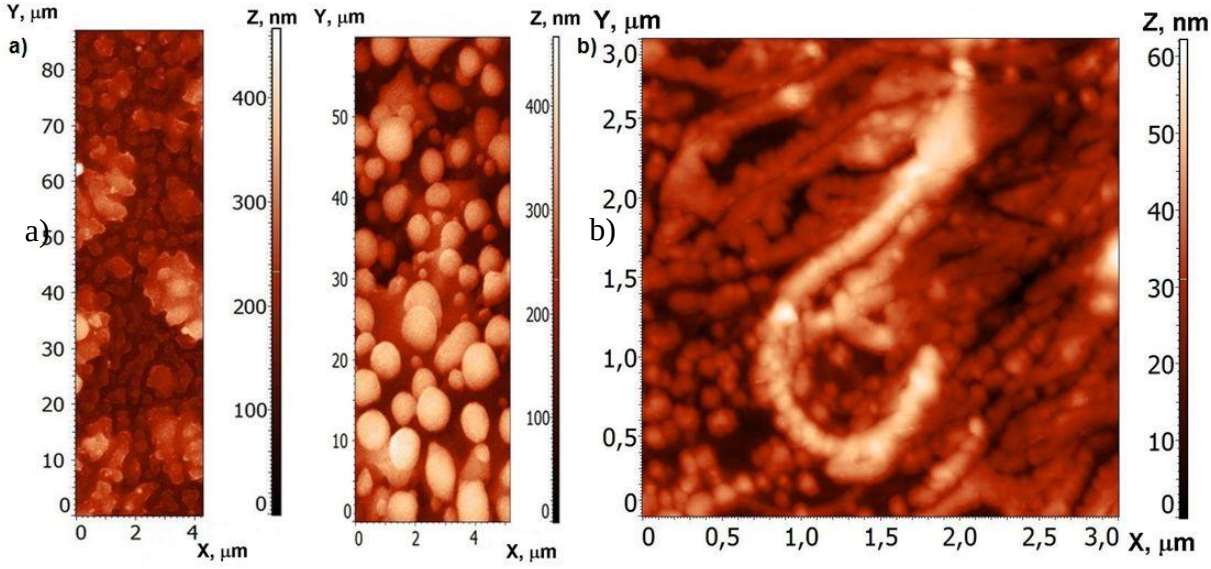

Atomic clusters of Ni on a quartz substrate Nanoparticles of PbTe on the glass substrate

3. A correlated state for the system of nanoparticles will be as an analogue of a coherent state of the type of Bose-Eienstein condensation (BEC). In fact, the conditions of low temperatures near absolute zero, which correspond to the values of the momentum of a particle p~0, we consider the conditions of «the energy trap» due to the surface effects, being the suppress factor for the temperature effects for nanoparticles.

Characteristic parameters of the problem with the dimension of length are, in the first place, «heat wave length» $\lambda_B = \sqrt{\frac{2\pi\hbar^2}{m\,k_B\,T}}$ (the de Broglie wavelength of a particle with mass m and the energy $k_БT$), and secondly, is the average distance between particles $\upsilon^{1/3} = \left(\frac{V}{N}\right)^{1/3}$. We

will be interested in a case of occurrence of the correlations in the system, i.e. when $\lambda_B \sim \upsilon^{1/3} \gg R$, where R is the radius of influence of the interaction potential of the particles.

The principal question to the quantum behavior development is, the estimation for effective mass m for λ_B. E.g. for electrical transport properties of semiconductors the reduced coefficient form is not more than 0.1, and results in the value $\lambda_B \geq 25$nm. For quasi- particles with coupled states of different kind in collective phenomena the fact takes place, as well. So, nanoclusters can demonstrate the quantum behavior in some effects for room temperature. The fact is true for nonhomogenous structures with hollow structures under the tunnel effects development. For structures in figure we demonstrated the superconductivity tendency to increase the electrical conductivity (in several times for our case) at room temperature in comparison with homogenous sample.

The relative contribution of thermal and quantum fluctuations is determined by the fact that first appear in the range of energies $\Delta E \leq k_B \cdot T$, usually with large number of populations, and the second – when $\Delta E > k_B T$ with small number of populations. At low temperatures the role of quantum processes increases for this reason; increases the corresponding number of populations, as well.

We will be interested in the question, how quantum phase transitions still appear in the properties of macroscopic systems, located at finite temperature. The key parameter is the violation of coherence in the system of quantum particles, which occurs on the defasing length l_{df}, which has the meaning of the average size of quantum fluctuations.

The analogy such a non-temperature phase transition with quantum phase transitions can be constructed proceeding from these ideas, that is, entering a characteristic energy parameter ΔE. We will be in the framework of the concept of cluster systems, i.e. ensembles of large numbers of coupling particles (atoms) with a pair of interaction.

In such a system can be two types of excitations, the configuration (structural) and the vibration (thermal), which are separated. The thermal movement is the equilibrium corresponding to a certain temperature T.

One can show that for configuration excitation of one of the structures (with dense packing and the dominance of the short-range forces) is a hexagonal structure, for which it is possible to formulate a method for constructing, i.e. the assembling of. An important parameter is the definition of the surface energy, which characterizes the cluster energy and has a minimum for an optimal (hexagonal, in particular) structure.

In the limit of large cluster the surface energy is proportional to $n^{2/3}$. For specific (per a particle) of the surface energy it can obtain the following relation

$$E_{os}(n) = \frac{E_o n + E}{n^{2/3}} \quad ,$$

where E is the total energy of the cluster, E_o is its specific value. These two energy parameter in the framework of this model views are defined by the number of links between nearest neighbors.

The last requirement of the physically means that the characteristic energy ties more than the energy of thermal fluctuations, i.e. is not important in itself condition $T \rightarrow 0$, but the stability of the structure of the medium to the influence of temperature factors.

Such a generalization allows us to talk to nanoparticles on the conservation of correlation, in particular in cluster systems, and at high (room) temperature – analogue of the attraction between the atoms at low temperatures in the conditions of the BEC.

LASER PRINTING OF NANOPARTICLES AND LIVING CELLS

Boris N. Chichkov

Laser Zentrum Hannover e.V., Nanotechnology Department, Hollerithallee 8, 30419 Hannover, Germany

I will report on our recent progress in the development of laser printing technologies for applications in photonics and regenerative medicine.

Semiconductor vertical-cavity lasers and single photon emitters

V.A. Haisler

A.V. Rzhanov Institute of Semiconductor Physics of SB RAS,
Pr. Lavrentyeva 13, Novosibirsk, 630090, Russia
E-mail: haisler@isp.nsc.ru

In this contribution the recent progress in the development of semiconductor microcavity based lasers (vertical-cavity surface-emitting lasers, VCSELs) and single photon emitters (SPE) is reviewed. The VCSELs structure may provide a number of advantages as follows: a) ultralow threshold operation is expected from its small cavity volume, reaching μA levels, b) wavelength and thresholds are relatively insensitive against temperature variation, c) dynamic single-mode operation is possible, d) large relaxation frequency provides high-speed modulation capability, e) long device lifetime is due to completely embedded active region and passivated surfaces, f) high-power conversion efficiency, i.e., >50%, g) vertical emission from substrate, h) low divergence of output light, easy coupling to optical fibers due to good mode matching from single mode through thick multimode fibers, i) a number of laser devices can be fabricated by fully monolithic processes yielding very low cost chip production, j) the initial probe test can be performed before separating devices into discrete chips, easy bonding and mounting, cheap modules and package cost, k) densely packed and precisely arranged two-dimensional (2-D) laser arrays can be formed.

The details of VCSELs design, growth and fabrication technology, as well as lasing characteristics are discussed. Next-generation short-distance optical networks, such as chip-to-chip or backplane applications require temperature-robust ultrahigh bit rate sources with low integration costs. Ultrahigh speed VCSELs (up to 40 Gb/s) are believed to be the best candidates for these applications. Single mode VCSELs with a wavelength corresponding to 5S-5P transition of Rb or Cs are very attractive for the development of miniature chip-scale atomic clocks (CSAC).

The absolute limit in miniaturization of light emitters is the development and design of single-photon emitters. The ideal single photon emitter is determined as a device that, when one pulls the trigger, and only then, emits one and only one photon. The ideal SPE generates nonclassical light states or photon *Fock states.* A mode which is excited in *Fock states* is occupied by exactly N photons and the variance $\Delta N = 0$, as distinct from photon *Glauber states* which are generated by classical light sources there the photon number distribution is determined by *Poisson statistics*. Effective single-photon emitters are most important for systems of quantum cryptography and quantum calculations; they are also of great interest for producing precise spectral equipment and optical power standards. Single photons can be emitted only by isolated quantum systems: single atoms, single dye molecules, single crystal defects and “artificial” atoms - semiconductor quantum dots (QDs). The indisputable advantages of QDs systems is a possibility of a creation of the miniature and efficient completely solid state electrically driven SPE. An single-photon electrically driven emitter containing a single InAs quantum dot and a Bragg microcavity has been designed and fabricated. Developed SPE generates single polarized photons at repetition rate 1GHz and demonstrates a second-order correlation function $g^2(0) = 0$. The developed SPE is one of the first optoelectronic component whose operation actually relies CQED, through the Purcell effect.

Energy sinks in optics of metamaterials: Fundamentals and applications

V. V. Klimov

Lebedev Physical Institute, Leninskij prospect 53, Moscow, 119991 Russia
E-mail:vklim@sci.lebedev.ru

Due to energy conservation law the energy emitted by one body (source) will be always absorbed by other bodies (sinks). Usually people do not worry about sinks because far fields are of primary interest. However in nano-optics and especially in nano-optics of metamaterials the role of sinks becomes very important. In fact even in usual media (vacuum) absorbing point dipole drastically disturbs the field distribution and can be neglected by no means (see Fig.1).

In the case of closed cavities and metamaterials the situation becomes more complicated because in the stationary lossless regime strong spatial singularities arise there. From our point of view these singularities indicate that sinks (absorbers, detectors) should be explicitly incorporated in description of wave phenomena in metamaterial [1-4]. Our approach is not to try to avoid the appearance of new singularities by overdamping or changing geometry, but to include these singularities into wave propagation theory. So we suggest to put real sources and sinks (absorbers) in the places of possible singularities and to see what will happen. This expanded description results in new systems which turn out to be full of new physical sense. Moreover, such systems can serve as a base for a development of new applications of nano-optics. We have analyzed several negative refraction geometries (slab, sphere, wedge etc.) and closed elliptical cavities where singularities appear in formal solution of Maxwell equations. In all cases we found that it is possible to attribute real physical meaning to them. As an example of possible application of our paradigm the scheme of a perfect nano-absorber is shown in Fig.2.

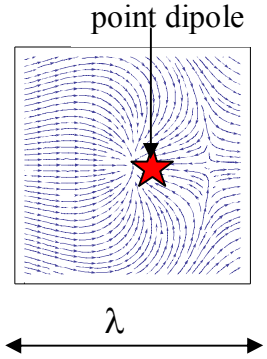

Fig.1. Resonant light absorption by point dipole.

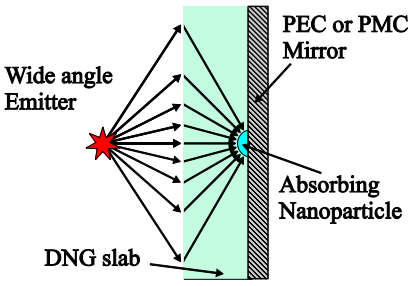

Fig. 2. Schematic diagram of a perfect nanoabsorber based on our paradigm.

It is proved by full scale simulations that this system can absorb 100% of wide angle incoming energy in deep subwavelength region. Other applications of our paradigm (e.g. preparation of entangled states of atoms for quantum computers) will be also discussed.

The author thanks the Russian Foundation for Basic Research and the Russian Quantum Center for financial support of this work.

References

1. V. Klimov *JETP Letters*, **89**, 270 (2009).
2. V. Klimov, J. Baudon, and M. Ducloy, *Europhysics Lett.*, **94**, 20006 (2011).
3. V. Klimov, S. Sun, G.-Y. Guo, *Optics Express,* **20**, 12, 13071 (2012).
4. G.-Y. Guo, V. Klimov, S. Sun, W.-J. Zheng, *Optics Express,* **21**, 9, 11338 (2013).

Experimental observations of temperature effects in the near-field regime of the Casimir-Polder interaction

A. Laliotis[1], T. Passerat de Silans[1,2], I. Maurin[1], M-P Gorza[1], M. Ducloy[1], D. Bloch[1]

[1] *Laboratoire de Physique des Lasers, UMR 7538 du CNRS et de l'Université Paris 13, 99 Av. J.B. Clément, 93430 Villetaneuse, France*

[2] *Federal University of Paraiba, Physics Department, Joao-Pesoa, Brazil*

E-mail: laliotis@univ-paris13.fr

Experimental studies on the Casimir-Polder interaction are of fundamental importance because they provide a physical insight on the interaction of atoms with the fluctuating vacuum. Since the first direct high-precision measurements of the atom-surface interaction [1] in the near-field (van der Waals) regime, many experiments have followed, that bring forth fundamental aspects of the interaction, such as retardation effects [2] or more recently temperature effects in the specific case when the surface is out of thermal equilibrium with the surrounding environment [3] and at a distance range of 5-10μm.

Due to the ever present nature of black body radiation photons, the effects of thermal fluctuations are an important consideration for any comparison between theory and Casimir-Polder (atom-surface) or Casimir (surface-surface) experiments, whose significance spans from fundamental measurements of Non Newtonian forces to nanotechnology applications. In the near field, thermal emission, usually considered as incoherent, has been shown to have a coherent almost monochromatic character due to the influence of surface excitations [4]. Moreover it has been demonstrated that excited atoms can be resonantly coupled to surface polariton excitations [5]. This coupling makes atoms an ideal probe for sensing thermal fields in the vicinity of planar or even nanostructured surfaces. Conversely thermal effects can provide an extremely useful way of tuning the atom-surface interaction via temperature.

In the van der Waals regime the interaction is usually described as an interaction between an oscillating electric dipole and its image. The close proximity of the atom to the surface assures that both dipoles oscillate in phase without retardation, resulting to a universally attractive potential and a free energy shift given by $-C_3/z^3$ where z is the atom-surface distance and C_3 is the van der Waals coefficient. In most cases the interaction is almost independent of temperature, except when atomic resonances are close to surface polaritons. In this case the interaction depends on the number of black body photons in the corresponding frequency, which becomes important when the thermal energy (k_BT) becomes comparable to that of the atomic transition ($\hbar\omega_{tr}$). Observing the thermal effects on the van der Waals interaction is thus feasible with excited atoms which have numerous couplings in the IR domain. In theory, the interaction can be tuned at will if one chooses the appropriate atomic state and dielectric material.

Initial experiments were performed with Cs ($8P_{3/2}$) in the vicinity of a CaF_2 surface in a specially designed vapor cell [6]. In this case, the $8P_{3/2}\rightarrow 7P_{5/2}$ at 36 μm weakly couples to a surface polariton at 25 μm [7], leading to a reduction of the C_3 coefficient with temperature. However, selective reflection measurements of the van der Waals coefficient were in sharp disagreement with theoretical predictions [8]. This result is attributed to the chemical instability of fluorine surfaces at high temperature and in the presence of alkaline vapors.

Here we report on spectroscopic selective reflection measurements of the interaction between a Cs ($7D_{3/2}$) atom and a sapphire surface. In this case the Cs $7D_{3/2}\rightarrow 5F_{5/2}$ transition at 10.8 μm, which couples to the surface resonance of sapphire at 12.1 μm, greatly influences the atom-surface interaction. Reaching the temperatures required to observe thermal effects is extremely challenging ($k_BT = \hbar\omega_{tr}$ indicates that T~1500K). For this reason our experiment is performed in an all-sapphire vapor cell. The cell windows are super polished with an annealing

post-treatment. The C_3 coefficient increases almost linearly with temperature up to almost 1000 K, in agreement with a full QED calculation [9].

A typical measurement of the C_3 coefficient consists of fitting reflection spectra to a theoretical model [5,6]. The experiment is performed for different vapor densities and different spots on the window to eliminate the influence of surface contaminants surface charges or vapor impurities. Statistical and systematic uncertainties have been reduced compared to our previous experiments performed on a different all-sapphire cell with windows of uncertain surface quality. The chemical stability of sapphire under these extreme conditions seems to be a key factor for this successful experimental achievement contrary to previous attempts that were compromised due to chemical degradation of CaF_2.

For the foreseeable future we plan on performing similar measurements with Cs($7P_{3/2}$) atoms for which the atom-surface attraction is expected to go down to zero at ~1000°C. This experiment is the first to provide a sensitive measurement of temperature effects on the atom-surface interaction in thermal equilibrium and highlights the QED nature of van der Waals regime. *Work partly supported by Capes-Cofecub Ph 740/12.*

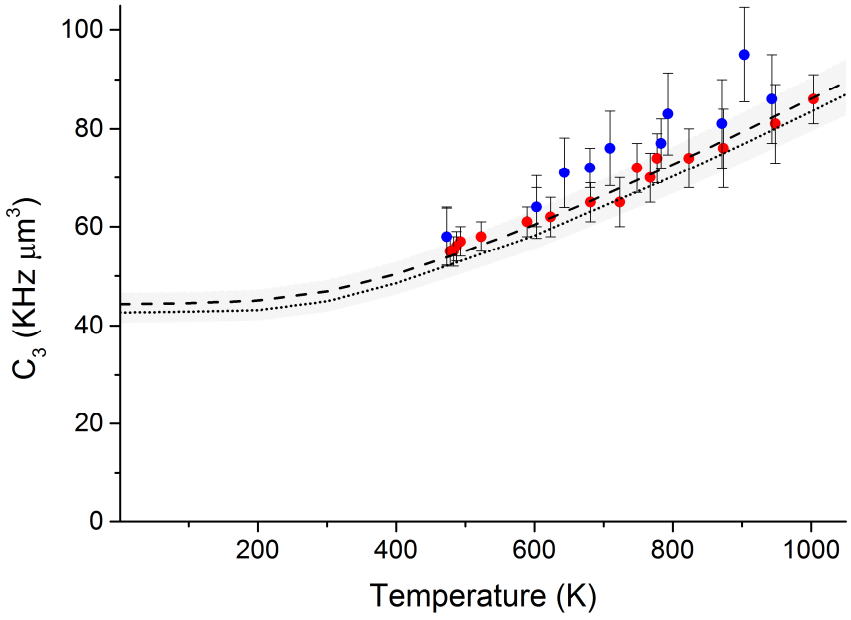

Fig.1. Temperature dependence of the C_3 van der Waals coefficient between Cs($7D_{3/2}$) and a sapphire surface. Red points represent measurements made on a super-polished sapphire window whereas blue points represent measurements performed on a window of uncertain but clearly inferior quality. Theoretical predictions using two different measurements of the sapphire dielectric constant reported in [7] (dotted) and [10] (dashed).

References

1. V. Sandoghdar, . C.I Sukenik, E.A. Hinds and S. Haroche, *Phys. Rev. Lett*, **68**, 3432 (1992).
2. C.I Sukenik, M.G. Boshier, D. Cho, V. Sandoghdar and E.A. Hinds, *Phys. Rev. Lett.*, **70**, 560 (1993).
3. J.M. Obrecht, R.J. Wild, M. Antezza, L.P. Pitaevskii, S. Stringari, E.A. Cornell, *Phys. Rev. Lett*. **98**, 063201 (2007).
4. A. V. Shchegrov, K. Joulain, R. Carminati and J. J. Greffet, *Phys. Rev. Lett*. **85**, 1548 (2000).
5. H. Failache, S. Saltiel, M. Fichet, D. Bloch and M. Ducloy, *Phys. Rev. Lett.*, **83**, 5467 (1999).
6. A. Laliotis, I. Maurin, M. Fichet, D. Bloch, M. Ducloy, N. Balasanyan, A. Sarkisyan, A. and D. Sarkisyan,. *Appl. Phys. B*. **90**, 415 (2008).
7. T. Passerat de Silans, I. Maurin, P.C.S Segundo, S. Saltiel, M-P Gorza, M. Ducloy,D. Bloch, D.S. Meneses and P. Echegut, *J. of Phys.: Condens. Matter* **21**, 255902 (2007).
8. T. Passerat de Silans, *PhD Thesis, Université Paris13* (2009).
9. M-P. Gorza and M. Ducloy, *Eur. Phys. J. D*. **40**, 343-356 (2006).
10. A.S. Barker, *Phys. Rev*. **132**, 1474-1481 (1963).

Plasmonic nanolaser

A. I. Plekhanov

Institute of Automation and Electrometry of the SB RAS, Koptyug Ave. 1, 630090 Novosibirsk, Russia

There is a tremendous interest in nanoplasmonic systems with gain initiated by the introduction of the spaser [1]. The spaser (Surface Plasmon Amplification by Stimulated Emission of Radiation) should have a medium with optical gain in close vicinity to a metallic nanostructure that supports surface plasmon oscillations. It is analogous to the conventional laser, but in a spaser photons are replaced by surface plasmons and the resonant cavity is replaced by a nanoparticle (NP) that supports plasmonic modes [2]. Spasers could find a wide range of applications, including nanoscale lithography, probing, and microscopy because it allows beating the diffraction limit and focusing electromagnetic energy to spots much smaller than a wavelength.

Here for the first time we experimentally show that by combining the photonic crystal (PhC) and spaser ideas one can create a coherent source of electromagnetic radiation that is based on plasmonic oscillations. We have demonstrated a three dimensional PhC infiltrated by plasmonic resonators supporting coherent current excitations with high quality factor can act as a source of spatially and temporally coherent radiation. In-phase plasmonic oscillations in individual resonators lead to emission of spatially- and temporarily-coherent light propagating in the direction normal to the PhC film.

We consider a system where Au NPs are located on monodisperse spherical silica particles (MSSP). These MSSPs are packed into an ordered face-centered cubic lattice structure forming a PhC with a photonic band gap. The diameter of the silica spheres is chosen so that the Bragg reflection wavelength of the PhC films overlaps with the optical-gain spectrum of the light-emitting Au NPs. This leads to a feedback similar to the distributed feedback (DFB) lasers. Thus, the emitters (spasers) lase in an external DFB cavity.

We have used Au NPs (D = 7-10 nm) with the surface resonance band at the wavelength λ_{spr} = 524 nm covered by fluorescein-doped silica shell (h = 6 – 10 nm thick) and PhC films with the photonic band gap at the wavelength λ_{phb} = 580 nm. The film thickness of PhCs is 4-5 μm.

Low-threshold spasing at the high-frequency side of the photonic band gap has been obtained in the PhC film infiltrated by the spasers. It was shown that the threshold of the lasing spasers in PhC is forty time less than in the colloid consisting of spasers (P_{thresh} = 140 kW/cm^2)

Thus, the lasing spaser in a PhC film allows high amplification and lasing in a very thin layer of material with a more modest gain level, making it a promising device. The thin-layer geometry is a desirable feature for some highly integrated devices (ultra-bright nanofilm lasers and displays, etc.), in particular, because of improved heat management and integration.

This work was partially financially supported by the Samsung Electronics Co., Ltd. I am also especially indebted to A.S.Kuchyanov, E.O Maltseva, I.K.Igumenov, B.M.Kuchumov, Chang-Won Lee, Yeonsang Park, Sangmo Cheonin, Kinam Kim and M.I.Stockman for sharing the fruits of their efforts.

References

1. Bergman, D. J., Stockman, M. I.. *Phys. Rev. Lett*. **90**, 027402 (2003).
2. Noginov, M. A. et al. *Nature*. **460**, 1110-1113 (2009).

Coherent Spontaneous Emission of Light by Solids

E. A.Vinogradov[1], I. A. Dorofeyev[2]

[1] *Institute of Spectroscopy, Russian Academy of Sciences,142190, Moscow, Troitsk, Russia.*
[2] *Institute for Physics of Microstructures, Russian Academy of Sciences,603950, GSP-105 Nizhny Novgorod, Russia*
E-mail: evinogr@isan.troitsk.ru

The study of emission spectra in the near field has shown that thermal emission can be quasi-monochromatic due to the excitation of resonant surface waves. From the point of view of coherence theory, this also demonstrates that such thermal sources exhibit a high degree of temporal coherence. This large time-coherence in the near field is due to the peak of the local density of states due to the presence of surface waves. A well-established result of coherence theory states that light across a planar thermal source at a given wavelength λ is spatially correlated over a distance on the order of $\lambda/2$ [1-3]. In deriving this result, the near-field part of the emitted light is disregarded, because it plays no role in the far-field properties of emission from planar sources. As it was shown [2-6] the non-propagating (evanescent) fields play a substantial role in the spectral properties of thermal sources. Fig.1 shows normalized spectrum of the E_z component of the field for the ZnTe half space at a temperature of $300K$. The dip corresponding to the negative values of the dielectric function is shown in more detail in the insert.

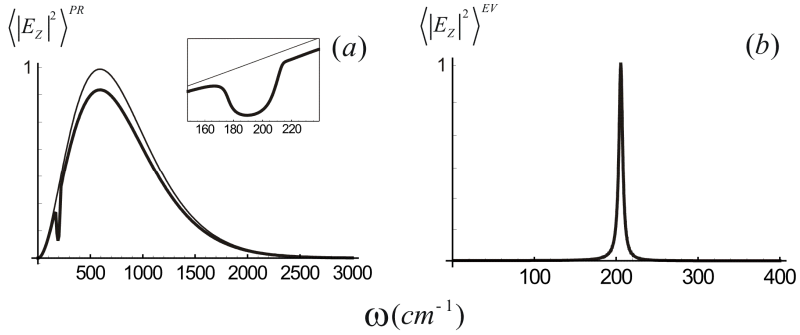

Fig. 1. The normalized spectrum of the E_z component of the field for the ZnTe half space at a temperature of $300K$: (a) spectrum of the propagating waves (thick line) and the Planck spectrum (thin line) and (b) spectrum of the evanescent waves at the distance from the surface that is significantly less than the wavelength corresponding to the spectral maximum.

At a distance from surface of 100 nm and less, the emission is almost monochromatic at a frequency of surface phonon which is not represented in the far-field spectrum [3-6]. The field of surface-polariton may be coherent along the interface.

Figure 2 shows the normalized correlation functions for the propagating component of the thermally stimulated field generated by the ZnTe half space at a temperature of $300K$ and the evanescent component of the field vs. normalized times $\tau/\vartheta_{\Pr}$ and τ/ϑ_{Ev}, respectively. The characteristic times in centimeters are $\vartheta_{Ev} = 2\pi/\omega_{QP} \approx 0.03cm$, where $\omega_{QP} \cong 205cm^{-1}$ is surface phonon of ZnTe and $\vartheta_{\Pr} = 1.37\hbar 2\pi c/\pi k_B T \approx 0.0021cm$.

However, since this coherence is only due to surface waves, it cannot be detected in the far field. To transfer the near-field coherence into the far field, we can use the coupling of an ATR prism over sample with the surface polariton of the sample [3-6]. Also a dielectric film on metal surfaces transforms the surface plasmon-polariton field into Fabry-Perot interference modes well observed in far field. Fig.3 shows the absorption (emission) spectra of ZnSe (1μm thick) film on Al substrate. $\omega_{ex} \approx 20000cm^{-1}$ - is exciton frequency in ZnSe, $\gamma_{ex} = 1500cm^{-1}$ is the decay

constant of the exciton at room temperature and $\Delta\varepsilon_{ex} = 0{,}05$ is the exciton oscillator strength [4,5].

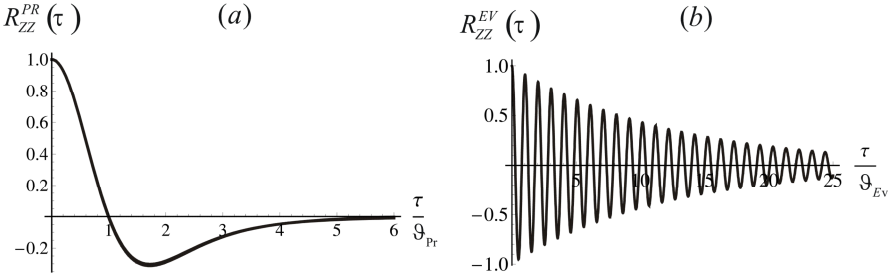

Fig. 2. Plots of the normalized correlation functions for (a) the propagating component of the thermally stimulated field generated by the ZnTe half space at a temperature of $300K$ and (b) the evanescent component of the field vs. normalized times $\tau / \vartheta_{\Pr}$ and τ / ϑ_{Ev}, respectively.

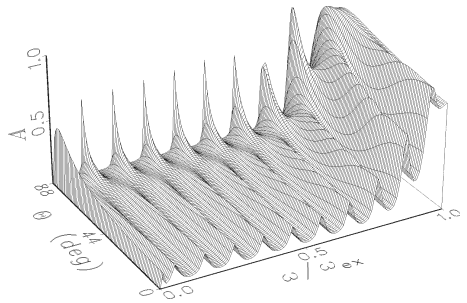

Fig.3. p-polarized absorption (emission) spectra of ZnSe (1μm) film on Al substrate.

The interference modes in the frequency range $\omega << \omega_{ex}$ are the radiative (propagating) part of noradiative (evanescent) surface plasmon-polariton of Al surface without the film. They are eigenstates of the structure "vacuum-film-substrate" as whole but not excitations of the film or the metal.

The correlation properties of the thermally stimulated electromagnetic fields of material objects are directly related to the internal dynamics of the lattice and electron subsystems of the field source, including the features of motion in the near-surface region. In particular, the electromagnetic fluctuations provide the heat transfer between objects in vacuum; the trapping of atoms, molecules, and coherent material states in electromagnetic traps; and several important physical-chemical phenomena in the vicinity of the surface (e.g., adsorption and desorption of atoms and molecules). Note that the electromagnetic fluctuations cause variations in the emission and absorption of a quantum system in the vicinity of the surface (e.g., variations in the conditions for and characteristics of the spontaneous emission of atoms and molecules, the shift of energy levels, and the complete or partial removal of the degeneration of levels) which can substantially affect the dynamics of heterogeneous effects. The analysis of the resonance states in the spectra of the thermally stimulated fields and various correlation characteristics enables one to characterize the eigenmodes of the system (volume and surface polaritons), whose properties are determined by the electrodynamical and geometrical parameters of the system.

1. L. Mandel, E. Wolf: *Optical Coherence and Quantum Optics* (Cambridge University Press, Cambridge 1995)
2. J. J. Greffet, R. Carminati, K. Joulain, J.P. Mulet, S. Mainguy, Y. Chen: *Coherent emission of light by thermal sources,* Nature **416**, 61 (2002).
3. I.A. Dorofeyev, E.A.Vinogradov, Laser Physics, **21,** 1 (2011).
4. E.A. Vinogradov, Physics Reports, **217**, 159 (1992).
5. E.A.Vinogradov, I.A. Dorofeyev, *Thermally stimulated electromagnetic fields from solids* (Fizmatlit, Moscow, 2010) (in Russian).
6. I.A. Dorofeyev, E.A.Vinogradov, Physics Reports, **504**, 75 (2011).

Random fiber laser: new efficient laser source with unique properties

S. A. Babin

Institute of Automation and Electrometry of SB RAS, Ac. Koptug ave. 1, Novosibirsk, 630090 Russia
Novosibirsk State University, Pirogova str. 2, Novosibirsk, 63009, Russia
E-mail: babin@iae.nsk.su

Attractive features of fiber lasers such as high-efficiency and stable hands-free generation of high-quality beam in broad range of output powers impel to development of new all-fiber laser schemes. One of recent advances in this direction concerns demonstration of random lasing in a piece of standard telecommunication fiber without any cavity elements [1]. The positive feedback required for laser generation in such fiber laser is provided by the Rayleigh scattering on refractive index inhomogeneities randomly distributed along the fiber. Although integral reflection coefficient due to the Rayleigh scattering (RS) is extremely small (~0.1%) the lasing threshold may be exceeded when sufficient distributed Raman gain is provided by means of optical pumping coupled into the fiber core.

Such one-dimensional random distributed feedback fiber laser has a number of new features, which make it different from conventional fiber lasers as well as from random lasers of other types. In particular, the generated radiation is featured by narrow-band quasi-continuous spectrum that is free of mode structure, whereas the output beam is stationary with nearly Gaussian profile corresponding to fundamental transverse mode.

In this paper, a review of recent endeavours in the development of various configurations of the RS-based random fiber lasers and corresponding studies of the basic physical process defining its operation is presented.

The reviewed configurations provide operation in widely tunable [2], multi-wavelength [3], cascaded [4] and other regimes in telecom (around 1.55 μm) as well as in other spectral ranges (1.1-1.3 μm), with fiber length varying from ~100 to ~1 kilometers.

Fundamental properties of the random fiber lasers are analysed, in particular generated power distribution along the fiber and its generation efficiency [5], as well as spectral features of the laser exhibiting usual line narrowing near the threshold and its nonlinear broadening with increasing power well above the threshold. Possibility to reach an efficiency close to 100 % with spectrum narrower than 1 nm is demonstrated.

In conclusion, possible applications of random fibre lasers are discussed including telecommunication and sensor systems.

References

1. S. K. Turitsyn, S. A .Babin, A. E. El-Taher, P. Harper, D. V. Churkin, S. I. Kablukov, J. D. Ania-Castañón, V. Karalekas, E. V. Podivilov, *Nature Photonics* **4**, 231 (2010).
2. S. A. Babin, A. E. El-Taher, P. Harper, E. V. Podivilov, S. K. Turitsyn, *Phys. Rev. A*. **84**, 021805(2011).
3. A. E. El-Taher, P. Harper, S. A. Babin, D. V. Churkin, E. V. Podivilov, J. D. Ania-Castanon, S. K. Turitsyn, *Opt. Lett.* **36**, 130 (2011).
4. I. D. Vatnik, D. V. Churkin, S. A. Babin, S. K. Turitsyn, *Opt. Exp*. **19**, 18486 (2011).
5. I. D. Vatnik, D. V. Churkin, S. A. Babin, *Opt. Exp*. **20** 28033 (2012).

Mode-locked fibre lasers with high-energy pulses

S. Kobtsev
Novosibirsk State University, Novosibirsk, Russia

Elongation of the resonator of a mode-locked fibre master oscillator can raise its pulse energy up to several μJ without application of Q-switching or cavity dumping techniques, as well as without additional optical amplifiers [1, 2]. However, increased energy may lead to changes in the pulse shape [3]. It is therefore important to control both pulse duration and pulse energy in various-length cavities of mode-locked fibre lasers that use different methods of mode locking. Recent studies [4–8] have demonstrated such possibilities, and the aim of the present work is to analyse and discuss them. Thus, it has been shown that a considerable elongation of the resonator of a mode-locked fibre master oscillator (up to 25 km) brings both pulse energy and pulse duration close to those of a Q-switched fibre laser with the same pulse repetition rate, although the structure of pulses generated in such a mode-locked laser is markedly different. The laser output in this case consists of nanosecond-long envelopes stochastically filled with femtosecond pulses. Unusual composition of these pulses stimulates active research on physical mechanisms that give rise to such pulses and on their application in different fields.

1. S. Kobtsev, S. Kukarin, and Y. Fedotov, "Ultra-low repetition rate mode-locked fiber laser with high-energy pulses," Optics Express 16, 21936–41 (2008).
2. S.V. Smirnov, S. M. Kobtsev, S.V. Kukarin and S.K.Turitsyn, Mode-locked fibre lasers with high-energy pulses (Laser Systems for Applications, InTech, 2011), Chapter 3.
3. S. Smirnov, S. Kobtsev, S. Kukarin, and A. Ivanenko, "Three key regimes of single pulse generation per round trip of all-normal-dispersion fiber lasers mode-locked with nonlinear polarization rotation," Optics Express 20, 27447–53 (2012).
4. N. N. Akhmediev and A. Ankiewicz, Dissipative Solitons, Springer, 2005.
5. B. Oktem, C. Ülgüdür, and Ö. Ilday, "Soliton-similariton fibre laser," Nature Photonics 4, 307–311 (2010).
6. W. H. Renninger and F. W. Wise, Dissipative soliton fiber lasers (Fiber lasers, Wiley-VCH Verlag GmbH & Co. KgaA, 2012), Chapter 4.
7. P. Grelu and N. Akhmediev, "Dissipative solitons for mode-locked lasers," Nature Photonics 6, 84–92 (2012).
8. D. Radnatarov, S. Khripunov, S. Kobtsev, A. Ivanenko, S. Kukarin, "Automatic electronic-controlled mode locking self-start in fibre lasers with non-linear polarisation evolution", Optics Express **21**, 2013 (accepted for publication).

High energy pulsed fiber lasers and applications for nonlinear frequency conversion

Wei Shi

College of Precision Instrument & Opto-electronics Engineering, Tianjin University, Tianjin, China
E-mail: shiwei@tju.edu.cn

Fiber lasers pumped by semiconductor lasers are becoming more and more important in laser applications. Monolithic all fiber-based pulsed fiber lasers are particularly promising sources for laser sensing, imagery, velocimetry, anemometry, and coherent LIDAR owing to their high spatial and spectral qualities, as well as their rugged, compact, maintenance-free, efficient, lightweight, and high beam quality features. For applications involving spectroscopic sensing and LIDAR, a high precision measurement highly depends on the linewidth or coherence length of the fiber laser pulses. For example, for active remote sensing spectroscopy, the oxygen absorption linewidth at standard temperature and pressure is in the range of a few gigahertz [1-2], so the linewidth and stability of the laser should be less than 10 MHz for high precision (fractions of a percent) measurements of the absorption lineshape and strength. Therefore, it is highly desirable to have fiber laser pulses with transform-limited linewidth, and pulse duration in 100 ns-500 ns range. In order to achieve a narrow linewidth pulsed fiber laser seed, it is possible to modulate a distributed feedback fiber laser (DFBL) or a single-frequency fiber laser by using electro-optic modulator or acoustic modulator [1-2, 3-5]. Most recently, narrow linewidth pulsed fiber lasers in the nanosecond time regime were demonstrated by using actively Q-switching, which are more efficient, compact and less expensive compared with the modulated fiber laser pulses.

For sub-microsecond pulses with single spatial mode and very narrow linewidth, the laser power scaling has been difficult in fiber amplifiers due to limitations primarily from the stimulated Brillouin scattering (SBS) nonlinear effect [1-3]. SBS builds up strongly in the fiber for narrow linewidth pulses of long pulse duration [6]. So it has been difficult to achieve high peak power, single-mode, and narrow linewidth operation simultaneously in a fiber laser system, especially for a monolithic master oscillator and power amplifier (MOPA) structure. Therefore, increasing the SBS threshold for the fiber amplifiers is crucial to scaling the peak and average power for the SM PM narrow linewidth sub-microsecond fiber laser pulses. There are three main approaches to reducing the SBS effect or increasing SBS threshold. One is to reduce the transverse overlap integral between the optical and acoustic fields as accomplished by proper profile design [7-8]. The second is using a temperature gradient or strain gradient to essentially shorten interaction length by altering the SBS spectrum along the fiber. The last one that is the well-known approach to reduce the SBS effect is to make fibers with LMA. The mode area is increased by lowering the core numerical aperture (NA) and increasing the core diameter. However, the challenge is to decrease the core NA. For example, for the lowest commercial core NA of 0.06 the fiber is still multimode in the c-band when the core diameter is larger than 20 μm. Single mode operations can be achieved by modal discrimination induced by coiling the fiber. A side effect of this method is that for large core size, bending deforms the mode field distribution and thus reduces the mode area. One of the promising approaches to achieve the high SBS threshold is based on the single-mode PM large core highly doped fibers in the power amplifier stage of a monolithic MOPA configuration [8-9]. Kilowatt-level SBS threshold and mJ-level pulse energy are discussed in this paper.

The all-fiber-based narrow linewidth nanosecond pulsed lasers in MOPA configuration have been successfully used in nonlinear frequency THz generation.

References

1. M. Stephen, M. Krainak, H. Riris, and G. R. Allan, "Narrowband, tunable, frequency-doubled, erbium-doped fiber-amplifed transmitter," Opt. Lett. **32**, 2073-2075 (2007)
2. C. E. Dilley, M. A. Stephen, and M. P. Savage-Leuchs, "High SBS-threshold, narrowband, erbium co-doped with ytterbium fiber amplifier pulses frequency-doubled to 770 nm," Opt. Express **15**, 14389-14395 (2007)
3. Wei Shi, Matthew Leigh, Jie Zong, Zhidong Yao, and Shibin Jiang, "Power scaling for narrow linewidth C-band pulsed fiber lasers using a highly Er/Yb co-doped phosphate glass fiber," SPIE Photonics West 2008, OPTO, Optical Components and Materials V, **19-24**, 6890-20 (2008)
4. B. Steinhausser1, A. Brignon1, E. Lallier1, J. P. Huignard1, P. Georges, **"**High energy, single-mode, narrow-linewidth fiber laser source using stimulated Brillouin scattering beam cleanup," Opt. Express, **15**, 6464-6469 (2007)
5. Valery Philippov, Christophe Codemard, Yoonchan Jeong, Carlos Alegria, Jayanta K. Sahu, and Johan Nilsson, "High-energy in-fiber pulse amplification for coherent lidar applications," Opt. Lett. **29**, 2590-2592 (2004)
6. G. P. Agrawal, *Nonlinear Fiber Optics*, Third Edition, (Academic, 2001)
7. Ming-Jun Li, Xin Chen, Ji Wang, Stuart Gray, Anping Liu, Jeffrey A. Demeritt, A. Boh Ruffin, Alana M. Crowley, Donnell T. Walton, and Luis A. Zenteno, "Al/Ge co-doped large mode area fiber with high SBS threshold," Opt. Express, **15**, 8290-8299 (2007)
8. J. Nilsson, "SBS Suppression at the kilowatt level," SPIE Photonics West 2009, 7195-50
9. W. Shi, E. B. Petersen, Zh. Yao, D. T. Nguyen, J. Zong, M. A. Stephen, A. Chavez-Pirson, and N. Peyghambarian, "Kilowatt-level stimulated-Brillouin-scattering-threshold monolithic transform-limited 100 ns pulsed fiber laser at 1530 nm," Opt. Lett. **35**, 2418-2420 (2010).
10. W. Shi, E. B. Petersen, D. T. Nguyen, Zh. Yao, A. Chavez-Pirson, N. Peyghambarian, and J. Yu, "220 μJ monolithic single-frequency Q-switched fiber laser at 2 μm by using highly Tm-doped germanate fibers" Opt. Lett. **36**, 3575-3577 (2011).

Laser performance of the erbium-ytterbium-codoped fiber with high concentration

Feng Song
School of Physics, Nankai University
fsong@nankai.edu.cn

Erbium-ytterbium heavy co-doped phosphate glasses with different concentrations have been fabricated. Absorption spectra, excitation spectra, emission spectra have been measured and optical parameters are calculated with J-O theory and Dexster theory. With the glasses of a few millimeters with good optical performance, the laser emission was demonstrated. More than 80 mW laser output was obtained with a 1mm Er-Yb-codoped phosphate glass. The glasses with good absorption and fluorescence performance were chosen to draw fibers. Laser emissions of the fibers were demonstrated. A propagation equation and rate equation model for the lasers, which considers the cumulative transfer and double-energy transfer processes, is established. The simulation for the lasing operation of a short Er^{3+}-Yb^{3+}-codoped phosphate fiber laser is investigated. A 10.4 cm compact fiber laser with an output power of 170.4 mW, a bandwidth of 0.053 nm and a slope efficiency of 35.3% is demonstrated in experiments. The experimental results show that the theoretical model we used is more accurate than former models. The dependence of output power on output coupler reflectivity, active fiber length and Er^{3+}-Yb^{3+} concentrations are also investigated numerically. We also demonstrated the super fluorescence source with 8-15cm fibers. An Er doped ZBLAN fiber laser by inserting a Fe^{2+}: ZnSe crystal as the saturable absorber to the free space part of the fiber laser cavity was also investigated.

Capacity of nonlinear channels

S.K. Turitsyn

Aston Institute of Photonic Technologies, Aston University, Birmingham, UK
Novosibirsk State University, Novosibirsk, 630090, Russia

Recent fast progress in development of coherent optical communication systems, exploiting optical phase for coding of information, resulted in the drastically new ways in which optical fibre channels are operated. In recent concepts of coherent transmission the optical fibre dispersion is not compensated at all in the optical domain and signal is recovered through digital signal processing using high speed electronics at the receiver [1]. However, nonlinear propagation effects still have critical impact (together with the accumulated noise) on the capacity of optical fibre channels [2-12]. The reason is rather evident - increase of input signal power to improve signal-to-noise ratio at some power level inevitably leads to nonlinear signal interactions and nonlinear mixing of signal with noise. Therefore, nonlinearity is critically important and the significance of an accurate evaluation of nonlinear transmission effects for analysis of nonlinear fibre channel capacity cannot be overestimated.

In general, signal transmission in fibre channels is described by nonlinear partial differential evolution(s) that makes analysis of capacity of such channels a very complex problem, indeed. Therefore, there is a strong demand on analytical approximate models of nonlinear fibre channel similar to available in linear channels.

The seminal Shannon's result [14] for capacity of the linear additive white Gaussian noise (AWGN) channel: $C = B\log_2(1+S/N)$ is one of the celebrated equations in science and engineering. In practical communication channels that are well approximated by the linear AWGN channel the Shannon capacity can be approached very closely (by a fraction of dB) by using low density parity check codes and turbo codes. The linear AGWN channel is nowadays a textbook material and is virtually wholly understood.

There is, however, a growing interest in studies of a capacity of more complex communication channels including nonlinear channels for which the limits have yet to be defined. The optical fibre channel is the most important example of such channels [2-9].

The definition of the Shannon capacity per unit bandwidth for arbitrary channel [13] involves maximizing the mutual information (MI) functional:

$$C = \max_{P_x} \int DxDyP_xP_{y|x} \log_2 \frac{P_{y|x}}{\int DxP_xP_{y|x}} \quad (1)$$

over all valid input probability distributions subject to power constraint $\int dxP_x(x)|x|^2 \le S$. Here statistical properties of the channel are given by the conditional input-output probability density function (PDF) P(y|x). Thus, from the view point of the information theory there is no much difference between linear or nonlinear channels as long as PDF P(y|x) is known. Yet, the modern information theory is mostly developed for linear channels, simply because it is often technically challenging to derive P(y|x) for practical nonlinear channels. This reflects both difficulty of analysis of nonlinear systems with noise and the fact that there are varieties of nonlinear communication channels that hardly can be described by any single generic theory.

An important new feature introduced by constructive nonlinearity is a possibility of signal filtering from noise or signal regeneration. Whenever the nonlinear filter transformation has multiple fixed points, consequent interleaving the noise with nonlinear filter will produce suppression of the noise [11].

I will overview a systematic approach [14] to design of nonlinear regenerative systems with increased channel capacity. The introduced classes of nonlinear devices can be used for construction of nonlinear communication channels with capacity exceeding the Shannon capacity of the linear AWGN channel.

The support of the EPSRC project UNLOC (Unlocking the capacity of optical communications) EP/J017582/1 and the Ministry of Education and Science of the Russian Federation (grant No. 14.B25.31.0003) is acknowledged.

References

1. S. J. Savory, IEEE J. Sel. Top. Quan. El. 16, 1164 (2010).
2. A. Splett, C. Kurzke, and K. Petermann, In Proceedings of the European Conf. on Opt. Com., ECOC'93, 2, 41, (1993).
3. A. D. Ellis and J. Zhao, in *Impact of Nonlinearities on Fibre Optic Communications*, S. Kumar edt., Chapter 13, p. 507 (Springer, New York, 2011).
4. A.Mecozzi, J. Light. Techn., 12(11), 1993 (1994).
5. P. P. Mitra and J. Stark, Nature, 411, 1027 (2000).
6. E. E. Narimanov and P. P. Mitra, J. Lightw. Technol., 20(3), 530 (2002).
7. K.-P. Ho and J. M. Kahn, In Proceedings of Opt. Fibre Comm. Conf. OFC'02, ThGG85 (2002).
8. K. S. Turitsyn, S. A. Derevyanko, I. V. Yurkevich, and S. K. Turitsyn, Phys Rev. Lett. 91, 203901 (2003).
9. R.-J. Essiambre, GJ Foschini, G. Kramer, PJ Winzer, Phys Rev. Lett., 101, 163901 (2008).
10. E. Agrell, The Channel Capacity Increases with Power, http://arxiv.org/pdf/1108.0391.pdf (2011).
11. K. S. Turitsyn and S. K. Turitsyn: Nonlinear communication channels with capacity above the linear Shannon limit, *Opt. Lett*. Vol. 37. pp. 3600-3603, Sept. 2012.
12. E. Agrell and M. Karlsson: WDM Channel Capacity and its Dependence on Multichannel Adaptation Models, *in Proc. OFC/NOFC 2013*, OSA Technical Digest, OTu3B.4.
13. C. E. Shannon, "A mathematical theory of communication," Bell Syst. Tech. J., vol. 27, (1948).
14. M. Sorokina and S.K. Turitsyn, Shannon capacity of nonlinear regenerative channels, http://arxiv.org/abs/1305.1537

Measuring general relativity effects in a terrestrial lab through laser gyroscopes

N. Beverini[1,2], **J. Belfi**[1], **M. Calamai**[1,2], **G. Carelli**[1,2], **D. Cuccato**[3], **A. Di Virgilio**[2], **E. Maccioni**[1,2], **A. Ortolan**[3], **A. Porzio**[4,5], **R. Santagata**[6], **S. Solimeno**[5], **A. Tartaglia**[7]

[1] *Dipartimento di Fisica, Università di Pisa, Largo B. Pontecorvo 3, I-56127 Pisa. Italy*
[2] *INFN, sezione di Pisa, Largo B. Pontecorvo 3, I-56127 Pisa. Italye*
[3] *INFN,Laboratori di Legnaro, I-35020 Legnaro, Italy*
[4] *CNR-SPIN, Monte sant'Angelo, via Cinthia 26, Naples, Italy*
[5] *INFN, Sezione di Napoli,via Cinthia 26, Naples, Italy*
[6] *Dipartimento di Fisica, Università di Siena, via Roma 56, Siena, Italy,*
[7] *Politecnico of Torino and INFN, Torino, Italy*
E-mail: beverini@df.unipi.it

The Sagnac Effect is based on the fact that two light beams counter-propagating inside a ring complete the path with a time difference Δt, if the ring is rotating with angular velocity Ω. These gyroscopes are sensitive to the absolute (i.e. with reference to an inertial frame) angular velocity. No mechanical moving parts are present, and no couplings between longitudinal and rotational degrees of freedom, unavoidable using mechanical apparatuses. Large-size ring lasers can reach very high sensitivity and accuracy; pushing to the shot noise limit, their performance makes possible not only important measurements in the field of Geodesy, but as well General Relativity tests.

Soon after the introduction of the general theory of relativity, it was manifest that the relative motion between an observer and a massive source should produce peculiar effects on the gravitational field measured by the observer. In particular, the proper rotation of a massive source gives a dragging of the inertial frames, or Lense-Thirring (LT) effect.

Gravity-Probe B (GP-B) experiment, whose development has taken almost 40 years, consisted in a satellite, with four superconducting gyroscopes and a telescope on board, in polar orbit around the Earth, and finally detected the LT precession within 19%. Further, Ciufolini and Pavlis by a technique, based on laser ranging of the LAGEOS and LAGEOS II satellites, measured LT precession within 8% accuracy and plan to reach 1% by exploiting the LARES satellite.

An unequivocal measurement of the LT effect performed on the Earth using a laser gyro will complement what has been done so far with measurements already performed in space and will allow to shed new light on the reliability of those measurements. Optical laser gyroscopes, exploiting the Sagnac effect, equipped with super-mirrors with an extremely high reflectance (R > 99,999%) and enclosing an area larger than a few tens square meter, are able to detect and measure angular movements with an extremely high sensitivity. The 16 m^2 square G gyrolaser, located in an underground laboratory in Wettzell, Bavaria, has a resolution for rotations better than 10^{-12} rad/s, attained in approximately one hour of data taking ($\sim 4 \cdot 10^3$ s), and is at present the most accurate ring-laser in the world. It is based on a monolithic design, which uses a single block of Zerodur, a practically thermal expansion glass.

The measurement of LT effect requires an accuracy around 10^{-14} rad/s that is Earth angular velocity must be measured with accuracy of one part in 10^9. This can be achieved by increasing the gyro dimension (shot noise reduces more than quadratically with the optical cavity length), and by increasing long term stability by Kalman filtering techniques.

GINGER (Gyroscopes IN GEneral Relativity) is a INFN proposal for measuring LT effect in an Earth laboratory environment [1]. It will consist in a structure in three gyroscopes mutually orthogonal with about 6 m of side, located in a deep underground

location, possibly the Gran Sasso INFN laboratory. The triaxial structure will allow the full determination of the laboratory frame angular velocity modulus that will be compared to the angular Earth rotation rate with respect to the fixed stars frame given by IERS through VLBI in order to derive the LT effect.

The required accuracy imposes very strong constrains to the geometrical shape of each gyro and to their orthogonality. However it is possible to build an octahedral structure where each mirror is shared by two orthogonal rings, and the Fabry-Pérot cavities between the opposite mirrors are kept at identical length values by locking them to an optical frequency standard. In this configuration the deviations of the mirrors position from the wholly symmetrical configuration will give only second order contributions to inaccuracy.

The laboratory measurements will be complementary to the ones provided by space experiments in orbiting satellites that are crucially sensitive to the exact knowledge of the Earth gravitational field.

References

1. F. Bosi, G. Cella, A. Di Virgilio, A. Ortolan, A. Porzio, S. Solimeno, M. Cerdonio, J.P. Zendri, M. Allegrini, J. Belfi, N. Beverini, B. Bouhadef, G. Carelli, I. Ferrante, E. Maccioni, R. Passaquieti, F. Stefani, M.L. Ruggiero, A. Tartaglia, K.U. Schreiber, A. Gebauer, and J-P. R. Wells, Phys Rev D 84, 122002 (2011)).

Detection of ultra weak interactions with the help of nuclear spin isomers of molecules

P.L. Chapovsky

Institute of Automation and Electrometry, SB RAS,
Physics Department of Novosibirsk State University,
630090 Novosibirsk, Russia
E-mail: chapovsky@iae.nsk.su

Detection of ultra weak interaction is simplified if there is a physical phenomenon that arises solely due to the interaction under the study. For the hyperfine interactions in molecules such specific phenomenon was recently discovered. This is a conversion of nuclear spin isomers of molecules.

Nuclear spin isomers of molecules are the specific quantum states of symmetrical molecules. The well-known example is the nuclear spin isomers of the molecular hydrogen, the famous ortho- and para-hydrogen. These molecules are different by the total spin of the two hydrogen nuclei: $I = 1$ for the ortho-hydrogen (the allowed values of the molecular angular momentum are odd) and $I = 0$ for the para-hydrogen (the allowed angular momentum are even). The hydrogen isomers appears to be extremely stable having the life time nearly 1 year at the gas pressure of 1 atm and ambient temperature.

Many other symmetrical molecules have the nuclear spin isomers too. As an example, we can mention here the symmetric top molecules, CH_3F. These molecules have the ortho and para isomers different by the total spin of the three hydrogen nuclei: I=3/2 for ortho-CH_3F and I=1/2 for para-CH_3F. Another example is the asymmetric top molecules, C_2H_4. These molecules have 4 nuclear spin isomers different by the symmetry of the nuclear spin wave functions.

In order to study the isomer conversion one needs to produce the enriched gas samples. Enrichment of the hydrogen nuclear spin isomers is easily performed by deep cooling of the hydrogen gas. The enrichment is possible due to the anomalously large rotational constant of the hydrogen molecules and consequently very large energy gap between the lowest ortho and para rotational states of the hydrogen isomers. The nuclear spin isomers of hydrogen were first enriched in the late 1920s.

For the heavier molecules, e.g., CH_3F or C_2H_4, the relevant rotational level splitting is very small and isomer enrichment by cryogenic methods fails. All attempts to enrich the isomers of heavy molecules were unsuccessful for a long time. Presently, the most efficient and the most widely used method for the isomer enrichment of heavy molecules is based on the Light-Induced Drift (LID) effect. The LID effect allows to spatially separate the gas components by laser radiation. Using the LID effect, the nuclear spin isomers of a number of molecules were enriched and their conversion was studied.

The main result of these studies was the prove that the isomer conversion is governed by the specific process, named **quantum relaxation**. The isomer conversion by quantum relaxation is induced by the intramolecular hyperfine mixing of the quantum states of the nuclear spin isomers. Thus, by studying the conversion of the nuclear spin isomers one obtains an access to the intramolecular hyperfine interactions.

The mixing of the isomer states is more efficient if the rotational states of the molecule are close in energy to each other. The mixing becomes stronger if the isomer rotational level gaps are decreased, or levels are even crossed, by external electrical or magnetic fields. At the level crossings, the isomer relaxation rate is increased by a few orders of magnitude resulting in the level-crossing resonances in the isomer conversion. The level-crossing resonances are the most sensitive and efficient detection method of the intramolecular hyperfine interactions

by the isomer conversion. Our estimations predict that by using this method one can detect very weak intramolecular interactions being on the order of 10 – 100 Hz.

So far, the level-crossing resonances in the isomer conversion were used to detect the two main types of hyperfine interactions: nuclear spin-spin interactions (having the magnitude of 10 – 100 kHz) and the nuclear spin-rotation interactions (1 – 10 kHz).

In the talk we will review the investigations of the intramolecular spin-spin and spin-rotation interactions performed with the help of the conversion of the nuclear spin isomers. We will analyze also which other hyperfine interactions in molecules can be detected and studied using the conversion of nuclear spin isomers.

This work was financially supported by RFBR (projects No 12-02-01130), the Presidium of SB RAS (project No 61) and the Department of Physical Sciences of RAS, (the program "Fundamental Optical Spectroscopy and Applications").

New perspectives on the search for a parity violation effect in chiral molecules

B. Darquié[1], S.K. Tokunaga[1], F. Auguste[1], A. Shelkovnikov[1,2], P.L.T. Sow[1], S. Mejri[1], A. Goncharov[1,3], O. Lopez[1], C. Daussy[1], A. Amy-Klein[1], C. Chardonnet[1]

[1] *Laboratoire de Physique des Lasers, Université Paris 13, Sorbonne Paris Cité, CNRS, 99 Avenue Jean-Baptiste Clément, F-93430 Villetaneuse, France*
[2] *P.N. Lebedev Physics Institute, Russian Academy of Sciences, Leninsky prosp. 53, 119991 Moscow, Russia*
[3] *Institute of Laser Physics of SB RAS, Pr. Lavrentyeva 13/3, Novosibirsk, 630090 Russia*
E-mail: benoit.darquie@univ-paris13.fr

Parity violation (PV) effects have so far never been observed in chiral molecules. Originating from the weak interaction, PV should lead to a frequency difference in the rovibrational spectra of the two enantiomers of a chiral molecule. We have been working towards measuring this difference using Doppler-free two-photon Ramsey interferometry in the mid-infrared (at around 10 µm) using ultra-narrow line width CO_2 lasers referenced to atomic clocks in Paris via an optical link. We previously used this technique on a continuous supersonic molecular beam of SF_6 and demonstrated an absolute frequency measurement with an uncertainty of 2×10^{-14}. By alternating between beams of left- and right-handed molecules within a single apparatus, several systematic effects including blackbody shifts cancel. We can thus expect to reach a fractional sensitivity of around 10^{-15} (corresponding to a few tens of millihertz) on the frequency difference between enantiomers[1].

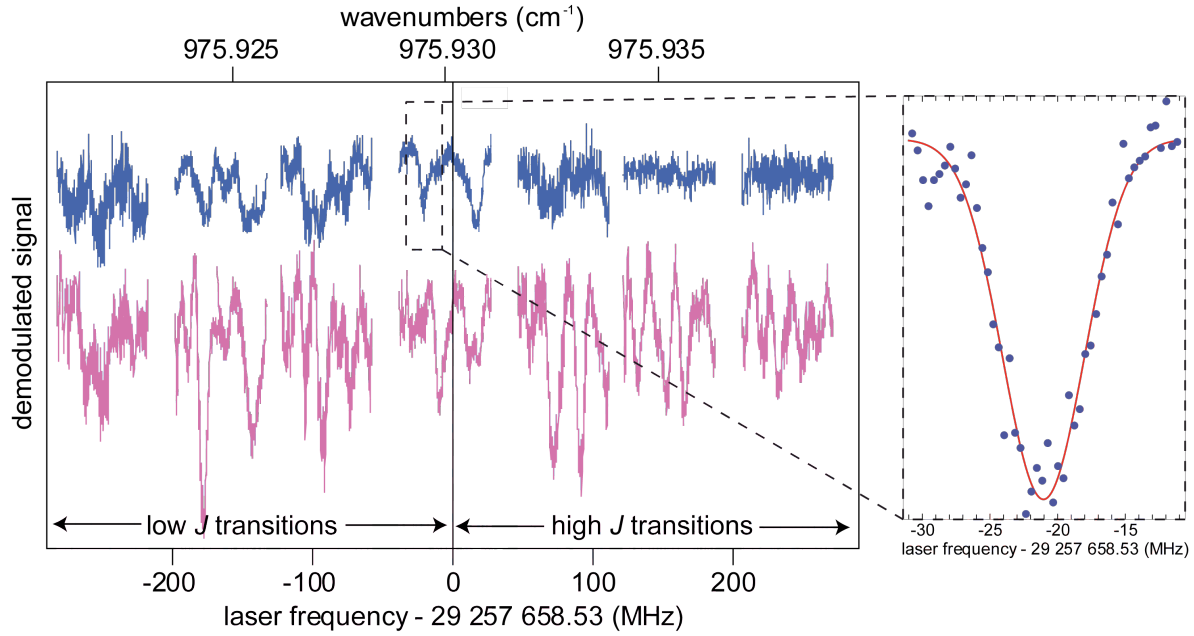

Fig.1. Linear absorption spectroscopy of a MTO-seeded supersonic jet, in the vicinity the R(20) CO_2 laser line frequency (corresponding to 0 MHz on the bottom axis). Lower pink curve: translational temperature ≥ 5 K. Upper blue curve: translational temperature ~ 1 K. The inset is a zoom on a single line (1 point every 400 kHz, 4 s of integration time per point, signal-to-noise ratio ~10).

We present the results of preliminary investigations conducted on methyltrioxorhenium (MTO), an achiral test molecule whose chiral derivatives have recently been synthesized and are estimated to have a $\sim10^{-14}$ level PV effect[2]. We report on the high-resolution spectroscopy of MTO[3], both in a cell and in a supersonic beam (Figure 1). This work has enabled us to identify several key elements of the current experiment needing improvement prior to making a PV measurement. Firstly, the current molecular beam source only yields a modest flux for

species such as MTO which are solid at room temperature. We plan to overcome this by developing a buffer gas beam source. The second is the lack of tunability of our CO_2 lasers.

The CO_2 laser's overall gain curve (roughly 100 MHz per emission line) puts constraints on species we can study. By comparison, quantum cascade lasers (QCLs) offer broad and continuous tuning[4] over several hundred gigahertz. We present our on-going work towards the replacement of the CO_2 lasers with QCLs. We conducted a careful frequency noise characterization on these new lasers. Demonstrating their potential as sources of high-resolution mid-infrared radiation, we show that the excellent spectral features of our CO_2 laser are copied to the QCL when the two are phase-locked. With a locking bandwidth of 1 MHz, we estimate our QCL's line width to be below 100 Hz, a world record as far as we know. Spectroscopic applications using this source will be reported. In particular, spectra of MTO over several GHz using our QCL source will be presented.

References

1. B. Darquié, C. Stoeffler, A. Shelkovnikov, C. Daussy, A. Amy-Klein, C. Chardonnet, S. Zrig, L. Guy, J. Crassous, P. Soulard, P. Asselin, T.R. Huet, P. Schwerdtfeger, R. Bast and T. Saue, *Chirality* **22**, 870 (2010).
2. N. Saleh, S. Zrig, L. Guy, R. Bast, T. Saue, B. Darquié and J. Crassous, *Phys. Chem. Chem. Phys.* **15**, 10952 (2013).
3. C. Stoeffler, B. Darquié, A. Shelkovnikov, C. Daussy, A. Amy-Klein, C. Chardonnet, L. Guy, J. Crassous, T.R. Huet, P. Soulard and P. Asselin, *Phys. Chem. Chem. Phys.* **13**, 854 (2011).
4. R.F. Curl, F. Capasso, C. Gmachl, A.A. Kosterev, B. McManus, R. Lewicki, M. Pusharsky, G. Wysocki and F.K. Tittel, *Chem. Phys. Lett.* **487**, 1 (2010).

Bioeffects of terahertz radiation: Possibility of biohazard

V.I. Fedorov
Institute of Laser Physics of SB RAS, ,Pr. Lavrentyeva 13/3, Novosibirsk, 630090, Russia
E-mail: vif41@mail.ru

Nonthermal low intensive terahertz radiation can be hazardous to biological systems under certain conditions as it initiates impairment of cell membrane permeability and resistance, organelle destruction, genomic instability, disturbance of cellular functional state, impairment of intercellular relationship, fall of cell viability, polymorphism,sterility, and stress. Recently application of terahertz technologies in several fields of human activity (medicine, security, food quality monitoring, military, environmental monitoring, scientific research etc) is increasing. Using these technologies associates with exposure to man as an object and service staff. But it does not pay attention to the biohazard of terahertz radiation. However, it was demonstrated in our and other laboratories that nonthermal low intensive terahertz radiation influences several bioobjects (biomolecules, cells, organisms). This influence has a dual character. Terahertz radiation initiates a cascade of physico-chemical and biochemical reactions that lead to either a positive effect or to cause different disturbances. It is depends on irradiation parameters (frequency, duration, intensity, type of THz source) and on a conditions of bioobject. Research of biohazard of terahertz radiation is not investigated properly. However, the data of investigations can raise the question of a more intensive study of terahertz biohazard. In this report the first systematization of negative bioeffects of terahertz radiation is present. Terahertz radiation in nonthermal doses induces damage at cellular level. This has a different appear.1. Impairment of membrane permeability and resistance. It was demonstrated that terahertz radiation (3.68 THz) does not influence spontaneous hemoglobin output from human red blood cells but increases hemoglobin output induced by water adding to isotonic buffer solution (hypoosmotic hemolysis). Terahertz radiation causes a pronounced shorting of duration of full hypoosmotic hemolysis of human red blood cells (3.68 THz) and decreases an osmotic membrane resistance of rat red blood cells (0.6-2.2 THz). 2. Organelle destruction. It was demonstrated that terahertz radiation (0.89 THz) induces an impairment of sheep sperm motility due to the deformation and dissociation of axial complex flagellar microtubules and disruption of mitochondrial cristae. 3. Genomic instability. It was demonstrated that terahertz radiation (0.1 THz) induces increased levels of aneuploidy and increased levels of asynchronous replication of centromeres, in human lymphocytes. It was demonstrated that in irradiated (1.5 THz) cell cultures of rat kangaroo kidney and of Chinese hamster ovary percentage of 3H-thymidine marked cells was reduced. Radiation did not induce reduction in 3H-uridine incorporation. Thus, terahertz radiation inhibits DNA synthesis. 4. Disturbance of cellular functional state. It was demonstrated that terahertz radiation (0.89 THz) induces a decrease in production of antibodies by rat spleen cells and an inhibition of migration ability of these cells in antigen presence at expressed initial level of migration. 5. Impairment of intercellular relationship. Terahertz radiation (3.68 THz) influences neuron network regeneration. Irradiation of pond snail pharyngeal ganglion neurons on the stage of connectional processes formation induces a emergence of heterogeneous cell surface and arbitrary directed process-like structures. After THz irradiation (3.68 THz) of neurons, which

have formed processes there are an alteration of growth zone and a disturbance of interneuron connection formation. 6. Fall of cell viability. It was demonstrated that terahertz radiation induces a dose-dependent fall of pond snail pharyngeal ganglion neurons (2.5 THz) and human lymphocytes (3.68 THz) viability. Besides THz irradiated (3.68 THz) human monocytes initiates a decrease in viability of nonirradiated lymphocytes. Terahertz biohazard at organism level was demonstrated by experiments on bacteria, plants, drosophilae, and mammals. THz radiation (0.89 THz) induces inhibition of mitosis, cell membrane destruction, and death of the part of bacterial cells of Shigella sonnei colony. THz influence on gene activity. After THz irradiation (3.68 THz) of Fusobacterium necrophorum colony there is an induction of leucotoxin gene with following increase of gene activity by rise of irradiation dose and besides an increase of hemagglutinin gene activity by THz radiation with following dose-dependent decrease of activity. A confirmation of THz effect on gene activity is the polymorphism of bacterial colony and an decrease of magnitude of subpopulation of some forms of Bacillus thuringiensis induced by THz radiation (3.68 THz). THz influence on plant productivity. THz exposure (2.5 and 0.67 THz) of rice seeds initiates the mutagenic effects in offspring (F2-F5) and phenotypic variations (induction of sterility, elongation of complete growing period and maturity, decrease of chlorophyll content up to albino, decrease of culm and panicle length, grain weight, grain number per panicle, grain number per plant etc, reduction of protein content). It is indicates that THz radiation induces gene expression and mutations. THz influence on fertility. THz exposure of fruit fly imago during 45 min at power 1 mW (0,89 THz) induces a rise of fertility in F1, but exposure during 1.5-2.5 hours at 2,5 and 0,67 THz at power 60 and 23 mW induced a sterility and emergence of recessive mutations. THz exposure (0.6–2.2 THz) of fruit fly females induces an impairment of the sex ratio of mature offspring F1 from 1:1 due to a decrease in total number of males. Stress and anxiety sensation. THz radiation (0.89 THz) induces typical stress reaction in laboratory rats. It is appears in activation of spleen, thymus, and adrenal glands, in increase corticosteroid hormones level in plasma, and change of proportion of lymphocytes and polynuclear neutrophils in blood. Irradiation (3.68 THz) of mouse (C57BL/6J line) induces escaping reaction and motor agitation. Anxiety sensation continues in the next day after irradiation. Irradiated animals do not drop in opened sleeves of cross-shaped labyrinth. Thus, THz radiation may be biohazarded at several conditions.

Advances in the optics and photonics in the terahertz region at the SPIN workstation of Novosibirsk free electron laser facility

B. A. Knyazev[a,b], I. A. Azarov[a,c], V. S. Cherkassky[b], Yu. Yu. Choporova[a,b], V. V. Gerasimov[a,b], Ya. V. Getmanov[a,b], E. V. Grigorieva[j], M. A. Dem'yanenko[c], D. G. Esaev[c], A. K. Kaveev[h], I. N. Kotelnikov[a,b], V. N. Kruchinin[c], M. V. Kruchinina[k], V. V. Kubarev[a,b], G. N. Kulipanov[a], S. N. Makarov[b,i], M. S. Mitkov[a,b,m], L. A. Mostovich[j], A. K. Nikitin[b,d], P. A. Nikitin[e], I. G. Palchikova[b,i], V. S. Pavelyev[f], D. G. Rodionov[a,b,m], S. V. Rykhlitsky[c], T. V. Salikova[a], M. A. Scheglov[a], O. A. Shevchenko[a], V. A. Shvets[b,c], S. S. Serednyakov[a], D. A. Skorokhod[a,b], M. F. Stupak[b,i], N. A. Vinokurov[a,b], M. G. Vlasenko[a,b], B.O. Volodkin[g], V. B Voloshinov[e], M. A. Zavyalova[b,i], G. N. Zhizhin[d]

[a] Budker Institute of Nuclear Physics SB RAS, Novosibirsk, 630090, Russia
[b] Novosibirsk State University, Novosibirsk, 630090, Russia
[c] Rzhanov Institute of Semiconductor Physics SB RAS, Novosibirsk, 630090, Russia
[d] Scientific and Technological Center for Unique Instrumentation RAS, 117342 Moscow, Russia
[e] Lomonosov Moscow State University, Moscow, 119991, Russia
[f] Image Processing Systems Institute RAS, Samara, 443001, Russia
[g] Samara State Aerospace University, Samara, 443086, Russia
[h] TYDEX, J. S. Co, St. Peterburg, 194292, Russia
[i] Technological Design Institute of Scientific Instrument Engineering (TDISIE) SB RAS, Novosibirsk, 630090, Russia
[j] Institute of Molecular Biology and Biophysics, SB RAMS, Novosibirsk, 630117, Russia
[k] Institute of Internal Medicine, SB RAMS, Novosibirsk, 630017, Russia
[m] Novosibirsk State Technical University, Novosibirsk, 630092, Russia

Novosibirsk free electron laser (NovoFEL), based on an energy recovery linac, was commissioned in 2003. The first stage, consisting of a one-turn track and a laser resonator, has been operating for users in the far infrared (110 – 240 μm) region from 2004. Nowadays, a four-turn accelerator system has been assembled; radiation from the second laser resonator (40 – 80 μm) is available to users; the third laser resonator (5 – 20 μm) is under commissioning. Investigators from about twenty research institutions, universities and high-tech companies are carrying out experiments in the fields of physics, chemistry, biology, medicine, and technology at six user stations.

One of the user stations, the SPIN station, was first destined for optics and spectroscopy studies. Until recently, the terahertz (THz) region was "a blank spot" in the spectrum, and the researchers had to design or adapt optical elements for performance in this range, as well as to examine peculiarities of operation of optical systems at such wavelengths. It was found that, owing to the multiple-beam interference effect, thin polypropylene films appeared to be optimal beam splitters in quasi-optic systems, whereas, because of the high power of the FEL beam, commercially available refractive TPX lenses are often damaged, and application of diffractive optical elements becomes necessary. Hot-pressed 0.8-mm thick polypropylene kinoform lenses with a large numerical aperture have been designed and used in many quasi-optical systems. Four binary high-resistivity-silicon diffractive optical elements (DOE) with antireflection layers designed to focus Gaussian beam into arbitrary curves or volumes ("focusators") (a binary Fresnel lens, a beam splitter, and focusators into a square and into a needle) have demonstrated rather high diffraction efficiency and resistivity to THz radiation.

Great attention has been paid to the development of devices for imaging of terahertz radiation. A thermal sensitive luminescent plate was applied as a wide-field terahertz imager,

in particular, to recording of terahertz holograms. A thermal sensitive glass-plate Fizeau interferometer was applied to both imaging of intense radiation and absolute measurement of radiation power. A 360x240 microbolometer focal plane array (MBFPA), first designed for mid-infrared radiation, was adapted to terahertz imaging in real time with a NEP of $3.8 \cdot 10^{-9}$ $W/Hz^{1/2}$ and a maximum dynamic range of up to 4000. A record repetition rate of 90 fps was achieved in experiments on detection of metal and dielectric objects, including hidden ones. These imagers also enabled conduction of a series of experiments on terahertz speckle metrology. With FEL radiation and the MBFPA, the Talbot effect in the terahertz range has been first demonstrated and applied to the measurement of distances, radiation wavelength and wavefront curvature and detection of optical inhomogeneities. It was shown that the Talbot interference pattern remains even if the diameter of openings in the 2D array is reduced to the wavelength.

Surface diagnostics and optical communication are also a practical implementation of terahertz devices. Surface plasmon polaritons (SPPs) are widely exploited in these applications. In contrast to the visible spectral range with a very short length of SPP propagation, the experimentally measured propagation lengths of THz SPPs appeared to be macroscopic. THz plasmons can be used for thin layer detection and for information transmission in integrated optical systems. We thoroughly studied THz SPP formation, transport and diffraction at edges. In the latter case, the emerging radiation was found to be highly directional, which can be employed for remote probing, for instance. Surface plasmon characteristics are very sensitive to surface conditions and enable sensing of even sub-micron scale films. Another technique, which is now under development at the user station, involves a terahertz ellipsometer.

Terahertz spectroscopy is a subject of special interest in biomedicine, chemistry and material science. FEL radiation is monochromatic, but, in contrast to other lasers, it can be continuously tuned within a wide spectral range. This feature enables developing spectroscopy techniques that require neither dispersion elements nor inverse Fourier transform processing. The advantage of high throughput is automatically applied to the FEL-based spectrometer. Since most substances of practical interest strongly absorb THz radiation, the absorption spectroscopy is often inapplicable in this region. For this reason, we have developed and implemented an imaging attenuated total reflection (ATR) spectrometer. It was applied to examination of numerous biologically important molecules. It is well known that enantiometry is an essential feature of such molecules. In particular, polysaccharide enantiomers can be used as markers of cancer risk. A Michelson-interferometer-based polarimeter with a movable mirror and ATR module has been developed and applied to study of enantiomers. Terahertz spectroscopy and ellipsometry were also used in the experiments on diffuse liver disease diagnostics via erythrocyte examination.

Among other current studies we could mention the acousto-optic experiments and the development of a near-field terahertz microscope.

High power all-solid-state laser and its application

X. C. Lin

Laboratory of All-solid-state Light Sources, Institute of Semiconductors, Chinese Academy of Sciences, Beijing, 100083, China.
Tel. 0086-18610566218, e-mail: xclin@semi.ac.cn

Using master oscillator power-amplifier, we successfully realized 7.13 kW high power laser with instability of ±0.98% within 8 hours. Fiber-coupled output power of 6.82 kW with coupling efficiency 95.1% was achieved. Using orthogonal placed two acousto-optic modulators, 1 kW Q-switched laser with repetition rate of 20 kHz was obtained.

Laser-induced synthesis in liquids, solids, liquid-solid interfaces

A.Manshina[1], A. Povolotskiy[1], A. Povolotskaya[1], M. Bashouti[2], M. Dubov[3]

[1] Chemical faculty, St.Petersburg State University, St.Petersburg, Russia
[2] Max-Plank institute for the science of light, Erlangen, Germany
[3] Photonics Research Group, Aston University, Birmingham, UK
E-mail: manshina@chem.spbu.ru

The appropriate choice of laser parameters can provide initiation of specific channels of matter transformation resulting in creation of new materials and structures. That is why laser-induced synthesis is considered now to be the most inquiring approach allowing realization of non-equilibrium substance state followed by peculiar routes of matter formation/reconstruction. The significant interest in this field is also stimulated by possibility to initiate nano- and micro-scale effects and as a result to carry out highly efficient bottom-up synthesis of nanomaterials. It should be noted that such approach can be applied for any media and systems, for example liquids, solids and liquid-solid interfaces.

The direct laser effect on liquid media is a new way to generate colloidal suspensions of nanoparticles. In this case laser focal volume acts as a chemical reactor localizing the process area and the amount of reacting substance (spatial localization), whereas duration of laser pulse can provide the temporal localization. The specific conditions in chemical reactor (focal volume) generate the optical breakdown of the medium (liquid phase with peculiar chemical composition) followed by the production of highly charged ions succeeded by formation of various particles and structures.

Laser irradiation of liquid-solid interfaces allows creation of localized coatings and structures with specified parameters (structure, composition, morphology) on the substrate surface. From the chemical viewpoint the deposition process includes chemical reduction of metal ions initiated by the laser irradiation. The deposition process can be divided into three main stages: 1) surface activation by the laser irradiation; 2) initial metal ion reduction onto active sites of the surface; 3) autocatalytic reduction processes to yield bulk metal phase.

Our latest experiments demonstrated possibility of deposition of different structures like nanoparticles, flakes (mono-crystalline structures) and stars (poly-crystalline structures). It should be mentioned that the indicated structures consist of heterometallic Au-Ag nanoparticles (3-5 nm) incorporated into the carbon matrix (amorphous in case of nanoparticles or crystalline – for flakes and stars). Variation of experimental parameters provides directed control of the deposits morphology. Figure 1 shows examples of deposited structures.

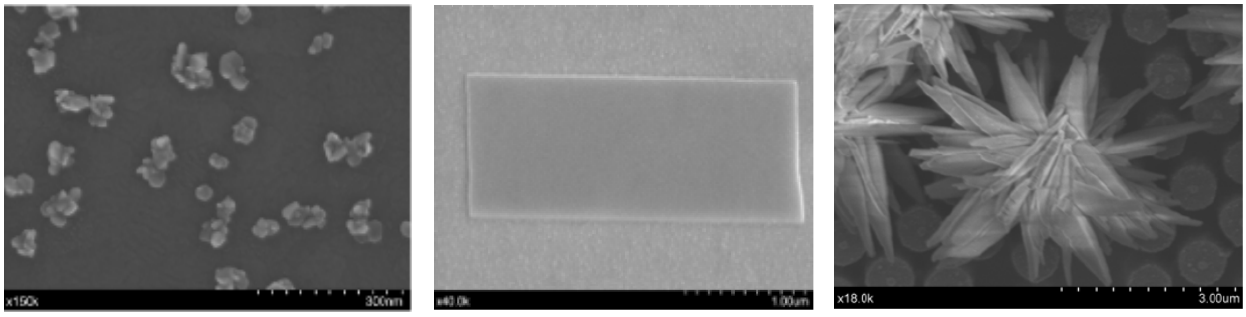

nanoparticles *flakes* *stars*

Fig. 1. Microphotos of deposited nanostructures

Preliminary studies of our deposited structures demonstrated their plasmon activity: surface-enhanced luminescence, surface-enhanced Raman scattering, surface-enhanced photovoltaic properties.

Femtosecond laser writing in bulk solids is another technique allowing formation of functional elements like waveguides, splitters, gratings, etc. for optical signals manipulation. The method is based on focusing fs laser radiation inside the bulk of a transparent material. The intensity in the focal volume may become high enough to cause nonlinear absorption, which leads to localized plasma formation, followed by the structure modification in the focal volume. This laser-induced structure modification results in the optical parameters change (refractive index, absorption coefficient), which allows creation phase- or amplitude-type elements in a one step process. Typically such technique allows one to obtain refractive index change about $10^{-4} – 10^{-3}$.

Our experiments have demonstrated that achievement of high refractive index contrast up to 10^{-2} can be based on laser induced alternation of local chemical composition of the optical material caused by chemical elements diffusion. Change of chemical composition can result in much stronger optical parameters variation in comparison with case of chemical structure reorganization. Local diffusion of ions in bulk glass may be induced by laser heating of the material, at that the diffusion length and rate are determined by temperature gradient, time of treatment and nature of chemical species. As these parameters can be controlled (by fixing/optimization of laser power, sample translation rate and glass chemical composition), laser induced element/ion diffusion can be considered as an efficient way to create high contrast optical phase elements.

Study of potassium titanyl phosphate nonlinear optical crystals by the method of wideband terahertz spectroscopy

V.D. Antsygin[1], **A.A. Mamrashev**[1, 2], **N.A. Nikolaev**[1], **O.I. Potaturkin**[1, 2]

[1] *Institute of Automation and Electrometry, SB RAS, Academician Koptug ave. 1, Novosibirsk, 630090 Russia*
[2] *Novosibirsk State University, 2 Pirogova str., Novosibirsk, 630090 Russia*
e-mail: potaturkin@iae.nsk.su

The development of terahertz (THz) spectrometers with high efficiency of generation and detection of terahertz radiation is essential for a wide spreading of terahertz diagnostic methods. One of the most promising approaches in terahertz spectroscopy is conversion of femtosecond laser pulses to wideband terahertz radiation on the surface of semiconductors. It is due to its high efficiency, compactness and simplicity. Its usage widens the dynamic range of the spectrometers and allows gathering information on the terahertz properties of nonlinear materials.

We present the results of a comparison of terahertz emission power from the surface of InSb, InAs, and GaAs pumped with the radiation of the first (1550 nm) and the second (775 nm) harmonics of an Er-doped fiber laser with pulse duration of 100 fs. The generation of terahertz radiation from the surface of *p*-InAs proved to be much more efficient in terms of power than in GaAs and InSb at both wavelengths of 775 nm and 1550 nm (fig. 1).

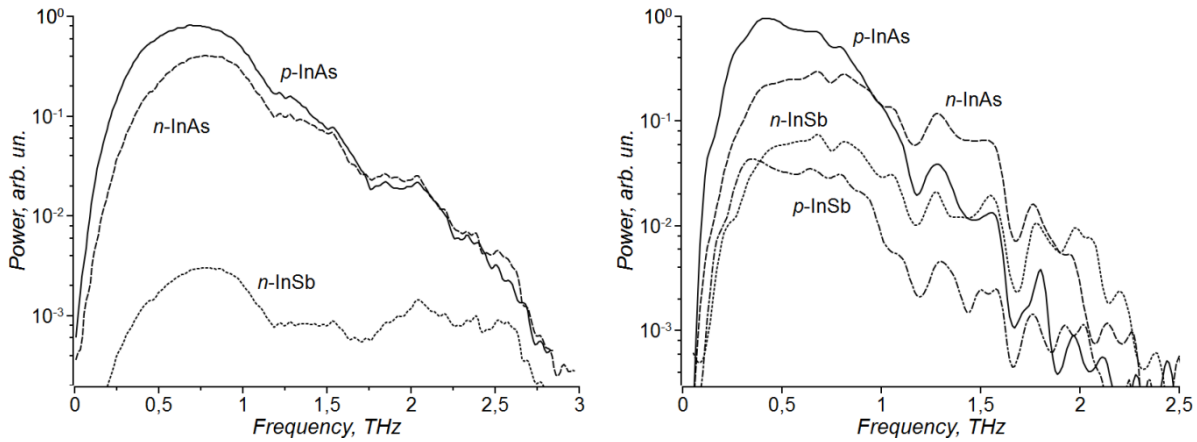

Fig. 1. Power spectra of terahertz pulses generated from the surface of different semiconductors pumped by 775 nm (left) and 1550 nm (right) laser.

However terahertz emission intensity can be further increased by placing the semiconductor into a magnetic field which is explained by rotation of electrical vector of photo-Dember field [1]. In our setup, the magnetic field was of the order of 1 T. The terahertz emission power under these conditions increases up to 3 and 10 times in InAs pumped at 775 and 1550 nm correspondently. In case of InSb pumped at 1550 nm the efficiency increases up to two orders of magnitude.

We designed a Time-domain terahertz spectrometer based on the studies described above [2]. It allowed us to investigate the properties of high-resistance and low-resistance potassium titanyl phosphate (KTP) crystals in terahertz spectral range at different temperatures.

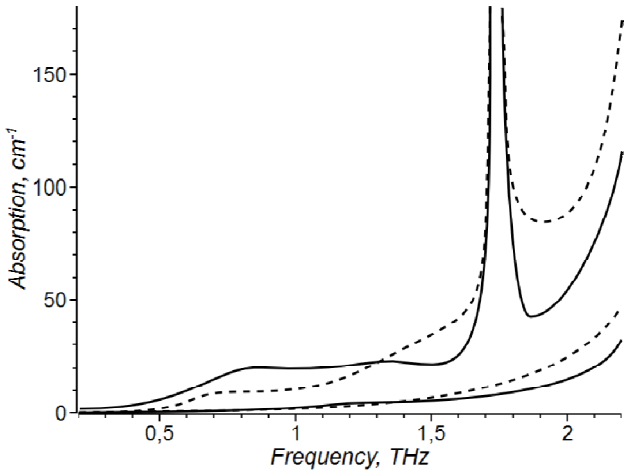

Fig. 2. The absorption spectrum of Z (two upper curves) and X (two lower curves) axis of high-resistance (solid curve) and low-resistance (dashed curve) KTP crystals at 80 K.

The KTP crystals are widely used in optics, particularly as electrooptic modulators. Such application fundamentally depends on the electrical conductivity of crystals. We studied the influence of conductivity on absorption in the terahertz spectral range. The Lorenz approximation of the experimental results is presented in Figure 2. It is shown that an increase in electrical conductivity leads to the broadening of the eigenmodes near 1.75 and 3 THz.

References

1. G. Klatt et al., *App. Phys. Let.* **98**, 021114 (2011)
2. V.D. Antsygin et al. *Optoelectronics, Instrumentation and Data Processing*. 46, 294 (2010)

Development and creation of pulsed UV lasers for medical applications in ophthalmology

A. M. Razhev

Institute of laser physics SB RAS, Ac. Lavrentyev's prosp., 13/3, Novosibirsk, 630090 Russia
Novosibirsk state university, Pirogova str., 2, Novosibirsk, 630090 Russia
Tel. +7(383) 330-62-14
E-mail: razhev@laser.nsc.ru

In the report the most wide-spread in ophthalmology diseases like anomalies of eye refraction (myopia, hyperopia, astigmatism, simplex herpes virus, open-angle glaucoma) are considered. Results of experimental investigations of interaction of high-power pulsed UV laser radiation with human eye tissues (cornea, sclera and eye-lens) are described. Possibilities of the creation of new laser methods of treatment of eye diseases are studied.

In the present work the development and creation of pulsed UV lasers with wavelengths of 193 nm, 223 nm, 248 nm, 308 nm, 353 nm and using of these lasers in medical systems for applications in ophthalmology are reported. Constructions and conformations of medical systems with wavelengths of 193 nm and 223 nm for correction of anomalies of eye refraction are described.

Fig. 1. UV ophthalmic laser complex "Medilex™"

Results of treatment of simplex herpes virus on eye cornea with laser radiation at λ = 223 nm and λ = 248 nm are presented. The high efficiency of laser method of treatment is demonstrated. Results of experimental investigations of treatment of open-angle glaucoma by laser methods using lasers with wavelengths of 248 nm, 308 nm, and 353 nm are described. Advantages of laser methods comparing with traditional mechanic methods are shown.

Fig. 2. UV laser complex "ExciLight™" for medical applications

Usage of pulsed UV laser radiation in medicine technologies is contactless, bactericidal, high-effective harmless method. It allows not only increase quality of treatment but significantly cut the recovery time. As result in Institute of laser physics SB RAS number of UV laser ophthalmic systems "Medilex™" has been developed. These systems successfully have been used during number of years in The S.N. Fyodorov FSI IRTC "Eye Microsurgery", Novosibirsk Division. Most of results are novel and have been achieved for the first time.

Low frequency signals of large scale GW-interferometers

A. V.Gusev[1], V. N.Rudenko[1], I. S.Yudin[1,2]

[1]Sternberg Astronomical Institute , Lomonosov Moscow State University
[2] Institute of Laser Physics of SB RAS, Pr. Lavrentyeva 13/3, Novosibirsk, 630090 Russia

Recently several long base laser interferometers with a few km scale were constructed and put in scientific operation with the principal goal of detecting a gravity purturbation associated with gravitational radiation of extraterrestrial nature [1,2]. As the physical devices these instruments present gravity gradiometers measuring some specific tensor gravity field structure (so called "tidal type" field) carried by gravitational waves. The maximum sensitivity belongs to the frequency range $10^{-22} Hz^{-1/2}$ were the spectral noise density defined mainly by the optical shot noise achieves $10^{-22} Hz^{-1/2}$ in term of metric perturbations.

During the more successful scientific runs it was detected that these instruments can react also at very slow tidal variations of the gravity potential at the earth surface. Correspondent signal at the interferometer appears as amplitude modulation of different harmonics at wide frequency range. The mechanism of arising of such signals is not completely clear at present time so as the interferometer mirrors keep fixed position during its operation due to feedback circuits providing the interference condition. In our talk we consider several explanation of this phenomenon with calculation of expected value the relativistic effect of direct gravity-optical interaction.

This phenomenon was first observed in the LIGO antenna [3]. Configuration of LIGO anntenas is a Michelson interferometer with Fabry-Perot cavity in the arms, for increasing an effective optical length. In a study noise properties of the output signal near FP-cavity free spectral range the low frequency noise variance was calculeted. In the paper [3}the nature of this phenomenon was considered as the "redshif" effect in the tidal gravitational field. However it was proved [4] that redshift can not be the reason of the observed effect. We have studied the mechanism associated with the relativistic gravity change in the optical refractive index.. But also estimates have shown the deficit of such effect more then 3 orders of magnitude compare with the observed one. It was necessary to abandon the assumption of fixed mirrors and consider the observed signal as a residual effect of tidal deformation [5]. The model of residual arm deformation below the mirror position control accuracy of 10^{-10} cm [2] provided a good agreement with the observed value [3]. Although in the low frequency region interferometer can be considered as a strain meter its signal at free spectral range frequency is too small due to the noise illumination of neighbors modes of arm FP cavities. We propose some new configuration of the GW interferometer with two mode laser pump to increase the signal-to-noise ratio for geophysical signal at the main interferometer output.

Geophysical signals were found also in VIRGO setup [6] in a process of search for GW radiation from Vela pulsar at a frequency close to 22 Hz. It appears as a modulation of the noise variance near this frequency. A further analysis showed that such modulation took place at all output harmonics in the range (10-1000 Hz). We have proposed an explanation for this phenomenon [7]. as a parametric mechanism of optical resonance frequencies modulation by

geophysical low frequency perturbations. The effect exists even with monochromatic pump does not require illumination of neighbors modes.

Further work will be devoted to a more detailed study of the possibility of using large scale interferometers as complex geophysical instruments.

References

1. Acernese, F. et al. Status of Virgo. //Class. Quantum Grav. 25, 114045 (2008)
2. Abbott, B. P. et al. LIGO: the Laser Interferometer Gravitational-Wave Observatory. Rep. //Prog. Phys. 72, 076901 (2009)
3. Meliessinos A.,(Talk at MG-12 Paris, July 12-18, (2009) http://xxx.lanl.gov/PS, cache/arxiv/pdf/1001/1001.558 v.2.pdf.)
4. Гусев А.В., Руденко В.Н.. Гравитационная модуляция оптической длины большебазовых лазерных интерферометров., Письма в ЖЭТФ, т.91, в.10, с.543 – 547, 2010
5. Гусев А.В., Руденко В.Н., Юдин И.С. Регистрация медленных геофизических возмущений на гравитационно-волновых интерферометрах. Измерительная техника, № 10, с
6. Sabrina D'Antonio, Pia Astone, Sergio Frasca, Cristiano Palomba, Alberto Colla, Noise Sidereal Analysis, talk given at Orsay LSC-Virgo meeting, June 2011
7. А.В.Гусев, И.С.Юдин. Локально-оптимальный алгоритм обнаружения слабых геофизических сигналов на выходе лазерных гравитационных антенн. ВМУ Серия 3. Физика и астрономия 2012г, No3.

Terahertz optics in biology and nanotechnology

A.V. Borodin[1], M.M. Nazarov[2], A.P. Shkurinov[1]

[1] Department of Physics, Lomonosov Moscow State University, Moscow, Russia.
[2] Institute on laser and Information Technologies of the Russian Academy of Sciences, Shatura, Moscow region, Russia.
E-mail: alexandershk@bk.ru

Terahertz time-domain spectroscopy (THz-TDS) [1] has revealed the extraordinary sensitivity to crystalline order [2], temperature of the sample [3] and the conformational form of the molecule [4]. In molecular crystals the assignment is complicated, for instance, by the presence of both internal and external modes (vibrations within molecules and intermolecular ones). There have been numerous attempts to distinguish the signature of external and internal modes in the THz spectra of various molecular crystals by comparing the spectra of samples with similar crystalline structures, by analyzing temperature dynamics of the spectra or by comparing the experimental data with simulations of an isolated molecule.

In the present paper we aim at studies of the influence of changes of intermolecular bonding in molecular crystals on those of vibrational spectra by means of THz-TDS and Raman spectroscopy on the example of several biological molecular systems. The studied molecular crystals are related to the weakly associated solid-state systems where most intermolecular interactions are dominated by Van der Waals and hydrogen forces. Modeling of these systems with the DFT calculations using standard quantum chemical packages (e.g. Gaussian 03) in general allows one to identify internal vibrational modes of isolates molecules that in some types of molecular crystals permits quality interpretation of low frequency spectra.

We present the review of the recent results on the interaction of terahertz radiation with the complex biological molecular systems and nanostructures. The influence of the radiation on the fictional activity of enzymes is also discussed. A sufficient part of the lecture will be directed to the discussion of the prospect of the THz diagnostics of biopolymers.

We also discuss the study the dielectric properties of nanodispersed materials, such as nanostructured aluminum oxyhydroxides (NOA) and their modification by surface silica (NOAM) in terahertz (THz) frequency range. We discuss the structural sensitive spectra if we change of the material's annealing temperatures and their chemical composition.

[1] E. B. Wilson, P. C. Cross, J. C. Decius, Dover publ., New York, 1955.
[2] M. Walther, B. M. Fischer, P. Uhd Jepsen, Chem. Phys. 288 (2003) 261-268.
[3] Y. Yomogida, Y. Sato, R. Nozaki, T. Mishina, J. Nakahara, J. Mol. Struct. 981 (2010)173-178.
[4] I.N. Smirnova, A. Cuisset, F. Hindle, G. Mouret, R. Bocquet, O. Pirali, P. Roy, J. Phys. Chem. B 114 (2010) 16936–16947.

Electro-optic sampling detection of THz pulsed radiation based on Cherenkov phase-matching

M. Tani[1], T. Kinoshita[1], T. Nagase[1], S. Ozawa[1], S. Azuma[1], S. Tsuzuki[1], D. Takeshima[1], T. Joja[1], A. Iawamae[1], S. Funkner[1], G. Niehues[1], E. Estacio[2], K. Kurihara[3], K. Yamamoto[1], M. Bakunov[3]

[1] *Research Center for Development of Far-Infrared Region, University of Fukui, 3-9-1 Bunkyo, Fukui 910-8507, Japan*
[2] *University of Philippines Diliman, 1101 Philippines*
[3] *Faculty of Education and Regional Stduies, Uiversity of Fukui, 3-9-1 Bunkyo, Fukui 910-8507, Japan*
[4] *University of Nizhny Novgorod, 603950, Russia*
E-mail: tani@fir.u-fukui.ac.jp

Cherenkov radiation mechanism is an established technique to achieve phase matching between ultrashort optical pulses and terahertz (THz) waves having a large collinear velocity mismatch, in a nonlinear optical material such as $LiNbO_3$ (LN). Phase matching is achieved with the optical and THz pulses propagating at an angle with respect to each other. Recently, we have experimentally demonstrated that Cherenkov phase matching mechanism can also be used for efficient electro-optics (EO) sampling of broadband THz pulses [1]. When we use a Si coupling prism, the Cherenkov phase-matching condition is determined by the ratio of the group index of the EO crystal at the sampling optical wavelength, n_g^{LN}, and the refractive index of Si in the THz frequency region, n_{THz}^{Si}:

$$\sin\alpha = n_g^{LN} / n_{THz}^{Si} \quad (1)$$

Here α is the apex angle of the coupling Si prism. Figure 1 shows THz waveforms detected with an LN crystal coupled to a Si prism (Si-prism/LN). The Cherenkov phase-matched EO sampling was achieved at optical sampling wavelengths of 780 nm and 1.55 μm using the same Si-prism/LN. For comparison, the THz waveform detected with a standard collinear EO sampling scheme using a 4-mm thick ZnTe crystal is also shown. The results indicate that by using a Si-prism/LN, we can obtain an EO signal comparable in magnitude to that obtained by standard, ZnTe-based collinear EO sampling. It must be noted that this EO sampling's sensitivity at 1.55 μm is about half of that at 780 nm, as expected from the wavelength dependence of the EO signal.

In a standard EO sampling scheme, a phase retardation of the sampling optical wave induced by a THz electric field is detected as a change of polarization. Because of this, polarization optics, such as a quarter wave-plates and polarizing beam splitters are necessary in standard EO sampling to enable polarization-sensitive detection. In addition, if a birefringent EO crystal (such as LN) is used, the EO sampling optics become more complicated due to the additional optics to compensate for the intrinsic birefringence of the EO crystal. Recently, we have proposed and demonstrated a new EO sampling scheme, where the intensity modulation of the optical sampling beam is directly detected without utilizing any polarization-sensitive optics [2]. In this "heterodyne EO sampling" scheme, the modulation of the sampling optical beam intensity is achieved through the interference of the sampling optical wave and the sum frequency generation (SFG) or difference frequency generation (DFG) arising from its interaction with the incident THz radiation. Thus, the detection optics needed to implement heterodyne EO sampling is significantly simpler compared with ordinary EO sampling. Figure 2 shows a comparison of the THz waveforms detected using the heterodyne EO sampling and ordinary EO sampling by using the same Si-prism/LN device. The sensitivity of the heterodyne EO sampling is comparable to that of the ordinary EO sampling.

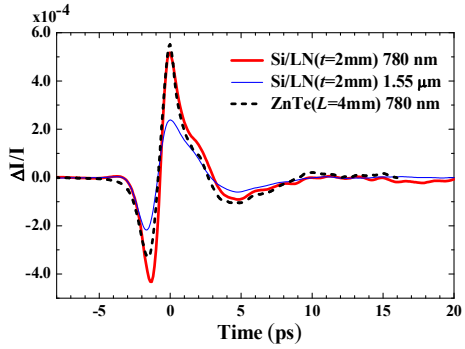

Fig. 1. THz waveform detected with Si-prism/LN in Cherenkov phase-matching scheme at 780 nm and 1.55 □m. For comparison, THz waveform detected with a 4-mm ZnTe is also shown.

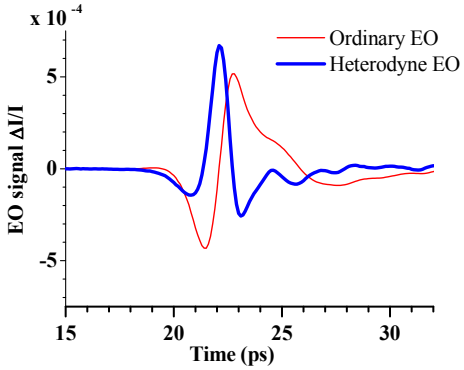

Fig. 2. THz waveforms detected with heterodyne and ordinary EO sampling.

The detection sensitivity of an EO crystal is limited by its EO coefficient r_{ij}. In the materials science aspect, however, it is difficult to control these material properties. Therefore, to enhance the EO sampling signal, it is necessary to tightly focus the THz beam onto the EO crystal. Due to the diffraction limit, however, it is not possible to focus the THz wave to an area smaller than its wavelength. To overcome this fundamental limit and to enhance the THz field, we use a tapered metallic parallel plate (V-groove) waveguide to focus THz waves at an area much smaller than the wavelength via a super-focusing effect. We used a parallel plate waveguide illustrated in Fig.3. The tapered parallel plates (taper angle = 10 degrees) focused the incident THz wave onto a parallel plate waveguide, wherein a thin Si plate (thickness D = 0.1 mm) was inserted. The end of the parallel plate waveguide and the Si plate were cut at an angle to achieve the Cherenkov phase matching condition between the sampling optical pulse and the THz wave in a LN crystal attached to the end face of the parallel plate waveguide. The THz waves were generated by a photoconductive dipole antenna. The heterodyne EO sampling signal was detected using a photodetector. The THz waveforms detected with the V-groove waveguide structure in conjunction with a LN crystal in the heterodyne EO sampling are shown in Fig. 4. The waveforms are compared with signals detected without using the metallic waveguide structure and an enhancement factor of 10 times was observed. The signal was further enhanced by using a thinner (40 μm-thick) LN crystal and the enhancement was about 20 times compared with the signal levels taken without using the metallic waveguide structure.

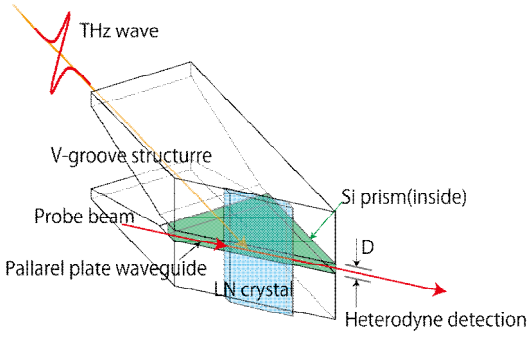

Fig. 3. Metallic, V-groove, waveguide structure to enhance EO sampling signal.

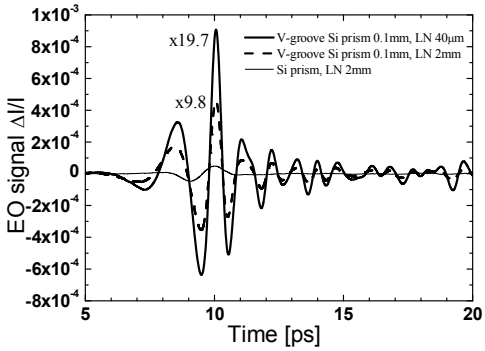

Fig. 4. THz waveforms with and without the parallel plate waveguide.

References

1. M. Tani, K. Horita, T. Kinoshita, Ch. T. Que, E. Estacio, K. Yamamoto, and M. I. Bakunov, *Opt. Express*, **19**, 19901 (2011).
2. M. Tani, T. Kinoshita, T. Nagase, K. Horita, Ch. T. Que, E. Estacio, K. Yamamoto, and M I. Bakunov, *Optics Express*, **21**, 277 (2013).

Atomic magnetometery based on coherent population trapping effect excited with polarization modulated light

E. Breschi[1], Z. Grujic[1], P. Knowles[1], A. Weis[1]

[1] *Department of Physics, University of Fribourg, Switzerland*
E-mail: evelina.breschi@unifr.ch

Atomic magnetometry is attractive for both fundamental and applied research, and, in the past 10 years several review articles have been devoted to this subject [1, 2]. In particular, many efforts are oriented to the development of so-called magnetically silent magnetometers as an interesting alternative to standard optical-rf double-resonance magnetometers. Magnetically silent magnetometers operate by resonant modulation of a light beam parameter, either amplitude, frequency, or polarization. The main advantage in the approach is that not rf magnetic field is applied to the atoms, then the magnetic perturbations of the environment to be measured are reduced.

We report on magneto-optical spectroscopy using polarization modulation of light that is resonant with the $F_g=4 \rightarrow F_e=3$ transition of the cesium D_1 line. The light polarization is square wave modulated between left- and right-circular polarizations, and, a transverse (i.e., orthogonal to the laser propagation vector) magnetic field is applied to the atoms. When either the transverse magnetic field or the modulation frequency is varied, we observe a rich spectrum of resonances occurring if $m \cdot \omega_L = \omega_{mod}$ (or $\omega_L = m \cdot \omega_{mod}$) where ω_{mod} is the polarization modulation frequency (varied between 100 Hz and 10 kHz), and ω_L is the Larmor frequency. The amplitudes of the different resonances harmonics have an oscillatory dependence on the modulation duty cycle, η [3, 4]. Figure 1 shows the relative amplitudes of the absorptive and dispersive part of the lock-in signal for the resonance at the first harmonic of the spectrum, i.e., $\omega_L = \omega_{mod}$, as a function of the modulation duty cycle, η. We have performed the detection at different harmonics of ω_{mod}, e.g., from the 1st (upper line in fig. 1) to the 6th (bottom line in fig. 1). The relative amplitude plotted here is defined by the resonance normalized with respect to the resonance at $\eta=0.5$ detected at the 2nd harmonic. Black dots and red lines of Fig. 1 represent experimental and model results, respectively. When $\eta=0.5$, the interaction scheme is analogous to push-pull optical pumping, which has been used to increase the contrast in the hyperfine clock resonance [5]. The original push-pull technique refers to the populations of atomic sublevels being migrated to selected sub-levels by the resonant interaction with laser radiation whose polarization is modulated between left- and right- circular polarization at the clock frequency. The fundamental concept behind push-pull is to drive a resonance with modulated light, whose modulation is phase-coherent with the harmonic evolution of the atomic quantum state. The dispersive part of the lock-in signal can be used as a reference signal for magnetic field measurements. We evaluate the push-pull magnetometer performance by measuring the noise-equivalent-magnetic field (NEM). The estimated shot-noise-limited NEM is 20 $fT/Hz^{1/2}$. The status of magnetometer performance will be presented.

References

1. D. Budker, W. Gawlik, D. F. Kimball, S. M. Rochester, V. V. Yashchuk, and A. Weis, *Rev. Mod. Phys.* **74,** 1153 (2002)
2. D. Budker and M. V. Romalis, *Nat. Phys.* **3** 227, (2007).
3. I. Fescenko, P. Knowles, A. Weis, and E. Breschi, submitted to Optics Express, (2013).
4. Z. Grujic, and A. Weis, submitted to Phys. Rev. A, (2013).
5. Y.-Y. Jau, E. Miron, A. B. Post, N. N. Kuzma, and W. Happer, *Phys. Rev. Lett.* **93** 160802, (2004).

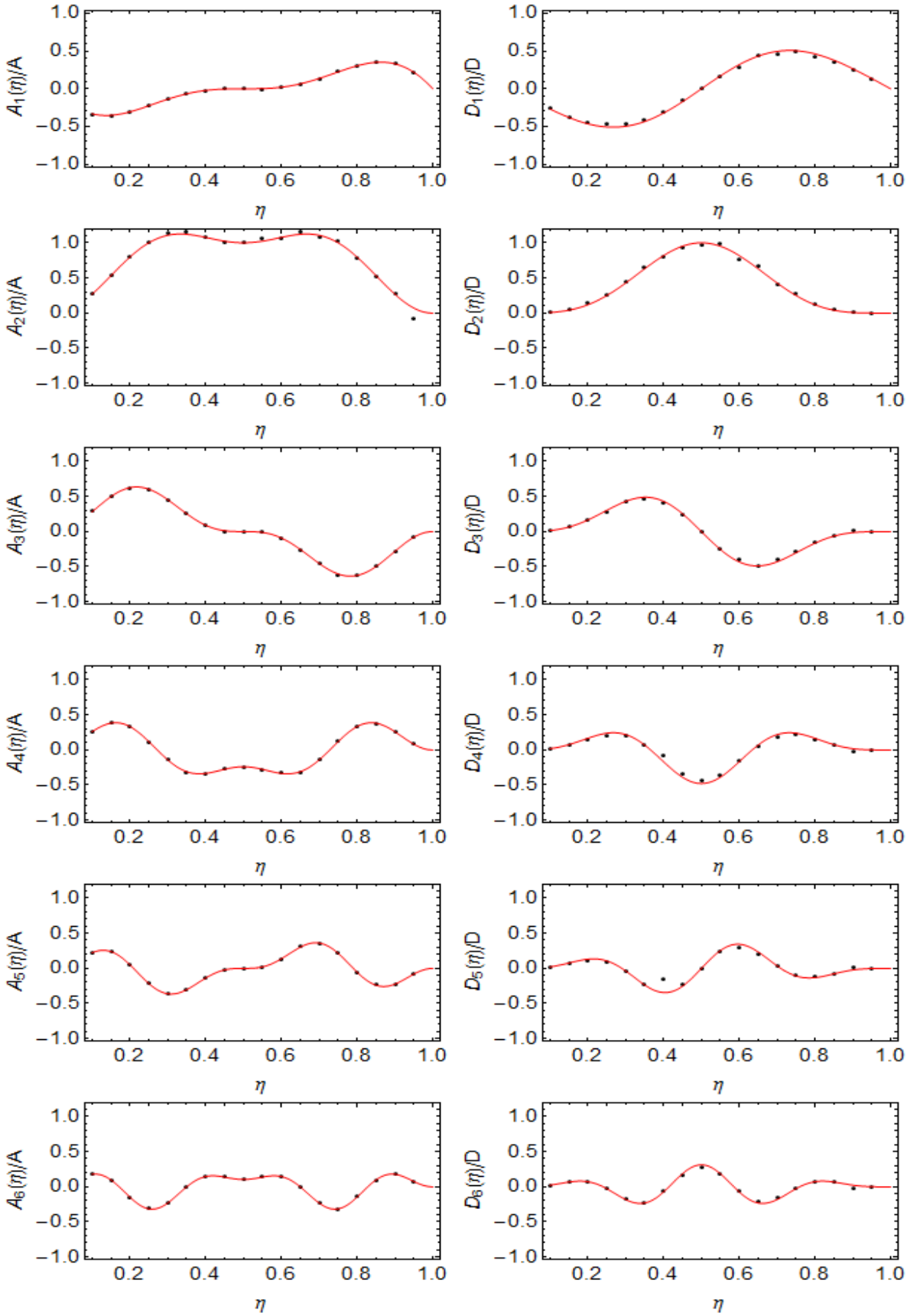

Fig.1: Relative amplitude of absorptive, $A_q(\eta)/A$ (left), and, dispersive $D_q(\eta)/D$ (right) lock-in signal for $\omega_L = \omega_{mod}$ as a function of modulation duty cycle (η), where $A= A_2(0.5)$, and $D= D_2(0.5)$. The index $q=1,\ldots,6$ indicate the harmonics of ω_{mod} at which the detection is performed. Black dots and red lines are experimental and model results respectively.

Chip-Scale Atomic Magnetometers for Biomagnetics and NMR

J. Kitching

Time and Frequency Division, National Institute of Standards and Technology
MS 847, 325 Broadway, Boulder, CO 80305
E-mail: john.kitching@nist.gov

Optical or atomic magnetometers[1,2] have advanced rapidly in recent years and the best sensors of this type now achieve sensitivities below 1 fT/√Hz, competitive with SQUID-based instruments. Our group at NIST has been developing microfabricated or "chip-scale" atomic magnetometers based on microfabricated alkali vapor cells integrated with diode lasers and optical fibers. These magnetometers have now achieved a sensitivity near 10 fT/√Hz and in addition are compact, low-power and well-suited to low-cost large-scale parallel fabrication.

Two main designs have been developed. In the first design[3], shown in Figure 1(a), a vertical cavity surface emitting laser is integrated with the vapor cell and a stack of optics that conditions the light. This type of chip-scale atomic magnetometer is well-suited to applications where a single stand-alone low-power sensor is needed. In the second design[4], shown in Figure 1(b), light from a remotely located laser is coupled to the sensor head with optical fibers. In this case a single higher-power laser can be used to drive many sensor heads. This design is best suited to the simultaneous operation of many sensors for magnetic imaging applications.

The magnetometers have been operated in a scalar spin precession (Mx) mode in which they have achieved sensitivities of 6 pT/√Hz. They have also been operated in a low-field vector mode in which spin-exchange collisions are suppressed[5]. In this mode, sensitivities approaching 10 fT/√Hz are obtained. However, these sensors can only be operated in ambient magnetic fields below about 10 nT and hence require magnetic shielding. The sensitivity achieved with a variety of these sensors over the last decade is shown in Figure 1(c). Typical bandwidths are in the range of a few hundred Hz.

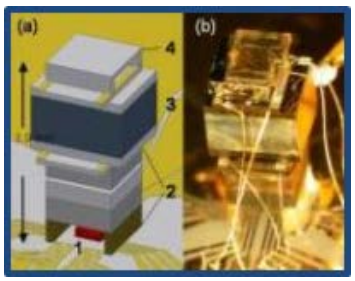

(a)

(b)

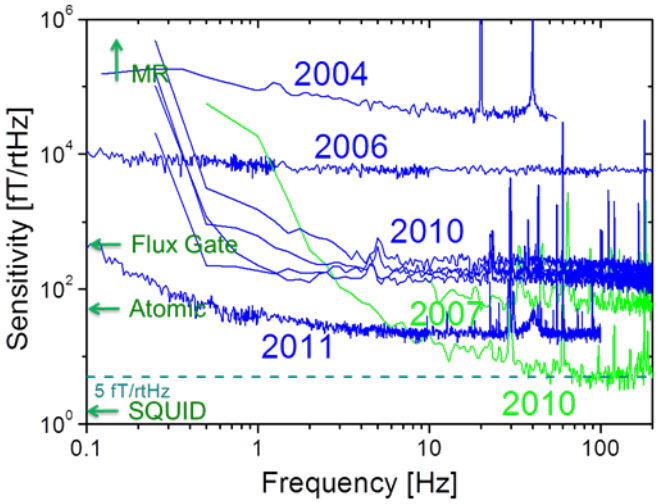

(c)

Figure 1. (a) Integrated chip-scale atomic magnetometer, in which light from a vertical-cavity surface-emitting laser is emitted upwards through an optics stack and microfabricated vapor cell. (b) Fiber-optically coupled sensor head in which light is brought to the sensor head from a remotely located laser via optical fibers. (c) Sensitivity of several types of chip-scale atomic magnetometers developed in our laboratory over several years.

We have used these chip-scale atomic magnetometers in experiments to monitor magnetic fields produced by the human body. In particular, we have measured magnetic fields produced by the human heart[6] in near-simultaneous measurements with SQUID-based magnetometers. We have also measured magnetic fields produced by the human brain[7] and successfully resolved both evoked response signals and spontaneous alpha-rhythm activity, shown in Figure 2(a).

These magnetic sensors also have application to problems in NMR. Because they are sensitive to DC magnetic fields, atomic magnetometers enable NMR measurements at low or even zero magnetic field[8]. Using CSAMs, chip-based remote detection of NMR signals is possible, which may lead to more general chip-scale NMR applications.

Finally, we describe very recent work on the development of a chip-scale hyperpolarized Xe source. This device consists of four chambers etched in a silicon wafer and connected by thin channels through which Xe gas is flowed, as shown in Figure 2(b). The Xe interacts with an alkali vapor confined in one of the chambers and becomes polarized via spin-exchange optical pumping. We achieve polarization fractions of 0.5 % with a flow rate of 5 μL/s and can efficiently transfer the polarization from one chamber to the next. We also use in situ detection of the Xe polarization by alkali atoms confined in the same cell as the Xe, which leads to an enhancement of the detection sensitivity by a factor of ~500 due to the Fermi contact interaction.

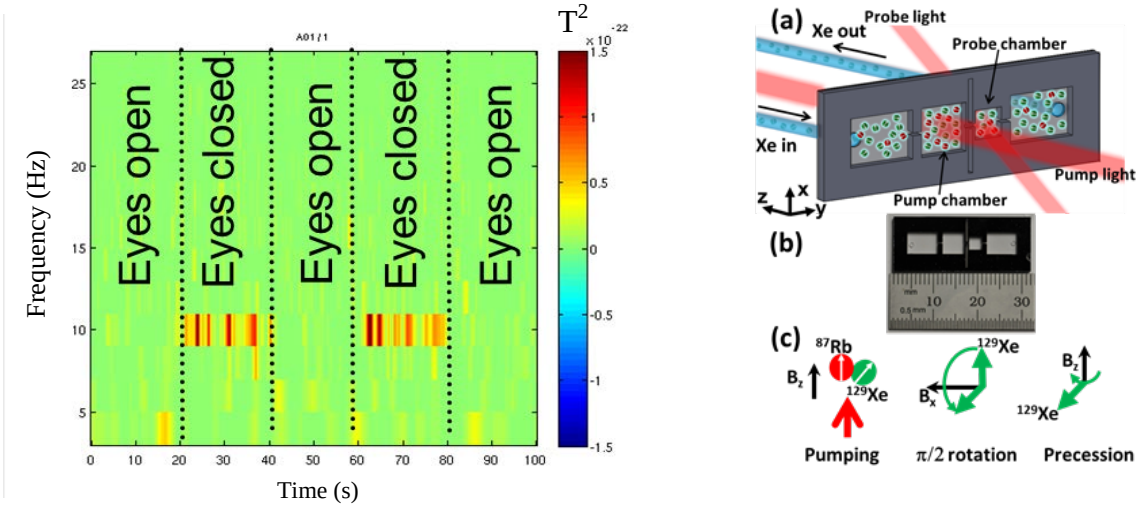

Figure 2. (a) Measurements of magnetic fields of the human brain with a chip-scale atomic magnetometer showing the change in alpha-rhythm signal at 10 Hz when the subject closes his eyes. (b) A chip-scale hyperpolarized Xe source.

References

1. W. E. Bell and A. L. Bloom, Phys. Rev. **107** (6), 1559 (1957).
2. D. Budker and M. Romalis, Nat. Phys. **3** (4), 227 (2007).
3. P. D. D. Schwindt, B. Lindseth, S. Knappe, V. Shah, J. Kitching, and L.-A. Liew, Appl. Phys. Lett. **90**, 081102 (2007).
4. R. Mhaskar, S. Knappe, and J. Kitching, Appl. Phys. Lett. **101**, 241105 (2012).
5. J. C. Allred, R. N. Lyman, T. W. Kornack, and M. V. Romalis, Phys. Rev. Lett. **89** (13), 130801 (2002).
6. S. Knappe, T. H. Sander, O. Kosch, F. Wiekhorst, J. Kitching, and L. Trahms, Appl. Phys. Lett. **97** (13), 133703 (2010).
7. T.H. Sander, J. Preusser, R. Mhaskar, J. Kitching, L. Trahms, and S. Knappe, Biomed. Opt. Exp. **3** (5), 981 (2012).
8. M. P. Ledbetter, I. M. Savukov, D. Budker, V. Shah, S. Knappe, J. Kitching, D. J. Michalak, S. Xu, and A. Pines, Proc. Nat. Acad. Sci. **105** (7), 2286 (2008).

Laser-pumped Cs magnetometer

A.N. Kozlov[1,2], D. I. Sevostianov[2,3], V.V. Shutov[2,3], A.V. Taichenachev[4,5], V. L. Velichansky[2,3,6,7],V. V. Vassiliev[2,7], V.P. Yakovlev[3], V. I. Yudin[4,5,6,8], E.V. Zhivun[3,9], S. A. Zibrov[2,7]

[1]N.V. Pushkov Institute of Terrestrial Magnetism, Ionosphere and Radio-vave Propagation, 142190 Troitsk
[2]Advanced Energy Technologies LTD, 100 Novaya St., Skolkovo Moscow 107045, Russia
[3]National Research Nuclear University (MEPhI), Moscow, 115409, Russia
[4]Institute of Laser Physics, Siberian Branch of RAS, Novosibirsk, 630090, Russia
[5]Novosibirsk State University, Novosibirsk, 630090, Russia
[6]Russian Quantum Center, 100 Novaya St, Skolkovo, Moscow Reg., 143025, Russia
[7]Lebedev Physical Institute, RAS, Moscow, 117924, Russia
[8]Novosibirsk State Technical University, Novosibirsk, 630073, Russia
[9]Department of Physics, University of California-Berkeley, Berkeley CA 94720

Optically pumped Cs magnetometers operating in Mx configuration are widely used in geological exploration, archeology, searching for unexploded ammunition. Their advantage is a high sensitivity which allows for detection of small relative variations (of about 10^{-5}) of terrestrial magnetic field. Such a magnetometer (to be carried by an explorer) has typically weight of about 10 kg. Large part of the weight comes from the battery which provides power to a resonance lamp. Power consumption can be decreased at least by an order of value by replacing discharge Cs lamp with a diode laser (DL).

Working Cs cell of investigated magnetometer was a glass cylinder with a length of 20 mm, and anti-relaxation coating of the walls. The DL frequency can be tuned to the four components of the D_1 line of Cs (895 nm) corresponding to transitions $F_g=3,4\rightarrow F_e=3,4$ or to the two components of the D_2 line (852,1 nm) in which the hyperfine structure of the excited state is not resolved. The experiments with tunable extended cavity diode lasers (ECDL) have shown that the best choice is the $F_g=4\rightarrow F_e=3$ transition of the D1 line or the $F_g=4\rightarrow F_e=3,4,5$ component of the D_2 line. In the last case the laser frequency should be off-tuned to the red wing of the line. For the experiments carried in the lab the ECDL is convenient but for the field operation a more reliable vertical-cavity surface-emitting laser (VCSEL) is needed. Thus most of experiment was made with a VCSEL tuned to the long wavelength component of the D_2 line. We studied the dependencies of the signal to noise ratio, magnetic resonance linewidth, and sensitivity of magnetometer on the laser intensity and frequency. To measure metrological characteristics of the magnetometer we used commercial Cs magnetometer optically pumped with a gas-discharge lamp. We confirmed that by using laser pumping the weight and the power consumption of the magnetometer can be dramatically decreased without decreasing the sensitivity.

The sensitivity of the magnetometer in measuring the variations of the terrestrial fields are found to be $\sim 5\ 10^{-2}$ nT. Parameters of the magnetometers are compared for three different sources of optical pumping: a gas discharge resonant lamp, a vertical cavity surface emitting laser (VCSEL), and an extended cavity diode laser. The problem of excess phase noise of VCSEL is discussed.

New magnetometric methods using "classical" quantum optical sensors

AntonVershovskii[1]

[1] *Ioffe Phys.-Tech. Institute of RAS, Polytechnisheskaya 26, St.-Petersburg, 194021 Russia*
E-mail: antver@mail.ioffe.ru

Application of lasers to the tasks of magnetic resonance optical pumping and detection has resulted in the development of various magnetometric systems using substantially new principles. In comparison to these systems, magnetometric sensors that use "classical" optically detected magnetic resonance (with or without laser pumping) may be somewhat controversially characterized as “Classical Quantum” Optically Pumped Magnetometers (CQOPM).

The present report is devoted to various modifications of CQOPMs, developed by Prof. E.Alexandrov and colleagues (Ioffe Phys.-Tech. Institute of RAS, Vavilov State Optical Institute), and demonstrating a set of absolutely new features, or new combinations of features.

The main, and most relevant, task that can be solved using CQOPM is a measurement of the scalar value of the magnetic field (usually the Earth’s field, and its natural and artificial variations). For a long time the Potassium Optically Pumped M_X Magnetometer (M_X-POPM, also developed by Prof. Alexandrov and his group) demonstrated the most impressive combination of time response, short-term resolution and stability among all the devices suitable for measuring geomagnetic field [1]. However, even though the M_X-POPM accuracy exceeds the accuracy of a Cs magnetometer by two orders of magnitude, it is still two orders of magnitude lower compared to the potential accuracy of Potassium M_Z Magnetometer (M_Z-POPM); the main reason for this is the M_X signal phase determination error. Recently we have developed a prototype of a magnetometer that combines the advantages of these M_X and M_Z devices, built on a single sensor and using the classical M_X pumping scheme [2]. A slow modulation was introduced into M_X-POPM scheme, allowing us to pick out from the ordinary M_X signal a relatively slow M_R signal proportional to the amplitude of the transverse component of the rotating magnetic moment. This M_R signal has all the advantages of the M_Z signal, including the line stability and symmetry, and independence from the detection phase; but unlike the M_Z signal, it can be observed on Larmor frequency together with the M_X signal in a transverse registration scheme.

Various methods of measuring components of the magnetic field with scalar sensors placed in an auxiliary field system are widely known. We have also developed two devices using this principle – K and Cs vector variometers [3]. While all the existing devices used fast switching of the auxiliary field direction, we applied rotating auxiliary fields, which allowed us to retain the total field module, and therefore to obtain much faster time response.

The idea of an absolute three-component magnetometer was suggested as an extension of these projects. In this scheme the total magnetic field vector in the sensor rotates, retaining its length, around the initial field direction. In each rotation cycle it passes through the three positions such that in each position, two components of the measured magnetic field are compensated with high accuracy, while the third one is fully uncompensated and amenable to measurement [4].

We have also suggested a concept of the M_X device that is able to measure the field scalar value with the accuracy and resolution achievable in M_X-POPM, and simultaneously indicate the direction of the magnetic field with the same laser beam that is used for optical pumping. The angular accuracy of such a laser compass is extremely high – when converted to the intensity of transverse field components, it is no more than one or two orders of magnitude lower than the resolution of M_X-POPM. This scheme has been modeled numerically [5], but at this time it has yet to be implemented experimentally. This scheme does not require

recalculation of its readings from the local coordinate system to the world coordinate system, and its accuracy does not depend on the precision of its positioning in space. Its additional advantage is the absence of generated magnetic fields, which enables its use in magnetometric observatories jointly with other devices.

Thus, new methods using CQOPMs allow us to solve various classes of magnetometric tasks, including the simultaneous measurement of the magnetic field modulus and components, and the optical indication of the direction of the magnetic field.

References

1. E.B. Alexandrov, M.V. Balabas, A.S. Pazgalev, A.K. Vershovskii, N.N.Yakobson, *Laser Physics*, **6**, 2, 244-251 (1996).
2. A.K. Vershovskii, A.S. Pazgalev, *Tech. Phys. Lett.*, .**37**, 1, 23-26 (2011).
3. A.K. Vershovskii, M.V. Balabas, A.E. Ivanov, V.N. Kulyasov, A.S. Pazgalev, and E.B. Aleksandrov, *Tech. Phys.*, **51**, 1, 112-117 (2006).
4. A.K. Vershovskii, *Opt. Spectr.,* **101**, 2, 309-316 (2006)
5. A.K. Vershovskii, *Tech. Phys. Lett.*, **37**, 2, 140-143 (2011).

New trends in atomic magnetometry and its applications

A. Weis[1]

[1] *Department of Physics, University of Fribourg, Switzerland*
E-mail: antoine.weis@unifr.ch

Atomic magnetometry is one of the most prominent applications of optically pumped atomic media. In atomic magnetometers, the transfer of angular momentum from resonance radiation to the atoms creates a macroscopic spin polarization (pump process). The magnetization associated with the spin polarization evolves under the torque exerted by the magnetic field to be measured, and the altered magnetization is detected by the same-or an auxiliary-resonant light field (probe process). The central detection feature for the field-atom interaction is the fact that the complex optical susceptibility, i.e., both the absorption and the index of refraction of a spin-polarized medium, depend on the magnitude and orientation of the spin polarization. The field information is imprinted onto the medium's optical susceptibility tensor, and can thus be retrieved from the properties (intensity, phase, polarization) of the transmitted probe light.

Early atomic magnetometer implementations used resonance light from discharge lamps, and the advent of compact tunable diode lasers has given the field a new boost in the past decade [1]. In recent years, a large number of novel atomic magnetometry methods and applications have been proposed [2], too many to be reviewed here. In my presentation I will focus on the atomic magnetometry research carried out in recent years by the Fribourg Atomic Physics group (FRAP) at the University of Fribourg.

For many years we have studied and deployed optical-magnetic double resonance magnetometers (ODMR) in the so-called M_x-geometry [3]. In this type of magnetometer, spin depolarizing magnetic resonances are driven by a weak oscillating magnetic field. In view of multi-sensor applications we have developed compact magnetometer modules (recent version shown in Fig. 1).

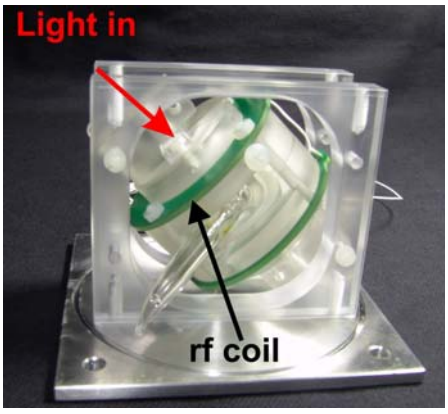

Fig.1. Magnetometer module containing a spherical (30 mm diameter) paraffin-coated Cs vapor cell [4], and a pair of rf coils (laid out on printed circuit boards) for applying the magnetic resonance driving oscillating field. The laser beam is fed to the sensor by a multimode fiber (not shown). It is collimated and made circularly polarized by optics contained in the block on the top left. The transmitted light power is detected by a photodiode at the lower right. The module is connected to the control optics/electronics by the fiber and two miniature coaxial cables. The structure is assembled with high-vacuum compatible non-magnetic materials.

Using an array of 25 similar sensors, we have mapped the dynamics of the magnetic field pattern produced by the beating human heart [5] (magneto-cardiography). We are currently deploying a large number of such sensors (16 are operational) for monitoring the spatial distribution and variations of the magnetic field (1 μT nominal value) in the ultrahigh vacuum chamber of an experiment [6] aimed at detecting a permanent electric dipole moment of ultracold neutrons (experiment carried out at the Paul Scherrer Institute, Switzerland). In the same experiment we will be using two large ^{3}He cells for monitoring the overall flux (and hence the gradient) of the magnetic field applied to the neutron storage volume. An array of auxiliary Cs magnetometers detects the free induction decay (FID) of nuclear spin polarized ^{3}He gas thereby providing a systematics-free measure of the absolute field value.

The M_x magnetometers are operated by a feedback loop that locks the oscillating field frequency to the Cs Larmor frequency. The relative sensitivity to magnetic field changes (in a 1 Hz bandwidth) in the shot noise limit is given by

$$\frac{\delta B}{B} = \frac{1}{Q}\frac{1}{SNR_{1Hz}}, \quad (1)$$

where Q is the quality factor of the magnetic resonance, and SNR_{1Hz} the signal/noise ratio in a 1 Hz bandwidth. With typical values of $Q \geq 350$ and $SNR_{1Hz} \geq 3\times10^5$, our M_x magnetometers have a *relative* sensitivity $\delta B/B \approx 10^{-8}$, and hence an *absolute* sensitivity of $\delta B \leq 10$ fT to changes of the 1 μT field. Although very sensitive, phase-feedback driven magnetometers do, in general, not have an accuracy that matches their sensitivity. In order to yield identical readings within the quoted δB value, the relative phases of all sensors in a large array have to be controlled at the μrad level, which is extremely difficult to implement. Systematic reading errors are detrimental when field gradients are to be inferred from pairs of nominally identical sensors.

In contrast to feedback driven magnetometers, FID-based magnetometers (such as the ^{3}He magnetometer mentioned above) do not suffer from this drawback. We are currently exploring the implementation of FID schemes in Cs sensors by monitoring the decaying magnetization with one (or several) weak probe beams following a short but strong pump pulse. By using several probe beams full vector information on the field can be retrieved. We note that the FID-magnetometer is an implementation of a magnetically silent magnetometer, so-called since it does not use an oscillatory drive field.

In recent times we have also become interested in other forms of magnetically silent magnetometers that rely on the modulation of the laser frequency, amplitude, or polarization (see contribution by E. Breschi *et al.* at this conference [7]).

I will further report on our efforts to use arrays of Cs sensors for detecting the magnetic field produced by superparamagnetic nanoparticles (SPIONs). When functionalized, such particles can be made to attach to specific biological entities, such as tumors or organs, where they serve as tagging agents. Mapping the magnetic field produced by embedded SPIONs opens new perspectives for contact free, non-invasive biomedical imaging.

Work funded by the Swiss Nation Science Foundation (grants 2200020 and CRSII2_144257).

References

1. D. Budker and M. V. Romalis, *Nature Phys.* **3**, 227 (2007).
2. S. Gröger, A. S. Pazgalev, and A. Weis, *Appl. Phys. B* **80**, 645 (2005).
3. S. Groeger, G. Bison, J.-L. Schenker, R. Wynands, and A. Weis, *Eur. Phys. J. D* **38**, 239 (2006).
4. N. Castagna, G. Bison, G. Di Domenico, A. Hofer, P. Knowles, C. Macchione, H. Saudan, and A. Weis *Appl. Phys. B* **96**, 763 (2009).
5. G. Bison, N. Castagna, A. Hofer, P. Knowles, J.-L. Schenker, M. Kasprzak, H. Saudan, and A. Weis, *Appl. Phys. Lett.* **95**, 173701 (2009).
6. P. Knowles, G. Bison, N. Castagna, A. Hofer, A. Mtchedlishvili, A. Pazgalev, and A. Weis, *Nucl. Inst. Meth. A* **611** 306 (2009).
7. E. Breschi, Z. Grujic, P. Knowles, and A. Weis, Poster presentation at this conference.

Vector magnetometer based on EIT resonances in linearly polarized light

V.I. Yudin[1-3], A.V. Taichenachev[1,2], Y.I. Dudin[4], V.L. Velichansky[4,5], A.S. Zibrov[6], S.A. Zibrov[5]

[1]*Laser Physics Institute, Siberian Division RAS, Novosibirsk, 630090, Russia.*
[2]*Novosibirsk State University, Novosibirsk, 630090, Russia.*
[3]*Novosibirsk State Technical University, Novosibirsk 630092, Russia*
[4]*Moscow State Engineering and Physics Institute, 115409 Moscow, Russia.*
[5]*Lebedev Physical Institute, RAS, 117924 Moscow, Russia.*
[6]*Physics Department, Harvard University, Cambridge, MA, 02138, USA.*
viyudin@mail.ru

We develop the generalized principle of the atomic vector magnetometry based on EIT. It is shown that this principle is valid for any atoms. We achieved a compass sensitivity 10^{-3} deg/Hz$^{1/2}$ at intermediate magnetic fields. We found that major contribution to the sensitivity gives the noise level mostly related to the intensity fluctuation of the laser system. A proper choice of the buffer gas type, pressure, the cell with the anti-relaxation coating walls, and the cell volume enables the varying of sensitivity, the spatial resolution, and the working range of the magnetic field.

A compass with one laser beam could be used as a 2D device, while using of two non-parallel laser beams allows to measure the orientation of the magnetic field in three dimensions. The proposed vector magnetometer has an exclusive importance for non-invasive biomedical studies of the temporal and spacial distribution of the brain and heart currents. Recent success in the developing the chip-size magnetometer and atomic clock gives the ligimate optimism on the creation of the small size compass-magnetometer, which could find a broad variety of application in navigation, geology and biology.

Our work is supported by the Ministry of Education and Science of the Russian Federation in the frame of the Program “Scientific and scientific-pedagogical personnel of innovative Russia” (Contract no. 16.740.11.0466 and Agreement no. 8387), by the Russian Foundation for Basic Research (grants nos. 12-02-00454, 12-02-00403, 11-02-00775, 11-02-01240), by the Russian Academy of Sciences and the Presidium of Siberian Branch of Russian Academy of Sciences, and the Russian Quantum Center.

Photo-desorption of nitrogen molecules from glass surface

S. N. Atutov, N. A. Danilina, S. L. Mikerin, A. I. Plekhanov

Institute of Automation and Electrometry SB RAS, Academician Koptug ave. 1, Novosibirsk, Russia, 630090
E-mail: atutov@fe.infn.it

There are several fields of research and application for which the ability to collect and then release by a pulsed light a large number of atoms or molecules can be a useful tool. For example, it is possible to collect by sorption on coated (or non coated) surface a large number of toxic or radioactive elements during tens of minutes and then release by photo-desorption all these elements to a volume with detector inside in a short time of milliseconds by a powerful pulse of light. In a case of low loss of collected particles and high efficiency of photo-desorption, a ratio of a pulsed signal from burst of desorbed particles to noise, is proportional to the ratio of the collection time to the release time which can be of several orders of magnitude.

We present the results of the experiment and a theoretical model of photo-desorption of nitrogen molecules from non coated inner surface of evacuated glass cell. The main goal of the study is to define optimal experimental conditions for the maximal manifestation of this phenomenon.

In the model we have considered two types of glass cell: spherical and cylindrical ones. By assuming a very low density of the detectable gas n_0, when the surface density of the absorbed molecules is proportional to the collection time T, we have obtained the following expression for the peak density of collected molecules n_{peak} after applying of the desorbing pulse light:

$$n_{peak} = 3\alpha n_0 T \frac{W}{R_s} \tag{1}$$

where W is the power of the pulse light, R_s – radius of the cell, α – some constant which is generally a function of the wavelength of the incident radiation, the binding energy of the molecules with the surface, the temperature of the surface and etc. From eq. (1) we can conclude that the peak density of desorbed molecules increases with the accumulation time, the total energy of the light pulse and with decreasing of the radius of the spherical cell. In the case of cylindrical cells with an inner radius R_l, and a length l the peak density of the photo-desorbed molecules can be written in the following form:

$$n_{peakl} = 2\alpha n_0 TW \frac{(R_l + l)}{R_l l} \tag{2}$$

In the experiment, we determine the magnitude of the effect by the ratio n_{peak}/n_0 that is the relative increasing of the density after applying flash light. Note that some cylindrical cells with a fixed wall area, which is limited by the power of the flash lamp, can have very small cell volume with respect of spherical cell with same wall area. Hence the peak density of the photo-desorbed gas in the case of employing of the cylindrical cell can be much greater than one of spherical cell. Therefore use cylindrical cell more preferably in order to further increasing of the detection signal.

Our first experimental setup shown in Fig.1. The cell 1 is evacuated by a turbo-molecular pump 2 through the vacuum valve 3. Letting of the cell by nitrogen is provided through a valve 4. The density of molecular nitrogen in the cell was measured using a mass spectrometer 5 connected to the system via the vacuum valve 6. The residual pressure in the system was controlled by a gauge 7. We use as a pulsed light source a commercial photographic lamp 8 with an energy density of the light pulse at the cell walls of 0.2 J/cm2.

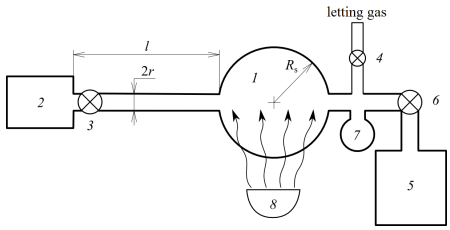

Fig.1. Experimental setup with a spherical glass cell.

In this experiment we measure $n_{peak}/n_0 \sim 0.2$. The reasons of that why we obtained a minor relative increase of the gas density are: not optimal spherical shape and too large volume of the cell used, the external to the cell position of the light source and detector. An inefficient use of the flash lamp light is due to the inability to concentrate fully all of the light from the lamp to the cell, and with a single passage of light through the cell walls, when only a small fraction of light absorbed by the surface of the glass is involved to the process of photo-desorption.

We have constructed the second setup shown in Fig.2, which utilized a cylindrical cell with a small volume. Both vacuum gauge and flash lamp were inserted inside of the cell.

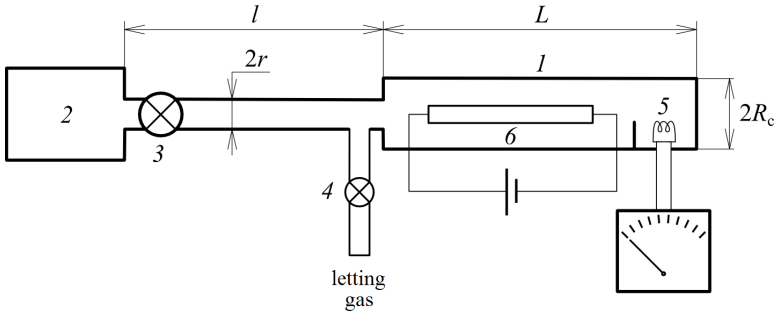

Fig.2. Experimental setup with a cylindrical glass cell.

Here 1 – cylindrical cell made of molybdenum glass, 2 – turbo, 3, 4 – vacuum valves, 5 – vacuum gauge, 6 – flash lamp. For providing of many passages of the desorbing light inside of the cell its walls were made mirror like with a high enough reflectivity. A typical signal taken under the improved conditions is shown in Fig.3.

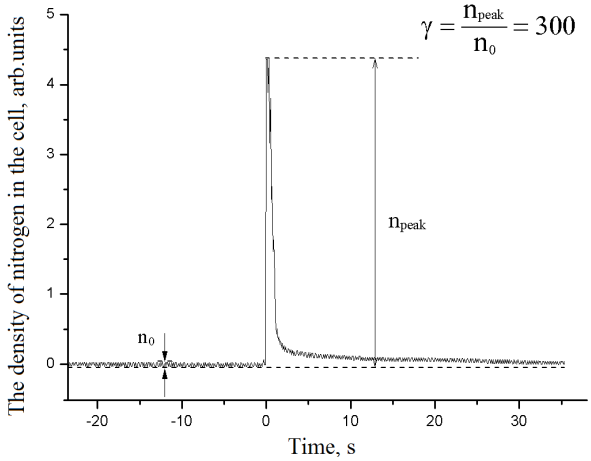

Fig.3. Dependence of the density of nitrogen molecules in the cell vs. time.

From the Fig.3 one can clearly see that the density of nitrogen in the cell increases very quickly, and then, reaching a maximum, decreases with a time of 1.2 seconds. In the experiment we have found that the relative increase of the detecting signal $n_{peak}/n_0 = 300$.

This method could be used for enhancement of sensitivity of existed sensors for the trace detection of various elements (including toxic or radioactive ones) which is important to environmental applications, in medicine, in geology and etc.

Optical frequency standard based on the coherent population trapping resonance

E.V. Baklanov, S.N. Bagayev, A.K. Dmitriev, A. V. Taichenachev, V. I. Yudin

Institute of Laser Physics SB RAS, pr. Ac. Lavrentyeva, 13/3, Novosibirsk, 630090 Russia
Novosibirsk State University, ul. Pirogova, 2, Novosibirsk, 630090, Russia
Novosibirsk State Technical University, pr. K. Marksa, 20, Novosibirsk, 630073, Russia
E-mail:baklanov.ev@gmail.com

We propose an optical frequency standard, which uses as a reference the coherent population trapping resonance. This frequency standard is based on a self-mode-locked laser with the frequency of pulse repetition directly locked to the hyperfine splitting of ^{133}Cs. An important feature of the proposed standard consists in the absence of source of microwave radiation.

The use of femtosecond lasers substantially simplified the process of measurements of optical frequencies. A self-mode-locked femtosecond laser emits a periodic train of pulses. The spectrum of such laser represents the so-called frequency comb covering the entire width of the spectrum. If one of the spectral components of the comb generator is locked to the microwave frequency standard used as a reference, the absolute values of frequencies of all other components will be known. In fact we have an efficient optical ruler for absolute measurements of optical frequencies. This allows a series of fundamental physical experiments, such as measurements of the Rydberg and fine structure constants.

A system of precision measurement of optical frequencies contains, at least, two main units – the microwave standard and the frequency converter to optical region, for example, a femtosecond laser. In this work we consider an optical standard which does not contain the microwave standard (as the device), and is a self-mode-locked laser directly exciting the coherent population trapping (CPT) resonance [1] in a Cesium vapor. As a result the pulse repetition rate is directly locked to a microwave reference transition. We analyze the basic theory of CPT resonance (for a three-level Lambda-atom), and extend it to the case of self-mode locking radiation, following to the main ideas of ref.[2] and ref.[3].

It is worth to note an important feature of the proposed frequency standard – the absence of the external microwave frequency reference. All optical frequencies are automatically measured, because we use as reference the microwave clock transition of ^{133}Cs. This fact could simplify significantly absolute frequency measurements in optical range. In addition, the use of CPT resonances in the multi-mode regime allows the light shift cancellation leading to a good frequency stability of the standard.

Our work is supported by the Ministry of Education and Science of the Russian Federation in the frame of the Program “Scientific and scientific-pedagogical personnel of innovative Russia” (contract no. 16.740.11.0466 and agreement no. 8387), by the Russian Foundation for Basic Research (grants nos. 12-02-00454, 12-02- 00403, 11-02-00775, 11-02-01240), by the Russian Academy of Sciences and the Presidium of Siberian Branch of Russian Academy of Sciences, and the Russian Quantum Center.

References:

[1] E. Arimondo, Prog. Opt. **35**, 257 (1996).
[2] A.V. Taichenachev, V.I. Yudin et al., Phys. Rev. A **67**, 033810 (2003).
[3] E.V. Baklanov, A.K. Dmitriev, Laser Physics **20**, 52 (2010).

Quantum gates with mesoscopic atomic ensembles based on adiabatic passage and dipole blockade

I. I.Beterov,[1, 2] M.Saffman,[3] E.A.Yakshina,[1, 2] V.P.Zhukov,[4] D.B.Tretyakov,[1] V.M. Entin,[1] I. I. Ryabtsev,[1, 2, 5] C. W. Mansell,[6] C. MacCormick,[6] S. Bergamini,[6] and M.P. Fedoruk[2]

[1]*A.V.Rzhanov Institute of Semiconductor Physics SB RAS, 630090 Novosibirsk, Russia*
[2]*Novosibirsk State University, 630090 Novosibirsk, Russia*
[3]*Department of Physics, University of Wisconsin, Madison, Wisconsin, 53706, USA*
[4]*Institute of Computational Technologies SB RAS, 630090 Novosibirsk, Russia*
[5]*Russian Quantum Center, Skolkovo, Moscow Reg., 143025, Russia*
[6]*The Open University, Walton Hall, MK7 6AA, Milton Keynes, UK*
E-mail: beterov@isp.nsc.ru

Quantum information can be stored in collective states of ensembles of strongly interacting atoms [1]. This idea can be extended to encoding an entire register of qubits in ensembles of atoms with multiple ground states which opens up the possibility of large quantum registers in a single atomic ensemble or of coupling arrays of small ensembles in a scalable atom chip based architecture. Our proposal for implementing high fidelity quantum gates in ensembles is thus of interest for several different implementations of quantum computing.

The enhanced coupling of the mesoscopic ensembles to the radiation field by a factor of $\sqrt{N}$ in the regime of dipole blockade [1], with N the number of atoms, is useful for coupling matter qubits to single photons. However, due to the increase of the Rabi frequency of oscillations between different collective states proportional to $\sqrt{N}$, with the one atom Rabi frequency, it is difficult to perform gates with well defined rotation angles in the situation where N is unknown [2]. Adiabatic passage techniques have been widely used for deterministic population transfer in atomic and molecular systems [2,3]. Although Stimulated Raman Adiabatic Passage (STIRAP) or Adiabatic Rapid Passage (ARP) methods provide pulse areas with strongly suppressed sensitivity to the Rabi frequency N, and therefore suppressed sensitivity to N, the phase of the final state is in general still strongly dependent on N.

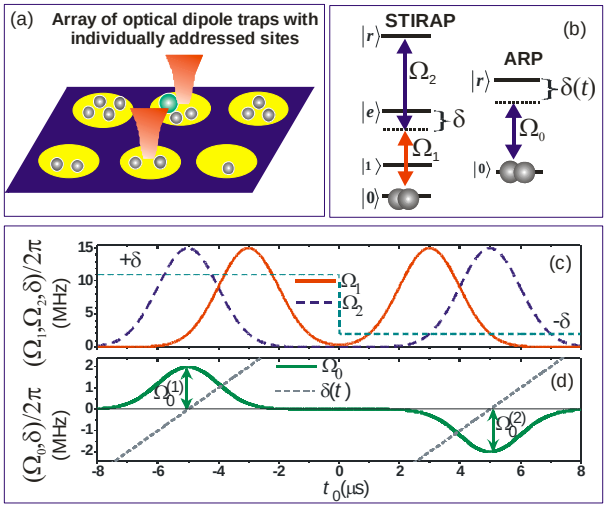

Fig.1 (a) Scheme of the quantum register based on individually addressed atomic ensembles in the array of optical dipole traps. Laser pulses are used to excite atoms into the Rydberg state. Only one atom in each site can be excited due to Rydberg blockade. Simultaneous excitation of Rydberg atoms in the neighboring sites is also blocked; (b) Energy levels for two-photon STIRAP and single-photon ARP excitation; (c) Time sequence of STIRAP laser pulses; (d) Time sequence for ARP laser excitation;

We propose double adiabatic sequences using either STIRAP or ARP excitation which remove the phase sensitivity, and can be used to implement gates on collectively encoded qubits without precise knowledge of N. The quantum register consists of individually addressed atomic ensembles in arrays of optical dipole traps or optical lattices [Fig. 1(a)]. The energy levels scheme for STIRAP and ARP is shown on Fig. 1(b). A sequence of two STIRAP pulses is produced with fields having Rabi frequencies $\Omega_{1,2}$ and detuning δ from the intermediate state. In the regime of strong Rydberg blockade, the first STIRAP (ARP) pulse deterministically prepares the ensemble in a collective state with a single Rydberg excitation, as we demonstrated in [2]. The second reverse STIRAP pulse, as

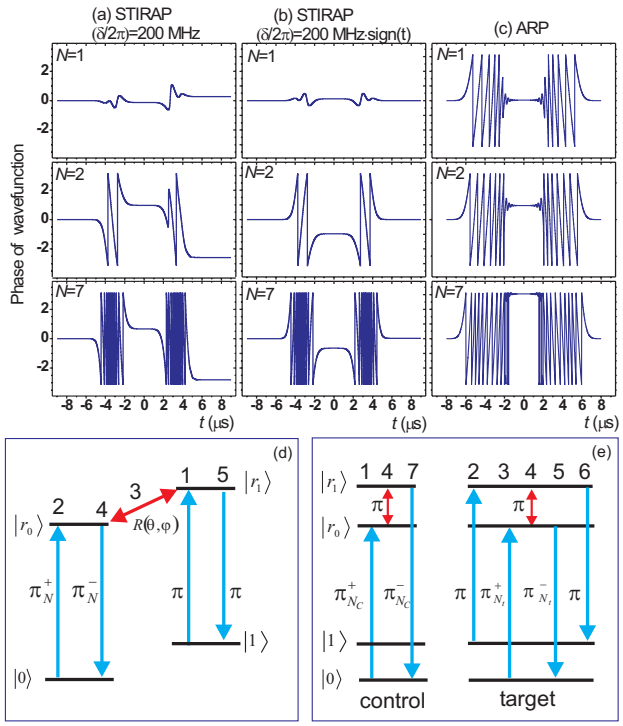

Fig. 2. Calculated time dependence of the phase of the collective ground state amplitude for N =1, 2, 7 atoms (top to bottom). Double STIRAP sequence with $\delta/2\pi$ = 200 MHz (a), with $\delta/2\pi$ = 200 MHz ×sign (t) (b), and for a double ARP pulse sequence with phase inversion (c). All other parameters are as in Fig. 2. (e) Single qubit gate for a mesoscopic qubit with N atoms. Pulses 1 − 5 act between the qubit states $|\,|0\rangle,|1\rangle$ and the Rydberg states $|r_0\rangle,|r_1\rangle$. Pulses 1, 2, 4, 5 are optical transitions and pulse 3 is a microwave frequency transition between Rydberg states. (b) CNOT gate between mesoscopic qubits with N_c atoms in the control qubit and N_t atoms in the target qubit.

shown in Fig. 1(c), returns the Rydberg atom back to the ground state. Similar scheme can be implemented using linearly chirped ARP pulses, as shown in Fig. 1(d).

At the end of a double STIRAP sequence the population is returned back to the collective ground state $|0000\rangle$ of the atomic ensemble, but a geometric phase is accumulated. This phase shift of the ground state is dependent on the Rabi frequency and leads to gate errors. The phase of the atomic wavefunction can be compensated by switching the sign of the detuning between two STIRAP sequences, or by switching the phase between two ARP pulses, as shown in Fig. 1(c). For a double STIRAP sequence with the same detuning throughout the accumulated phase depends on N [Fig.2(a)], while the phase change is zero, independent of N, when we switch the sign of detuning between the two STIRAP sequences [Fig.2(b)]. A similar phase cancellation occurs for phase shifted ARP pulses [Fig.2(c)].

The phase compensated double STIRAP or ARP sequences can be used to implement a universal set of quantum gates as we now describe. Consider atoms with levels $|0\rangle,|1\rangle,|e\rangle,|r\rangle$ as shown in Fig. 1. A qubit can be encoded in an N atom ensemble with the logical states $|\bar{0}\rangle=|00000\rangle$, $|\bar{1}\rangle=\left(1/\sqrt{N}\right)\sum_{j=1}^{N}|0..1_j0\rangle$. Levels $|0\rangle,|1\rangle$ are atomic hyperfine ground states with coupling between these states and implementation of quantum gates mediated by the singly excited Rydberg state $|\bar{r}\rangle=\left(1/\sqrt{N}\right)\sum_{j=1}^{N}|0..r_j0\rangle$. Single-qubit rotations are implemented using transitions between Rydberg states $|r_0\rangle\rightarrow|r_1\rangle$, driven by microwave radiation, as shown in Fig.2(d). Single-atom addressability is necessary when the atoms are excited into the Rydberg states. The scheme of CNOT gate, shown in Fig.2(e), is an extension of the method implemented in Ref.[4].

This work was supported by the grant of the President of Russian Federation MK.7060.2012.2, EPSRC project 5EP/K022938/1, FP7-PEOPLE-2009-IRSES “COLIMA”, RAS, RFBR and Russian Quantum Center. MS was supported by the NSF and the AFOSR MURI program.

[1] M. D. Lukin et al., Phys. Rev. Lett. 87, 037901 (2001).
[2] I. I. Beterov et al., Phys. Rev. A 84, 023413 (2011).
[3] I. I. Beterov et al., arXiv:1212.1138
[4] L. Isenhower et al., Phys. Rev. Lett. 104, 010503 (2010).

Improving accuracy of a frequency instability estimation of optical standards by means of optimal smoothing frequency fluctuations

B. D. Borisov, E. V. Upenik

Institute of Laser Physics, Siberian Branch, Russian Academy of Sciences,
pr. Akademika Lavrent'eva 13/3, Novosibirsk, 630090 Russia
E-mail: borisov@laser.nsc.ru

The frequency instability - the value of Allan's variance $\sigma_y^2(2,\tau)$ of a modern optical standards is down to $10^{-14} - 10^{-16}$ [1, 2].

$$\sigma_y^2(2,\tau) = \frac{1}{2} < (\bar{y}_i - \bar{y}_{i-1})^2 >= \frac{1}{2}\left[\left\langle \bar{y}_i^2 \right\rangle + \left\langle \bar{y}_{i-1}^2 \right\rangle\right] - 2\left\langle \bar{y}_i \cdot \bar{y}_{i-1} \right\rangle = \frac{1}{2}\left(D_{\bar{y}_i} + D_{\bar{y}_{i-1}}\right) - \rho_{i,i-1}. \quad (1)$$

Herein $\bar{y}_i, \bar{y}_{i-1}$ are the mean values of a frequency fluctuation y_i, *i* and *i – 1* are paired adjacent intervals each of finite duration τ seconds and with a pause of $\tau_p = 0$ between them, $\rho_{i,i-1}$ is the correlated moment for adjacent readings $\bar{y}_i, \bar{y}_{i-1}$, $D_{\bar{y}}$ are variances of $\bar{y}_i, \bar{y}_{i-1}$ on time intervals τ. The averaging operator over an infinite time interval is enclosed into broken brackets [3].

We need to determine the potential accuracy of measurements of a frequency instability characteristic and to identify other factors that influence the efficiency of estimating (1).

In practical measurements the efficiency of the estimates depends on:

A. the finite size of the paired samples *M* against the infinite one $\langle\ \rangle$,

B. the duration of time intervals τ and the quality of smoothing frequency fluctuations over τ,

C. the value $\rho_{i,i-1}$,

D. the value $\tau_p \neq 0$

and is specified by the sample variance (variance of variance) $\hat{G}^2\left[\hat{\sigma}_y^2(2,\tau)\right]^2$ [3, 4].

Lesage and Audon is determined to depend of $\hat{G}^2$ on *M* [4]. Borisov eliminates the dependence of (1) on *M* and finds the true (nonsampling) variance of the Allan variance depending on $\sigma^2(\bar{y})$ and $\rho_{i,i-1}$ only [5]

$$G^2\left[\hat{\sigma}_y^2(2,\tau)\right] \cong 2\left[\sigma^2(\bar{y}_i) - \rho_{i,i-1}\right]^2. \quad (2)$$

Yoshimura determined the contribution of $\rho_{i,i-1}$ to (1) for frequency and phase fluctuations with spectral power density obeys the power law flicker-type [6]. Borisov developed an optimal filtering procedure for these types of frequency noises which provides minimum smoothing variances of a samples y_i in a finite time interval τ taking into account the edge effects at its ends [7].

Reasoning from analysis and comparison the factors A, B, C, and D it is clear that the main contribution to the variance (2) of the estimate of the frequency instability characteristic comes not from the correlation of the paired averages, not from the $\tau_p \neq 0$ and samples size *M* but from the quality of averaging of fluctuations of y_i in the interval τ, the value $\sigma^2(\bar{y})$. For

example frequency flicker noise is weakly suppressed by increasing the averaging time and the only method suitable for improving the estimation efficiency in this case is optimal filtering for obtaining $\bar{y}_i, \bar{y}_{i-1}$ in intervals τ [7].

The following table consists of the models of nonstationary frequency fluctuations with a spectral power density obeying the power law (column 1), same models in a stationary approximation with a finite variance and correlation function (column 2) and results of smoothing samples y_i over τ by counter (column 3), by optimal filter (column 4) and profit-ratio variances $\hat{\sigma}_y^2(\bar{y})_{opt}$ to $\hat{\sigma}^2(\bar{y})_C$ (column 5). It is obvious that the perfect integrator used in the counter meter is an optimal filter only for the white frequency noise with $S(\omega) = N_0$.

Noise type, $S(\omega)$	Model of integrated noise type	Variance of estimation $\hat{\sigma}^2(\bar{y})_C$ by counter	Variance of estimation $\hat{\sigma}^2(\bar{y})_{opt}$ by optimal filter	Ratio variances $\hat{\sigma}_y^2(\bar{y})_{opt}$ to $\hat{\sigma}^2(\bar{y})_C$
White FM $\omega^0 = N_0$	ω^0	N_0/τ	N_0/τ	1
Flicker FM ω^{-1}	$\frac{a+\omega}{a^2+\omega^2}$ [7]	4.46, [7]	2.27, [8]	$\cong 0.5$

The main factors influencing efficiency of estimating the fundamental frequency instability characteristic (Allan's variance) of oscillators of any spectral range were compared. The variance of the average frequency estimate in finite time interval τ was shown to make the major contribution to the Allan variance. For frequency fluctuations of a flicker type with a spectral power density obeying the power law a decrease in these variances is achieved predominantly by using an optimal filtering operator in comparison with counter frequency meter.

References

1. S.N. Bagaev, S.V. Chepurov, V.M. Klementyev, S.A. Kuznetsov, V.S.Pivtsov, V.V. Pokasov,V.F. Zakharyash, *Appl.Phys. B,* **70**, 375 (2000).
2. J Reichert, R. Holzwarth, Th. Udem, T.W. Haensch, *Optics Comms,* **172**, 59 (1999).
3. J. Rutman, *Proc. IEEE* **66** (9) (1978).
4. P. Lesage and C. Audon, *IEEE Trans. Instrum. Meas.* **22** (2), 157–161 (1973).
5. B. D. Borisov, *Optoelectronics, Instrumentation and Data Processing*, **45,** 282 (2009)
6. K. Yoshimura, *IEEE Trans. Instrum. Meas.* **27** (1) (1978).
7. B. D. Borisov, *Optoelectronics, Instrumentation and Data Processing,* **44**, 317 (2008).
8. G. P. Pashev, *Izv. Vuzov, Ser. Radiofizika* (in russian) **24** (8), 1030 (1981).

Laser testing of dosimetric detectors based on anion-defective sapphire crystal

V. V. Bourtsev[1,2], E. V. Milyutina[1,2], V. S. Kortov[3], E. F. Martynovych[1,2]

[1]Irkutsk Branch of Institute of Laser Physics SB RAS, 130a Lermontov Str., Irkutsk, 664033 Russia,
[2]Irkutsk State University, 20, Gagarin Blvd, Irkutsk, 664003 Russia
[3]Ural Federal University named after the first President of Russia B.N.Yeltsin, 19 Mira, Ekaterinburg, 620002, Russia,
E-mail: filial@ilph.irk.ru

Sapphire crystals (a-Al_2O_3, corundum) are widely used in various fields of science and technology, due to a favorable combination of optical, thermal, mechanical, dielectric, radiation and other properties, the highly developed industrial production, the opportunity to grow large and perfect single crystals. One of the important achievements in the field of application of these crystals was the creation on their basis of thermoluminescence gamma-radiation detectors [1,2] and photoluminescent nuclear track detectors for the detection of fast neutrons and high-energy heavy charge particles [3]. Crystals of these detectors are grown in a reducing atmosphere, resulting in defects that occur in the anion sublattice - color centers F^+ and F-type, and also more complex centers are formed from the oxygen vacancies [4]. These color centers are the working centers in dosimetric processes. They are to a large extent determine the shape of the spectra of the dosimetric fluorescent signals.

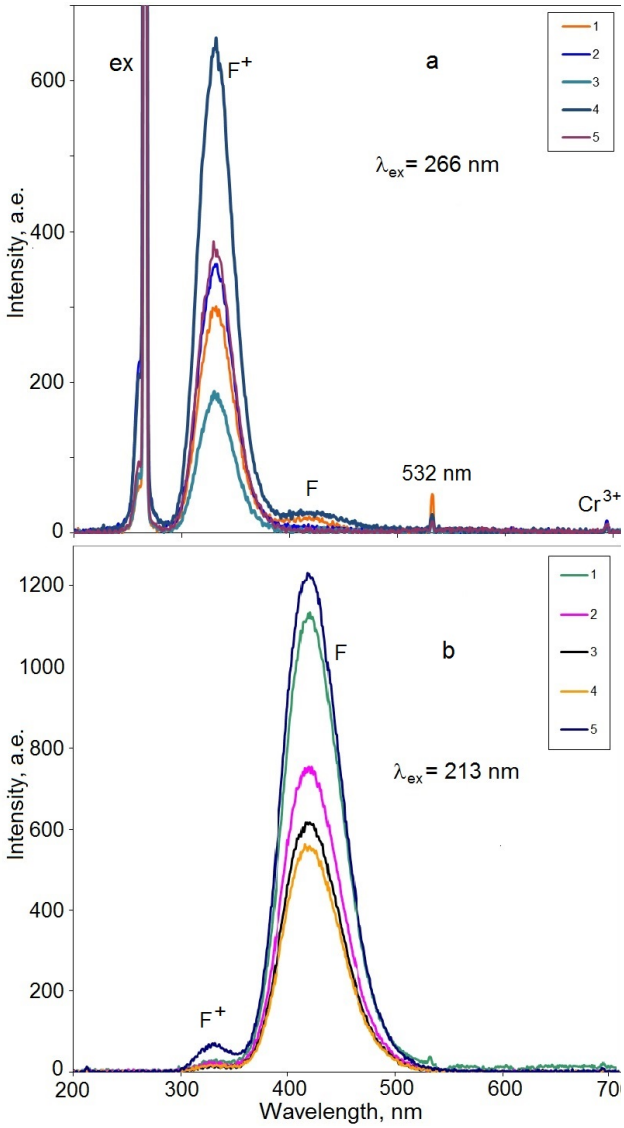

Fig. 1. The luminescence spectra of corundum crystals excited by the 4th harmonics (266 nm) and 5th (213 nm) harmonics of Nd: YAG laser.

The aim of this work was the study of laser testing of gamma-ray detectors based on anion-defective sapphire with using harmonics of Nd: YAG laser. 10 samples of the single crystal detector of anion-defective corundum with form of cylindrical tablets with diameter 5 mm and a thickness of 1 were studied in the experiments. The luminescence spectra of the studied detectors were studied in experiments with excitation by second, fourth and fifth harmonics of the neodymium laser. Moreover, diode lasers are used with additional wavelengths 405, 450 and 640 nm. The spectra were recorded by 65000 Ocean Optics spectrometer with a cooled matrix in the range of 200-1000 nm. The intensities of the luminescence spectral bands belonging to individual centers were measured by obtaining the spectra and their relationships were determined for the different harmonics of the exciting radiation. The scaling of the intensities used in the measurement to obtain more accurate values.

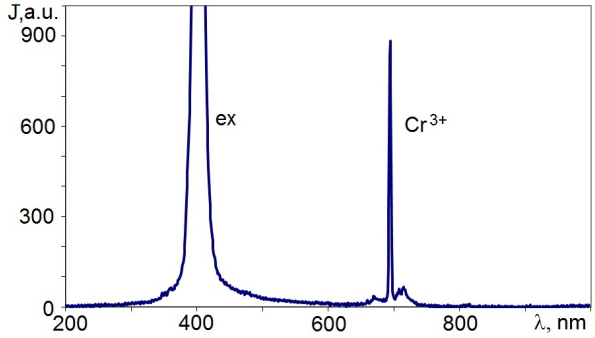

Fig. 2. Luminescence of crystals

Fig. 1a, we see that, F^+-centers fluoresce more intensely than the F-centers at the excitation wavelength at 213 nm. The opposite picture is seen in Fig. 1b, where the F centers fluoresce more intensely. Luminescence when excited by the second harmonic of the laser radiation with a wavelength of 532 nm and a diode or a laser (405 nm) was recorded in all crystals of chromium lines Cr^{3+} (Fig. 2).

№	213 нм			266 нм			$J_{F(213)}/J_{F+(266)}$
	J_F	J_{F+}	J_F/J_{F+}	J_F	J_{F+}	J_F/J_{F+}	
1	1134	26	43,6	22	301	0,073	3,8
2	752	24	31,3	12	357	0,034	2,1
3	617	11	56,1	8	188	0,043	3,3
4	559	16	34,9	31	657	0,047	0,9
5	1232	67	18,4	8	387	0,02	3,2
6	1569	49	32,1	25	563	0,044	2,8
7	714	27	26,4	9	440	0,02	1,6
8	721	29	24,9	20	753	0,027	0,96
9	613	19	32,3	9	70	0,129	8,8
10	1450	48	30,2	37	636	0,058	2,3

The study found that the studied radiation detectors based on sapphire crystals have different concentrations of the major (F and F^+) and related (Cr^{3+}) luminescence centers. These concentrations can be measured by the intensity of photoluminescence excited by a Nd:YAG laser harmonics.

Thus, using a neodymium laser (2, 4 and 5 harmonics), we record the spectral photoluminescence band of working centers of crystals (F, F) and related impurity centers. Harmonic of the Nd: YAG laser are useful for evaluating the properties of radiation detectors based on anion-defective crystals of sapphire. Calibrating the fluorescent spectrometer with the standard sample, we can determine the absolute concentration of centers and classify detectors for their more effective use. The development of the laser method of testing and classification of detectors makes them more efficient and more accurate.

The research was supported by the Presidium of RAS (Programme No. 13, project № 4.12) and by the Siberian Branch of RAS (Programme No. II.8.1, project № 6).

1. M.S.Akselrod, V.S.Kortov, D.J.Krasnetsky, V.I.Gotlib. Highly sensitive thermoluminescent anion-defect α-Al_2O_3:C single crystal detectors. Radiation Protection Dosimetry, 1990, v. 33, No 1/4, pp. 119-122.
2. S.V. Solov'ev, I.I. Milman, A.I. Syurdo. Thermal- and photo-induced transformations of luminescence centers in α-Al_2O_3 anion-defective crystals. Physics of the Solid State. 2012, V. 54, No 4, pp 726-734.
3. Sykora, G.J. and Akselrod, M.S.. Spatial frequency analysis of fluorescent nuclear track detectors irradiated in mixed neutron-photon fields. Radiation Measurement, 2010, V. 45, No 10, pp. 1197-1200.
4. E.F. Martynovich. Color Centers in Laser Crystals. Irkutsk: Publishing House of the ISU, 2004, 227 p. (in Russian).

Study of the possibility of deep laser cooling of magnesium atoms

D.V. Brazhnikov[1,2], A.E. Bonert[1], A.N. Goncharov[1-3], A.M. Shilov[1,2], A.V. Taichenachev[1,2], V.I. Yudin[1-3]

[1]*Institute of Laser Physics SB RAS, pr. Lavrent'eva 13/3, 630090 Novosibirsk, Russia*
[2]*Novosibirsk State University, ul. Pirogova 2, 630090 Novosibirsk, Russia*
[3]*Novosibirsk State Technical University, pr. Karla Marksa 20, 630092 Novosibirsk, Russia*
LLF@laser.nsc.ru

Frequency standards play significant role in many fundamental and applied investigations. At present, microwave frequency standards, based on the cold cesium atoms, have relative uncertainty of the order of 10^{-16} [1]. These types of standards, most likely, have reached their limit of potential accuracy. Major hopes for significantly enhancing metrological properties of frequency standards are connected with the optical spectral band. In this direction in the past few years an increased attention have been being paid to optical clocks based on a laser-cooled single ion confined in an electromagnetic trap [2] or on large number of atoms trapped in an optical lattice [3]. The relative frequency uncertainty of these standards of the orders of 10^{-17}-10^{-18} is expected.

For a few reasons, ones of the main candidates for producing the new-generation frequency standards are alkaline earth and alkaline-earth-like atoms: Yb, Ca, Sr, Hg and Mg. To date, atoms of the first four elements can be effectively cooled down to the recoil energy limit [4,5] and even below to obtain the Bose-Einstein condensate [6]. But long time researchers have not been able to reach the same success with Mg atoms [7]. Recently some good experimental results have been achieved in the Hannover University [8]. In the experiments small number of ultracold atoms (N=5000, T=5 μK) was confined in a dipole trap.

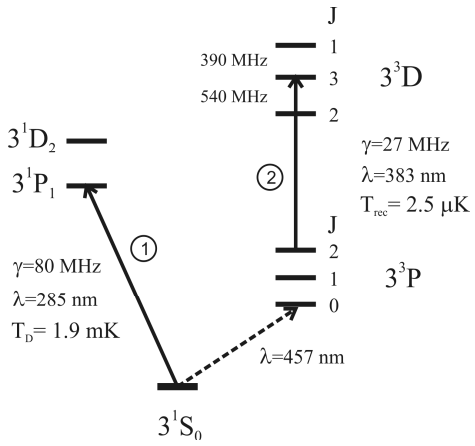

Fig. 1. Relevant energy levels of ^{24}Mg: solid lines denote the cooling transitions (the 1st and the 2nd stages with corresponding temperature limits), dashed line corresponds to the highly-forbidden transition that can be used for the laser stabilization ("clock" transition). The distances between the levels are not in scale

The present research is aimed to theoretical analysis of deep laser cooling of magnesium atoms, using electro-dipole transition $3^3P_2 \rightarrow 3^3D_3$ (see Fig.1) and to make recommendations for maximizing the fraction of cold atoms in a cloud. The energy levels of the transition are degenerate, what allows one to realize the sub-Doppler laser cooling by polarization gradients [9]. The regular semiclassical approach, based on the Fokker-Planck equation for the momentum distribution function, is exploited. At that, the problem is solved out of limits of the slow atoms approximation. By overcoming this limit we are able to investigate kinetic properties of the atomic cloud in a wide range by intensity and frequency detuning of the light field. Here, without going into mathematical details, we present a number of graphical results. The one-dimensional light field configuration, composed of two counterpropagating plane waves with opposite circular polarizations, is considered. Figures 2a and 2b represent the dependences of average atomic kinetic energy on the laser field intensity (or more exactly on the ratio R^2/γ^2, with R the Rabi frequency and γ the spontaneous decay rate) and on the frequency detuning δ in γ units. By analyzing such plots for different intensities one can figure out that the lowest achievable kinetic energy is about $20\times E_{rec}$ [10], where E_{rec} is the recoil energy. This value is sufficiently large for further applications of cooled atoms (e.g. for loading

an optical lattice). In the present work we suggest the way for overcoming this problem with keeping of essential part of cold atoms in a cloud. Let us consider the momentum distribution of cold atoms in various cases of the light field intensity. As it follows from Fig.2c, the distribution profile can be quite "nonmaxwellian" with narrow and high-contrast spike at the center (solid line). This spike corresponds to the coldest atoms, while the wide base characterizes "hot" ones. The new task hereby arises: what conditions do maximize the relative area under the spike? Assume the atoms to name "cold" if their momentum is less than, for example, $3\times\hbar k$. Fig.2d shows that the relative number of cold atoms has maximum at the certain intensity. In other words, the relative number of cold atoms in a cloud can be maximized by proper choice of the field parameters. After the sub-Doppler laser cooling the atoms can be loaded into a dipole trap. Its depth can be selected so that the only cold atoms (corresponding to the spike) will be confined in it. In that case an effective temperature of the cloud will be defined by the width of the narrow spike (just several μK).

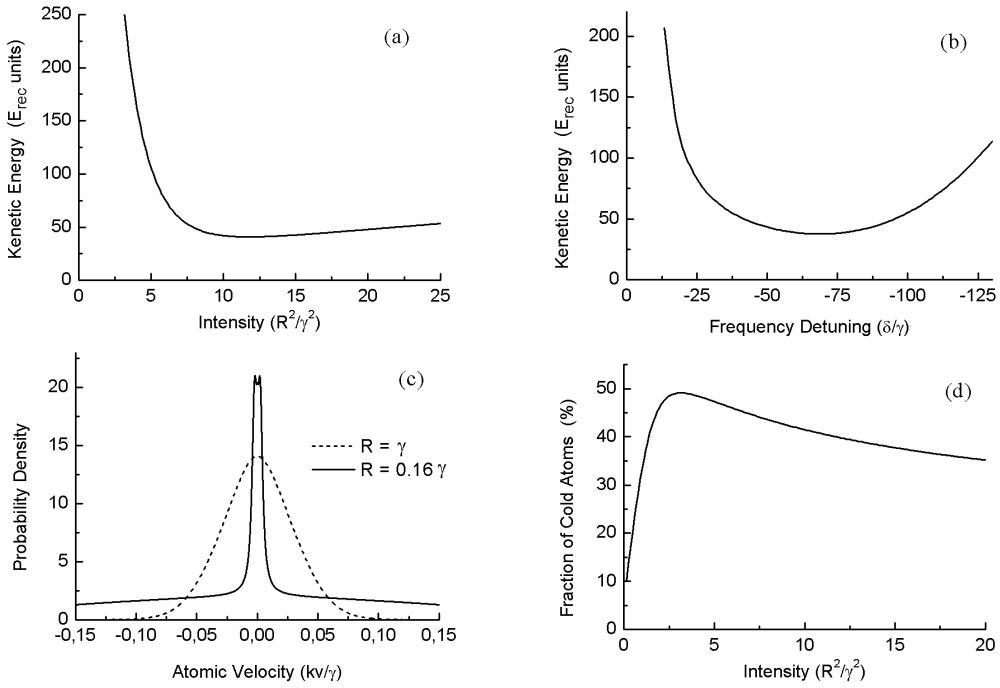

Fig. 2. Average kinetic energy of atom in a cloud as the functions of *a)* light intensity (proportional to the Rabi frequency in a square) and *b)* frequency detuning at R=0.7γ. *c)* The examples of momentum atomic distributions in various light-field intensity regimes. *d)* Relative fraction of cold atoms in a cloud as the function of the light intensity. For the figures a), c) and d) frequency detuning equals to -2γ

The work is supported by the Ministry of Education and Science of the Russian Federation in the frame of the Program "Scientific and scientific-pedagogical personnel of innovative Russia" (the Contract no. 16.740.11.0466 and the Agreement no. 8387), by RFBR (grants nos. 12-02-00454, 12-02-00403, 11-02-00775, 11-02-01240), by the Presidium of Siberian Branch of Russian Academy of Sciences and the Russian Quantum Center. The young scientists D.V. Brazhnikov, A.M. Shilov and K.S. Tabatchikova are also supported by the Presidential Grant MK-3372.2912.2 and the RFBR Grant 12-02-31208-"mol_a".

[1] T.E. Parker, "Long-term comparison of caesium fountain primary frequency standards", Metrologia **47**, 1-10 (2010).
[2] T. Rosenband, D.B. Hume, P.O. Schmidt et al., "Frequency ratio of Al^+ and Hg^+ single-ion optical clocks. Metrology at the 17th decimal place", Science **319**, 1808-1812 (2008).
[3] H. Katori, "Optical lattice clocks and quantum metrology", Nature Photonics **5**, 203-210 (2011).
[4] C. Degenhardt, H. Stoehr, Ch. Lisdat et al., "Calcium optical frequency standard with ultracold atoms: Approaching 10^{-15} relative uncertainty", Phys. Rev. A **72**, 062111 (2005).
[5] S. Mejri, J.J. McFerran, L. Yi et al., "Ulraviolet laser spectroscopy of neutral mercury in a one-dimensional optical lattice", Phys. Rev. A **84**, 032507 (2011).
[6] S. Sugawa et al., "Bose-Einstein condensate in gases of rare atomic species", Phys. Rev. A **84**, 011610 (2011).
[7] T.E. Mehlstäubler, K. Moldenhauer, M. Riedmann et al., "Observation of sub-Doppler temperatures in bosonic magnesium", Phys. Rev. A **77**, 021402 (2008).
[8] M. Riedmann, H. Kelkar, T. Wübbena et al., "Beating the density limit by continuously loading a dipole trap from millikelvin-hot magnesium atoms", Phys. Rev. A **86**, 043416 (2012).
[9] J. Dalibard and C. Cohen-Tannoudji, "Laser cooling below the Doppler limit by polarization gradients: simple theoretical models", J. Opt. Soc. Am. B **6**(11), 2023-2045 (1989).
[10] D.V. Brazhnikov, A.E. Bonert, A.N. Goncharov et al., "Study of a possibility of deep laser cooling of magnesium atoms for designing the new-generation frequency standard", Vestnik NSU, Series "Physics", Vol. **7**, Is. 4, 6-18 (2012) [in Russian].

Characteristics of the free space laser line telecommunications and quantum key distribution

B.V. Poller [1], A.V. Britvin[1], U.D. Kolomnikov[1], S.I. Konyaev[1], V.L. Kurochkin[2], A.V. Zverev[2], Y.V. Kurochkin [3]

[1] *Institute of Laser Physics of SB RAS, Pr. Lavrentyeva 13/3, Novosibirsk, 630090 Russia*
[2] *Institute of Semiconductor Physics of SB RAS, Pr. Lavrentyeva 13, Novosibirsk, 630090 Russia*
[3] *Russian Quantum Center,Novaya str., 100, BC "URAL", SKOLKOVO, Moscow region, 143025, Russia*
E-mail: jeepo@yandex.ru

Increase of volumes of information transfer between various continents on Earth, growth of networks of television, development of satellite systems of navigation defines interest to use laser ground-space communication lines.

The use of laser lines can significantly increase the data rate, increase the accuracy of navigation. However, the biggest problem of creating ground-space communication is to overcome the attenuation of laser radiation in the cloud. One method of transmitting data from spacecraft in cloudy conditions is the use of optics-radio repeaters placed on unmanned aerial vehicles, or balloon, clouds above that makes a major contribution to the attenuation of the optical signal.

At top of the mountain 2100 m high experiments on distribution of laser signals on lengths of waves 405, 450, 530, 910 nanometers on the horizontal route of 1100 m and on the inclined route of 8500 m with difference of height of 1100 m in the conditions of the range "Kaytanak" of Mountain Altai for definition of operating conditions of laser systems on land point were made. Characteristics of optical backgrounds in UV, visible and near infrared ranges at the heights of 1000 and 2100 m above sea level were received. Besides, characteristics of backgrounds in the spectral range for quantum cryptography were in addition investigated.

We suggested to use a planar polymeric wave guide with additives as the receiver of a laser signal. This receiver has the directional pattern about 360, the small weight (rather classical reception systems), can have the big area, is simple in production, can use available fiber devices.

Quantum cryptography is a field of research in telecommunications whose ultimate goal is to ensure absolute security of data communications over fiber or free-space optical channels [1]. The idea behind quantum cryptography is to create a secret quantum key during the transmission of single photons from a sending to a receiving party, commonly called Alice and Bob, respectively. The security against eavesdropping by a third party called Eve comes from laws of quantum mechanics: (1) Any measurement of the state of a quantum entity changes this state. (2) It is not possible to reliably identify an unknown state of a quantum entity by a single measurement. Consequently, any attempted attack on the data transmission will unavoidably cause an irreversible change in the quantum states of data-carrying single photons, providing unambiguous evidence of the attack.

This paper reports on experimental demonstrations of free-space QKD with polarization coding of single photons by the BB84 protocol, for which purpose a quantum-cryptography communication system was built. The aim was to investigate methods for the generation of single photons in a given polarization state, their detection, and original-state identification. The basic experimental device used in this work consists the transmitting unit and the receiving unit [2,3]. The four laser beams are combined by a system of mirrors into one beam, which is attenuated by an absorbing filter at the exit. Alice produces single linearly polarized photons whose polarization can have one of the four possible orientations 0°, +45°, +90°, and –45°, which make up a rectilinear (0°, +90°) and a diagonal (+45°, –45°) basis. The receiving unit of the setup consist of four single photon detectors. Measurements happen in v rectilinear and basis diagonal. The specially chosen avalanche photodiodes C30902S, which are the most sensitive photodiodes in the range

of 0.8ηm, served as single-photon detectors. With the aim of counting single photons, the avalanche diodes were connected so that they operated in the Geiger mode, when one photon can induce an avalanche of charge carriers. The diodes were connected in a passive avalanche quenching circuit. The signal was picked off the load resistor 50Ω, amplified by an amplifier, and fed into a shaper of standard TTL pulses for the interface with a computer. The probability of detecting a single photon at a wavelength of 830 nm reaches 50%. In order to decrease intrinsic noises, the diodes were cooled to -20°C with the use of Peltier semiconductor microrefrigerators. The frequency of noise pulses in the avalanche photodiodes operating in the Geiger mode depends on the temperature and the excess of the applied voltage over the threshold value. During a communication session, Alice sends a sequence of single photons whose polarizations are chosen at random. Bob detects the photons and chooses at random a polarization measurement basis for each of them, using a polarization beam splitter. Over an additional, open channel, Bob then informs Alice which basis he has taken for the measurement but does not communicate the result. Calculations of the loss of a quantum channel, depending on the distance and the parameters of the optical system are given.

The organization of the channel of laser communication of ground-space with use of optics-radio repeaters in the atmosphere allows to provide information transfer with overcast on the route. Methods of creation of the laser line, including with quantum and cryptographic coding of data, taking into account change of windows of transparency of the atmosphere depending on height of lifting of repeaters and characteristics of the laser radiation accepted by means of the special planar and fiber antenna were investigated.

References

1. Gisin, N., Ribordy, G., Tittel, W., and Zbinden, H., Quantum Cryptography, Rev. Mod. Phys., 2002, vol. 74, pp. 145–175.
2. Kurochkin V. L., Ryabtsev I. I., and Neizvestny I. G., 2004,Optics and Spectroscopy, ***96,*** 703.
3. V.Kurochkin et al., Optoelectronics, Instrumentation and Data Processing 45, 374 (2009).

THz and Raman spectroscopy of steroid hormones

O.P. Cherkasova

Institute of Laser Physics of SB RAS, Pr. Lavrentyeva 13/3, Novosibirsk, 630090 Russia
E-mail: o.p.cherkasova@gmail.com

The steroid hormones differ only by the position of functional groups attached to this four-ring core and by the oxidation state of the rings. The biological action of steroids is closely related to some features of their chemical structure. The steroids are aggregated into the molecular crystals of two space groups P_{212121} and P_{21}, in general. The molecules could be bound by van der Waals and/or stronger hydrogen forces in molecular crystals. Thus, steroids are convenient object for study of a nature of low-frequency vibrations and affects of hydrogen bonds.

The steroid hormones influence on many physiological processes in humans and animals is well known. Their crucial role in regulating life processes led to a widespread research in steroid chemistry and biochemistry, creating new and fast methods of steroid analysis in biological samples, as well as in food, sewage and pharmaceutical production. Steroids have rather complex molecular structure, show significant reactivity with similar physico-chemical properties and are often located in low quantities in multicomponent matrices. The determination of steroids and their metabolites in biological samples and pharmaceutical drugs can be done by chromatography, mass spectrometry and other methods of analysis with high accuracy. However, these methods are time consuming and expensive. In this regard, the development of new operational methods of analysis is highly relevant. The methods of terahertz time-domain spectroscopy (THz-TDS) can be helpful for the study of steroids. This type of spectroscopy has a number of advantages such as the possibility to analyze a wide frequency band in a single measurement, to obtain time resolution and phase information, and to measure the complex dielectric permittivity which completely characterizes the optical response of the matter. At the same time, THz-TDS is able to penetrate many opaque materials, but unlike X-rays, it is non-ionizing radiation and can detect the samples without influence or destroys. Moreover, THz spectra of molecular crystals show rich information about collective vibrations and are highly sensitive to the changes of the molecular conformation, structure, environment elements and intermolecular interaction. The aim of our research is to study a wide range of steroids by THz-TDS and Raman spectroscopy.

For THz-TDS measurements the samples were prepared by pressing the pure polycrystalline powder to disks of thickness 0.4 mm, diameter 5 mm and average density 1.2 mg/mm^3 by applying a pressure about 50 MPa. For the case of thin films and solutions we developed total internal reflection (TIR) scheme using silicon right angle Dowe prism [1]. The description of the THz-TDS apparatus was given in [2]. The Raman spectra were recorded as in [3].

Spectral properties of steroids are well described in UV and IR spectral range, but those spectra are similar. Only in THz region substances have several intensive unique features. The substances have several intense spectral features in the frequency range 0.1-3.0 THz. The features are uniquely determined by a hormone structure. This allows one to analyze a complex mixture on specific frequencies and to obtain information about individual components.

References

1. M.M. Nazarov, A.P. Shkurinov, E.A. Kuleshov, V.V. Tuchin, *Quantum Electronics*, **38** (7), 647-654 (2008).
2. I. N. Smirnova, D. A. Sapozhnikov, A. V. Kargovsky, V. A. Volodin, O. P. Cherkasova, R. Bocquet, A. P. Shkurinov, *Vibrational Spectroscopy*, **62**, 238–247 (2012).
3. O. P. Cherkasova, V.A. Volodin, V.A. Minaeva, B.F. Minaev, G.V. Baryshnikov, *Vestnik Novosibirsk State University, Series: Physics*, **5** (4), 176- 180 (2010).

About shape of the saturated absorption resonance and spectrum of magnetic scanning

E.G. Saprykin [1], A.A. Chernenko[2], A.M. Shalagin[1]

[1]Institute of Automation and Electrometry of SB RAS, Pr. Koptuga 1, Novosibirsk, 630090 Russia
[2] Insitute of Semiconductor Physics of SB RAS, Pr. Lavrentyeva 13, Novosibirsk, 630090 Russia
E-mail: chernen@isp.nsc.ru

Results of the theoretical analysis of physical processes leading in experiment [1] to essential distinction of the magnetic scanning spectra at change of mutual orientation of the plane polarized counter spreading waves of one frequency are submitted.

In the simple model of atomic transition with full level moments J=1 stationary and non-stationary numerical solutions of equations for a density matrix are received. It is shown that for a long-living lower state (as in [1]), in stationary conditions the basic process determining features of behavior of amplitudes of the saturated absorption resonance and spectra of magnetic scanning from mutual orientation of the polarization planes of light waves, is the magnetic coherence induced by the linear polarized strong field between levels at the lower state of atomic transition. The maximum contribution due to the transfer process of magnetic coherence from the upper to the lower levels doesn't exceed 10% from amplitude of a nonlinear resonance, and the contribution of nonlinear polarization at a combinational frequency makes still smaller value.

It is revealed that in case of the orthogonally polarized fields the type of a form of the nonlinear resonance significantly depends on the openness degree of atomic transition (value of branching parameter a0) and can have both a dip, and a peak form on the Doppler absorption line contour. While at parallel polarizations of fields influence of the transition openness degree is not enough, and the nonlinear resonance is always exhibited by the dip way.

It is shown that in the flying area behavior of the saturated absorption and magnetic scanning spectra for transitions from the ground atomic states at the stationary and non-stationary solutions of equations for a density matrix coincide qualitatively.

Researches of the more complex models of atomic transition (J=2-J=1 and J=2-J=2) in a stationary case give qualitative consent with results of calculations of J=1-J=1 transition both on spectra of nonlinear resonance, and on spectra of magnetic scanning.

References

1. D.V. Brazhnikov, A.V. Taichenachev, A.M. Tumaikin, et.al., *JETP Lett* **91**, 694 (2010).

About double structure of the saturated absorption resonance on open atomic transition

E.G. Saprykin [1], A.A. Chernenko[2], A.M. Shalagin[1]

[1]*Institute of Automation and Electrometry of SB RAS, Pr. Koptuga 1, Novosibirsk, 630090 Russia*
[2] *Insitute of Semiconductor Physics of SB RAS, Pr. Lavrentyeva 13, Novosibirsk, 630090 Russia*
E-mail: chernen@isp.nsc.ru

Recently in work [1] at research of the nonlinear resonance shapes in a spectroscopy of the counterpropagating waves of rubidium vapor the unusual inverted resonances in saturated absorption of a strong wave were found. Such statement of experience is used seldom. Authors couldn't explain the nature of resonances within the physical effects and phenomena known for them list of which, on our opinion, looks not full. As a result they interpreted the found effect as unusual solution of the balance equations for a density matrix of the nondegenerate two level resonant medium. However, among the mentioned by them phenomena there is no effect of magnetic coherence of levels without of which it is impossible to consider the spectroscopic phenomena in real degenerate atomic systems, in particular, in rubidium atom.

In this report we present results of numerical researches of the saturated absorption spectra of the strong wave in a resonant atomic medium with degenerate structure of levels (the full moment of levels J=1 and J=2). It is shown that the spectrum of the saturated absorption resonance of a strong wave in the wide range of change of the relaxation characteristics of atomic transitions and parameters of saturation is represented, as well as in work [1], in the form of the narrow inverted peak in a traditional wide dip. Thus the peak structure of a resonance is caused generally by the magnetic coherence between levels of the lower state induced by the strong field which contribution to the peak amplitude considerably surpasses contribution of the populational mechanism in the two level model [1]. Influence of an extremity of the interaction time of atoms with optical fields on shapes of nonlinear resonances for transitions from the ground state is discussed.

References

1. V.I. Vasilyev, V.L. Velichanskii, A.S. Zibrov, et.al., *JETP* **130**, 883 (2011).

Spectropolarimetric resonance shapes at the transitions between excited states of the neon atom

I.A. Kartashev, A.A. Chernenko, A.V. Shishaev

Insitute of Semiconductor Physics of SB RAS, Pr. Lavrentyeva 13, Novosibirsk, 630090 Russia
E-mail: chernen@isp.nsc.ru

Results of experimental and theoretical studies of the spectropolarimetric resonance shape of the probe light wave of linear polarization in the presence of a strong counter propagating circularly polarized wave of the same frequency tunable near the transitions between degenerate excited states $1s_5$ - $2p_2$ ($J = 2 \rightarrow J = 1$) and $1s_5$ - $2p_4$ ($J = 2 \rightarrow J = 2$) of the neon atom placed in a longitudinal magnetic field are presented.

Spectropolarimetric resonance on studied neon atom transitions in the absence of a magnetic field is shown experimentally in the form of a narrow peak near the line center. The magnetic field effect at low values of intensity ($H \leq 2Gs$) leads to splitting of the probe wave shape resonances into two asymmetrical components having dip near the line center. By increasing the magnetic field strength in the range of $2Gs \leq H \leq 20Gs$ a decrease in the amplitude of the doublet components, the frequency distance enhancement between them and a significant increase in the dip amplitude are observed.

With further increase of the magnetic field ($H>20Gs$) along with the mentioned behavior of components of the doublet splitting occurs in additional splitting of the resonance dip. Moreover, the pattern of the dip splitting for studied transitions are different: if for transition $1s_5$ - $2p_2$ this splitting has doublet character, in case of transition $1s_5$ - $2p_4$ a more complex structure is observed.

A theoretical interpretation of the observed dependence of the spectropolarimetric resonance behavior on the magnetic field is proposed. Based on numerical modeling effect in a degenerate atomic system with level moments of $J = 2$ and $J = 1$ the impact nature of the atomic transition parameters, g-factor of levels and the ellipticity degree of polarization of the strong light wave on the spectropolarimetric resonance shape of the probe field has been studied. Numerical calculations are showed that the polarization ellipticity of the strong light wave determines the shape of the resonance peak at zero magnetic field and spectrum of the doublet splitting of the resonance in a magnetic field. The peculiarities of the additional splitting of resonance dips for studied transitions in a strong magnetic field are caused by the difference in the value of g-factors of the upper levels of these transitions.

.

Phase transitions with trapped atomic polaritons

A.P. Alodjants[1,2], I.Yu. Chestnov[1], S.M. Arakelian[1]

[1] *Vladimir State University named after A.G. and N.G. Stoletovs, Gorky Str. 87, Vladimir 600000, Russia*
[2] *Russian Quantum Center, Novaya Str.100, Skolkovo, Moscow 143025, Russia*
E-mail: alodjants@vlsu.ru

We consider problem of high temperature thermodynamic properties and phase transitions with coupled atom-light states (dressed states and polaritons). We examine the optical collision (OC) problem for system consisting of a hot (530 K) two-level Rubidium atomic gas and ultra-dense buffer gas (the pressure is up to 500 bars) in the presence of non-resonant laser irradiation.

In a coupled atom-light states picture OCs cause transitions between dressed state energy levels. We argue that quick enough OC processes can lead to establishment of thermodynamically equilibrium population of dressed states. We propose a theoretical approach of a dressed-state thermalization that accounts for the evolution of pseudospin Bloch vector components and characterizes the essential role of the spontaneous emission rate in the thermalization process which limits the lifetime of coupled state and prevents thermalization. For experimental conditions [1] the predicted thermalization time is in nanosecond domain that is approximately ten times shorter the natural lifetime of Rb 5^2P excited states.

For polariton thermalization we propose to use a waveguide cavity in described system for providing necessary atom-field interaction and achieving suitable polariton lifetime, as a result. In fact, we consider metallic tube with round cross section. The lifetime of photon-like polaritons trapped in such a waveguide can be longer than the thermalization time, and is mainly determined by the cavity *Q*-factor. The radius of proposed waveguides should be sub-wavelength, yielding a low-frequency cutoff close to the atomic resonance.

The problem of second order phase transition to "superradiant" state of photonic field under dressed state thermalization condition is discussed. Using a thermodynamic approach (partition function calculation) we established a gap equation under a mean-field approximation for order parameter λ - normalized on atom number average amplitude of optical field. Nontrivial solution of this equation shows that for large negative detunings $\delta = \omega_{\text{laser}} - \omega_{\text{atom}}$ a macroscopic stationary polarization of the atomic medium, that is proportional to the order parameter λ, appears. Such a transition can be connected with superfluid (coherent) properties of photon-like low branch polaritons, representing a superposition of quantum optical field and macroscopic polarization of atomic medium. In this case order parameter λ can be recognized as a polariton wave function.

Figure 1 demonstrates phase transition behavior for order parameter λ for the system under discussion. In the low density limit, when $\lambda^2 << 1$, this dependence is described by the easy expression (see [2]) $\lambda(\varepsilon) \cong \sqrt{\rho}\left[1-(\rho)^{\varepsilon/\varepsilon_c - 1}\right]^{1/2}$, where $\varepsilon_c = -\ln[(1-\rho)/\rho]$, $\varepsilon \equiv \hbar\delta/k_B T$.

For positive detunings the fulfillment of thermalization condition for coupled atom-light states permits us to create a population inversion in a two-level atomic ensemble. But this state isn't stable and for any finite laser power the variation of atom-field detuning δ drives a coupled atom-light system out of thermal equilibrium even if such an equilibrium (or quasi-

equilibrium) has been initially achieved. Due to the inversion of atomic states this system is appropriate candidate for lasing (see [3]).

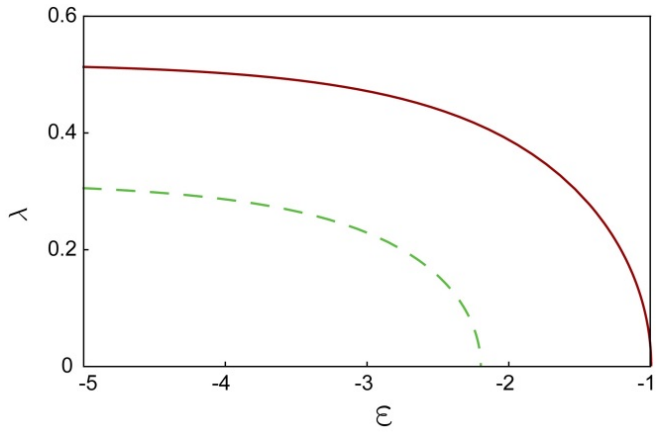

Fig. 1.The dependence of order parameter λ on normalized atom-field detuning (ε parameter) for temperature of atomic gas $T = 530\,\mathrm{K}$. Value $\rho = 0{,}27$ (solid red curve) corresponds to experimental condition (see. [1]), $\rho = 0{,}1$ (dashed green curve) was plotted under low density limit $\lambda^2 << 1$.

Finally, the problem of high temperature Bose-Einstein condensation (BEC) of low-branch atom-light polaritons in a waveguide cavity was studied – [4]. Specifically, we propose a special biconical waveguide cavity (BWC), permitting localization and trapping of LB polaritons imposed by the variation of the waveguide radius in longitudinal direction – see [3]. In particular, we consider waveguides with a form $R(z) = R_0/[1+\alpha\,|\,z\,|^{\nu}]$, with $\nu \neq 0$ and $\alpha \neq 0$, where α characterizes the curvature of waveguide profile. The solution of Maxwell equations for the field inside waveguide shows that photon (and, respectively, photon-like polariton at negative detuning) is effectively trapped in potential, that is linearly proportional to $|\,z\,|^{\nu}$, i.e. represents power-law potential. In a quasiclassical approximation we determined the critical temperature of Bose-Einstein condensation of low-branch polaritons, that can be high enough – a few hundred kelvins; it is connected with the photon-like character of LB polaritons and strongly depends on waveguide-cavity parameters.

References

1. I. Yu. Chestnov, A. P. Alodjants, S. M. Arakelian et al., *Phys. Rev. A***81**, 053843 (2010).
2. A. P. Alodjants, I. Yu. Chestnov, and S. M. Arakelian, *Phys. Rev. A***83**, 053802 (2011).
3. R. V. Markov, A. I. Parkhomenko, A. I. Plekhanov, A. M. Shalagin, Zh. Eksp. Teor. Fiz. 136, 211 (2009) [JETP 109, 177 (2009)].
4. I. Yu. Chestnov, A. P. Alodjants, S. M. Arakelian et al., *Phys. Rev. A***85**, 053648 (2012).

Pulsed IR Inductive Lasers

A. M. Razhev[1,2], D. S. Churkin[1,2], E. S. Kargapol'tsev[1]

[1] *Institute of laser physics SB RAS, Ac. Lavrentyev's prosp., 13/3, Novosibirsk, 630090 Russia*
[2] *Novosibirsk state university, Pirogova str., 2, Novosibirsk, 630090 Russia*

Pulsed inductive discharge is alternative method of pumping gas lasers [1–6]. In contrast to conventional pulsed longitudinal and transverse discharges, a pulsed inductive discharge is formed due to the magnetic field induction produced by the pumping system without any electrodes in the active medium. An appropriate choice of the tube material may ensure the purity of the active medium considerable endurance of lasers. The formation of such a discharge is not accompanied by the appearance of cathode spots on the surface of the electrodes, which are responsible for the instability and contraction of the discharge, deterioration of the homogeneity of the discharge, contamination of the gas mixture, quenching of lasing, and limitation of the pulse repetition rate.

To form pulsed inductive discharge two different excitation systems are developed. The first one is based on well known of Blumlein-type scheme and is described by us in [5]. Another system is developed using 144 MHz homemade RF power supply.

Pulsed inductive discharge allows pump active gas media with different types of inversion population formation. Using Blumlein-type excitation scheme near IR hydrogen inductive laser is created.

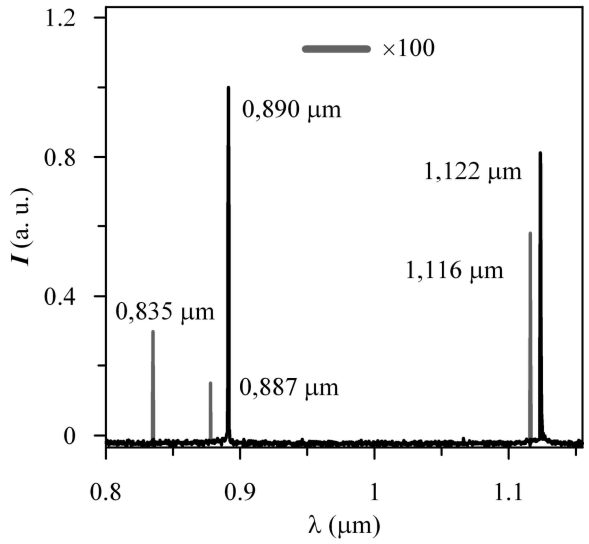

Fig. 1. Generation spectrum of H2 inductive laser

The generation is observed on 4 lines. The wavelength λ_1 =0.835 μm, λ_2 =0.89 μm, λ_3 =1.116 μm, the λ_4 =1.122 μm that corresponds to $2s\sigma^1\Sigma^+_g(\boldsymbol{E}) \rightarrow (2ps)^{21}\Sigma^+_g(\boldsymbol{B})$ transition. Maximum of laser emission peak power is at two lines: 7 kW for wavelength λ_2 =0.89 μm and 5 kW for wavelength λ_4 =1.122 μm, respectively. Pulse duration of generation is 18–20 ns (FWHM). Laser is working both on one wavelength and on two wavelengths simultaneously with competition between these transitions. The active medium is hydrogen at optimal pressure 0.5-0.8 Torr.

The next IR inductive laser created is chemical HF laser working on vibrational-rotational transitions of HF molecules. As a fluorine donor one used F_2, NF_3 and SF_6, as hydrogen donor – H_2. The highest power has been obtained with SF_6 as the fluorine donor. For the mixture of H_2-NF_3 one has also obtained the lasing, but its parameters were not studied due to dusting of the resonator's windows with the products of discharge. For H_2-F_2 one has not been able to obtain the infrared lasing. Despite of the electric discharge HF lasers, the pulsed inductive HF one reaches its maximum power when has added Ne but not He as a buffer gas in the mixture. During the experiments one obtained 10 mJ for H_2-SF_6-Ne mixture (Fig. 2), which is 10% higher than lasing in H_2-SF_6-He mixture.

Lasing on vibrational-rotational transitions of CO_2 molecules (10.6 μm) is achieved using both types of excitation systems. The maximum generation energy for Blumlein-type excitation system of 150 mJ is achieved at the CO_2:N_2:He – 1:4:12 mixture pressure of 15 Torr. However total efficiency doesn't exceed 0.3%, because in this type of pulsed inductive

discharge major energy of the inductive discharge is used to excite nitrogen molecules to electronic levels $C^3\Pi_u$ and $B^3\Pi_g$. Therefore, to increase the efficiency of the CO_2 laser it is necessary to optimize the excitation parameters of the active medium by an inductive discharge.

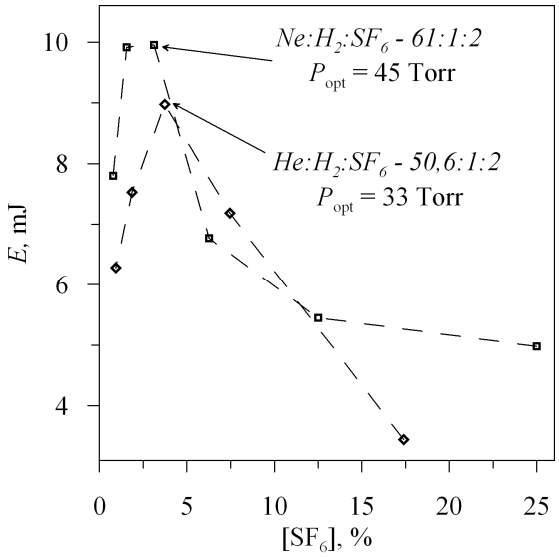

Fig. 2. Dependence of the HF inductive laser generation energy on concentration of SF_6 with He (◆) and Ne (■) as buffer gas

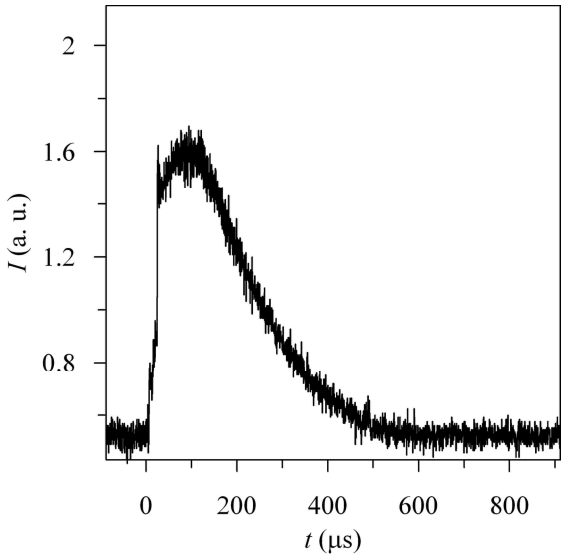

Fig.3. Oscillogram of the CO_2 inductive laser optical pulse

To solve this problem the excitation system based on RF power supply is developed. This system allows form pulsed RF inductive discharge with respectively low-energy electrons. Thus major energy in this case is used to excite CO_2 molecules directly (first thin peak shown on Fig. 3) and low vibration levels of N_2 molecules. Laser can operate with either only N_2-CO_2 mixture or multi component mixtures. In the latter case the generation energy is about 3–5 times higher. The maximum generation energy for this system is 17 mJ and is achieved for $He:N_2:CO_2$–8:1:1. Energy loaded from RF power supply is 100 mJ, therefore total efficiency is 17%.

The lasing shape is also investigated. For pulsed high voltage excitation system lasing has a ring shape. For pulsed RF excitation system lasing has a circle shape. Characteristic feature of inductive lasers is high pulse-to-pulse stability. The reproducibility of the amplitude from pulse to pulse is equal to about ±1%.

References

1. A.M. Razhev, V.M. Mkhitaryan, D.S. Churkin, “703 to 731 nm FI laser excited by a transverse inductive discharge”, *JETP Lett.*, 2005, **82(**5) p. 259-62
2. A.M. Razhev, D.S. Churkin, “Inductive ultraviolet nitrogen laser”, *JETP Lett.*, 2007, **86**(6) p. 420-423
3. A.M. Razhev, D.S. Churkin, A.S. Zavyalov, “Pulsed inductive discharge molecular hydrogen laser”, *Vestnik NSU*, *Seria Fizika*, 2009, **4**(3) p. 12–19 (in Russian)
4. A.M. Razhev, D.S. Churkin, A.A. Zhupikov, “Study of the UV emission of an inductive nitrogen laser”, *Quantum Electronics*, 2009, **39**(10) p. 901-905
5. A.M. Razhev, D.S. Churkin, “Pulsed inductive discharge CO_2 laser”, *Optics Communications*, 2009, **282** (7), p. 1354–1357
6. A.M. Razhev, D.S. Churkin, E.S. Kargapol’tsev, “Chemical HF laser with pulsed inductive discharge initiation”, *Laser Physics Letters*, 2013, **10**(7)

Multiple ultrashort pulses generation and related experiments

D. Ursescu[1,2], Romeo A. Banici[1], Constantin Blanaru[1], Gabriel V. Cojocaru[1], Razvan Dabu[1],Laura Ionel[1], Liviu Neagu[1], Sandel Simion[1], Razvan Ungureanu[1], Holger Stiel[3]

[1]Lasers Department, National Institute for Lasers, Plasma and Radiation Physics, Magurele, Ilfov, Romania
[2]National Institute for Nuclear Physics and Engineering – Horia Hulubei, Magurele, Ilfov, Romania
[3]Max Born Institut für Nichtlineare Optik und Kurzzeitspektroskopie im Forschungsverbund Berlin, Berlin, Germany
E-mail: gabriel.cojocaru@inflpr.ro

Abstract:

Multiple pulses generation, characterization and coherent control are at the core of a broad range of experiements with ultraintense laser pulses.

A multiple pulses chirped pulse amplification laser system was developed at INFLPR by modification of a commercial 15 TW laser system. The system can be used for multiple pulses generation in collinear pump-probe experiments. In order to generate the multiple pulses, a simple passive pulse shaping technique in the spectral domain is implemented directly in the stretcher. The resulting pulses have complementary spectra. The ratio of the intensity of the pulses and the delay between them can be easily controlled. The pulses generated in this way were used in experiments related to coherent combination of ultrashort pulses and in experiments related to plasma X-ray lasers.

Multiple pulses generation

Two and three spectrally separated pulses with duration of 300 fs and energies in the mJ range were generated at the GIWALAS facility (2kHz, 200fs, 775nm, 0.6mJ), with intensity ratios from few percent to 100% and delays up to 600 ps. The method was also implemented at TEWALAS facility (10Hz, 30fs, 800nm, 300mJ).

Coherent combining of ultrashort pulses

At TEWALAS, the generation of two complementary spectra pulses was used for extending the collinear coherent combination method to ultrashort and intense pulses in Chirped Pulses Amplification systems. It was experimentally shown that the addition of the pulses is quadratic in power with the number of pulses. The method is scalable to few tens of PW pulses. Moreover, a method to measure and control the delay between the pulses with sub-radian resolution was demonstrated .

New X-Ray Laser pumping scheme

Based on the same multiple pulse generation method, optimization of a plasma-based X-ray laser was performed. The novel X-ray laser pumping scheme, based on one long and two short (1L2S) pump pulses, in a grazing incidence pumping configuration allowed us to produce lasing in Zr, Mo, Pd, Ag and Sn x-ray lasers with wavelengths from 22nm to 11.9nm. The total pump energy in one 360ps long and two short pulses was only 200 mJ on the target .

Plasma x-ray lasers (XRL) are the coherent sources in the EUV range with the highest peak brilliance. With the introduction of the normal incidence, transient colli-sional excitation (NICE) pumping scheme in mid 1990s[1]. and, later, with the introduction of the grazing inci-dence pumping (GRIP) scheme [2,

3], the pump energy needed for XRLs decreased to the Joule level for the sat-urated plasma emission, e.g. in an Ag X-ray laser emiting at 13.9 nm, in the EUV domain [4].

The success of the GRIP scheme was related to the spatial control of the short pulse pump energy depo-sition in the XRL plasma. While in the NICE scheme the pumping used normal incidence pulses, the pump pulse energy deposition was realized in the plasma crit-ical density region, tens of micrometers away from the sub-critical plasma density region where the XRL gain
was efectively useful. With the GRIP scheme, this spa-tial mismatch was eliminated. It became possible to con-trol the density region where the energy of the pump pulse is deposited by varying the incidence angle of the short pulse.

In the present study we report the demonstration of a novel pump scheme based on one long pump pulse with 360 ps duration and two subsequent short pump pulses (1L2S), with the duration in the range of few ps. It is shown that 1L2S scheme allows to operate a high gain Ni-like Ag XRL nearly to saturation level, with a pump energy as low as 200 mJ. The key issue in the fur-ther reduction of the pump energy is the removal of thetemporal mismatch between the moment of the highest plasma temperature and the moment of generation of the optimal ionization stage.

To conclude, a new pumping scheme using two short pulses was proposed and implemented for Ni-like Ag XRL, based on a modication in the optical stretcher of the pump laser. The new 1L2S scheme provides better control of ionization and temperature dynamics in the XRL plasma. An XRL output up to 12 times higher than in the 1L1S was found. The small gain signal of 55 cm^{-1} is comparable with the gain obtained for Mo XRL in [3] at longer wavelength. The higher gain obtained experimentally is in accordance with EHY-BRID simulations indicating an increase of both gain and electron temperature in comparison with the 1L1S scheme. The reported results pave the way to XRLs in the EUV region using high repetition rate pump lasers in the hundred of Hz range. They may prove useful in the extension of the XRL operating wave-lengths towards the water window using multi-Joule, 10Hz repetition rate pump lasers.

References

1. P. V. Nickles, V. N. Shlyaptsev, M. Kalachnikov, M. Schnrer, I. Will, and W. Sandner, *Phys. Rev. Lett. 78*, 2748 (1997).
2. V. N. Shlyaptsev, J. Dunn, S. Moon, R. Smith, R. Keenan, J. Nilsen, K. B. Fournier, J. Kuba, A. L. Osterheld, J. J. G. Rocca, B. M. Luther, Y. Wang, and M. C. Marconi, in Soft X-Ray Lasers and Applications V, vol. 5197, E. E. F. S. Suckewer, ed. *(SPIE, 2003), vol.5197*, pp. 221-228.
3. R. Keenan, J. Dunn, P. K. Patel, D. F. Price, R. F. Smith, and V. N. Shlyaptsev, *Phys. Rev. Lett. 94*, 103901 (2005).
4. Y. Wang, M. A. Larotonda, B. M. Luther, D. Alessi, M. Berrill, V. N. Shlyaptsev, and J. J. Rocca, *Phys.Rev. A 72*, 053807 (2005).

The research leading to these results has received funding from the EC's Seventh Framework Programme (LASERLAB-EUROPE, grant agreement n° 228334). We acknowledge suport from COST Action MP0601 “Short Wavelength Lab Sources”. This work was supported by National Authority for Scientific Research in Romania, Project LAPLAS3, Project IDEI RP6/2007, No. PN-0939/2012 and project PARTENERIATE 1/2012.

Optimization of the length standard error

A.K. Dmitriev[1,2], N.N. Golovin[1], A.A. Lugovoy[2]

[1]*Novosibirsk State Technical University, K. Marx av. 20, Novosibirsk, 630073 Russia*
[2] *Institute of Laser Physics of SB RAS, Pr. Lavrentyeva 13/3, Novosibirsk, 630090 Russia*
E-mail: alexander_dmitriev@ngs.ru

At the present time the wavelength of optical frequency standards is accepted as a reference length [1]. To transfer the size of the wavelength to the geometric length Michelson interferometer is commonly used. It is known, when a plane electromagnetic wave passing through a vacuum interferometer its transmission bands are equidistant with the interval equals to half-wavelength. This was the basis for creating the optical ruler (meter), where wavelength of stabilized laser, which frequency at present can be measured with an accuracy of a primary standard, acts as a reference length [2].

In the present article the studies of interference pattern that occurs during the passage of a Gaussian beam through a Michelson interferometer were performed. That allows finding error of length measurement which is caused by diffraction divergence and by the wavefront curvature of the light beam.

Studies were performed to assess the additional error of length measurement, which arises due to the diffraction divergence and wavefront curvature of the Gaussian beam. The calculation of the diffraction pattern and shift of the absorption band maximum relative to the case of a plane light wave (when the distance between the bands is exactly equal to the wavelength of magnitude) was performed with the distance z_2 variation for various positions of the photodetector and various crossections of beam. For definiteness, the wavelength was assumed to be 1μm.

Since the interval length is determined by the number of bands when moving the measuring mirror between two selected points z'' and z', then $\Delta l = (z_2'' - z_2') / 2$. The systematic error when using a Gaussian beam Δ is equal to the difference of shifts of transition bands: $\Delta = \delta(z_2'') - \delta(z_2')$. In other words, the error Δ is qualitatively proportional to the derivative of the total shift. Errors of the meter measuring Δ were plotted according to the $Z = (z_2'' - z_2') / 2$, with Δl=1m.

As can be seen in Fig. 1a, for ω0 = 1 mm value of Δ at z1 = 0 has a maximum when z2 = 0 and not exceeds 5×10^{-2} λ (in relative units 5×10^{-8}). For z1 = 3m maximum value closes to the previous case, but its position is shifted approximately by 1 m in the negative region. The contrast of the interference pattern in the first case is equal to 100%, in the second - slightly less than 1. With increasing the distance Z error decreases with degradation of the resonance contrast. Some oscillations in the wings of the curves associated with the error of the calculations.

Dependences on the error in determining meter for ω0 = 2 mm (Fig. 1b) have significant differences from the previous case. In both cases, there are zero values of Δ when Z equals about 2 m. Contrast of interference fringes in both cases is close to unity.

Thus, at a wavelength of 1 micron and small size of the beam (ω_0 = 1 mm) choice of the mirror tuning limits in the measuring arm is to achieve a compromise between the accuracy of the adjustment on the center of band and the systematic error at the expense of diffraction divergence and the wavefront curvature of Gaussian beam.

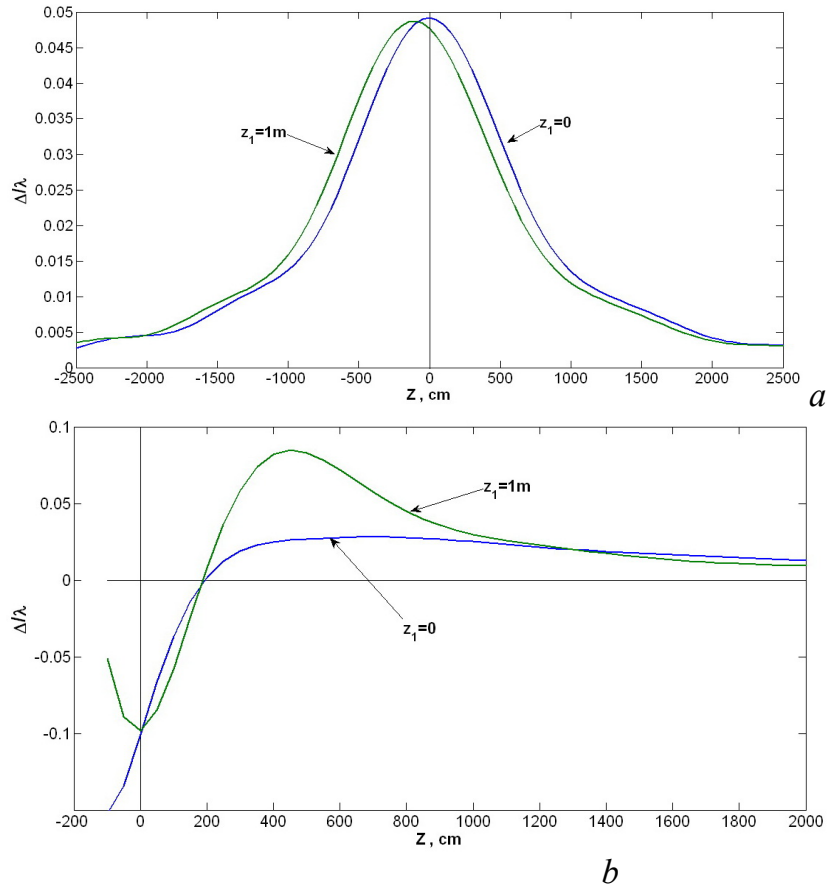

Fig.1. The systematic error of a meter when a) ω_0 = 1 mm, b) ω_0 = 2 mm.

When increasing a cross-section of the beam (up to ω_0= 2 mm) values of Z are in the near field, in which the total error Δ depending on the diffraction divergence and wavefront curvature of the Gaussian beam is equal to zero. In this case contrast of the interference fringes is close to unity.

References

1. Quinn T.J. *Metrologia* **40**, 103 (2003).
2. Udem Th.,Reichert J., Haensch, T.W. *Phys. Rev. Lett.*, **82**, 3568 (1999).

Saturation rotational structure inside magnetospectral optical resonance

K. Gus'kov[1], A. Rudavets[2]

[1] *Institute of Automation and Electrometry of SB RAS, pr. Koptyuga 1, Novosibirsk, 630090, Russia*
[2] *Moscow Institute of Physics and Technology, per. Institutsky 9, Dolgoprudny, 141700, Russia*
E-mail: guskiv@yandex.ru

We derive exact formula for nonlinear resonance absorption of monochromatic arbitrarily intense laser radiation propagated along molecular gas cell within quasi-stationary homogeneous longitudinal magnetic field. It permits us to analyze frequence, intensity and magnetic dependences of the absorption. The derivation uses superoperator representation of magnetooptical Hamiltonian operator of the gaseous medium. The formula is nonperturbative and describes the spectral structure of optical electrodipole resonance for optically coupled pair of molecular multiplet levels with any equal or unit-difference rotational angular momenta and with simple single-constant collisional relaxation. Normally thermal motion of gas molecules is also taken into account. The specified structure appears not only inside Voigt profile but also inside saturation-broadened Lorentz one. Nonperturbative form of the solution permits to escape divergent series with respect to saturation parameter and to span practically the whole of its possible values. The practically important spectral peculiarity of the solution for noncircularly polarized radiation is that the saturation sub-Lorentz rotational structures manifest themselves against Voigt background with magnetic scanning only and completely do not with frequency one.

Magneto-optical Hamiltonian operator via standard spherical tensor operators of rank 1 and via projection operators is

$$\overset{\vee}{H}{}^{(\omega)} \overset{def}{=} \sum_j \left(\tfrac{\Omega}{2}(-1)^j \overset{\vee}{1}{}^{(p)}_{jJ_j} - \vec{\tilde{\Delta}}^{(0)}_J \cdot \overset{\vee}{\vec{J}}{}^{(p)}_{jj}\right) - \left(\vec{G}^{(\omega)}_{mn} \cdot \overset{\vee}{\vec{T}}{}^{(p)}_{(mn)1} + h.c.\right) \qquad (1)$$

$$= \sum_{j_1,J_{j_1},M'_{j_1};\, j_2,J_{j_2},M_{j_2}} H^{(\omega)}_{j_1,J_{j_1},M'_{j_1};\, j_2,J_{j_2},M_{j_2}} \overset{\vee}{P}_{j_1,J_{j_1},M'_{j_1};\, j_2,J_{j_2},M_{j_2}} \ .$$

$j \in (m,n) \overset{def}{=} (1,0)$, $\Omega \overset{def}{=} \omega - \omega_{mn}$, $\omega_{mn} \overset{def}{=} \omega_m - \omega_n > 0$, $\vec{G}^{(\omega)}_{mn} \overset{def}{=} \vec{E}^{(\omega)}(m, J_m \| \vec{d} \| n, J_n)/(2\hbar)$, and $\vec{\tilde{\Delta}}^{(0)}_J \overset{def}{=} \vec{\Delta}^{(0)}_{J_j}(j, J_j \| \overset{\vee}{\vec{J}} \| j, J_j) = g_J \mu_N \vec{B}^{(0)}/\hbar$ with $g_{J_j} = g_J$.

Light absorption power volume-density for molecules with suppressed motion

$$\mathrm{P}^{(J_m,J_n)}_{\nu}(G^{(\omega)}_{mn}, \tilde{\Delta}^{(0)}_J, \Omega) = 2\hbar\omega \tilde{N}_{nm}\, tr\{\overset{\vee}{P}_{n,J_n} \overset{\vee}{H}{}^{(\omega)} \overset{\vee}{P}_{m,J_m} [L^{(\mathrm{lm})}(\overset{\vee\vee}{H}{}^{(\omega,ad)}/\nu) : \overset{\vee}{P}_{n,J_n}]\} . \qquad (2)$$

Here projector $\overset{\vee}{P}_{j,J_j} \overset{def}{=} \overset{\vee}{P}_{j,J_j;\,j,J_j} \overset{def}{=} \sum_{M_j} \overset{\vee}{P}_{j,J_j,M_j;\,j,J_j,M_j}$, Lorentz function imaginary-part $L^{(\mathrm{lm})}(\xi) \overset{def}{=} \xi(1+\xi^2)^{-1}$, adjoint superoperator $\overset{\vee\vee}{O}{}^{(ad)} \overset{def}{=} \overset{\vee}{O} \otimes \overset{\vee}{1} - \overset{\vee}{1} \otimes \overset{\vee}{O}$, Frobenius colon product $[\overset{\vee\vee}{O}{}^{(1,ad)} : \overset{\vee}{O}{}^{(2)}]_{\alpha_1,\alpha_2} \overset{def}{=} \sum_{(\alpha_3,\alpha_4)} O^{(1,ad)}_{\alpha_1,\alpha_2;\,\alpha_3,\alpha_4} O^{(2)}_{\alpha_3,\alpha_4}$. Collisional relaxation constant $\nu = \nu_j$, saturated collisional constant $\nu_\varsigma \approx \nu[1 + \varsigma/(3(2J_n+1))]^{1/2}$ with saturation parameter $\varsigma \overset{def}{=} (2G^{(\omega)}_{mn}/\nu)^2$. In fact, the expression (2) is only a rational function of the magnetooptical and relaxational parameters.

Light absorption power volume-density or light intensity decrement per unit length for molecules with thermal motion:

$$\mathrm{P}_{\nu,\omega_D}^{(J_m,J_n)}(G_{mn}^{(\omega)},\tilde{\Delta}_J^{(0)},\Omega)=-\partial_{r_\kappa}I(r_\kappa)=\int_{-\infty}^{\infty}\frac{du_\kappa}{\sqrt{\pi}\,u_M}\,e^{-(u_\kappa/u_M)^2}\,\mathrm{P}_{\nu}^{(J_m,J_n)}(G_{mn}^{(\omega)},\tilde{\Delta}_J^{(0)},\Omega-\kappa u_\kappa)\,. \qquad (3)$$

Thermal Doppler constant $\omega_D=\kappa u_M$. If ν, Ω, and $\tilde{\Delta}_J^{(0)} << \omega_D$ then in magnetic spectrum only the saturation rotational structure of sub-Doppler dip against Doppler background is

$$\mathrm{P}_{\nu,\omega_D}^{(J_m,J_n)}(G_{mn}^{(\omega)},\tilde{\Delta}_J^{(0)},0)\approx\int_{-\infty}^{\infty}\frac{d\omega'}{\sqrt{\pi}\,\omega_D}\,\mathrm{P}_{\nu}^{(J_m,J_n)}(G_{mn}^{(\omega)},\tilde{\Delta}_J^{(0)},\omega') \qquad (4)$$

$$\le\mathrm{P}_{\nu,\omega_D}^{(J_m,J_n)}(G_{mn}^{(\omega)},(\nu<<)\tilde{\Delta}_J^{(0)\prime}(<<\omega_D),0)\approx 2\hbar\omega\tilde{N}_{nm}\nu^2\sqrt{\pi}/\omega_D\,.$$

An simple example of ${}_{nnn}\mathrm{P}_V(\Delta=\tilde{\Delta}_J^{(0)},\Omega)\overset{def}{=}\mathrm{P}_{\nu,\omega_D}^{(J_m,J_n)}(G_{mn}^{(\omega)},\tilde{\Delta}_J^{(0)},\Omega)/\mathrm{P}_{\nu,\omega_D}^{(J_m,J_n)}(G_{mn}^{(\omega)},0,0)$ is represented on Fig. 1. In general case we have the same picture when two Voigt ridges stretch along $\Omega=\pm\tilde{\Delta}_J^{(0)}$ and add in the cross top. Saturation there forms gap-like dip of Voigt type along Ω-axis and of folded Lorentz type along $\tilde{\Delta}_J^{(0)}$-axis. If $J_j\in\mathrm{N}_1$, then the fold amount is equal to $(2J_{\max}-1)$, else if $2J_j\in\mathrm{N}_1$, then to (J_m+J_n-1).

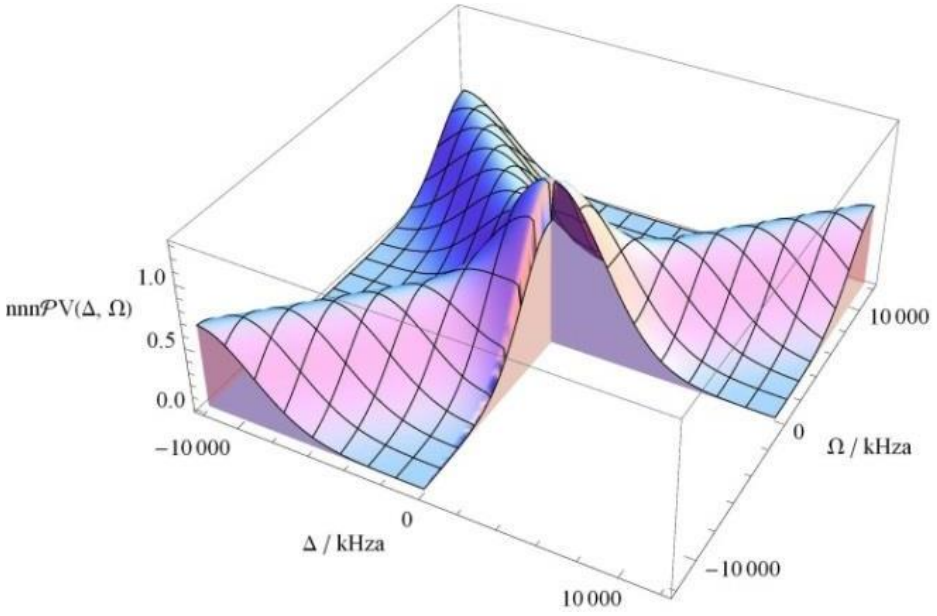

Fig.1. Normalized magneto-frequency spectrum of optical resonance for transition $\left[{}^{J_m=0}_{J_n=1}\right.$;
ω_D = 4000 kHza, ν = 40 kHza, $G_{mn}^{(\omega)}$ = 80 kHza, ς = 16, ν_ς = 66.7 kHza.

We have given the exact formula derivation and graphical analysis for the saturation rotational structure specific to magnetic spectrum of optical resonance. We get rid of all restrictions of [1, 2]. It is quite possible within superoperator formalism framework to make the problem extension on resonance fluorescence of an atomic gas with spontaneous relaxation in the form of Lindblad superoperator, e.g. for the case [3], and to take into account parity doubling or sub-Lorentz hyperfine structure of a molecular line, e.g. for the case [4]. It is important that one can make all these and similar extensions precisely with saturation parameter optimization.

References

1. S.G. Rautian, A.G. Rudavets, *Pis'ma Zh. Eksp. Teor. Fiz.* **35**, 309 (1982) [*JETP Lett.* **35**, 379 (1982)].
2. K.A. Nasyrov, A.M. Shalagin, *Zh. Eksp. Teor. Fiz.* **81**, 1649 (1981) [*JETP* **54**, 877 (1981)].
3. M. Ducloy, *Phys. Rev. A* **8**, 1844 (1973); **9**, 1319 (1974).
4. K.I. Gus'kov, V.I. Kovalevsky, A.G. Rudavets, and E.G. Saprykin, *J. Mol. Spectrosc.* **228**, 160 (2004).

Laser cooling of two-level atoms with full account of recoil effects: Anomalous Localization and Quantum Regime

R.Y. Ilenkov[1], D.V. Brazhnikov[1], A.V. Taichenachev[1,2], V.I. Yudin[1-3],

[1]Institute of Laser Physics SB RAS Ac. Lavrentyev's prosp., 13/3, Novosibirsk, 630090 Russia
[2]Novosibirsk State University, ul. Pirogova 2, Novosibirsk, 630090 Russia
[3]Novosibirsk State Technical University, pr. Karla Marksa 20, Novosibirsk, 630073 Russia
e-mail address: ilenkov.roman@gmail.com, taichenachev@hotmail.ru, viyudin@mail.ru

The idea to control matter by electromagnetic fields originated in the minds of the scientists at the beginning of the last century. However only invention such precise and powerful tool as a laser has opened before us a wide range of capabilities for atom manipulation: acceleration, deceleration, localization, deflection, and focusing. So laser cooling has become an integral part of both fundamental science and many practical applications (high-precision frequency and time standards, nanolithography, quantum information and many others) In addition, strong evidence of the importance and interest to this area is the Nobel Prize 1997., which have been awarded some of the pioneers in the field of laser cooling (eg, Nobel lecture [1]).

The theoretical description of the kinetics of neutral atoms in the polarized light fields with all the atomic levels, the coherence, the recoil effect is both important and challenging problem. The first step toward understanding mechanisms of interaction between atoms and light was called quasi-classical approach. [2] It lies in the fact that the equations for the density matrix can be reduced to the Fokker-Planck equation for the Wigner function in the phase space. Simplicity of this approach has allowed understanding many of cooling mechanisms in the usual and ordinary terms of force and diffusion. However, this approach can only be applied in certain cases. First, the small recoil frequency parameter compared to the rate of spontaneous decay, and secondly, the momentum of a light field photon should be much smaller than the width of the momentum distribution of the atoms. Later quantum methods were developed [3,4], for example, the secular approach which describes cooling and localization of atoms in the optical potential. In this approximation distance between the energy bands in the optical potential is greater than their broadening caused by optical pumping. At a fixed depth of the optical potential this approximation is valid in the limit of large detuning, and thus, for a given configuration is disrupted in a deep optical potential. Moreover, the secular approximation is valid only for the lower vibrational levels, and fails for the higher, where the distance between the levels becomes smaller due to the effects of anharmonicity. This approximation is not applicable to atoms undergo above-barrier motion.

We have developed an own quantum method [5] to obtaining the stationary distribution of two-level atoms in a standing wave of arbitrary intensity, allowing full account the recoil effect. The method used is to decompose the density matrix elements in the Fourier series for the spatial harmonics, which is possible due to periodicity of the light wave.

Using the developed method kinetics of atoms in light fields of varying intensity was investigated. The new and most important result was mode which we called the anomalous localization (Fig. 1). Usually at a low recoil and weak field stationary momentum distribution has a typical Gaussian profile and atoms are located in the region of minimum optical potential (at the antinodes of the standing wave in the red detuning). This result is well known and has been studied previously (see monograph [2,6] and references) However, in strong standing wave (Rabi frequency greater than the constant spontaneous relaxation) was detected a anomalous behavior of atoms, namely, the concentration at the peaks of the optical potential.

Research showed that such localization is always accompanied by a pronounced double-humped distribution of atoms in momentum space (Fig. 1b). We proposed following

mechanism of anomalous localization: If in the case two-humped distribution the most probable kinetic energy of the atoms is greater than potential depth, atoms are concentrated in the peaks of the optical potential, but if the energy is less than depth of potential, localization will occur in the classical turning points. A bit later it has been successfully validated.

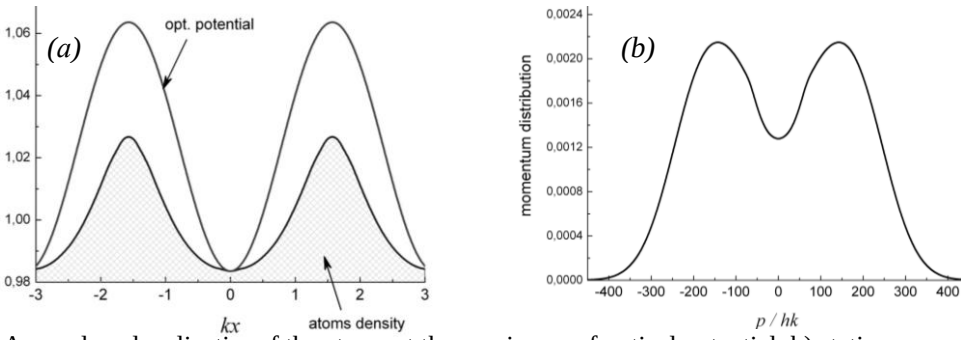

Fig.1. a) Anomalous localizationof the atoms at the maximum of optical potential; b) stationary momentum distribution of the atoms in a strong field.

The next step in study of atomic kinetic was to examine the stationary distribution destruction with decreasing detuning. For small detunings of the momentum distribution (Fig. 2a) loses its Gaussian shape, wing area is increased, and, finally, at the approach to the turn of $\delta = -1/200$ appear the non-physical narrow unstable structure (small peak around zero) . Total exact quantum calculation confirmed statements quasiclassics and responded about how far you can reduce the detuning.

Further, it was decided to carry out a detailed comparison of the results of our method with the results of other authors [7,8]. In general, was obtained qualitative agreement forms, including narrow structures of order of $\hbar k$, for an example (Fig. 2b) the momentum distribution in a weak field ($\delta = -0.5, \Omega = 0.1$) and for different parameters of recoil.

This work was supported by RFBR (grants nos. 12-02-31208, 12-02-00454, 12-02-00403, 11-02-00775, 11-02-01240), the Presidential Grant (SP-1518.2012.3, MK-3372.2912.2) and programs of RAS.

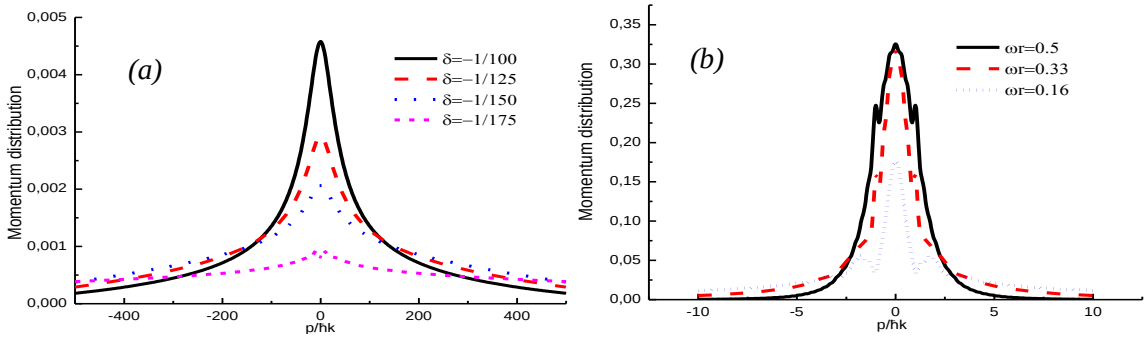

Fig.2. a) Stationary distribution destruction with detuning decrease ; b) Quantum regime. Narrow structures of order of single photon recoil.

References

1. C. Cohen-Tannoudji, «Manipulating atoms with photons», Nobel Lecture, December 8,1997.
2. A. P. Kazantsev, G. I. Surdutovich, and V. P. Yakovlev, «Mechanical Action of Light on Atoms», *World Sci., Singapore* (1990).
3. A. Aspect, E. Arimondo, R. Kaiser, N. Vansteenkiste, and C. Cohen-Tannoudji, *Phys. Rev. Lett.* **61**, 826 (1988).
4. S. M. Yoo and J. Javanainen, *J. Opt. Soc. Amer. B* **8**, 1341 (1991).
5. O. N. Prudnikov, R. Ya. Il'enkov, A. V. Taichenachev, A. M. Tumaikin, V. I. Yudin «Steady state of a low-density ensemble of atoms in a monochromatic field taking into account recoil effects», Journal of Experimental and Theoretical Physics June 2011, Volume 112, Issue 6, pp 939-945.
6. V.G. Minogin, V.S. Letochov, «Laser light pressure on atoms». New York u.a.: Gordon and Breach (1987).
7. Sung Mi Yoo and Juha Javanainen, Wigner-function approach to laser cooling in the recoil limit JOSA B, Vol. 8, Issue 6, pp. 1341-1347 (1991)
8. Doery M.R, Vredenbregt E.J, Bergeman T. Quantum dynamics and cooling of atoms in one-dimensional standing-wave laser fields: Anomalous effects in Doppler cooling. Phys Rev A. 1995 Jun; 51(6):4881-4899.

A novel scheme of quantum optomechanics

L. Il'ichov

Institute of Automation and Electrometry SB RAS, Novosibirsk State University, Novosibirsk, Russia
E-mail: leonid@iae.nsk.su

The interaction of vibrational quantum systems of various natures—photon modes and mechanical oscillators—is of current interest (this field was considered for the first time in [1]). This field studying methods for quantum control of mechanical motion [2], which is called quantum optomechanics, opens new prospects in quantum metrology, micro– and nanotechnologies, and engineering of correlated quantum systems of radiation and mechanical devices [3]. The traditional quantum optomechanical scheme includes an optical cavity, where one of the mirrors (which is usually totally reflecting) is a mechanical oscillator. Radiation in the cavity provides pressure on the mirror. The moving mirror changes the length of the cavity and, consequently, its resonance frequency. Such a coupling between two oscillators, photon and mechanical, makes it possible to prepare and control quantum systems of both subsystems. For example, if the photon subsystem is slower, adiabatically subordinating mechanical oscillations of the mirror, an effective Kerr nonlinearity appears in the dynamics of the photon subsystem. In particular, this allows the formation of squeezed field states [4]. It is important for the subject of this work that the mentioned coupling makes it possible to provide deep cooling of the mirror to an energy of several vibrational quanta [5, 6]. A new quantum optomechanical scheme involving two photon modes and a mechanical oscillator with a mirror is proposed in this work. The motion of the mirror will induce a change in the phase difference between the modes rather than a shift of the resonance frequency, as in the traditional scheme. As will be shown below, the mechanism of the photon exchange between modes and irreversible absorption of photons can lead to the bistability of the position of the mirror. This position can be efficiently controlled by varying the phase φ of the second mode.

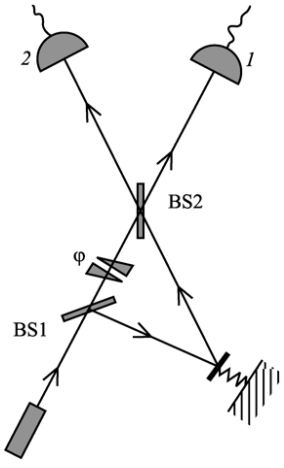

Fig. 1. Optomechanical scheme.

Beam splitter BS1 is used to prepare two modes. Photons of mode 2 are reflected from an oscillator mirror and are then "mixed" on beam splitter BS2 with photons of mode 1. Mode 1 has a controllable phase delay. The position of the mirror turns to depend on the phase φ. Stable and unstable branches appear. The equilibrium positions are bistable; controllable switching between them is possible by means of φ variation. The simplicity of the control is an important feature of the proposed scheme.

References

1. V. B. Braginsky and A. B. Manukin, Sov. Phys. JETP **25**, 653 (1967).
2. A. Cho, Science **430**, 516 (2010).
3. T. J. Kippenberg and K. J. Vahala, Science **321**, 1172 (2008); M. Aspelmeyer, P. Meystre, and K. Schwab, Phys. Today **65**, 29 (2012).
4. C. Fabre, M. Pinard, S. Bourzeix, et al., Phys. Rev. A **49**, 1337 (1994); S. Mancini and P. Tombesi, Phys. Rev. A **49**, 4055 (1994).
5. P. F. Cohadon, A. Heidemann, and M. Pinard, Phys. Rev. Lett. **83**, 3174 (1999).
6. S. Gigan, H. R. Bohm, M. Paternostro, et al., Nature **444**, 67 (2006); O. Arcizet, P._F. Cohadon, T. Briant, et al., Nature **444**, 71 (2006); D. Kleckner, Nature **444**, 75 (20 06).

Investigation of physical processes at laser isotope separation of thallium by the method selective excitation and field ionization of the Rydberg states

P.A. Bokhan, N.V. Fateev, V.A. Kim, Dm.E. Zakrevsky

Rzhanov Institute of Semiconductor Physics, Siberian Branch, Russian Academy of Sciences, prospekt Lavrent'eva 13, 630090 Novosibirsk, Russia

In Nature, thallium contains two isotopes, namely ^{203}Tl (29.5%) and 205Tl (70.5%). ^{203}Tl is used as a source material to produce the ^{201}Tl radioisotope. ^{201}Tl is produced in a cyclotron by irradiating an enriched ^{203}Tl target with a 19–31 MeV proton beam. ^{201}TlCl is used as a radiopharmaceutical for single photon emission computerized tomography to diagnose heart diseases and tumors.

The laser isotope separation (LIS) technique, which employs the isotope-selective photo ionization processes of atoms, has been suggested as an alternative to overcome the demerits of the other methods. With a medical demand of about 1 kg of ^{203}Tl per year, the laser setup for the isotope separation can be compact. A laser system can be created using low power commercially available lasers, and the required production rate can be reached at a working chamber length of up to 200 cm. For those cases where LIS is technically feasible, an economic evaluation can be performed by consideration of the cost competitiveness of this technique against other techniques, which requires knowledge of the physical and chemical properties of the element, the required laser power, the isotope selectivity and ionization efficiency of the photoionization process, etc. Thallium has no available autoionization levels. Accordingly, photoionization of thallium atoms through an autoionization level is not possible.

This report is devoted to experimental study of the population behavior of the $nF_{5/2}$ Rydberg states with principal quantum number n excited from the ground state by the two-step scheme $6P_{1/2} \rightarrow 6D_{3/2} \rightarrow nF_{5/2}$ through the intermediate state $6D_{3/2}$ by using a dense collimated atomic beam to reduce the width of the Doppler broadening and monochromatic radiation from two frequency tunable lasers λ_1 = 276,9 nm, λ_2 = 773÷808 nm). The lasers were pumped by the radiation of a copper vapor laser with a repetition rate of 11 kHz. The maximum mean output power for the second harmonic radiation with a wavelength of 276.9 nm was 1 W, line width 380MHz and the pulse duration 9 ns. In the second step line width at a wavelength of 800 nm were less than 1 GHz, pulse duration 14 ns and the mean output power 1.2 W.

The largest selectivity of excitation in this scheme takes place in the first step excitation. The splitting between the ^{203}Tl and ^{205}Tl isotopes were found to be 0.98 and 1.25 GHz for the transitions with the nuclear moments $F = 1 \rightarrow F' = 1, 2$ and $F = 0 \rightarrow F' = 1$, respectively, which is sufficient for a relatively high isotopic selectivity of the $6D_{3/2}$ state excitation with subsequent ionization for laser separation of the thallium isotopes. The effects that lead to the broadening of the resonance and a decrease in the selectivity are analyzed. The main contribution is related to the field broadening by the laser radiation, which limits the average laser power density. An intense selective excitation of a certain atomic state leads to a high population inversion of this state relative to a lower level that is not involved in the scheme of levels of the laser isotope separation. This fact causes amplification and superradiance at the corresponding wavelength. The superradiance results in depletion of the selectively excited level and broadening of the absorption line, so that the ionization quantum yield and selectivity decrease. A transition from a demonstration of the laser isotope separation to isotope production causes several problems. The first problem is related to the fact that the excitation selectivity and efficiency and the ionization must be provided in a relatively large volume at a small isotope shift. To solve the problems related to the ionization of the selectively excited atoms, we plan to employ excitation at a wavelength of 800 nm to the highly excited (Rydberg) states with subsequent effective

ionization in the presence of an electric field. The experiments are performed under conditions that are almost identical to the conditions in the setup for the laser isotope separation. We use a long (2×15 cm^2) and dense ($n \approx 3\cdot10^{11}$ cm^{-3}) collimated atomic beam excited by narrow-band laser sources with an average power of up to 1 W.

The experiments showed that the main reason for the limiting selectivity excitation of the Rydberg states is the field broadening of the absorption resonances at the first and second steps of the excitation scheme. The excitation efficiency of this scheme is considerably governed by the parameters of the laser radiation at the second step and an electric field pulse. To decrease the effects of field broadening the laser power density must be attenuated in the interaction region. The closeness of the two values resulting from the approximate calculations proves the above conclusions. A decrease in the lifetime of the excited $6D_{3/2}$ state due to the above physical effects imposes additional requirements on the radiation parameters in the second stage of excitation (in particular, power and duration). An increase in the power density of the radiation that interacts with the atoms leads to an increase in the number of atoms in the excited state. However, the maximum quantum efficiency is reached when the excitation rate approaches zero. The quantum efficiency decreases when the excitation intensity is saturated. In addition, note the absorption resonance broadening at relatively high radiation intensities, which leads to worsening of the isotope selectivity of excitation. Thus, we have revealed the physical reasons for the decrease in the isotope selectivity of the thallium isotope excitation and demonstrated the effects that cause a decrease in the efficiency of the laser excitation in the collimated atomic thallium beam. Figure 1 shows the ion current arriving at the ion collector versus the first-step laser frequency. This picture show good isotopic selectivity in the ionic current.

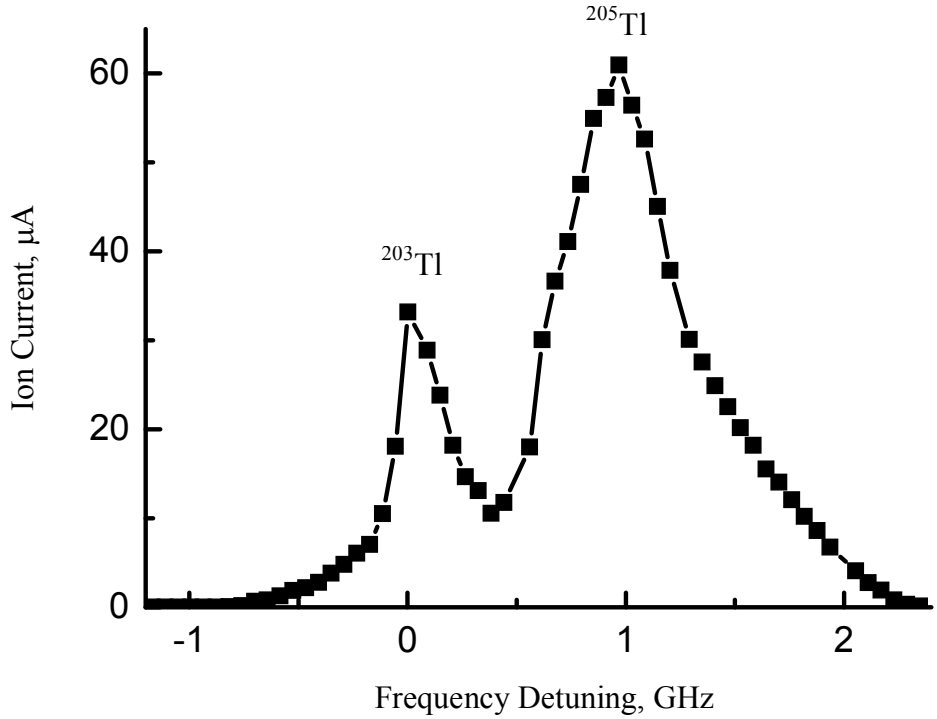

Fig.1. Plots of the ion current versus the first-step laser frequency (λ = 276.9 nm) detuned from the center of the transition $6P_{1/2} \rightarrow 6D_{3/2}$ (F = 1 – F´ = 1, 2) for mean power densities of $P_{1m} \approx 25$, $P_{2m} \approx 600$ mW/cm^2.

Application of femtosecond Laser-Induced Breakdown Spectroscopy for liquid analysis

A. V. Kolesnikov[1], **S. S. Golik**[1,2], **A. A. Ilyin**[1,2], **M. Yu. Babiy**[1] **and O. A. Bukin**[2]
[1]*Far Eastern Federal University, Laser Spectroscopy Lab., 690950, 8 Sukhanova St., Vladivostok, Russia*
[2]*Institute of Automation and Control Processes, Far Eastern Branch of the Russian Academy of Sciences, 690041, 5 Radio St., Vladivostok, Russia*
E-mail address: ***nucleo@land.ru***

In spite of the fact that femtosecond Laser-Induced Breakdown Spectroscopy (LIBS) shows more attractive results in comparsion with conventional nanosecond LIBS, increasing of femtosecond LIBS sensivity is very important for possibility of its application.

Recent investigations showed that femtosecond LIBS limits of detection (LOD, one of the basic characteristics of an analytical method) of different chemical elements are much lower - the difference reaches few orders for some elements [1]. As was shown lower LODs were obtained for Al, Cu, Fe, K, and Zn. The LOD for Mg is the same or a little higher than in [2, 3]. However, special data post-processing technology was used in the study in [2], while in [3] the plasma was formed in a liquid jet. For Na, Ba, and Ca, better LODs were obtained in [4], but in this case the plasma was formed in a liquid jet (HCl solution) by emission from an ArF laser with wavelength 193 nm. Thus the LODs obtained by femtosecond time-resolved LIBS showed that the proposed technique is suitable for real-time fast monitoring of the macro composition of sea water (such elements as Ca, Na, Mg, K), with reproducibility of the determinations <10%. The average concentrations in sea water for these elements significantly exceed the LOD values obtained in [5]. Regarding barium, a value of the same order of magnitude as the average Ba concentration in sea water was obtained. This allows to determine a slight increase in the Ba concentration relative to the average value, for example, at sites of barite deposits or oilfield development. The results obtained for aqueous solutions of Al, Cu, Zn, and Fe showed insufficient sensitivity of the method for quantitative analysis of trace concentrations of metals having an average concentration in sea water of $\approx 10^{-6}$ g/L [5]. They could be determined by this method if there is a substantial increase in concentration in sea water (up to three orders of magnitude). In order to determine the indicated concentrations, there is need of additional methods for increasing the sensitivity, for example, using the dual pulse mode for LIBS and resonant excitation of the corresponding atomic transitions (the transitions Fe I with λ = 794 nm, Al I with λ = 783.6 nm, and Cu I with λ = 809.2 nm are within the wavelength range 775–825 nm of the femtosecond titanium:sapphire laser).

In order to increase LIBS sensivity the influence of the focal spot radius on line and continuum intensity was investigated [6]. In our case the focal spot radius was varied by laser beam diameter changing. Spitfire Pro 40F Ti:Sapphire laser system (Spectra-Physics) was used as the source of femtosecond laser pulses (central wavelength is 800 nm, pulse duration is 40 fs, pulse energy is 0.8 mJ, repetition rate is 20 Hz). Laser beams with two different diameters (7 or 14 mm) by the plano-convex lens with 100 mm focal length (KPX094AR.16, Newport) was focused on the surface of the investigated solution (distilled water, $CaCl_2$ in water solution with Ca concentration of $3.5 \cdot 10^{-2}$ g/l, marine water). The angle of reflection of the HeNe laser beam (1137P, JDS) from the water surface was used to control the sample surface position. Plasma radiation was imaged by the quartz lens onto the 50 or 100-μm input slit of the 500 mm focal length imaging spectrometer SpectraPro 2500i (Princeton Instruments) equipped with a 600 or 1,200 groove/mm grating. A gated ICCD camera (PicoStar HR, LaVision, GmBH, 1,370 x 1,040 pixels) with an intensifier gating time of 200 ns was used as a detector. The gate delay of 55 ns was used to provide the time-

resolved measurements. Each spectrum was accumulated by CCD with 80 seconds exposition time. So the amount of the summed spectra was 1,600 with the 20 Hz laser repetition rate.

The significantly higher intensities of the Ca, H_α, O, N lines for 14 mm beam diameter were obtained. For example, the emission lines of Ca II (393.3 nm) and H_α (656.3 nm), measured with 14 mm and 7 mm beam diameter are presented in fig.1.

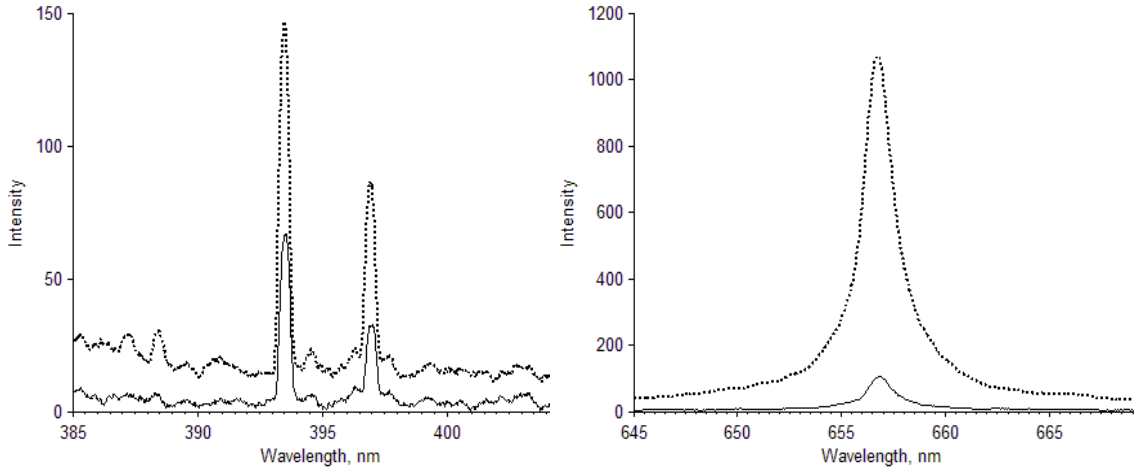

Fig.1. Emission spectra of CaII (393.3 nm) (on left) and H_α (656.3 nm) (on the right).

All other experimental parameters except laser beam diameter were constant. The dotted curves on Fig.1 correspond to 14 mm beam diameter and solid curves correspond to 7 mm one. As it can be seen intensity of Ca II (393.3 nm) line increased by more than twice and H_α (656.3 nm) intensity increased by order of magnitude. This effect can be used as a simple way to improve sensitivity of femtosecond LIBS.

References

[1]. S. S. Golik, O. A. Bukin, A. A. Ilyin, E. B. Sokolova, A. V. Kolesnikov, M. Yu. Babiy, Yu. N. Kulchin and A. A. Galchenko, *Journal of Applied Spectroscopy* **79**, 471-476 (2012)

[2] V. Lazic, F. Colao, R. Fantoni, and V. Spizzicchino, *Spectrochim. Acta B* **60**, 1002–1013 (2005)

[3] F.-Y. Yueh, R. C. Sharma, J. P. Singh, H. Zhang and W. A. Spencer, *J. Air Waste Magan. Assoc.* **52**, 1307–1315 (2002)

[4] K. M. Lo and N. H. Cheung, *Appl. Spectrosk.* **56**, 682–688 (2002)

[5] K. K. Turekian, Oceans, Prentice-Hall, Englewood Cliffs, New Jersey (1968)

[6] S. S. Golik, A. A. Ilyin, A. V. Kolesnikov, M. Yu. Babiy, Yu. N. Kulchin and O. A. Bukin, *Technical Physics Letters* **39**, 72-77 (2013)

PAD spectrometer at 2.5-11 mm based on fun-out PPLN and $HgGa_2S_4$ optical parametric oscillator

D. B. Kolker[1,2,3] , I. V. Sherstov[1,2] , A. A. Karapuzikov[1], A. I. Karapuzikov[1,2], M. K. Starikova[1,3], D. A. Kashtanov[1,2], F. A. Mayorov[4], M.Shtyrov[1], A.A. Boyko [1,3], K.Zenov[1], M.B.Muroshnochenko[1], I.B.Miroshnichenko[1,3], N. Yu. Dukhovnikova[1,3]

[1)] Special technologies, Ltd., Zelenaya Gorka 1/3, Novosibirsk 620060, Russia
[2)] Institute of Laser Physics, Siberian Branch, Russian Academy of Sciences, pr. Akademika Lavrent'eva 13/3, Novosibirsk 630090, Russia
[3)] Novosibirsk State Technical University, pr. K. Marksa 20, Novosibirsk 630092, Russia
[4)] HLS Hypertech Laser Systems GmbH, Luebeck, Germany
E-mail: kolker@ngs.ru

In recent years the method of laser photo acoustic spectroscopy (LPAS) has become an important method for monitoring of gas chemical agent in atmosphere because of its simplicity experimental realization, safety, high sensitivity (ppb-ppt level) [1-2]. LPAS makes to take measurements in real time with a minimal volume of gas sample or in continuous pumping mode of the analyzing gas sample. [3-5].

The experimental OPO setup combined with photo - acoustic detector was developed. The experimental setup consists of pump laser (Q-switched Nd:YLF) and two OPO: fun - out PPLN OPO-1 (2.4-3.9 μm) and HGS OPO-2 (figure 1). The photo-acoustic detector is used for registration of absorption spectra of gas samples. The monolithic fun - out PPLN OPO cavity consist of two high-reflectivity mirrors at the signal wave (SDPOPO). The output mirror is high transparent for the pump and idler wavelengths but for the signal wavelength this mirror is high reflected. The step motor moves crystal in relation to pumping beam for the wavelength tuning. Lasing threshold is 10 – 16 mJ/cm^2 at the spectral range 2.2 – 4 μm for fun – out PPLN OPO [6].

Optical parametric oscillator based on chalcogenide crystals allows covering wide spectral range from 2 to 11 μm. The advantage of HgG_2S_4 (HGS) crystal: high effective nonlinear coefficient and wide optical transmission in spectral range 0.5–12.0 μm, makes it realistic to generate infrared parametric radiation in wide spectra range [7-8].

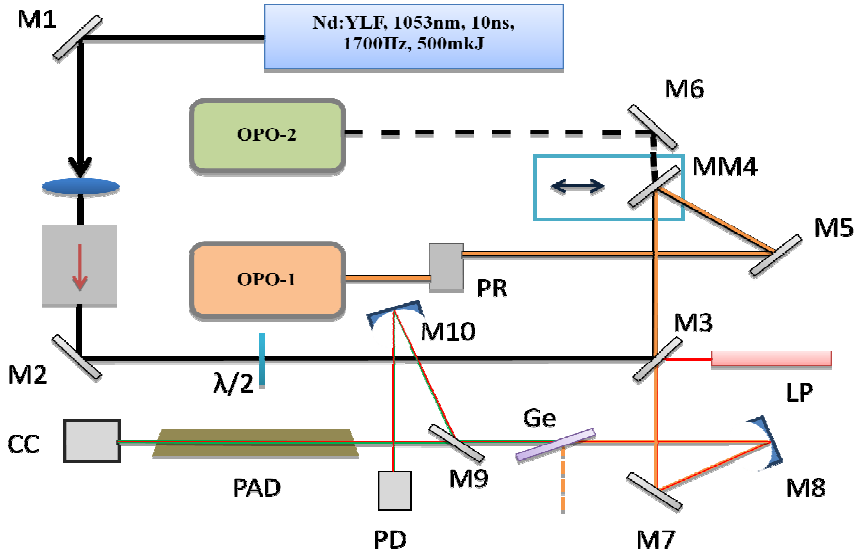

Fig.1

Absorption spectra of gaseous mixtures (CH_4, C_3H_8, C_2H_6, C_2H_4, CO2, acetone, NH3) and human's breath were studied by using tandem OPO-PAD. Absorption spectra of methane and NH_3 are presented on the figure 2, 3.

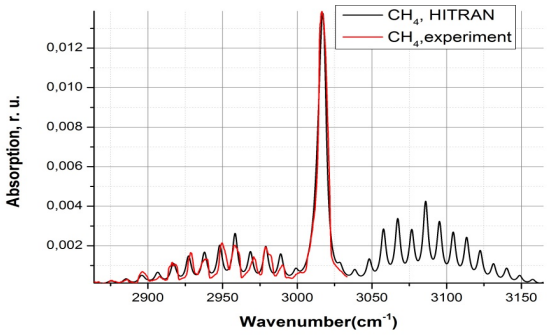

Fig 2. Absorption spectra: absorption spectrum of experimental gaseous mixture CH_4 (red line) and theoretical absorption spectrum of CH_4 (black line) from HITRAN

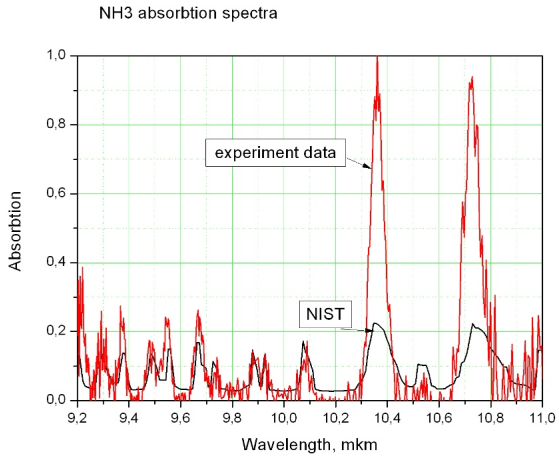

Fig3. Absorption spectra: absorption spectrum of acetone (red line) and theoretical absorption spectrum of CH_4 (black line) from HITRAN

This work was performed with support of Ministry of Education and Science of Russian Federation (contract 16.522.11.2001).

References

1. Photoacoustic Spectroscopy in Trace Gas Monitoring Frans J.M. Harren, Gina Cotti, Jos Oomens, and Sacco te Lintel Hekkert in Encyclopedia of Analytical Chemistry R.A. Meyers (Ed.) pp. 2203–2226 У John Wiley & Sons Ltd, Chichester, 2000
2. Miklos A, Hess P, Bozoki Z (2001) Application of acoustic resonators in photoacoustic trace gas analysis and metrology Rev Sci Instrum, 72 (2001) pp. 1937-1955
3. A. Lyakh., R. Maulini, A. Tsekoun, R. Go, C. PflËugl, L. Diehl, Q. J. Wang, F. Capasso, and C. Kumar N. Patel, “3 W continuous-wave room-temperature single-facet emission from quantum cascade lasers based on non-resonant extraction design approach,” Appl. Phys. Lett. 95, 141113 (2009).
4. Anadi Mukherjee, Manu Prasanna, Michael Lane, Rowel Go, Ilya Dunayevskiy, Alexei Tsekoun, and C. Kumar N. Patel Optically multiplexed multi-gas detection using quantum cascade laser photoacoustic spectroscopy Applied Optics Vol. 47, Iss. 27, pp. 4884–4887 (2008)
5. Michael E. Webber, Michael Pushkarsky, and C. Kumar N. Patel Optical detection of chemical warfare agents and toxic industrial chemicals: Simulation J. Appl. Phys. 97, 113101 (2005)
6. Kolker D.B., Pustovalova R.V., Starikova M.K., Karapuzikov A.I., Karapuzikov A.A., Kuznetsov O.M., Kistenev Yu. V. Optical parametric oscillator within 2.4-4.3 mkm pumped with a nanosecond Nd:YAG laser, Atmospheric and Oceanic Optics, 2012, Vol. 25, No. 1, pp. 77-81 (in Russian)
7. Marchev G., Tyazhev A., Vedenyapin V., Kolker D., Yelisseyev A. Nd:YAG pumped nanosecond optical parametric oscillator based on $LiInSe_2$ with tunability extending from 4.7 to 8.7 μm //Optics Express, 2009, Vol. 17, Issue 16, P. 13441-13446.
8. Petrov V., Zondy J.-J., Bidault O., Isaenko L., Vedenyapin V., Yelisseyev A., Chen W., Tyazhev A., Lobanov S., Marchev G., Kolker D. , Optical, thermal, electrical, damage, and phase-matching properties of lithium selenoindate //JOSA B, 2010, Vol. 27, Issue 9, P. 1902-1927.

Sensitivity of GW bar detector's optical-electronic readout

V.A. Krysanov, V.N. Rudenko

Institute for Nuclear Research RAS, Pr. 60-letiya Oktyabrya, 7a, Moscow 117312, Russia
Sternberg State Astronomical Institute, MSU, Universitetsky pr., 13, Moscow 119992, Russia

Sensitivity of GWD is defined by thermal noise of a bar and a threshold signal (sensitivity) of an acoustic disturbance registration system [1, 2]. Radio physical registration methods were developed in MSU; RF capacitor sensors were created [2 - 5], resolution $5\cdot10^{-17}$ cm was reached [5]. Data processing facilities had been developed [6]. The RF SQUID measurer is created [7, 8] in locked circuit with internal modulation, synchronous detection; sensitivity analysis is carried out, resolution of $2\cdot10^{-14}$ cm with averaging time 1 sec is reached [9].

Laser measurer on Fabry-Perot cavity is considered [2]. Changes of bar length $\boldsymbol{x}$ cause eigen frequency variations $\delta\nu_{\mathbf{R}} = (c/\lambda L)x$ (L- bar length). As well as in a capacitor sensor, on a slope of a resonant curve they are transdused into light power variations $\boldsymbol{\delta P}$ registered by photo detector: $\delta P/(P_0/2)=2\pi x/\lambda(1-R)$, ($P_0$ – resonant passable light power) [2]. It functions in a flare mode as an heterodyne optical receiver [10]. In a photo diode (PD) current variations δI_S are: $\delta I_S = (\eta\, e/h\nu)\delta P$. The overall steepness of signal transformation is

$$\alpha_S \equiv \delta I_S/x = \pi\eta e P_0[(1-R)\lambda h\nu]^{-1} . \qquad (1)$$

Shot noise current have the power spectral density (PSD) $N_{INE}(f)=2eI_E = e^2P_0/(h\nu)$, ($I_{NE}^2 = 2eI_E\Delta f$ [10]). Shot noise determines the threshold signal x_{N0} (η =1 in [2]):

$$x_{N0} = I_{NE}/\alpha_S = \pi^{-1}\lambda(1-R)[(h\nu/\eta P_0)\Delta f]^{1/2} \equiv (G_{xs0}\,\Delta f)^{1/2}. \qquad (2)$$

For P_0 = 0,1W, (1 - R) = 10^{-3}, $\lambda = 1{,}06\cdot10^{-6}$ m the forecast is: $x_{N0} = 5\cdot10^{-17}\,\mathrm{sm}(\Delta f)^{1/2}$.

The PSD of the equivalent fluctuation force F_N acting upon the bar-oscillator [2] is: $G_F = G_B+G_{ba}+G_{Seq}$ [11]. Here G_B – the Nyquist's strength: $G_B(\omega)=2kTM/\omega_\mu Q$, ($M$, ω_μ, Q – bar effective mass, eigen frequency and quality factor); the terms G_{Seq}, G_{ba} represent noise of the a measurer and force back action (FBA) - Poisson light pressure. It was estimated: $G_{ba} \ll G_B$ [11]; therefore, the measurer may be considered as an independent device [5, 7- 9].

The oscillator displacement PSD, caused by the force F_N, around resonance ω_μ is:

$$G_x(f) = \frac{4kTQ}{M\omega_\mu^3}\frac{1}{1+((\omega-\omega_\mu)/\delta_\mu)^2} + B\frac{h\nu}{\eta P_0}\left(\frac{\lambda}{\pi N}\right)^2 \equiv G_{xT} + G_{xs} \quad . \qquad (3)$$

The PSD G_{xT} represents thermal noise of the bar; $\delta_\mu = \omega_\mu/(2Q)$, ($\omega = 2\pi f$). For OGRAN values M ≈ $8\cdot10^2$ kg, $\omega_\mu = 2\pi\cdot1{,}3\cdot10^3$ s^{-1}, $Q = 10^5$ in resonance $G_{xT}^{1/2} \approx 2\cdot10^{-13}$ sm/Hz$^{1/2}$.

The term G_{xs} in (3) represents the threshold signal of the laser measurer; B – a factor taking into account excess laser noises; N = $(1–R)^{-1}$ [12], at B=1 the PSD G_{xs} is reduced to (2). The peak G_{xT} is observed [13]. There are frequencies f_1 and f_2, where $G_{xT} = G_{xs}$. In the band $\Delta f_{GD} = f_2 - f_1$ sensitivity of the GWD on metrics h is potential [1, 2, 12]: $h \approx 2\cdot10^{-20}$ Hz$^{-1/2}$. For $G_{xs} = 10^{-15}$ cm/Hz$^{1/2}$ Δf_{GD} is ~2 Hz, and for $h = 10^{-18}$ the receiving band is ~100 Hz.

Laser noises ($B = 10^4$ in [13]) reduce sensitivity; technical light power fluctuation (LPF) is expressed by the normalized PSD m_L: $N_P(f) = P^2 m_L$ [11]. For laser applied it is measured: $m_L \approx 10^{-12}$ Hz^{-1} at 1,3 kHz. The corresponding estimated PD current is $4\cdot10^{-8}$ A/Hz$^{1/2}$ whereas $I_{INE} \approx 10^{-10}$ A/Hz$^{1/2}$. This noise deposit, in principle, can be compensated [14].

In the OGRAN project [15-17] the Pound-Drever-Hall technique is applied: an internal light modulation, a synchronous detector (SD) and automatic laser frequency control (ALFC) are used. In [18] the simplified ($I_E = 2P_S\eta e/h\nu$) expression for the decrement D_P of the ALFC discrimination characteristic is derived: $D_P \equiv \delta P_{PD}/\delta\nu_R = 16\Phi(L/c)(P_C P_S)^{1/2}$. Here P_C, P_S - carrier and sideband power, Φ - finesse. With PD the overall signal steepness is:

$$\alpha_{PDH} = \delta I_E/x = 16\Phi(\eta e/h\nu)(P_C P_S)^{1/2}/\lambda . \qquad (4)$$

In PD $N_{IE} = 4\eta e^2 P_S/h\nu$. Formalized [18] expression for limit sensitivity of the method is:

$$x_{N1} = (\lambda/8\Phi)\,[(h\nu/\eta P_C)\Delta f]^{1/2}. \qquad (5)$$

For η = 1 [18], $\Phi = 10^4$, P_C = 0,5W (OGRAN) the estimation is: $x_{N1} \approx 10^{-18}\,\mathrm{sm}(\Delta f)^{1/2}$.

There is relation [18]: $\Phi \approx \pi/(1-R^2)=(\pi/2)/(1-R)$. Then (2) is: $x_{N0} = (\lambda/2\Phi)[(h\nu/\eta P_0)\Delta f]^{1/2}$. The distinction with expression (5) (for schemes [2, 12] and [15, 17]) is not essential.

In the report [19] the system of ALFC of the OGRAN measurer was presented and the equations, containing sources of noise, were written out. The changed ratios are:

$$U_{SD} = D(\delta\nu_R - \delta\nu_L) + U_N\,, \qquad U_C = K_C U_{SD}\,, \qquad \delta\nu_L = \delta\nu_N + \beta U_C\,. \tag{6}$$

Here D - decrement (D^{-1}= 5,8 kHz/V in [15]), U_N, $\delta\nu_N$ - LF random processes with PSD $N_U(f)$ and $N_\nu(f)$; $\delta\nu_N$ – intrinsic laser frequency fluctuation (LFF); $\delta\nu_L$ - laser LF variations. As well as in [19] the threshold signal displacement (for ALFC) is ($K_0 = K_C\beta D$):

$$x_N^2 = (\lambda L/c)^2(N_U/D^2 + N_\nu/|K_0|^2)\Delta f \equiv x_{NE}^2 + x_{NL}^2\,. \tag{7}$$

The condition $K_0 \equiv K_C\beta D = 10^3$ was suggested, validated and represented in [19]. It was inscribed before into OGRAN Requirements Specification. To avoid self-excitation the complicated ALFC circuitry was developed in ILP SB RAN; EOM was entered into the laser cavity, the third fast servo amplifier was included [15, 17]. So far addition data are obtained for the laser applied: it is measured N_ν =10 Hz/Hz$^{1/2}$ (±15%) at 1,3 kHz; value ~7 Hz/Hz$^{1/2}$ may be observed on diagram [15]; for $K_0=2\cdot10^3$, L=2 m the forecast is: $x_{NL} \approx 3\cdot10^{-15}$ sm/Hz$^{1/2}$.

Random process U_N is a product of RF noise transformation in SD. RF noise in PD is:

$$I_N^2 = I_{NE}^2 + I_{Nph}^2 + I_{Na}^2 + I_{Nm}^2 \equiv I_{NE}^2 F_E\,.$$

Here I_{Npd} – PD intrinsic noise current, I_{Na} – input noise of current preamplifier; I_{Nm} - current noise of residual RF LPF, $I_{Nm}^2 = I_E^2 m_{Lrf}\Delta f$ [10]; $F_E \approx 2$.

If a selective filter is inserted before SD, noise at it's enter becomes a narrow-band random process, having PSD $N_{in}(\Omega)$ at the modulation frequency Ω. Together with a signal it looks:

$$U_{SDin} = \mathrm{Const}(\delta\nu_R - \delta\nu_L)\sin\Omega t + (V_C(t)\cos\Omega t - V_S(t)\sin\Omega t)\,.$$

Here V_C,V_S - quadrature components. Then $U_{SD} = k_{SD}\,(\mathrm{Const}(\delta\nu_R-\delta\nu_L)-V_S)$, and in (6, 7) $U_N = -k_{SD}V_S$, $N_U = N_V(0) = 2k_{SD}^2 N_{in}(\Omega)$. Thus $x_{NE} =(\lambda/8\Phi)[F_E(2h\nu/\eta P_C)\Delta f]^{1/2}$ – analog (5).

The OGRAN discriminator adds noise [19]. It is discounted in the complete formula:

$$\frac{x_N^2}{\Delta f} = \left(\frac{\lambda}{8\Phi}\right)^2 \frac{2h\nu}{\eta P_C} F_E + \left(\frac{\lambda}{8\Phi_D}\right)^2\left(\frac{L}{L_D}\right)^2 \frac{2h\nu}{\eta_D P_{CD}} F_{ED} + \left(\frac{\lambda L}{c}\right)^2 \frac{N_\nu}{|K_0|^2}\,.$$

Here the last, LFF term dominates but, in principle, it can be compensated.

Information on LFF can be applied in the scheme [2]. On a slope $S_P = (\delta P/\delta\nu_R)^2 N_\nu$, and $x_{NL0} = (\lambda L/c)(N_\nu\Delta f)^{1/2}$. Frequency stabilization of a laser (K_0 »1) leads to expression x_{NL} (7). Technical LPF cause random force acting on the cavity mirrors and the bar (FBA). It's PSD is $G_{Fm} = m_L(2\Phi P_0/\pi c)^2$. For $\Phi = 10^4$, P_0 = 0,5W $G_{Fm} \approx 10^{-22}$ N^2/Hz, whereas $G_B \approx 10^{-18}$ N^2/Hz .

References

1. V.B. Braginskii, V.N. Rudenko, *Sov. Phys. Usp.***13,** 165, (1970)
2. V. B. Braginsky, *Physical Experiments with Test Bodies* (Moscow, Nauka, 1970).
3. V.B. Braginskii, V.P. Mitrofanov, V.N. Rudenko and A.A. Khorev, *Prib. Tekh. Eksp.*, No.4, 241, (1971)
4. V.A. Krysanov, M.I. Kuklachiov and V.N. Rudenko, *Prib. Tekh. Eksp*. No.4, 240, (1979)
5. V.B. Braginskii, V.I. Panov and V.D. Popel'nik, *JETP Lett*. **33**, No.8, 405, (1981)
6. V.A. Krysanov, V.N. Rudenko, *Plobl. Theory Gravitation & Element. Particles*, *M.*, No.8, 195, (1977)
7. V.A. Krysanov, V.N. Rudenko, *Proc. Int. Conf. GR-9* **2**, ed. E. Schmutzer, 394, (1980)
8. V.A. Krysanov, V.N. Rudenko, *Prib. Tekh. Eksp.*, .No.3,.199, (1984)
9. S.V. Yelfímov, B.A. Krysanov, V.N. Rudenko, *preprint* No.32/87, *MSU, dept. of physics*, (1987)
10. N.Sh. Khaikin, B.V. Yurist, *Radiotekhnika i Elektronika*; **16**, 373, (1971); **19**, 1852, (1974)
11. A.V. Gusev, V.V. Kulagin, V.N. Rudenko, *Gravitation & Cosmology* **2**, No.2, 68, (1996)
12. V.V. Kulagin, A.G. Polnarev and V.N. Rudenko, *Sov. Phys. JETP* **64**, No.5, 915, (1986)
13. Yu.M. Gavrilyuk, …, V.A. Krysanov, …, V.N. Rudenko, *Astronomy Reports* **56**, No.8, 638, (2012)
14. V.A. Krysanov, B.S. Kuruliov // Invent. Certificate No.555551, *Bull.of Inventions, USSR*, 1977, No.15
15. L.B.Bezrukov, N.L.Kvashnin, .., V.N.Rudenko, ., M.N.Skvortsov et al., *Instrum .& Exp.Tech.***53**, 423, (2010)
16. L.Bezrukov, , V.Rudenko, M.Skvortsov et al., *preprint gr-qc*/0411083. Proc.Conf."Astr.& Cosm.,Gamow"
17. V.N. Rudenko, S.M. Popov et al., *Proc. Int. Conf "PIRT'2007"/ ed. M. Duffy* - Moscow: BMSTU – P. 49
18. E.D. Black, *Am. J. Phys*. 69, No.1, 79, (2001)
19. V.A. Krysanov, *In Tech. Digest of V Int. Symp."MPLF'2008",* Novosibirsk, Russia. - P.168

The signal-to-noise ratio of the saturated absorption method in the multimode regime

A.A. Kurbatov, E.V. Baklanov

Institute of Laser Physics of SB RAS, Pr. Lavrentyeva 13/3, Novosibirsk, 630090 Russia
E-mail: aleksk@laser.nsc.ru

Is considered the possibility of increasing the signal-to-noise ratio in one of the main methods of laser spectroscopy without Doppler broadening – the method of saturated absorption. Normally, the saturated absorption method is related to the absorption power resonance in the presence of a standing wave (saturated absorption resonance). However, the effect is also possible upon the interaction of counterpropagating waves with different frequencies (see, for example, [1]). This circumstance makes it possible to increase the number of gas atoms that effectively interact with the field and, hence, the intensity of the narrow resonance in the line shape. The method is not widely used, in spite of the fact that an increase in the signal-to-noise ratio was experimentally demonstrated in [2]. We assume that the method may provide a significant increase in the signal-to-noise ratio, which can be employed in the modern frequency standards for an increase in the accuracy and stability. In this work, we analyze a possibility for an increase in the signal-to-noise ratio with the aid of the resonance of saturated absorption in the multimode regime of the counter propagating waves. We consider a scheme for the measurement of small oscillations of surface using the saturated absorption resonance. It is demonstrated that, for the photon noise, the signal-to-noise ratio can be increased by a factor of $\sqrt{N}$, where N is the number of modes. For the noises that significantly exceed the photon noise, the signal-to-noise ratio is proportional to the number of modes that interact with the gas. This result is due to the fact that each pair of oppositely directed waves interacts with different atoms and, hence, independently contributes to the power resonance. Therefore, the contribution of each pair of oppositely directed modes to the photodetector voltage can be considered as an independent measurement channel. When the voltages of N pairs are summed up at the photodetector, the signal (square of voltage) increases by a factor of N^2. The noise increases only by a factor of N, since the phases of noise in the independent channels are uncorrelated. It is shown that the signal-to-noise ratio can be increased proportional to number of modes.

References

1. E. V. Baklanov and V. P. Chebotaev, Usp. Fiz. Nauk **122**, 513 (1977).
2. F. Riehle, J. Ishikawa, and J. Helmcke, Phys. Rev. Lett. **61**, 2092 (1988).

The development of Yb-doped ceramic multipass amplifier operating at cryogenic temperatures

A.V. Laptev, V.V. Petrov, G.V. Kuptsov, V.A. Petrov, E.V. Pestryakov

Institute of Laser Physics of SB RAS, Pr. Lavrentyeva 13/3, Novosibirsk, 630090 Russia
E-mail: alaptev@laser.nsc.ru

Due to the rapid growth in technology of production new ytterbium-ion doped laser materials, the evolution of high repetition rate diode-pumped femtosecond laser systems became possible [1]. For example, Yb:Y_2O_3 material has higher thermal conductivity, broader absorption and emission bands than well-known laser crystal Yb:YAG [2]. The method of the creation of diode-pumped femtosecond laser systems is being developed based on the hybrid (parametric + laser) method [3] of an amplification of pulses generated by start femtosecond laser in the two parallel channels.

In the pump channel of a parametric amplifier Yb:KYW regenerative amplifier (pulse repetition rate – 1 kHz) is used as a preamplifier to increase the peak energy of a pulse up to 0.5 mJ. The main multipass amplifier with output energy up to 150 mJ and at the central wavelength of 1030 nm was developed.

The comparison of laser media was done, the result points at Yb:Y_2O_3 ceramic as the optimal choice for using as an active medium: at cryogenic temperature (80 K) Yb^{3+}-doped medium has a four-level energy scheme, leading to the significant increasing of the efficiency and decreasing thermal loading in the active medium. The advantage of operating at cryogenic temperature against room temperature was shown.

The relation between an output power, number of passes through the active medium of a signal pulse being amplified and pump power was established. In the calculation of the main multipass amplifier spectral characteristics of pump pulse, signal pulse and gain spectrum of the laser medium were taken into account [4]. Such consideration allowed to achieve more precise theoretical data, which is in agreement with our previous experimental results. It should be noted that the spectral narrowing of a signal pulse after amplification is significantly stronger at cryogenic temperatures than at room temperature. In both cases the central wavelength is shifted towards longer wavelengths by amount of approximately 2 nm.

To obtain multiterawatt power of pulses at the output of system the possibility of using in the pump channel an additional intermediate amplifier between the preamplifier and the main multipass amplifier was considered. Calculation of Yb:Y_2O_3 ceramic four-pass intermediate amplifier at cryogenic temperatures was performed. After passing through intermediate amplifier pulse energy increases from 0.5 mJ up to 15 mJ. That case will allow to reach the peak energy of a pulse after the main multipass amplifier up to 250 mJ.

This work is supported by RAS Program “Extreme light fields” and by The Ministry of education and science of Russian Federation, project 8387.

References

1. V.V.Petrov, E.V.Pestryakov, V.I. Trunov, A.V. Kirpichnikov, M.A. Merzliakov, A.V.Laptev, *Atmospheric and Oceanic Optics*, **25**, 285 (2012)
2. T.Y.Fan, D.J. Ripin, R.L. Aggarwal, J.R. Ochoa, B.Chann, M. Tilleman, J. Spitzberg, *IEEE J. Sel. Top. Quantum Electron.*, **13**, 448 (2007)
3. V.I. Trunov, E.V. Pestryakov, A.V. Kirpichnikov, V.V. Petrov, *Proc. SPIE.*, **6054**, 210 (2006)
4. M P Kalachnikov, G Sommerer, P V Nickles, W Sandner, *Quantum Electron.,* **24**, 403 (1997)

Laser-induced luminescence in diamonds from Yakutia and Brazil

V.P. Mironov[1], A.L. Rakevich[1], F.A. Stepanov[1,2], A.S. Emelianova[1,2], D.A. Zedgenizov[3], V.S. Shatsky[4], E.F. Martynovich[1,2]

[1]Irkutsk Branch of Institute of Laser Physics SB RAS,
130a Lermontov st., Irkutsk 664033, Russia,
[2]Irkutsk State University,
[3]V.S. Sobolev Institute of Geology and Mineralogy SB RAS
[4]A.P. Vinogradov Institute of Geochemistry SB RAS
filial@ilph.irk.ru

Luminescence and its distribution in diamond plates from Brazil and Yakutia was investigated. Pulsed diode lasers with a wavelength of 375 nm, 405 nm, 470 nm, 532 nm, 640 nm were used for excitation of luminescence. The pulse duration is about 70 ps, and the peak power reached 980 mW. The pulse repetition frequency may be adjusted in the range from 80 kHz to 31.25 MHz. Confocal scanning fluorescence microscope MicroTime 200 (PicoQuant GmbH) equipped with fiber-optic spectrometer QE65000 (Ocean Optics Co) were used for registration. This allows obtaining a spectra and carrying out investigation of the kinetics of luminescence with enough sensitivity to detect single molecules, including at a temperature of 77K.

The distributions of the luminescence in the plates are not homogeneously (Fig 1).

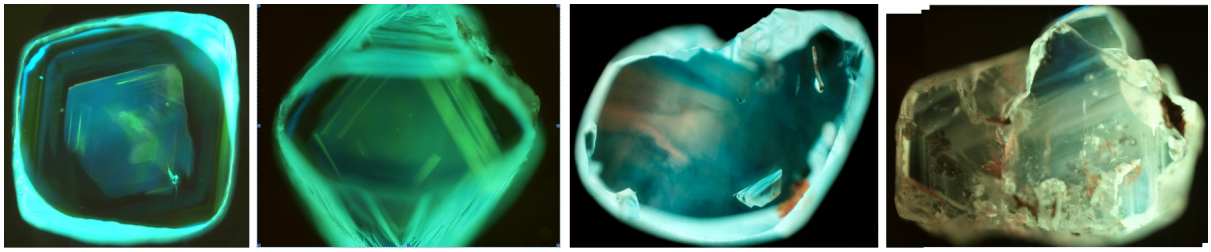

a b c d

Fig. 1. Distributions of luminescence in diamonds plates: a, b- from Yakutia; c, d – from Brazil.

Areas with a different color and intensity of the luminescence were observed. Local spectroscopy in different areas showed the following results.

In the diamonds from Yakutia centers (of varying luminescent intensity): N3, S2, 523 nm, 794 nm and 800 nm band recorded in the central parts of the crystals outlined grained zoning at 375 nm laser excitation. N3 luminescence centers are dominant. For 470 nm laser excitation the spectra contain centers: S1 523, 675, 694, 701 nm and 700 nm band. 532 nm laser excite a weak structure less band of red luminescence with a maximum at 800 nm. 375 nm laser excites only the N3 luminescence centers in the peripheral parts of the same crystals (outside grained zoning), sometimes accompanied by a faint red glow. 470 nm laser in those parts of the crystal excites H3 centers and sometimes accompanied by a band with ZPL at 612 and 675 nm. Laser 532 nm does not excite luminescence of the peripheral regions (fig 2).

In the diamonds from Brazil the laser 375 nm excites centers N3, 491, 496, 523, 536, 575, 700 nm band. 470 nm laser excites the centers 496, 536, 575, 700 band. 532 nm laser excites the centers 575 and a band with a maximum at 700 nm. Lines and bands vary in intensity from point to point, but a set of them is the same in all areas (fig. 3).

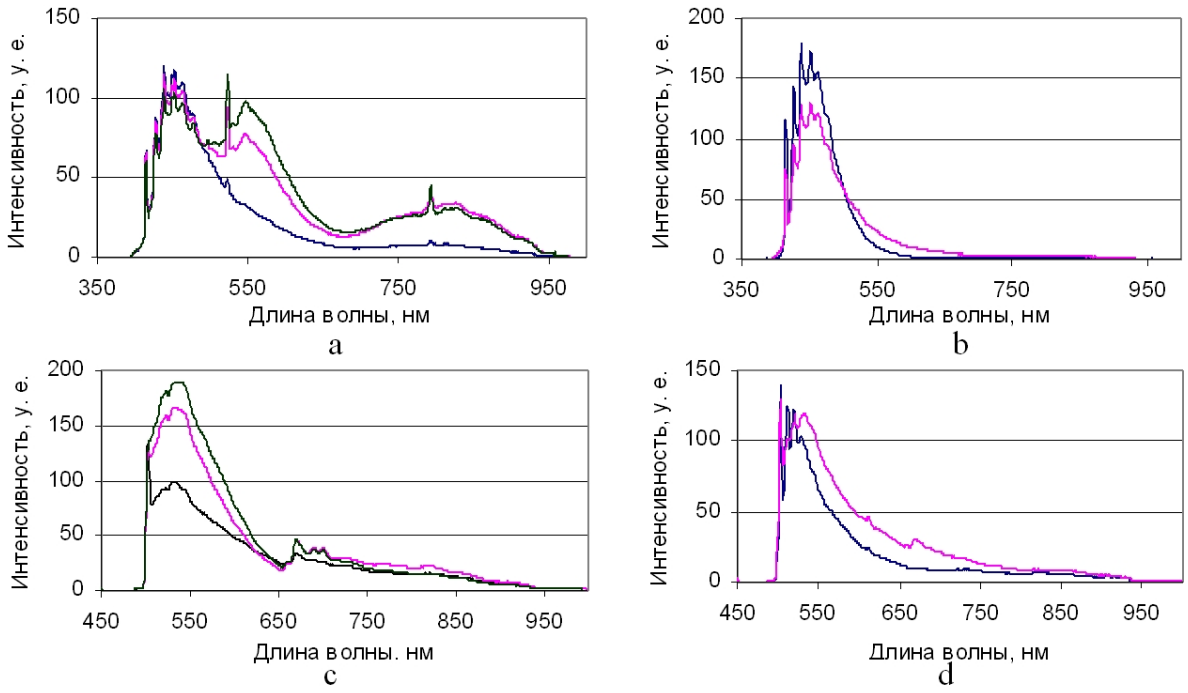

Fig. 2. Luminescence in diamonds from Yakutia: a, b –laser 375 nm, c, d - laser 740 nm, a, c – in central parts, b, d – in periphery parts.

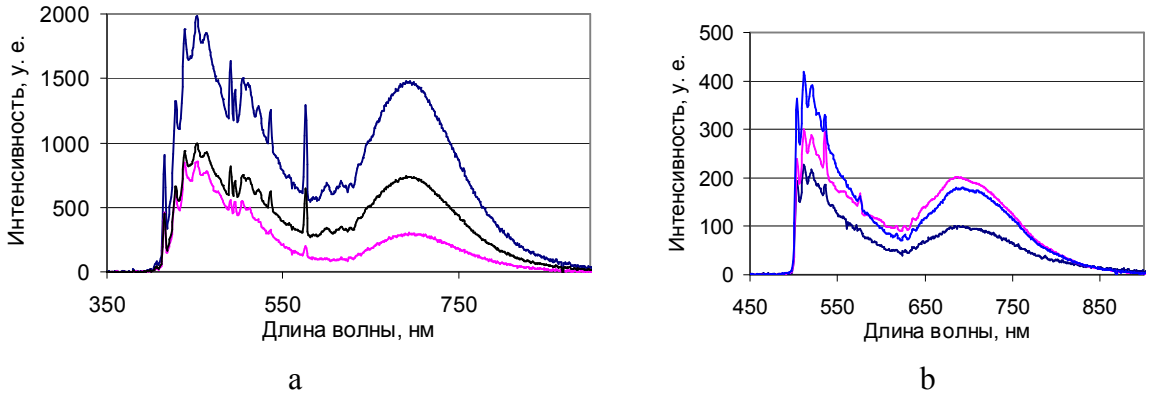

Fig. 3. Luminescence of different points of plates in the diamonds from Brazil: a –laser 375 nm, b - laser 740 nm,

Thus, using of lasers is effective in mineralogical investigation. Llocal study laser-induced luminescence in diamonds from two regions showed significant differences in the conditions of crystallization of diamonds from these regions. According to the research:

1. Diamonds of both regions were crystallized in unstable conditions, with fluctuations in pressure and temperature, as reflected in the respective zonal distribution of luminescence colors.

2. Physical-chemical conditions of crystallization were different, that is manifested in a different set of defects.

3. Diamonds from Yakutia were crystallized in at least two stages substantially different crystallization conditions, Brazil diamonds were crystallized in one step.

The research was supported by the Siberian Branch of the Russian Academy of Sciences as part of the interdisciplinary integration project number 16.

All Ti:sapphire 1-PW laser facility

L. Neagu[1], R. Dabu[1], G. Matras[2], F. Caradec[2], C. Radier[2], C. Simon-Boisson[2], L. Boudjemaa[2]

[1]*Department of Lasers, National Institute for Laser, Plasma, and Radiation Physics, 409 Atomiştilor Str., 071125 Măgurele, Romania*
[2]*Thales Optronics SA, 78995 Elancourt, France*
E-mail: liviu.neagu@inflpr.ro

Center of the Excellence for Advanced Laser Technology (CETAL) is the biggest running Romanian investment project in the research field. The CETAL project will cover several fields of physics such as high-power lasers and optics, relativistic plasma physics, particle physics, nuclear physics, ultrahigh pressure and nonlinear physics. One of the major CETAL laboratories is dedicated to a high intense and ultrafast laser system and its applications. This laboratory is equipped with a high power femtosecond laser system, which was developed by the French company Thales Optronics, beam delivery system, and reaction chamber for experiments.

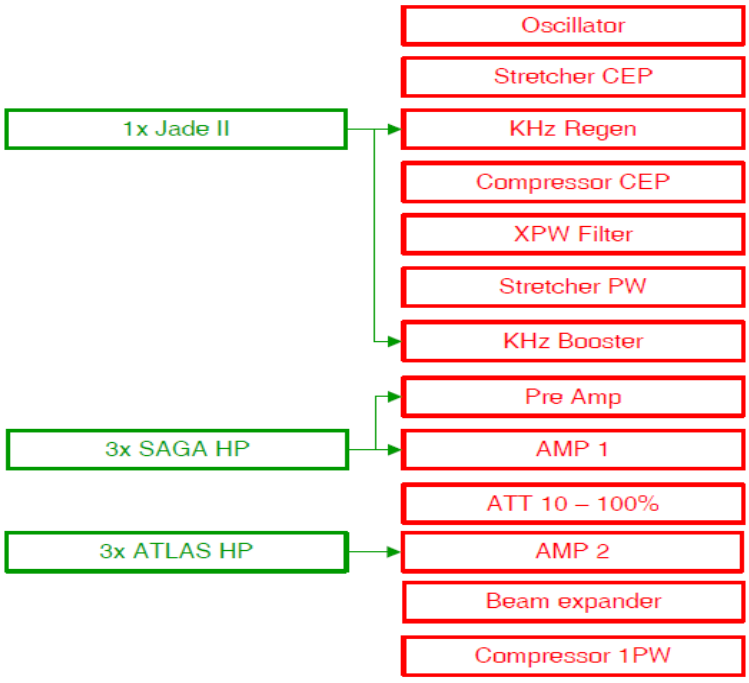

Fig. 1. CETAL 1-PW Laser System General description: oscillator, stretcher CEP, kHz regenerative amplifier, compressor CEP, Cross polarized wave (XPW) filter, stretcher PW, kHz booster, pre amplifier, first stage multi-pass amp, variable attenuator, Final bow-tie multipass amplifier, beam expander, compressor PW.

Based on the CPA amplification technique [1] in Ti:sapphire crystals, the laser system delivers sub-25 fs laser pulses of more than 1-PW peak power at 0.1 Hz repetition rate, centered at 805 nm wavelength.

The petawatt laser system with a modular configuration (see figure 1) consists in a high intensity contrast front-end amplifier and a final bow-tie multipass amplifier pumped by 3 Atlas lasers. It is seeded by a commercial Kerr Lens Mode-locked femtosecond oscillator (model Mantis from Coherent, US). The high intensity contrast and large spectral bandwith amplification is based on a double CPA configuration.

The first CPA consists of an aberration-free stretcher based on the Offner triplet, a kHz regenerative amplifier pumped by a diode-pumped solid-state laser (Jade 2 from Thales

Optronique) and a grating-based compressor using the Treacy configuration. The output of this first CPA is sent to the next stage which is a XPW (Crossed Polarized Wave) filter which allows to increase the temporal contrast of the femtosecond laser pulses by 4 to 5 orders of magnitude and to increase the spectral bandwidth by a factor 1.7 through the use of third order nonlinear optics effect in cubic crystals like BaF_2 [2].

The second CPA uses again a Offner-type stretcher providing longer stretched pulses in order to limit laser intensities on crystals and optical components. An Acousto-Optic Programmable Dispersive Filter (AOPDF) Dazzler from Fastlite (Orsay, FR) is implemented to optimize both spectral amplitude and spectral phase of the overall laser system. The spectral amplitude shaping provided by the Dazzler will compensate red-shift and gain narrowing effects generated by the following amplifier stages which consist in a kHz booster pumped by the remaining power of the Jade 2, a multipass pre-amplifier (PA) and 2 power stages, amplifiers Amp-1 and Amp-2, which works at 0.1 Hz. PA and Amp-1 are pumped by 3 flashlamp pumped 10 Hz lasers (Saga HP of Thales Optronique). Amp-2 is pumped by 3 high energy Nd:Glass flashlamp-pumped lasers (Atlas HP) developed by Thales Optronique in order to meet the requirements for Titanium Sapphire amplifier pumping in terms of beam profile homogeneity and energy stability. Each of these Atlas HP laser delivers at 532 nm 25 J of energy per pulse at 0.1 Hz. The high-energy laser amplifier design is based on techniques developed by Thales company for the management of transverse lasing effects and Amplified Spontaneous Emission [3,4]. By the spectral broadening in the XPW filter, the spectral profile and spectral phase optimization using Dazzler, sub-25 fs pulses where obtained for the first time in a PW-class laser amplifier [5]. In order to obtain a Strehl ratio higher than 0.75, the wave-front aberrations of the amplified femtosecond pulses were corrected by adaptive optics. Ultra-high laser intensity of more than 10^{22} W/cm^2 in the focused beam is expected.

The laser system can also operate at higher repetition rates for dedicated experiments. The laser system can be configured in order to deliver 45 TW pulses at a repetition rate of 10 Hz. An additional output placed before the XPW filter can be used to get a beam delivering sub-mJ pulses at 1 kHz repetition rate. The laser system, commissioned in the Thales factory on April 2013, will be installed during this summer in Magurele. The PW laser facility will come into operation in the second half of the year 2013.

References

1. D. Strickland and G. Mourou, “Compression of amplified chirped optical pulses”, *Optics Communications*, Vol. **56**, 219-221 (1985)
2. A. Jullien et al., “Highly efficient nonlinear filter for femtosecond pulse contrast enhancement and pulse shortening”, *Opt. Lett.* **33**, 2353-2355 (2008).
3. S. Laux et al., “Suppression of parasitic lasing in high energy, high repetition rate Ti:sapphire laser amplifiers”, *Optics Letters* **37**, 1913-1915 (2012)
4. F. Lureauetv al., “High repetition rate PetaWatt Titanium Sapphire laser system for laser plasma acceleration”, Ultrafast Optics 2013.
5. G. Matras at al., “First sub-25 fs PetaWatt laser system”, CLEO, San-Jose, USA, 9-14 June 2013.

THz time-domain spectroscopy of amino acids in the frequency range 0.1 – 1.0 THz.

A.V. Kapralova[1], E.F. Nemova[1], A.S. Pogodin[1], N.A. Nikolaev[2]

[1]Institute of Laser Physics of SB RAS, Pr. Lavrentyeva 13/3, Novosibirsk, 630090 Russia
Phone number: (383)330-99-22(20) E-mail: kapralova@ngs.ru
[2]Institute of Automation and Electrometry of SB RAS, Academician Koptyug ave. 1, Novosibirsk, 630090 Russia
Phone number: (383)330-90-33 E-mail: nazar@iae.nsk.su

THz spectroscopy is a convenient method to characterize many biological molecules. Previously, we have found that THz radiation affects on proteins [1]. But the mechanism of this effect has not been established. Thus, it is necessary to study amino acids as components of proteins using the THz spectroscopy. This method can help us to identify the targets of THz radiation influence.

The aim of this work is the THz time-domain spectroscopic study of amino acids (alanine, histidine, glycine, cysteine, methionine, tyrosine, tryptophan and phenylalanine) in the frequency range 0.1 – 1.0 THz.

We used dry tablet samples of the natural amino acids (Sigma) which were prepared by compression of lyophilized powders in metal frame. Every sample had its individual parameters: diameter was of 5 mm (for all samples) but thickness ranging was from 0.8 to 1.1 mm. Investigations were done in laboratory conditions. The description of the THz-TDS apparatus is given in [2].

In the work we have chosen the pairs of amino acids with the same (similar) structure, differ only by the formation of radicals [3]. For example, alanine and glycine are different of each other only by presence of methyl group and hydrogen in the radical. Methionine and cysteine are sulfur-containing amino acids. Tyrosine and phenylalanine differ only by the presence of OH group attached to an aromatic ring of tyrosine. Tryptophan and histidine are different by the structure of aromatic radicals. A pair of alanine and glycine has the most similar THz spectra. In other cases, although the structure of radicals similar, the spectra show differences, such as phenylalanine-tyrosine, which differ only by the presence of the hydroxyl group of tyrosine.

In the literature there are data of THz spectra of amino acids [4]. However, all the data are for the frequency range over 1 THz and there is no any information about peaks in the range 0.1 – 1.0 THz. It should be noted that water absorbs radiation in the range over 1THz. But the presence of water in the samples wasn`t taken into account in many studies. In the works with dry preparations it is also necessary to take into account the reflection of THz radiation.

In future studies we plan to take into consideration the presence of water in our samples. Moreover, in our further researches data of the radiation reflection will be obtained.

References

1. A.V. Kapralova, A.S. Pogodin, Influence of Terahertz radiation of different ranges on the conformation of molecules ov bovine serum albumin, *Vestnik NSU. Series of Physics*, Vol.5, No.4. P. 182-185 (2010).
2. V.D. Ancygin, A.A. Mamrashev, N.A. Nikolaev, *Avtometry Vol. 46, No.3, (2010).*
3. H.-D. Yakubke, H. Eshkait, Aminoacid. Peptides. Proteins. *M, «Mir»,* (1985).
4. B. Jin, C. Zhang, P. Wu, S. Liu, Resent progress of terahertz spectroscopy on medicine and biology in China. *Terahertz science and technology,* ISSN 1941-7411, Vol. 3, No. 4 (2010).

Ultra-stable lasers: from the cold to space

A.Yu. Nevsky

Institut für Experimentalphysik Heinrich-Heine-Universität Düsseldorf, Germany
Institute of Laser Physics SBRAS, Novosibirsk, Russia

We will present the ongoing activity at the Heinrich-Heine-University of Düsseldorf on the development of the ultra-stable oscillators based on cryogenic and room temperature high-finesse optical resonators as well as on the persistent absorption holes in the crystals. The application of the oscillators will be the new generation of the Michelson-Morley type experiment and a prototype development for the STE-QUEST space mission.

Elaboration of high power femtosecond diode-pumped Yb-laser system at high repetition rate

V.V. Petrov, E.V. Pestryakov, A.V. Laptev, A.V. Kirpichnikov, V.I. Trunov, S.A. Frolov

Institute of Laser Physics of SB RAS, Pr. Lavrentyeva 13/3, Novosibirsk, 630090 Russia
E-mail: vpetv@laser.nsc.ru

The current stage of development of laser physics is largely determined by research in the physics of extreme optical fields and their applications. High intensity femtosecond laser systems, working with a high repetition rate, are the basis for the improvement of inter-disciplinary areas for scientific and technological researches, including the bio-chemical and medical applications.

In the work the principles of creation of high intensity femtosecond laser system with 7-10 fs pulse duration and repetition rate up to 1 kHz are developed. Main units of the system are: start femtosecond Yb-laser; OPCPA channel of noncollinear parametric amplification of start Yb-laser pulses based on BBO and LBO crystals and optically synchronized with it CPA channel based on the cryogenic diode-pumped Yb-doped laser media. The CPA channel forms picosecond pulse radiation to pump parametrical amplifiers of OPCPA channel.

Numerical modeling of parametric pulse amplification was carried out [1]. Configurations and parameters of base elements, and radiation in OPCPA- and CPA-channels are determined for consecutive increasing of number of parametric amplifier cascades up to 1 TW, 10 TW, 100 TW and 1 PW peak power.

Formation of picosecond radiation with 515 nm wavelength by SHG in borate class crystals in the CPA channel is considered. The sizes of aperture and optical quality of the crystal allow to scale the CPA channel to run up to 100 J energy for output pulses.

Investigations show that realization of work of multiterawatt class laser system with repetition rate more than 1 Hz requires use of a cryogenic operating mode of the CPA-channel therefore in the work the considerable attention was paid to determination of availability of application of a number of Yb-doped crystal and ceramic laser media [2, 3].

Thus, in the work the basic principles of creation, element base and optimum schemes of consecutive scaling up to PW level of high-intensity laser system with parametric amplification of pulses in BBO and LBO nonlinear optical crystals pumped by SHG of radiation of cryogenic diode pumped Yb-doped ceramic and crystal media lasers are developed. The data should be used in the development of cryogenic multistage femtosecond laser systems working with high repetition rate in the kilohertz regime.

This work is supported by RAS Program “Extreme light fields” and by The Ministry of education and science of Russian Federation, project 8387.

References

1. V.V. Petrov, E.V. Pestryakov, V.I. Trunov, S.A. Frolov, et al., *15th International conference on Laser Optics*, St. Petersburg, Russia, June 25-29, 2012, TuR1-07.
2. J.-C. Chanteloup, D. Albach, *IEEE Photonics Journal* **3**, 245 (2011).
3. V.V. Petrov, E.V. Pestryakov, V.I. Trunov, A.V. Kirpichnikov, M.A. Merzlyakov, A.V. Laptev, *Atmospheric and Oceanic Optics* **25**, 285 (2012).

Terahertz spectroscopy as characterization tool for ordered media in living cells

S.S. Popova

Institute of Laser Physics of SB RAS, Pr. Lavrentyeva 13/3, Novosibirsk, 630090 Russia
E-mail: svetlanas_popova@mail.ru

Living cells inner media is ordered by a network of tubules forming the cytoskeleton. Landscape of almost all biological macromolecules and kinetics of biochemical processes are influenced by spatial characteristics. For this reason, spatial ordering in the cells is a subject of current interest.

Three types of cells inner media ordering are shown in Fig. 1: glass-like media (a), layered media (b), and crystal-like structure (c). Absorption features in terahertz (THz) region are sensitive to spatial structures of materials, which makes THz spectroscopy an excellent tool to analyze ordering properties.

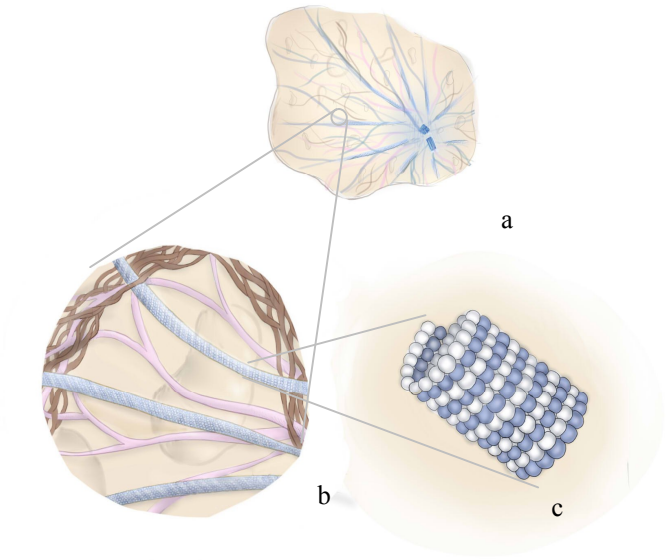

Fig. 1. Cells inner media: a) glass-like (with neglecting inhomogeneity and anisotropy) b) layered media near organelles c) crystal-like structure in the microtubule

Applications of THz spectroscopy include determination of glass media absorption features [1], studying water layer dynamic near proteins [2], and investigation intermolecular bonding in molecular crystals [3]. However, applicability THz methods for complex analysis the structures in living media has not been investigated.

The development of a sensitive tool to probe the inner cells structure can open up the possibility of non-invasive diagnostic and will shed new light on biochemical processes *in vivo*.

References

1. B. Champagnon, L. Wondraczek, T. Deschamps. *Journal of Non-Crystalline Solids* **355**, 712 (2009).
2. B. Born, M. Havenith *J. Infrared Milli Terahz Waves* **30**, 1245 (2009).
3. I.N. Smirnova, D.A. Sapzhnikov, A.V. Kargovsky, V.A. Volodin, O.P. Cherkasova, R. Bocquet, A.P. Shkurinov *Vibrational Spectroscopy* **62**, 238 (2012).

Localization of atoms in bichromatic lattices

O. N. Prudnikov, A. M. Tumaikin, V. I. Yudin

Novosibirsk State University, ul. Pirogova 2, Novosibirsk, 630090 Russia
Institute of Laser Physics, Siberian Branch, Russian Academy of Sciences, pr. Akademika Lavrenteva 13/3, Novosibirsk, 630090 Russia

Nowadays the optical lattices became a basic tool for experiments with ultracold atoms [1]. These are majorly used for quantum information experiments [2-8], with ultracold atoms as basic elements for storing and manipulation by quantum information. Optical lattices are widely used experiments with quantum gas [9], as well they can be applied in microscopy [10].

The theory of laser cooling is well studded now. The dipole force on atoms from light fields can capture and cool the atoms to ultralow temperature in optical potentials minimum. However, it is not possible to reach a strong localization and extremely low temperature of laser cooling simultaneously in monochromatic light fields, i.e. in the situation where the optical potential and dissipative processes in atomic kinetics are determined by a single field [11,12]. Bichromatic fields could be one of possible solution to overcome this problem. Really, the one field here can be used for optical potential, and the other one for cooling.

The first theoretical description of laser cooling in bichromatic fields was done in [13,14] where the optical transition of atom is exited by two fields with different frequency. One of the brightest effect was found here is the dipole force rectification over the length much exceed the wavelength [13] that allow to create deep and wide optical potential.

Resolved-sideband cooling [15,16] can also be considered as a particular case of bichromatic laser cooling, where the cooling is happened due to redistribution of atoms on vibration levels of optical potential generated by strong optical field, by using low pumping field for repumping. However, the theoretical description here is limited by a simple model where the strong field effects only to optical potential without taking into account dissipation effects on atomic kinetics, and the low field effects is limited by consideration of relaxation of Zeeman and vibration levels of optical lattices only [17, 18]. To consider atoms localization in optical lattices more accurately, it is important to take into account both fields effects on atomic kinetics. Really, the fluctuation in the processes of induced absorption and emission of photons of strong light field may lead to significant increment of atom diffusion and heating in optical potential that as well limits the atom localization and cooling.

In the following we consider the problem of the laser cooling and localization in bichromatic light filed where both fields are considered in equal manner, i.e. by considering all dissipative and non-dissipative effects from both fields. We perform detailed analysis of force on atom, friction and diffusion coefficients in bichromatic light fields that are resonant to single optical transition of atom. These expressions can describe basic effects of cooling in bichromatic filed. Apart from the well known results for atom in monochromatic light field new terms appear here that predict strong localization of atoms for some field parameters. For detailed analysis of localization of atoms in these fields a quantum simulation was also done. As a particular case, we consider the situation with one field produces a strong optical potential and the other one is low-intensity field realize dissipation in this optical potential. For this case

strong atom localization is possible. It happens in the points of global minimum of optical potential, where the mutual phase of these two fields is equal to 0 or $\pi/2$.

References

1. G. Grynberg, C. Robilliard, Physics Reports **355**, 335–451 (2001).
2. D. Jaksch, H.-J. Briegel, J. I. Cirac, C. W. Gardiner, and P. Zoller, Phys.Rev. Lett. **82,** 1975 (1999).
3. G.K. Brennen, C. M. Caves, P. S. Jessen, and I. H. Deutsch, Phys. Rev.Lett. **82,** 1060 (1999).
4. D. Jaksch, J. I. Cirac, P. Zoller, S. L. Rolston, R. Cote, and M. D. Lukin, Phys. Rev. Lett. **85,** 2208 (2000).
5. P. S. Jessen, I. H. Deutsch, and R. Stock, Quantum Inf. Process. **3,** 91 (2004).
6. A. J. Daley, M. Boyd, M. J. Ye, and P. Zoller, Phys. Rev. Lett. **101,** 170504 (2008).
7. I. Bloch, Nature (London) **453,** 1016 (2008).
8. K.-A. Brickman Soderberg, N. Gemelke, and C. Chin, New J. Phys. **11,** 055022 (2009).
9. I. Bloch, J. Dalibard, and W. Zwerger, Rev. Mod. Phys. **80,** 885 (2008).
10. A. Klinger, S. Degenkolb, N. Gemelke, K.-A. Brickman Soderberg, and C. Chin Rev. Sci. Instrum. **81,** 013109 (2010)
11. O.N. Prudnikov, A.V. Taichenachev, A.V. Tumaikin, V.I. Yudin, JETP **104,** 839, (2007).
12. O. N. Prudnikov, R.Ya. Ilenkov, A. V. Taichenachev, A. M. Tumaikin, and V. I. Yudin, JETP **112,** 939-945 (2011).
13. A. P. Kazantzev and I. V. Krasnov, JETP Lett. **46,** 420 (1987).
14. R. Grimm, Y. B. Ovchinnikov, A. I. Sidorov, and V. S. Letokhov, Phys. Rev. Lett. **65,** 1415 (1990).
15. Vladan Vuletic, Cheng Chin, Andrew J. Kerman, and Steven Chu Phys. Rev. Lett. **81,** 5768 - 5771 (1998).
16. A. J. Kerman, V. Vuletic, C. Chin, and S. Chu, Phys. Rev. Lett. **84,** 439 (2000).
17. A. V. Taichenachev, A. M. Tumaikin, V. I. Yudin, L. Hollberg Phys. Rev. A **63,** 033402 (2001).
18. G. Di Domenico, N. Castanga, G. Mileti, P. Thoman, A. V. Taichenachev, and V. I. Yudin, Phys. Rev. A **69,** 063403 (2004).

Processing of signals in optical echo-processors

I.A. Rusanova

Kazan federal university, Physics institute, Kremlin 18, 420008, Kazan, Russia
E-mail: irusanova@yandex.ru

Now the big attention to working out of optical memories (RAM) and optical echo-processors in which technically important operations different variants of compression of information signals dare, their parcel and transformation Fourier is paid [1]. During the interaction of the resonant medium with sequence of laser pulses, atoms can behave as the quantum gates carrying out logic operations. The realization of a set of elementary gates XOR and NOT allows to receive, basically, any quantum unitary operations on system qubits. Possibilities of quantum systems of information transferring and transformation depend on superdense coding of the quantum information and the quantum algorithms that allow to more effectively solve any problem. Any objects can be physical systems realizing qubits, provided they have two quantum conditions: polarizing conditions of photons, spin conditions of kernels, etc. The urgent problem of today is the organization of the management of separate qubits and the interaction between them, with providing sufficient time of decoherence.

The quantity of the transferred information can be increased at the expense of the quantum communication channel unmistakably transferring any quantum condition. In work quantum information processes in resonant two-level environments with phase memory are investigated at record of exciting laser (code) pulses, with certain order of the coding set in the form of "echelon" of present («1») and absent («0») pulses-codes by duration $n\partial t \ll T_1, T_2$ (where T_1 and T_2 - times of a longitudinal and cross-section irreversible relaxation), that allows to operate data recording process in the optical echo-processor (Fig. 1).

Let's consider realisation of logic element XOR in the phenomenon of a primary photon echo, consisting in a generated echo-signal the two-level resonant environment with phase memory after two-pulse influence. In case of the code Alphabet consisting of two symbols «0» and «1», at an information transfer on a communication channel with noise, the most direct way to be insured from errors repetition of messages [2]. In work earlier developed teoretiko-information method of research of quantum information processes in resonant environments with phase memory on the basis the algorithmic theory of the information of Kolmogorov [3,4].

The classical information which has been put in pawn in an exciting objective laser pulse, will be transformed to the potential quantum information of environment. The information in the environment appears put in pawn the transitive dynamic lattices described by the equation for an one-partial matrix of density

$$i\hbar \frac{\partial \rho}{\partial t} = [H, \rho].$$

Believing, that before influence of an object pulse the atom was in the basic condition, for matrix elements of a matrix of density we will receive

$$\tilde{\rho}(n\partial t) \approx P_{11}\left(cos^2\frac{\Theta}{2} + \frac{\Delta^2}{\Theta'^2}sin^2\frac{\Theta}{2}\right) + P_{12}\left(-i\frac{a^*}{2\Theta'}sin\Theta + \frac{a^*\Delta}{\Theta'^2}sin^2\frac{\Theta}{2}\right) +$$

$$P_{21}\left(i\frac{a}{2\Theta'}sin\Theta + \frac{2\Delta}{\Theta'^2}sin^2\frac{\Theta}{2}\right) + P_{22}\frac{|a|^2}{\Theta'^2}sin^2\frac{\Theta}{2}.$$

The quantity of the structural information falling separate isochromatic component of the inhomogeneously broadened line of the resonant transition of two-level atoms, will look like:

$$J_q = \int_{-\infty}^{\infty} g_1(\omega')d\omega' \int_{-\infty}^{\infty} g_2(\Omega')\frac{abs\left(\sum_{i\neq j}\rho_{ij}(t)\right)}{abs\left(\sum_{i\neq j}\rho_{ij}(t_0)\right)}(\omega', \Omega')d\Omega'.$$

Influence of capacity of an objective code pulse, its duration Δt_1 and the coding scheme N on efficiency of record of the quantum information in two-level system is considered.

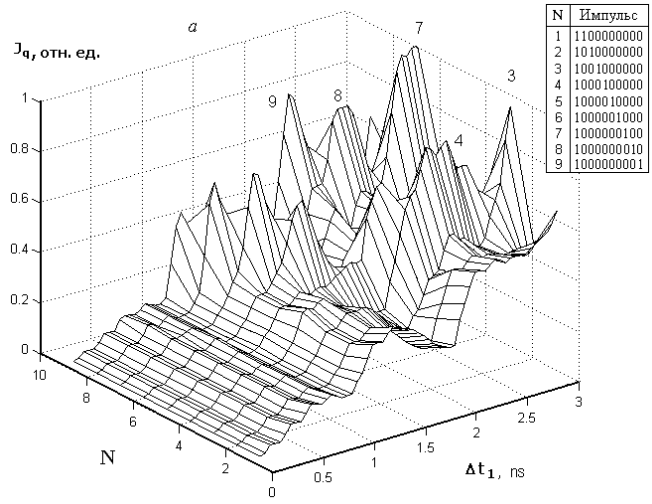

Fig. 1. Efficiency of record of the quantum information J_q of environment from capacity of an objective code pulse and the coding scheme N ($\sigma = 5ns^{-1},\ T_2 = 2\text{ns},\ T_1 = 10ns,\ \Delta t_1 = 0.5T_2$).

A possibility of managing the distribution of quantum bits within the inhomogeneous broadened line in the course of information recording and transformation on the basis of two-pulse excitation of the resonant medium with a phase memory is presented.

1. S. Kroll, P. Tidlund, *Appl. optics,* **32**, 7233 (1993).
2. A.C. Xolevo, *Usp. math. nauk*, **53**, № 6, 193 (1998).
3. L.A. Nefed'ev, I.A. Rusanova, *Opt. spektrosk.,* **90**, 1000 (2001).
4. I.A. Rusanova*, The bulletin of the Chelyabinsk SU*, **14**, 88 (2012).

Waves merging in magnetized space plasma

V.N. Ticshenko[1], I.F. Shaikhislamov[1], N.I. Yakunkin[2]

[1] *Institute of laser physics SB RAS, Pr. Lavrentyeva 13/3, Novosibirsk, 630090 Russia*
[2] *Institute of numerical mathematics and mathematical geophysics SB RAS, Pr. Lavrentyeva 6, Novosibirsk, 630090 Russia*
E-mail: ildars@ngs.ru

In [1-3] a mechanism of shock waves merging (SWM) was proposed for shocks generated by optical discharges in gas or surface of solids. It was suggested that SWM might act in various mediums, for example in magnetized plasma [4]. SWM is effective for generation of low-frequency wave trains because the length of the wave packet when created by a series of laser pulses is proportional to a total energy delivered by laser pulses. In contrast to gas, in a magnetized plasma a quasi-stationary wave or a thin and extended train of magneto-sonic waves (MWT) is formed which propagates along magnetic field for large distances. MWT forms at condition of resonance interaction of energy source with a medium such that compression phase of a successive wave overruns a previous wave and waves unite in a single train.

The aim of the work is to verify a possibility of MWT generation at conditions of purely electromagnetic interaction of source and background plasmas. Namely when transverse size of wave train is much smaller than ion gyro-radius, ion inertia length, collision free-path length and when velocity of source plasma expansion is much larger than the sound speed in background plasma. Reverse conditions were considered previously in a single fluid MHD frame [4]. Investigation was carried out by means of parallelized numerical simulations in the frame of two ion and common electron fluids.

$$m_i n_i \left(\frac{\partial}{\partial t}\mathbf{V}_i + (\mathbf{V}_i\nabla)\mathbf{V}_i \right) = -\nabla p_i - \frac{n_i z_i}{n_e}\nabla p_e + \frac{n_i z_i}{n_e c}[\mathbf{J}\times\mathbf{B}] + \left(\frac{n_i n_j z_i z_j}{n_e} \right)\frac{e}{c}(\mathbf{V}_i - \mathbf{V}_j)\times\mathbf{B}$$

Here an ion moment equation is given with terms (at the right) of thermal pressures, magnetic force and Lorentz force between interpenetrating plasmas (magnetic-laminar mechanism). Problem was solved in a cylinder geometry with symmetry axis Z parallel to magnetic field vector. As characteristic scale a dynamic radius is chosen $R_d = (Q/p_o)^{1/3}$ where p_o is total thermal and magnetic pressure of background medium. Stationary source releases at a time interval T_S a series of N_q plasma clouds each with energy Q and with initial size much smaller than R_d. Such situation might be related to sporadic flares at the Sun [4].

Fig. 1 illustrates MWT generated by 10 pulses. The source is positioned at Z=0. MWT propagates along magnetic field with velocity of ion-acoustic speed. The total pressure in MWT is equalized with that of background plasma due to partial expulsion of magnetic field and this precludes radial widening of wave packet. The source plasma interacts with background plasma through the Lorentz force as shown in Fig. 2. Each expanding plasma cloud courses the recoil pulse in the background resulting in compression of background plasma around symmetry axis. This compression in turn leads to excitation of the slow magneto-sonic wave propagating along the field. If the pulse periodicity corresponds to resonance $T_S \sim R_d/C_S$ then sequential perturbations overrun each other and unite in MWT.

Pulse periodicity ($\omega=1/T_S$) influences the MWT spatial structure. At low frequencies $\omega<0.1$ the condition of wave merging isn't fulfilled and one can see only separate waves from each pulse propagating along magnetic field. At large frequencies $\omega>1$ the dependence of MWT length on number of pulses and input energy is too weak. The optimal range for generation of

extended MWT is $\omega_p \approx 0.5 \pm 0.1$. Profile of wave packet along the axis of propagation at optimal periodicity is shown in Fig 3 for several moments of time.

In summary, it was shown that mechanism of waves merging acts not only in gases but in space collision-free plasmas as well. Extended wave packet propagating along magnetic field forms at resonance depending on periodicity of pulsating plasma source and background plasma parameters. Effective ~30 % transformation of source energy into wave packet can be reached at specific relation between mass and energy of a single pulse and at large number of pulses.

Fig. 1. Grey-scale plot of plasma density. Black color corresponds to MWT and grey to background.

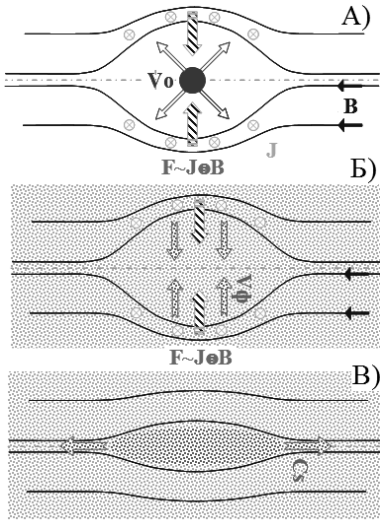

Fig. 2. Mechanism of MWT excitation by explosive plasma. A – expanding plasma cloud forms magnetic cavity. Б) – Lorentz force acts on background plasma and courses its motion across magnetic field. B – compression of background plasma around symmetry axis excites slow magneto-sonic wave.

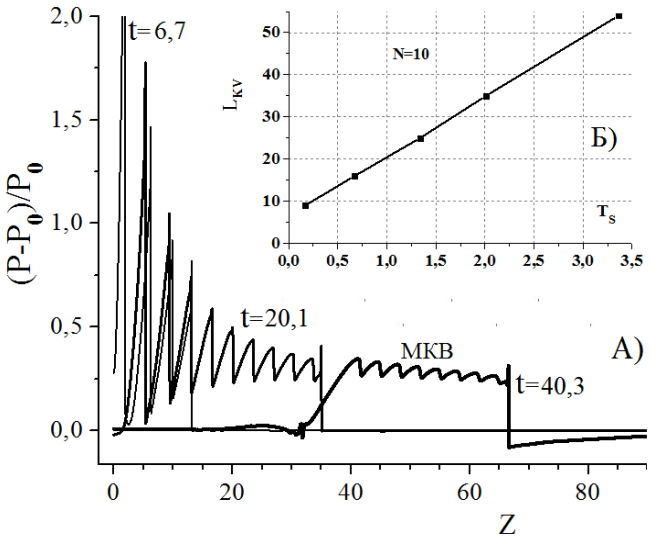

Fig. 3. Pressure in the wave train at Z axis at various times after beginning of source operation (A). Inserted panel (Б) - dependence of wave train length on a periodicity of pulses T_S. Other parameters are: sonic Mach number M_S~50, number of pulses N=10, thermal beta β=0.006, ion inertia length L_{pi}=10.

Acknowledgements: The work is supported by SB RUS project № 113 and RFFI project № 12-08-00587-a.

References

1. V.N. Ticshenko. *Quantum electronics*, in Russian. **33**, 823 (2003).
2. G.N. Grachev, A.G. Ponomarenko,V.N. Ticshenko, A.L. Smirnov. *Quantum electronics*, in Russian. **36**, 470 (2006).
3. V.N. Ticshenko, A.G. Ponomarenko, V.G. Posukh, A.I. Gulidov. *Quantum electronics*, in Russian. **41**, 895 (2011).
4. V.N. Ticshenko, I.F. Shaikhislamov. *Quantum electronics*, in Russian. **40**, 464 (2010).

Multiphoton coherent population oscillations

A. V. Sharypov[1,2] and A. D. Wilson-Gordon[3]

[1] *Kirensky Institute of Physics, 50 Akademgorodok, Krasnoyarsk, 660036, Russia*

[2] *Siberian Federal University, 79 Svobodny Ave., Krasnoyarsk, 660041, Russia*
[3] *Department of Chemistry, Bar-Ilan University, Ramat Gan 52900, Israel*
E-mail: asharypov@iph.krasn.ru

Nonlinear interaction between electromagnetic fields and matter can lead to the appearance of resonances with a bandwidth which is much narrower than the unperturbed natural line bandwidth. The most familiar effects which can give such narrowband response are electromagnetically induced transparency (EIT) [1] and coherent population oscillations (CPO) [2]. The narrowband resonances may appear not only in the spectrum of the effective linear medium response, but also in the spectrum of the higher-order susceptibilities. In the CPO case, the narrowband resonance is centered at the pump frequency [3, 4]; this raises problems for the filtration of weak signals, that either propagate or are generated in the region of the CPO resonance, from the strong pump and incoherent scattering.

Here we present the response of a two-level system (TLS) that displays long-lived coherent population oscillations in the presence of a bichromatic pump, and one or two weak fields. The two sidebands of the pump are symmetrically displaced from the frequency ω_0 and in the case where the scanning is realized by two probe fields, these fields are also symmetrically displaced from ω_0 (see Fig.1). In the bichromatic fields, resonances at the subharmonic frequencies $\omega_{sub}=\omega_0\pm(n+1/2)\delta$ [5] appear where δ is the frequency difference between the two pumps and n is an integer. Here we demonstrate that these resonances can appear under CPO conditions with a width determined by the effective longitudinal relaxation rate. We also demonstrate that the effective FWM process between two CPO resonances can appear at a pump Rabi frequency well below the transverse relaxation rate of the TLS.

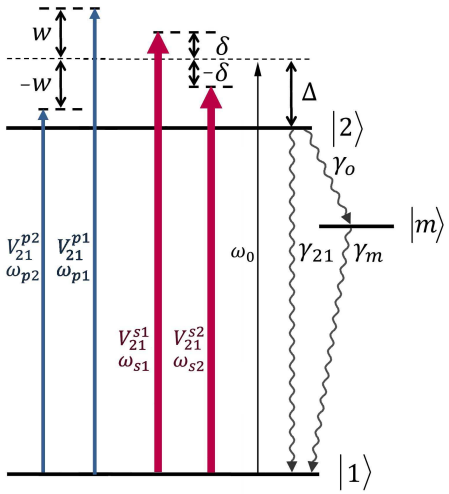

Fig.1. A two-level system |2>-|1> interacting with bichromatic pump field $V_{21}^{s1,s2}$ and bichromatic probe field $V_{21}^{p1,p2}$. γ_{21} longitudinal relaxation from the excited state to the ground, γ_o - longitudinal relaxation rate from the excited state to the intermediate metastable state |m> and γ_m is the longitudinal relaxation rate from intermediate state to the ground.

References

1. M. Fleischhauer, A. Imamoglu, and J. P. Marangos, Rev. Mod. Phys. 77, 633 (2005).

2. E. V. Baklanov and V. P. Chebotaev, Sov. Phys. JETP 33, 300 (1971); M. Sargent III, Phys. Rep. 43, 223 (1978); R. W. Boyd, et al. Phys. Rev. A 24, 411 (1981); R. W. Boyd and M. Sargent III, J. Opt. Soc. Am. B 5, 99 (1988).
3. A. V. Sharypov, A. Eilam, A. D. Wilson-Gordon, and H. Friedmann, Phys. Rev. A 81, 013829 (2010).
4. A. V. Sharypov and A. D. Wilson-Gordon, Phys. Rev. A 84, 033845 (2011).
5. Z. Ficek and H. S. Freedhoff, Spectroscopy in polychromatic fields. Progress in Optics 40, 389 (2000).

Parallel amplification and coherent beam combination as solution for increasing the power of ultrashort pulse lasers

Sandel Simion[1,2], Daniel Ursescu[1,3], Romeo Banici[1], Razvan Dabu[1]

[1]ISOTEST Laboratory, NILPRP, 409 Atomistilor Str., 077125 Magurele-Bucharest, Romania
[2]Doctoral School of "Politehnica" University of Bucharest, Faculty of Electronics, Telecommunication and Information Technology, Romania
[3]ELI-NP, Reactorului str. 34, 077125, Magurele-Bucharest, Romania
simion.sandel@inflpr.ro

Today ultrashort pulses laser based on chirped pulse amplification (CPA) technique, achieve a pulse energy range of tens Joules, up to one hundred Joules. That means a little over 1PW pulse power at a few tens of femtoseconds. The limitation mainly is given by geometrical restriction of laser active medium crystals (Ti-sapphire), and green pumping lasers.

A similar problem arises in microelectronics, when the microprocessor technology began to stagnate and no longer able to sustain the growth dynamics of computing capability as the market demand. The solution was to put two or more microprocessors cores to work together (or in parallel!), and creating the well-known today, the multi-core processor technology.

In the same way in ultrashort, high power pulse laser technology to overcome the limitations of technology, a solution could be given by coherent combining the multiple laser beams from separate laser amplifiers, in other words parallel implementation of these laser amplifiers. Coherent combination of laser beams has been made in CW (continuous wave) laser [1,2], and nanosecond pulse in laser amplifiers with optical fiber [3]. However, to realize parallel amplification and coherent combination in ultrashort (femtosecond) pulse, high power laser, is not an easy task and needs considerable research and engineering in order to overcome the specific difficulties and particularities met in this area. These limitations are given mainly by self phase modulation effect, dispersion, and optical path fluctuations (OPF) between the different beams that are to be combined [4].

In order to control the optical path in such high power lasers, the OPF control system in fact must be a feedback control loop. In general, a feedback loop contains four main blocks: the sensor, the reference, the controller, and the actuator. Because the system must be controlled at a tens of nanosecond scale, the sensor should be based on an interferometric principle. A real-time, high speed homodyne interferometer has been built for this purpose [5]. The resolution of the interferometer is 20nm, and is capable to work at maximum velocity of 2 m/s. Regarding the actuator several devices was tested, the best seems to be a piezo actuator. The next step is to install the interferometer and the actuator on two separate laser amplifiers, and performing tests in order to obtain coherent beam combination.

1. R. Xiao, J. Hou, M. liu, and Z. F. Jiang, "Coherent combining technology of master oscillator power amplifier fiber arrays", Optics Express 16(3), 2015-2022 (2008).
2. R. Uberna, A. Bratcher, T. G. Alley, A. D. Sanchez, A. S. Flores, and B. Pulford, "Coherent combination of high power fiber amplifiers in a two-dimensional re-imaging waveguide", Optics Express 18(13), 13547-13553 (2010).
3. E. Seise, A. Klenke, J. Limpert, and A. Tunnermann, "Coherent addition of fiber-amplified ultrashort laser pulses", Optics Express 18(26), 27827-27835 (2010).
4. A. Klenke, E. Seise, J. Limpert, and A Tunnermann, "Basic consideration on coherent combining of ultrashort laser pulses", Optics Express 25(19), 25379-25387 (2011).
5. S. Simion, C. Blanaru, D. Ursescu, "Design considerations for an interferometer for coherent combination of ultrashort laser pulses", Romanian Reports in Physics, 3(62), 644-651, 2010.

Suppression of residual amplitude modulation of electro-optical modulator in OGRAN project

V.I. Vishnyakov[1], S.M. Ignatovich[1], N.L. Kvashnin[1], S.M. Popov[2], V.N. Rudenko[2], A.A. Samoilenko[2], M.N. Skvortsov[1], I.S. Yudin[1,2]

[1] *Institute of Laser Physics of SB RAS, Pr. Lavrentyeva 13/3, Novosibirsk, 630090 Russia*
[2] *Sternberg Astronomical Institute, Moscow State University, Universitetsky pr. 13, Moscow, 119991 Russia*
E-mail: mskvortsov@mail.ru

Experimental methods for a suppression of residual amplitude modulation (RAM) of electro-optical modulator are considered in application to the problem of sensitivity of the opto-acoustical gw-detector OGRAN proposed in [1].

The idea of the OGRAN gravitational-wave detector consist in combination of bar-detector and a long-base interferometer. The sensitivity $\sim 4\cdot 10^{-16}\ m/\sqrt{Hz}$ was achieved on the pilot setup with the 50 kg detector [2]. On the full-scale setup with the detector of 2 m long and 2000 kg weight estimated sensitivity is about $5\cdot 10^{-18}\ m/\sqrt{Hz}$. However, using the same setup [2] we could not to overcome the sensitivity level $10^{-17}\ m/\sqrt{Hz}$. The noise budget analysis showed an importance of the RAM level for the setup sensitivity.

OGRAN setup uses the Pound-Driver-Hall method for feed back loops and signals readout. For this method it is necessary to use EOM for phase modulation of the laser beam and lock-in detector, but typical EOMs have unspecified level of the RAM. The special attention should be paid to thermal stabilization of the crystal in EOM to avoid fluctuation of RAM due to interference of the beams reflected from the input and output ends of the crystal.

We used another method to avoid such negative effects – the incident laser beam was directed to the input EOM surface on Brewster angle. In this case we exclude mutual interference of beams reflected from input and output surfaces of crystal as well as gain additional polarization purification of laser beam.

Nevertheless, the RAM amplitude and its phase along cross-section of the laser beam vary on several times of magnitude. It depends on the inhomogeneity and individual structural defects of the EOM crystal. The final RAM value detected by photodiode depends strongly on the point of the photodetector surface at which the beam falls. This point should be tuned as accurate as a small fraction of the laser beam diameter.

In order to achieve the homogeneity of the RAM level through the laser beam cross section after EOM, the beam was passed through the single-mode polarization maintenance optical fiber. The output laser light after optical fiber has stable RAM level and fixed phase along beam cross-section. Alignment of the laser beam entering point of the polarization maintenance optical fiber can achieve the desired RAM phase relative to the lock-in detector reference signal. The RAM phase should be chosen to minimize output signal DC level of the lock-in detector.

After minimization of the RAM level the final sensitivity of the full-scale OGRAN setup achieve the value of $2\cdot 10^{-17}\ m/\sqrt{Hz}$.

References

1. V.V.Kulagin, A.G.Polnarev, V.N.Rudenko // JETP N.64. p.915. (1986)
2. L.B. Bezrukov, N.L. Kvashnin, et al. *Instruments and Experimental Techniques*, **53**, №3, 423 (2010)

The luminescence quenching and photo-thermal transformation of color centersin LiF crystals with laser excitation

K.A. Slastnyh[1,2], S.V. Boychenko[1,2], A.L. Rakevich[1], E.F. Martynovich[1,2]

[1] *Irkutsk Branch of Institute of Laser Physics SB RAS, Lermontov str., 130a, Irkutsk, 664033, Russia*
[2] *Irkutsk State University, 664003, Irkutsk, Gagarin Blvd, 20*
E-mail: filial@ilph.irk.ru

Color centers are working quantum systems in a number of optoelectronic applications. They are used to record information in the form of images or in digital formats in 3D and multilayer fluorescent optical storage media [1-3] in the thermoluminescent detectors of hard radiation and long-wave femtosecond laser pulses [4], in the technology of electron-beam lithography [5], laser media and passive Q-switch [6].

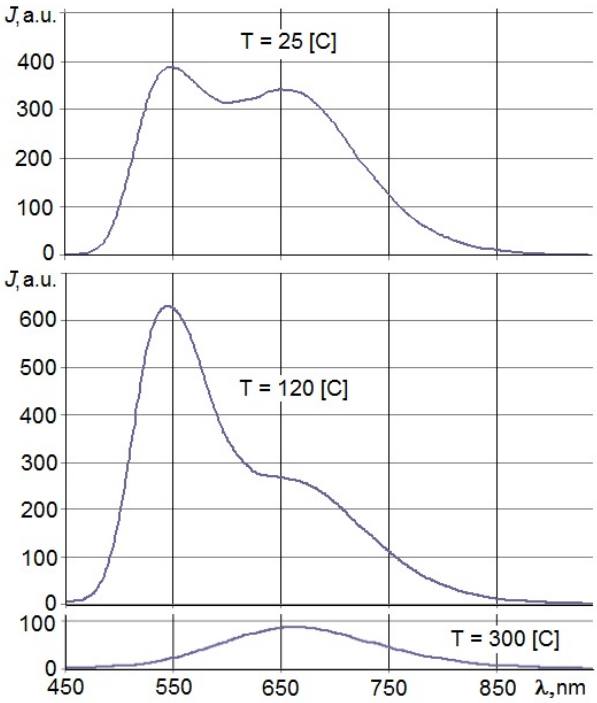

Рис. 1. Спектры фотолюминесценции при разных температурах. λ_{ex} = 405 nm.

In this study we investigated, firstly, the temperature dependences of the integrated luminescence intensity of the color centers excited by a continuous or pulsed laser radiation. Secondly, the temperature dependences of the decay time constants and the relative yields of the various time components of the luminescence due to F_3^+ (~ 8 ns) and F_2 (~16 ns) color centers under the picosecond laser excitation (Fig. 2c). Moreover, the temperature dependences studied both during heating and during cooling of the samples. Also the temperature dependences of processes were investigated with significantly different intensities of the exciting radiation.

The experiments were performed using a confocal scanning fluorescence microscope MicroTime 200 with a time resolution (Picoquant Gmbh), including picosecond laser sources for luminescence excitation. This microscope was equipped with an additional 65000 Ocean Optics spectrometer, a system of heating and cooling of samples and additional sources of continuous laser radiation of low power.

Fig. 1 shows the luminescence spectra in the three selected temperature points during continuous heating at low exciting laser radiation (~ 100 mW/cm^2). It can be seen that during the heating intensity F_3^+ band at first increases and then decreases substantially. At the same time and under the same conditions the temperature dependence of the luminescence intensity in the F_2 band is significantly different. In contrast to the above-described mode of continuous weak luminescence excitation, the integrated emission intensity decreases monotonically with picosecond pulsed excitation by a focused laser beam (Fig. 2a). The luminescence yield of the individual time components falls roughly in the same manner (Fig. 2b). However, this fall was not accompanied by a corresponding drop in the luminescence decay time constants F_2, F_3^+ centers (Fig. 2c), which are almost unchanged. This allows you to eliminate the effect of intracenter quenching at emitting transitions on the temperature dependence in the entire temperature range.

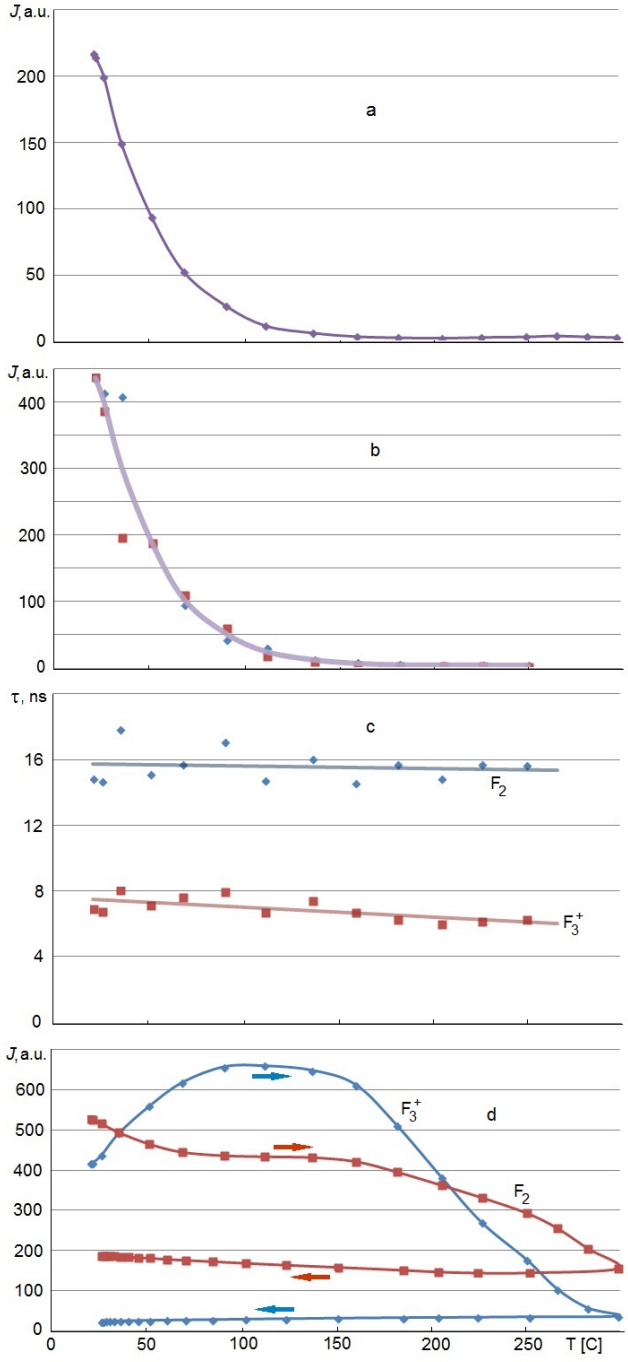

Fig. 2. Temperature dependences: the integrated luminescence intensity (a), the intensity of individual time components of the luminescence of F_2 and F^{3+} centers (b), the decay time of luminescence of individual time component (c). Measured under intense picosecond laser excitation (a-c). The temperature dependence of the intensity of the luminescence of individual spectral bands of F_2 and F_3^+ centers at low excitation (d), during heating and cooling (indicated by arrows).

A consistent increase in the intensity of luminescence F_3^+ centers and its fall of F_2 centers by raising the temperature to 100 °C (Fig. 2d) logically explained by thermal release of the anion vacancies from unidentified centers and their association with F_2 centers. Comparison of the temperature dependences of the direct and reverse temperature allows, first, to eliminate the influence of temperature changes in the spectral absorption and luminescence bands in the observed temperature dependence of the intensity of luminescence. Secondly, it is possible to conclude that the main contribution to the reduction of the intensity in the region above 150 °C makes the thermal destruction of the centers. Action of the intense exciting laser radiation accelerates this process.

The research was supported by the Presidium of RAS (Project № 4.12 of Basic Research Program № 13) and by the RFBR (Project № 13-02-92202 Mong_a).

References:

1. E.F.Martynovich, A.V.Kuznetsov, A.V.Kirpichnikov, E.V.Pestryakov, S.N.Bagayev. Formation of luminescent emitters by intense laser radiation in transparent media. Quantum Electronics, 43 (5) 463 – 466 (2013).
2. E.F. Martynovich, D.S. Glazunov, A.V. Kuznetsov, E.V. Pestriakov, A.V. Kirpichnikov and S.N. Bagayev. 3D Fluorescent Imaging with Highly Nonlinear Photosensitive Materials. Optical Sensors, Optical Society of America, 2011, paper SWD6.
3. Martynovych E.F., Balyunov D.V., Kuznetsov A.V., S.N. Bagayev. Optical information carrier. RF Patent № RU 85027 U1, published on: 20.07.2009.
4. D.S.Glazunov, V.P.Dresvyanskiy, N.S.Bobina, V.F.Ivashechkin, A.I.Nepomnyashchikh, A.V.Kirpichnikov, A.V.Kuznetsov, E.V.Pestriakov, B.Chadraa, O.Bukhtsooj, E.F.Martynovich. Thermostimulated luminescence of LiF:Mg,Ti, irradiated with femtosecond laser pulses in filamentation mode. Russian Physics Journal, 2012, 55, № 11/3, p.47-49.
5. F. Bonfigli M., Montecchi R.M., Montereali E., Nichelatti M., Piccinini F., Somma. Colour-centre concentrations in broad-band light-emitting strip waveguides in Lithium Fluoride. J. Phys.: Conf. Ser., 2010, 249 012004.
6. E.F. Martynovich. Color centers in laser crystals. Irkutsk: Irkutsk University Publishing. 2004, 227 p.

About nature of opto-magnetic resonances in light emission from gas mixture of even neon isotopes

Sorokin V.A.
Institute of automation and electrometry SB RAS, 630090, Pr. Koptyuga 1, Novosibirsk, Russia
E-mail: Vlad_sorokin@ngs.ru

In papers [1-3] were shown that the spontaneous emission of pair of identical static atoms is differ from the spontaneous emission of single atom too much. If only one atom is in excited state at initial time, then the creation of the tangled quantum states of atoms takes place during evolution.

$$\psi_e = \frac{1}{\sqrt{2}}\left(\psi_{1e}\psi_{2g} + \psi_{1g}\psi_{2e}\cdot e^{2\cdot\pi\cdot i\frac{R}{\lambda}}\right), \quad \psi_g = \psi_{1g}\psi_{2g}.$$

Here are: *Ψjs* – wave functions of single atoms (*j*=1,2; *s*=*e*(exited), *g*(ground)); *R* – distance between atoms; λ – wave length of the resonant quant of light. Matrix element of electric dipole for spontaneous decay $\psi_e \rightarrow \psi_g$ now is function of distance *R*. Amplitude of probability of the electro-dipole transition $\psi_e \rightarrow \psi_g$ can be to change from zero to value which exceed amplitude of probability of single atom to $\sqrt{2}$ time.

$$d_{eg} = \langle\psi_e|er|\psi_g\rangle = \frac{1}{\sqrt{2}}\left(d_1 + d_2 e^{2\pi i\frac{R}{\lambda}}\right), \quad d_1 = d_2 = d, \quad |d_{eg}|^2 = |d|^2\left[1+\cos\left(2\pi\frac{R}{\lambda}\right)\right].$$

Estimation of intensity of spontaneous emission for single atom W_1 and for pair of atoms W_2 one can find by using the simplest kinetic equation:

$$\frac{d}{dt}N_m + \Gamma N_m = Q_m, \; W = A_{mn}\cdot\hbar\omega_{mn}\cdot N_m, \quad \Rightarrow W_1 = A_{mn}\cdot\hbar\omega_{mn}\cdot\frac{Q_m}{\Gamma_1}, W_2 = A_{mn2}\cdot\hbar\omega_{mn}\cdot\frac{Q_m}{\Gamma_2},$$

$$\Gamma_2 = A_{mn2} + \alpha P, \quad \Gamma_1 = A_{mn} + \alpha P, \quad A_{mn2} = \frac{4\omega_{mn}^3}{3c^3}|d_{eg}|^2 = A_{mn}\left[1+\cos\left(2\pi\frac{R}{\lambda}\right)\right].$$

Here is $\Gamma=\Gamma_1$ or $\Gamma=\Gamma_2$, the both depend on pressure *P* and describe the collisional and radiation deactivation; Q_m – rate of excitation of the upper level *m*. $W_2(R)$ is periodical function and looks like potential. The minimum of this is the most probable state for atomic pairs where atoms can accumulate. Intensity of spontaneous emission W_2 depends on distance *R* and we must average it for gas. Assuming distribution of atoms is homogeneous, we can obtain:

$$W_{a2} = \frac{1}{\lambda}\int_0^{\lambda} W_2\left(2\pi\frac{R}{\lambda}\right)dR = \frac{\hbar\omega_{mn}\cdot Q_m}{1+B+\sqrt{B(1+B)}}, \quad B = \frac{\alpha P}{2A_{mn}}.$$

Difference between spontaneous emission of pair and single atom will be to have extremum (minimum) about –13% at $\alpha P/Amn \approx 0.6/\pi = 0.19$. Curve $dW(B)$ is shown in fig.1.

$$dW(B) = \frac{W_{a2} - W_1}{\hbar\omega_{mn}\cdot Q_m} = \frac{1}{1+B+\sqrt{B(1+B)}} - \frac{1}{1+2B}.$$

For gas it is too difficult to observe the spontaneous emission of pair because of there is the great emission from single atoms. However, if you have gas mixture of the different isotopes it is possible to select spontaneous emission of pair in far wing of spectral line when the emission from single atoms decreases when isotope shifts are large enough. Fig.2 demonstrates the evidence of these phenomena registered at 0.2 mmHg. One can see resonances at ±850 Gs and ±1300 Gs, formed by Zeeman compensation of isotope shifts of some transitions of 2*p*–1*s* multiplet [4]. The most contrast resonance at ±1300 Gs (see area 3) shows the decreasing of the spontaneous emission directly.

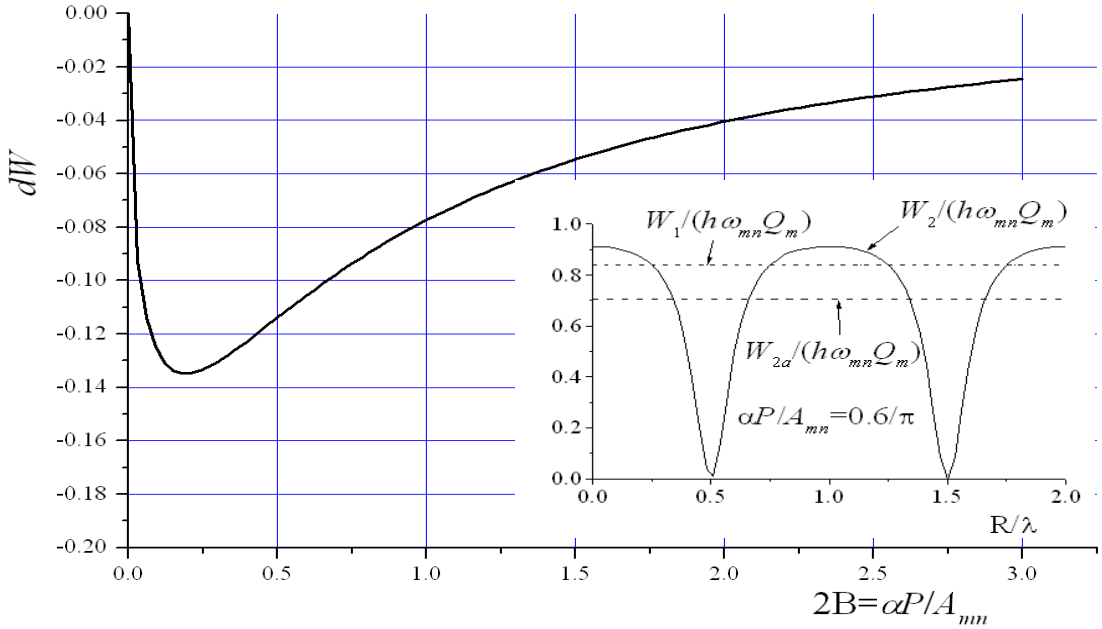

Fig.1. Difference between spontaneous emission of pair and single atom.

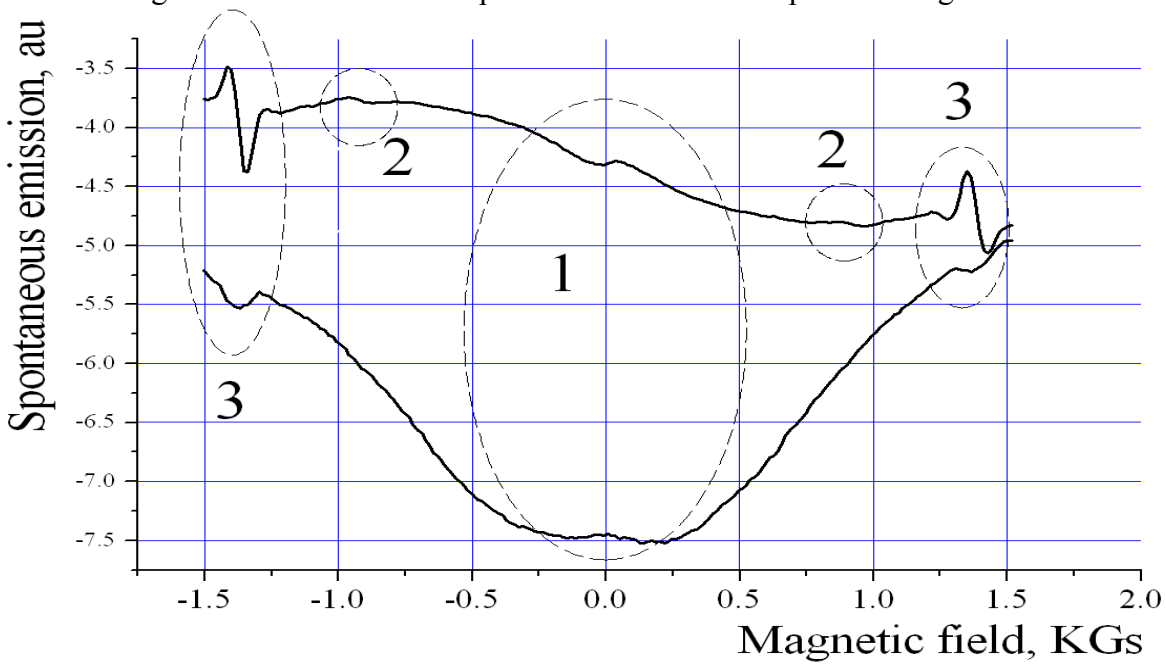

Fig.2. Spontaneous emission as function of magnetic field from glowing discharge in mixture of ^{20}Ne and ^{22}Ne. Upper curve is derivative on magnetic field. Down curve is direct registration of light.

The work has been support by the grant of President of RF for State supporting of leading scientific schools SS-2979.2012.2.

References

1. A.A.Makarov, V.S.Letokhov, JETP, **124,** 766 (2003).
2. A.M.Basharov, A.A. Bashkeev. Opt and spectr. **96**, 716 (2004).
3. L.V.Ilyichev. JETP, **131**, 30 (2007).
4. E.G.Saprykin, V.A.Sorokin, A.M.Shalagin JETP, **143**, 622 (2013).

Generalized Ramsey spectroscopy of ultracold atoms and ions: Effect of spontaneous relaxation and finite width of laser line

K. S. Tabatchikova[2,3], A. V. Taichenachev[1,3], V. I. Yudin[1,2,3]

[1]*Institute of Laser Physics SB RAS, Pr. Lavrentyev, 13/3, Novosibirsk, 630090, Russia*
[2]*Novosibirsk State Technical University, Pr. K. Marksa, 20, Novosibirsk, 630073, Russia*
[3]*Novosibirsk State University, Str. Pirogova, 2, Novosibirsk, 630090, Russia*
E-mail: k.tabatchikova@gmail.com

Presently, laser spectroscopy and fundamental metrology are among the most important and actively developed directions in modern physics. Ramsey's method of separated oscillatory fields was crucial for the progress in precision spectroscopy and the development of atomic clocks [1] and is an important tool in quantum information processing [2]. In the case of optical spectroscopy the high probe light intensities required to drive these transitions will unavoidably lead to level shifts through the dynamical Stark effect.

Several methods were investigated to compensate this shift, for example, linear extrapolation to zero intensity or the use of an additional inversely shifting field [3]. Nevertheless, a wide range of precise frequency measurements presently suffer from significant uncertainties due to light shift [4,5]. In work [6] a generalized Ramsey excitation scheme recently proposed by Yudin et al. (fig. 1), which cancels the light shift and efficiently suppresses the sensitivity of the spectroscopic signal to variations of the probe light intensity. The dominating dependence of signal frequency shift on atomic transition shift is cubic on certain ratio of pulse durations. First experiments on a laser-cooled single ^{171}Yb ion corroborated high efficiency of given method [7].

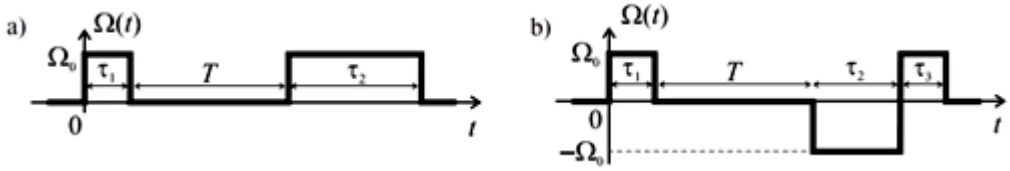

Fig. 1. Ramsey pulses with Rabi frequency Ω_0 of different duration τ_1, τ_2 and τ_3 with phase step in the second pulse and during dark time *T*.

In work [6] authors consider idealized case, which ignores spontaneous relaxation of atomic level and finite width of laser line. In this work we investigate the proposed scheme (fig. 1) with account for the spontaneous relaxation of atomic levels and finite width of laser line. The analysis is executed by numerical solution of system of quantum kinetic equations.

Theoretical analysis of excitation scheme indicates that the suppression efficiency of the field shift diminishes for scheme represented on figure 1a in the presence of typical experimental Rabi frequency fluctuation. The phase step in the second pulse (fig. 1b) provides the robust suppression of the field shift.

Therefore, we consider the scheme presented in figure 1b. Suppose that the spontaneous relaxation of atomic levels and the width of laser line are equal to zero. In this case, the effective suppression of the field shift and maximum amplitude of resonance are achieved when $\Omega_0\tau_1 = \pi/2$, $\Omega_0\tau_2 = \pi$ and $\Omega_0\tau_3 = \pi/2$. Dependence of signal frequency shift on atomic transition shift for calculated value is represented in figure 2a (solid line). The analogous dependence for calculated value of pulse durations has form represented on figure 2a (dashed line) when spontaneous relaxation of atomic level and finite width of laser line are taken into account. Influences of the spontaneous relaxation of atomic level and finite width of laser line lead to significant decrease of field shift suppression efficiency.

Further, we calculate optimal values of pulse durations canceling the field shift when spontaneous relaxation of atomic level and finite width of laser line are taken into account. Dependence of signal frequency shift on atomic transition shift is represented on figure 2b. When comparing dependences (fig. 2a,b) we summarize that spontaneous relaxation of atomic level and finite width of laser line must be considered. Spontaneous relaxation for forbidden transition is insignificant, so spectral line width has major influence on calculation results.

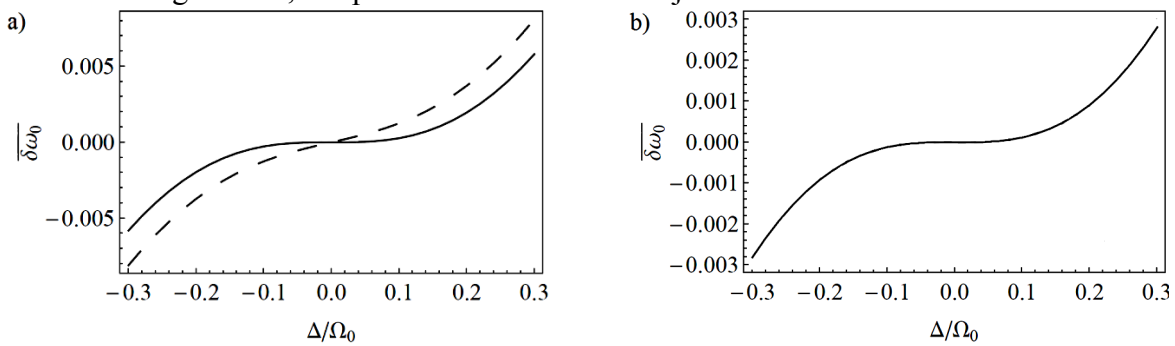

Fig. 2. Dependence of signal frequency shift on atomic transition shift a) $\Omega_0\tau_1 = \pi/2$, $\Omega_0\tau_2 = \pi$ and $\Omega_0\tau_3 = \pi/2$ to both case b) for optimal pulses $\Omega_0\tau_1 = 1.6$, $\Omega_0\tau_2 = 3.25$ and $\Omega_0\tau_3 = 1.65$ in the presence spontaneous relaxation of atomic level $\gamma/\Omega_0 = 0.01$ and the finite width of laser line $\gamma_d/\Omega_0 = 0.01$.

Thus, the theoretical analysis of the Ramsey scheme with pulses of different duration and with a phase step in the second pulse with account for the spontaneous relaxation of atomic level and the finite width of laser line. We define optimum features of pulses that correspond to maximum suppression of the field shift and maximum amplitude of resonance for both schemes. Ramsey scheme with a phase step in the second pulse provides effective suppression of the field shift and it is less sensitive to the Rabi frequency fluctuations in comparison with Ramsey scheme with pulses of different duration.

The work is supported by the Ministry of Education and Science of the Russian Federation in the frame of the Program “Scientific and scientific-pedagogical personnel of innovative Russia” (contract no. 16.740.11.0466 and agreement no. 8387), by the Russian Foundation for Basic Research (grants nos. 12-02-00454, 12-02- 00403, 11-02-00775, 11-02-01240), by the Russian Academy of Sciences and the Presidium of Siberian Branch of Russian Academy of Sciences, and the Russian Quantum Center. The young scientist K.S. Tabatchikova is supported by the Presidential Grant MK-3372.2912.2 and the RFBR Grant 12-02-31208-“mol_a”.

References

1. N. F. Ramsey, *Rev. Mod. Phys.* **62**, 541-552 (1990).
2. H. Häffner, C. Roos, and R. Blatt, *Phys. Rep.* **469**, 155-203 (2008).
3. H. Häffner, S. Gulde, M. Riebe, G. Lancaster, C. Becher, J. Eschner, F. Schmidt-Kaler, and R. Blatt, *Phys. Rev. Lett.* **90**, 143602 (2003).
4. C. G. Parthey, A. Matveev, J. Alnis, B. Bernhardt, A. Beyer, R. Holzwarth, A. Maistrou, R. Pohl, K. Predehl, T. Udem, T. Wilken, N. Kolachevsky, M. Abgrall, D. Rovera, C. Salomon, P. Laurent, and T.W. Hänsch, *Phys. Rev. Lett.* **107**, 203001 (2011).
5. N. Huntemann, M. Okhapkin, B. Lipphardt, S. Weyers, Chr. Tamm, and E. Peik, *Phys. Rev. Lett.* **108**, 090801 (2012).
6. V. I. Yudin, A.V. Taichenachev, C.W. Oates, Z.W. Barber, N. D. Lemke, A. D. Ludlow, U. Sterr, C. Lisdat, and F. Riehle, *Phys. Rev*. A **82**, 011804(R) (2010).
7. N. Huntemann, B. Lipphardt, M. Okhapkin, Chr. Tamm, E. Peik , A.V. Taichenachev, V. I. Yudin, *Phys. Rev. Lett*. **109**, 213002 (2012).

Investigation of resolution in multichannel confocal microscopy

V.P. Bessmeltsev[1], A.N. Raldugin, V.S. Terentyev, M.A. Korelina
[1]*Institute of Automation and Electrometry of SB RAS , Pr . Ac. Kuptug 1, Novosibirsk, 630090, Russia*
E-mail: bessmelt@iae.nsk.su

The effect of a background illumination by neighbour laser beams on the resolution of a multichannel confocal microscope (MCM) with the optical scheme shown in Fig.1 has been investigated in this work. [1].

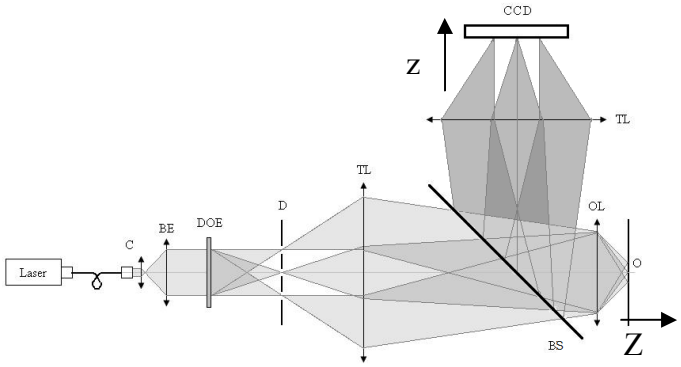

Fig. 1. Principal scheme of multichannel confocal Microscope.

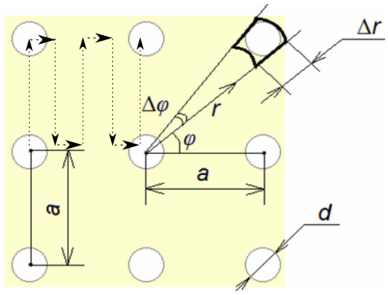

Fig. 2. Part of 3x3 rays in object plane of OL, a=300 mkm, d=80 μm.

Laser beam, widened by an optical expander BE, is then split into NxN beams by diffraction optical element DOE. The image is transferred from the plane matrix aperture D to the area of an object O by means of lenses TL. It is possible to scan the surface of an object in focal object plane OL by, as an example, moving consecutively beams in focal plane and reading simultaneously the signal from the confocal to the illuminating laser beam pixels CCD of receiving photo matrix. Standard way of scanning is shown in Fig.2. by dotted lines with arrows. Compare to common one -channel CM, in MCM scheme mutual noise or background, which comes out of neighbor beams focused in the plane of CCD matrix which at the same time is a program matrix aperture, may present.

For the assessment of the mutual effect, the calculation of the intensity in the investigated channel has been held depending on the displacement along Z from the optimal focus plane in the approximation of thin fluorescent layer with the thickness equal to the focal depth of the confocal system *FD* [2] on condition that the image of fluorescent layer ,illuminated by matrix rays 3x3, is formed on CCD (Fig.2). When scanning the object on depth, the total signal I_C that was brought on the central aperture from its nearest neighbors, was calculated. Calculations, carried out according to diffraction theory [3] using expression (1) (Fig.2):

$$I(d,a) = A\left(\frac{\omega_0}{\omega(Z)}\right)^2 2arctg\left(\frac{d}{2a}\right)\cdot\int_{a-d/2}^{a+d/2}\left|\int_0^1 J_0(\upsilon\rho)\cdot\exp\left(-\frac{1}{2}\cdot i\cdot u\cdot\rho^2\right)\cdot\rho\cdot d\rho\right|^2\cdot r\cdot dr \qquad (1)$$

$$I_C = 4I(d,a) + 4I(d,\sqrt{2}a)$$

Where $u = \frac{2\pi}{\lambda}\cdot\left(\frac{D_{TL}}{2f_{TL}}\right)^2\cdot z$, $\upsilon = \frac{2\pi}{\lambda}\cdot\frac{D_{TL}}{2f_{TL}}\cdot r$, $Z = -\frac{f_{OL}^2\cdot z}{f_{TL}^2}$, $\omega(z)^2 = \omega_0{}^2(1+\left[\lambda z/(\pi\omega_0{}^2)\right]^2)$,

$\omega_0 = 0.61\lambda / NA_{OL}$, λ - wave length of the light, D_{TL}=7 mm – aperture of ray on TL, A – normalization constant, have shown that at the displacement of an object from focus along Z axis, the background maximum from neighbor apertures is an amount less than 0.5% (focal length f_{OL}= 3 mm, magnification M_{OL} =60x, numerical aperture NA_{OL}= 0.9, f_{TL}=180mm, Fig.3).

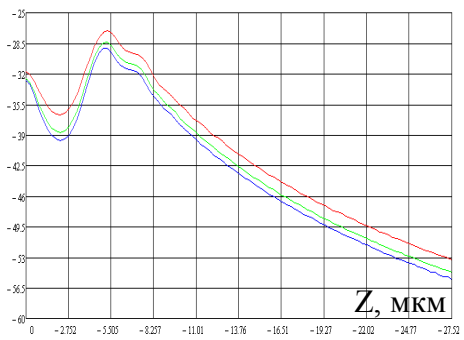

Figure 3 . Total background radiation.

The comparison of the background level estimated in Gaussian beams approximation with the experimentally observed background level has been carried out as well. In the experiment, the profile of light in the plane of CCD matrix from an objects that were thin and thick layers of the R6G solution in isopropyl alcohol placed in a plane parallel to the focal plane of objective OL has been measured.

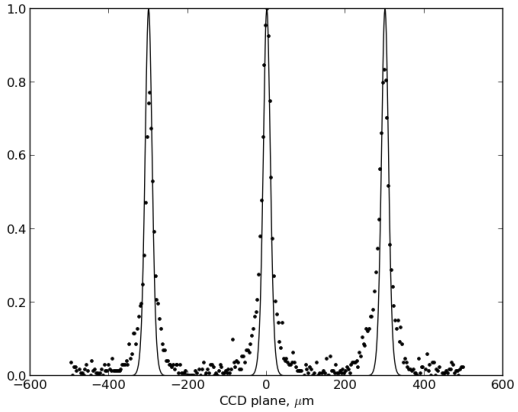

Figure 4. . Profiles of fluorescence 3x3 laser beams for thin layer (10 μm).

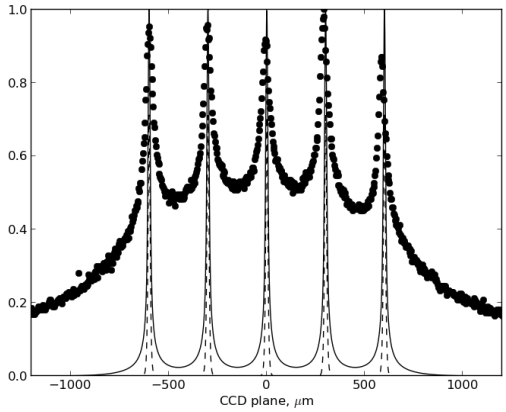

Figure 5. Profiles of fluorescence from 5x5 beams for thick layer (100 μm).

Fig. 4 shows the profiles of fluorophore fluorescence from 3x3 laser beams. The dots represent the experimentally measured signal from a thin 10 μm. The solid line represents the calculation in Gaussian beam approximation, at that it was supposed that the laser beam excited fluorophores only once and that there were no effects of re-reflection and excitation by repeated radiation. The dotted curve shows the calculation for layer thickness equal to the thickness of the focal depth of the objective OL (f_{OL} = 9mm, M_{OL}=20x, NA_{OL}=0.75, FD=5.1 mkm). In case 5x5 beams (Fig.5) for thick 100 μm layer, the profile of experimental signal has significant background , unlike the calculation. Formula for Gaussian beams approach included summation over all beams and over Z axis:

$$I_{\Sigma}(x) = \sum_{k=-K}^{K} \sum_{n=-N}^{N} \sum_{m=-N}^{N} I(x - na, ma, k \cdot \Delta z));$$

where $\Delta z = 10FD / K$, K=100, $I(x, y, z) = (\omega_0 / \omega(z))^2 \exp\left(-2\left(x^2 + y^2\right) / \omega(z)^2\right)$.

Thus, the usage of multichannel scheme shown in Figure1 allows to decrease significantly object scanning time in confocal fluorescence microscopy. A drawback is a possible influence of intermodulation distortions at high concentrations of investigated objects and fluorophore.

References

1. V.P.Bessmeltscev, A.N.Raldugin, V.S.Terentyev. Development of multi-channel confocal system for the study of surface microprofile. Conference «HOLOEXPO 2012», Suzdal 2012
2. S.Wilhelm. Confocal Laser Scanning Microscopy. Jena. Carl Zeiss. ISBN: 978-3-940885-02-9.
3. Max Born & Emil Wolf. Principles of Optics (4th.ed.) Pergamon Press (1970).

Mercury optical lattice clock at LNE-SYRTE

R. Tyumenev, Z. Xu, J. J. McFerran, S. Bize

SYRTE, 61 avenue de l'Observatoire, 75014 Paris, France
Email: rinat.tyumenev@obspm.fr

The SI second is currently realized by cesium microwave clocks with accuracy of 2×10^{-16}. New generation of optical atomic clocks will shift this limit down to 10^{-18}. Here we present our results in the development of an optical lattice clock based on neutral mercury atoms.

Laser cooling on the weak transition and trapping in an optical dipole trap of Tm atoms

G. Vishnyakova, D. Sukachev, E. Kalganova, A. Savchenkov, A. Sokolov, A. Akimov, N. Kolachevsky, V. Sorokin

P.N. Lebedev Physical Institute of the Russian Academy of Sciences, Leninsky prosp. 53, 119991 Moscow, Russia, +7 495 135 42 64
Moscow Institute of Physics and Technology, Institutsky per, 9, Dolgoprudny, Moscow region, 141700, Russia, +7 495 408 45 54
Russian Quantum Center, BC ñUralsò, Novaya st., 100, SKOLKOVO, Odincovsky rayon, Moscow region, 143025, Russia, +7 495 280 00 01 add. 5011
E-mail: gulnarav7@gmail.com

Laser cooling and trapping of neutral atoms is one of the most powerful tools for studying atomic ensembles at ultralow temperatures [1]. It has opened a new era in precision laser spectroscopy [2], the study of collisions, atomic interferometry, and the study of quantum condensates. During the last decade laser cooling of rare-earth elements with the hollow inner shell (Er, Dy, Tm) attract close interest. These elements possess high ground state magnetic moments which make them attractive for studying atom-atom interactions at ultralow temperatures. Inner shell transition can also be used in ultra-stable optical clocks. It is expected that Tm has a lot of Feshbah resonances. Laser cooling and trapping of rare-earths is a challenging task due to their rich level structure. Recently, laser cooling was demonstrated for Er, Dy and Tm rare earths with the hollow 4*f* subshell.

The transition at the wavelength 1.14 μm between two fine-structure components of Thulium ground-state is a good candidate to be a clock transition in optical lattice clock. This transition has narrow natural line width (1.2 Hz) and is strongly shielded by closed $6s^2$ and $5s^2$ shells that provide high frequency stability of Thulium-based optical clocks. In order to load atoms in a shallow optical dipole trap or optical lattice, they should be laser cooled to temperatures as low as 1-10 μK.

Thulium atoms were successfully laser cooled in our laboratory at LPI in 2010 [3]. We used a strong nearly closed transition with the natural line width of γ=9.4 MHz and the wavelength of λ=410.6 nm for Zeeman slowing and trapping of laser-cooled atoms in a magneto-optical trap (MOT). The Doppler limit for this transition is 240 μK. But due to similar magnetic sensitivity of the upper and lower cooling levels, sub-Doppler cooling mechanisms happened to be very efficient which allowed us to reach temperatures down to 25 μK directly in the MOT. In principle, such temperatures already allow loading atoms in a deep optical dipole trap which is forming by a strongly focused few-watt laser beam. However, such regime would be unfavorable for optical clock applications due to a strong dynamic Stark shifts from the trap field and low re-capturing efficiency due to tight focusing. To reach more favorable regime lower temperature is required.

We have demonstrated second stage laser cooling of Tm atoms on the closed transition $4f^{13}6s^2(J = 7/2) \quad 4f^{12}5d_{5/2}6s^2(J' = 9/2)$ with the wavelength of λ=530.7 nm and the natural line width of γ=360 kHz. In comparison with the first stage cooling transition it has much lower Doppler limit of 9 μK which should allow to easily load atoms in the optical dipole trap. For the second stage cooling we use a frequency doubled semiconductor laser providing a spectral line width of ~1 MHz. Such line width allows to cool atoms only using large red frequency detuning (30-50γ) which increases the velocity capture range, but, in turn, raises temperature. In our case the temperature of atoms in the green 530.7 nm MOT was in the range 20-30 μK. We demonstrated re-capturing of atoms from the blue MOT with nearly 100% efficiency, as well as direct capturing of atoms from decelerated atomic beam. To

further reduce the temperature we are going to narrow the laser spectral line width by locking it to external optical cavity which is under investigating now.

Laser cooled atoms were loaded from the MOT into the optical dipole trap (Fig.1a) operating near 532 nm. Radiation of frequency doubled Nd^{3+}-doped laser which was tightly focused into an atomic cloud (up to 10 W in the 30 μm beam waist) forms an optical trap with an estimated depth of 1 mK. To observe the optical dipole trap we switch off the cooling beams in the presence of trapping laser and after a few ms (typical time-of-flight of MOT) we illuminate cold atoms to make them visible and make a picture. Successful optical trapping of atoms in the beam waist was observed both in a trap formed by one beam and in two crossed beams. We also demonstrated trapping in the optical lattice (optical standing wave) (Fig.1b) by retro-reflecting the trapping beam. The life time of atoms in the trap corresponds to 200 ms which indicates low heating rates well suiting for further precision experiments. Relatively low re-capture efficiency (1.5%) is due to small spatial overlap between the initial atomic cloud and optical trap beams.

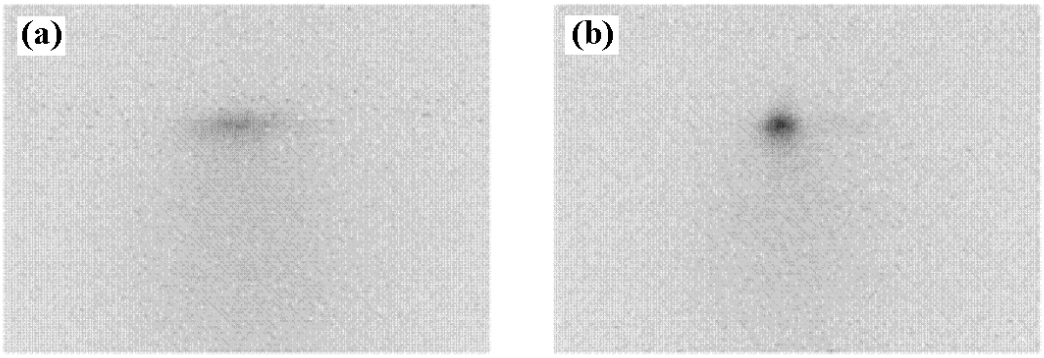

Fig.1. Optical dipole trap (a) and optical lattice (b). The wavelength of trapping laser is 532 nm, the power is 10 W, the beam waist is 30 μm. Time-of-flight (see the text) is 15 ms. The dipole trap is stretched because of the long size of the beam waist (about few cm).

References

1. W. D. Phillips, Rev. Mod. Phys. 70, 721 (1998).
2. F. Riehle, *Frequemcy Standards. Basics and Applications* (Wiley-VCH, Weinheim, 2004).
3. D. Sukachev et al., Phys. Rev. A 82, 011405 (2010).

Generation of Laser-Produced Plasma with a high energetic efficiency for various model experiments*

Yu.P. Zakharov, V.M. Antonov, E.L. Boyarintsev, A.V. Melekhov, V.G. Posukh, A.G. Ponomarenko, V.N. Tishchenko, I.F. Shaikhislamov

Institute of Laser Physics (ILP) SB RAS, Novosibirsk, 630090, Av. Lavrentyeva13/3
E-mail: ki1z@mail.ru

Despite of different approaches used for interpretation of angular structure of expanding Laser Produced Plasma (LPP) blobs ablated from plane targets, in the range of moderate intensities $q \le 10^{11}$ W/cm^2 a most grounded is Anisimov model [1]. This model of self-consistent 3-D expansion of semi-elliptical vapor cloud was developed for ablation and deposition problem. Nevertheless, according to numerous LPP experiments [2-5] it successfully describes a geometry of inertial stage of laser produced plasma expansion which starts after the end of laser pulse τ plus a few dynamical times. Characteristics of LPP at this stage we are interested in depends mostly on initial form of the cloud at a moment $t=\tau$ just after the end of laser pulse. LPP expands along the normal of a plane target with a velocity of the order of ion-acoustic speed C_s and reaches a size of $Z_0 \sim C_s\tau$, while in transverse dimensions X and Y remains of the same size X_0~D/2 which is a radius of irradiation spot. Therefore, a condition of plane target geometry [6] reads as $D>C_s\tau$. Model gives that a relation between initial aspect ratio $\alpha=Z_0/X_0 < 1$ and asymptotic aspect ratio $\beta \equiv K_z=Z_\infty/X_\infty \ge 1$ is approximated by $\beta \approx 1{,}1/\alpha^{1/2}$ [7]. In our case the ion-acoustic speed $C_s \approx (z_i T_{e0}/m_i)^{1/2}$ estimates for expected initial electron temperature $T_{e0} \sim 70 \div 80$ eV and average value of ion mass to charge ratio $\langle m_i/z_i \rangle \approx 2{,}5$ a.e.м. [8] as ~ 55 км/с. Taking other parameters (τ~100 ns and D~2÷3 cm) we find that $\alpha \approx 0{,}44$ and $\beta \approx 1{,}7$. This is close to the experimentally observed relation of ellipsoid half-axes $a/b = \beta \approx 2$, as can be judged from the plasma snap-shot image in Fig 1a from recent model experiments [5,12] at KI-1 facility of ILP.

The elliptical-type boundary $\rho(\theta)$ of LPP luminosity as shown in Fig. 1a is found to be in a good agreement with calculated one as shown in Fig. 1c (for angle θ from target normal along to which a half-axis $a = \rho_0$):

$$\rho(\theta) = \rho_0 \sqrt{1/(\beta^2 * Sin^2\theta + Cos^2\theta)} \equiv \rho_0 * F(Cos\theta) \qquad (1)$$

Based on this direct comparison of (1) it can be applied for calculation of LPP kinetic energy distribution in a solid angle $dE_k/d\Omega$. It can be done on the base of experimentally verified [2] dependence of ion number dN (in solid angle) on the LPP front velocity $\rho(\theta) = V*t$, as $dN \propto V$ for all angles $0 < \theta < \pi/2$. Due to $dE_k/d\Omega \propto dN*V^2$ the general dependence is $dE_k/d\Omega \propto V^3$ or $dE_k/d\Omega \propto F^3$ if normalized on the maximum of LPP energy flux at $\theta = 0$. A form of this function which is important for the calculation of the LPP total kinetic energy E_k is shown in Fig. 1d in a comparison with available measurements of $E_{0\theta}(\theta)$ based on the Langmuir probe's data of ion current density $J_p = ez_i nV$ (Fig 1b).

In both cases we employ a useful parameter of so called effective energy of LPP defined as $E_0 = (dE_k/d\Omega)_{\theta=0}*4\pi$ (~ 600 J for case A1 at Fig. 1b), or in general as $E_{0\theta} = (dE_k/d\Omega)_\theta*4\pi$ (~ 450 J for A2 at Fig. 1b). Such approach allows to determine angular distribution of energy density $(dE_{k\theta}/dE_{k0})$ based on equivalent relation $E_{0\theta}/E_0$. Namely this value was compared with function F^3 in Fig. 1d. Based on the satisfactorily agreement of this experimental data and expression F^3 near Cosθ ~ 1, we can estimate total LPP energy by numerical integration of F^3 as defined:

$$E_k = 2\pi \int_0^{\theta_{max}} \left(\frac{dE_0}{d\Omega}\right) * F^3 Sin\theta d\theta \equiv 2\pi \left(\frac{E_0}{4\pi}\right) * \int_{y=Cos(\theta_{max})}^{1} F^3(y)dy \qquad (2)$$

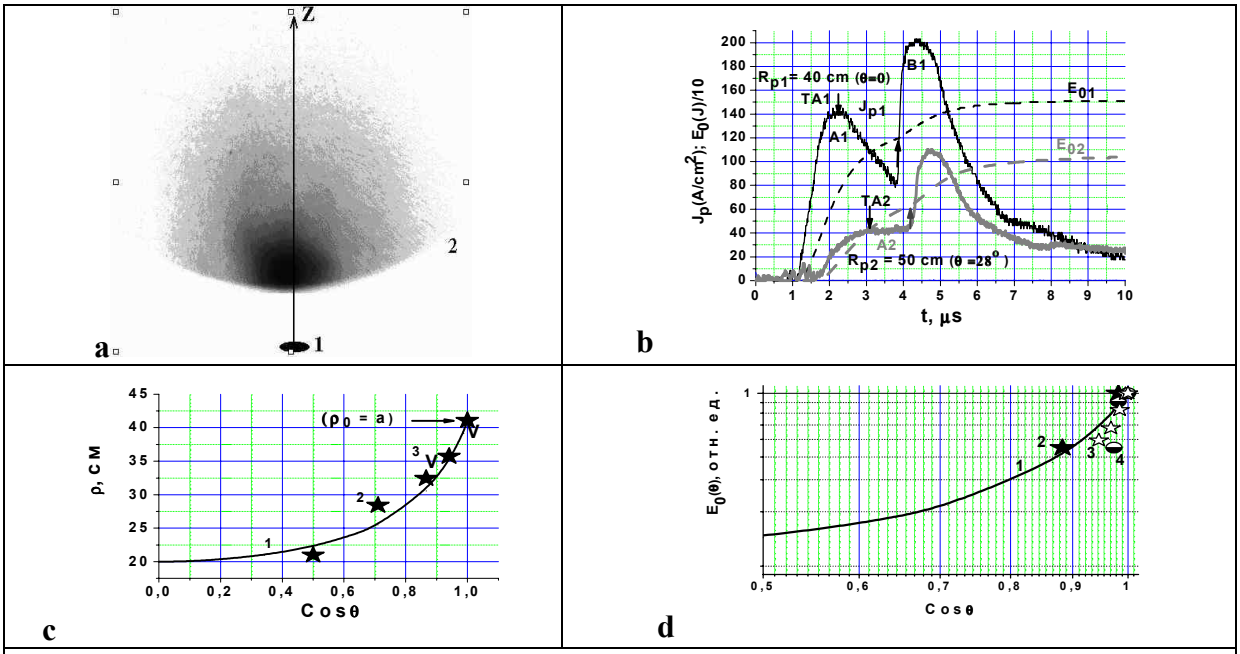

Fig. 1a) LPP shape (in a weak magnetic field 80 G) at a time of $t_* \approx 2{,}1$ μs: **1**– plastic target position; **2** – line of blocked field view of Gated Optical Imager (GOI). The whole vertical dimension of picture is near 40 cm.
1b) Dynamics of probe's current $J_p(t)$ obtained at 2 distances R_p from the target and calculated from them effective LPP energy E_0. **1c)** The model shape **(1)** of LPP-boundary via expression (1) in comparison with GOI-data **(2)** from **1a)** and probe data **(3)** from **1b) of** LPP's maxima in J_p recalculated to moment t_*. **1d)** Comparison of model [1] angular distribution **(1)** for LPP energy $\propto F^3$ (2) with a number of normalized probe data (Fig. 1b).

Thus, for the case 1b we get $E_k = (E_0/2)*\text{Integr}\{F^3\} \approx 400\text{J}*0{,}15 = 60$ J where numerical value of 0,15 is the value of integral (2) at $\theta_{max} = 60^0$. Then, at energy Q = 150 J in the main spike of the laser pulse we get effectiveness about $\eta \approx 40\%$ of laser to plasma energy' conversion, which is comparable to data of other recent works [9-11]. Therefore, due to combining of a) probe data on energy E_0 close to the target normal (Fig. 1b) and b) shot-time imaging of LPP boundary (Fig. 1a,c) one can estimate kinetic energy using function $\rho(\theta) \propto F(\text{Cos}\theta)$. Note that according to Anisimov model [1] and important relation $\beta \approx 1{,}1/\alpha^{1/2}$ [7], which more or less agrees with our data, one can operate the function $F(\theta)$ by varying initial coefficient α and using quasi-plane concave targets to increase the angular range θ_{max} of quasi-isotropic LPP expansion. This can be of prime importance to perform correctly various model experiments at KI-1 on magnetosphere's compression [5,12] or LPP blobs interactions with near-Earth magnetized plasma [13] and others high-energy active experiments [14].

**This work was supported by Siberian Branch RAS (Project II.8.1.4 of Basic Reasearch and Integrated Project № 113) and Russian Fund of Basic Research (Grant № 12-08-00587).*

References

1. S.I. Anisimov, D. Bauerle, B.S. Lukyanchuk, *Phys. Rev. B* **48**, 12076 (1993).
2. S. Gurlui, M. Sanduloviciu, M. Strat, et al., *J. Optoelectronics & Adv. Mater*. **8**, 148 (2006).
3. A.H. Dogar, B. Ilyas, H. Qayyum, S. Ullah, A. Qayyum, *Eur. J. Appl. Phys*., **54**, 10301 (2011).
4. B. Dogget, J.G. Lunney, *J. Appl. Phys*. **109**, #093304 (2011).
5. Yu. P. Zakharov, V.M. Antonov, E.L. Boyarintsev, et al., *In Proc. V ALL-RUSS. CONF. LASERS & PLASMA TECH. (CLAPT–2013, Novosibirsk 26-29 March, ITAM SB RAS)* **1**, 126 (2013)-In Russ.
6. P. Mora, *Phys. Fluids* **25**, 1051(1982).
7. A.M. Komashko, M.D. Feit, A.M. Rubenchik, *Proc. SPIE* **3935**, 9 (2000).
8. Yu.P. Zakharov, *High Energy Density Phys*. **8**, 329 (2012).
9. J. E. Sinko, A. V. Pakhomov, S. Millen, et al., *Proc. AIP* **997**, 254 (2008).
10. J. E. Sinko, C. R. Phipps, *Appl. Phys. Lett.* **95**. #131105 (2009).
11. E.Yu. Loktionov, A.V. Ovchinnikov, Yu.S. Protasov, D.S. Sitnikov, Techn. Phys. Lett. **36**, 588 (2010).
12. Yu.P. Zakharov, A.G. Ponomarenko, W. Horton, et al., *Astrophys. Space Science* **322**, 151 (2009).
13. L.R.O. Storey, *EOS* **48**, 1400 (1987).
14. B.G. Gavrilov, R.E. Erlandson, Y.N. Kiselev, C.-I. Meng, J.I. Zetzer et al., *Adv. Space Res.* **21**, 773 (1998).

Large-scale laboratory simulation of space Collisionless Shocks in magnetized background by using Laser-Produced Plasma blobs of kJ-range effective energy*

Yu.P. Zakharov[1], A.G. Ponomarenko[1], V.A. Terekhin[2], V.M. Antonov[1], E.L. Boyarintsev[1], A.V. Melekhov[1], V.G. Posukh[1], I.F. Shaikhislamov[1]

[1]*Institute of Laser Physics (ILP) SB RAS, Novosibirsk, 630090, Av. Lavrentyeva13/3*
[2]*All-Russian Scientific Research Institute for Experimental Physics (VNIIEF), Sarov, 607188, Av. Mira 37*
E-mail: ki1z@mail.ru

A physical model with new PIC-calculations [1,2], up-grated experimental set-up [3-5] and first results of experiments with Laser-Produced Plasma (LPP) blobs to study the generation processes for Collisionless Shock Wave (CSW) are presented. In spite of that LPP-based approach has a long history [4] and recent progress [6], only in experiment [3,4] at KI-1 laser facility of ILP with quasi-spherical LPP at high Alfven-Mach M_A number, a CSW-like disturbances of Background Plasma (BP) density $n_* \sim 2\div4*10^{13}$ cm^{-3} and the initial magnetic field $B_0 \sim 100$ Gs at scales of $R_* \sim 25$ cm were revealed. Here $R_* = (3N_e/4\pi n_*)^{1/3}$ is magnetic cavity size for the total number N_e of LPP electrons, and according to the theory [1,2] and numerical simulation [1,2,7,8] of so called Magnetic Laminar Mechanism (MLM or Larmor coupling [7]), namely under conditions, when a both ions (LPP and BP) have their directed Larmor radii R_L ($\propto$V, front velocity of LPP) comparable with R_*, an effective MLM-interaction between LPP and BP could occur. Energy gain of BP should be $\propto \delta = R_*{}^2/R_L R_{L*}$ (MLM-parameter), which was only $\delta \sim 0{,}7$ in our first experiment [3,4] with LPP kinetic energy $E_k \sim 40$ J , while now we have opportunity to increase it up to $\delta \geq 2$ by using LPP with the effective energy $E_0 = 0{,}3N_e\,(m/z)*V^2 \sim 1000$ J [4-5,9-10] from flat-type plastic target. Such kind of energy E_0 means, that namely into the main direction (along to target normal X at Fig. 1A, where $\theta = 0$), LPP has a real specific energy $dE_k/d\Omega = E_0/4\pi$, while for some critical θ_c, it could be < latter one, depending upon to angular function $F(\theta)$. We could find out experimentally [4-5,9-10] the regime of "plane target" [11] irradiation for production of LPP with the suitable F-function, both for LPP interaction with vacuum uniform and dipole magnetic field [5]. Here we are presenting the first results on cavity formation and MLM-action by such directed LPP, up to the cavity required large scale $R_* \geq 50$ cm [4] comparable with the diameter $\sim 70\div80$ cm of our highly-ionized hydrogen BP. Such scale supplies a necessary condition for generation of CSW in the given "BUW" experiment, by LPP as a piston expanding collision-free and super-alfvenically with V≥200 km/s, in a range of $\theta_c \sim 30^0$.

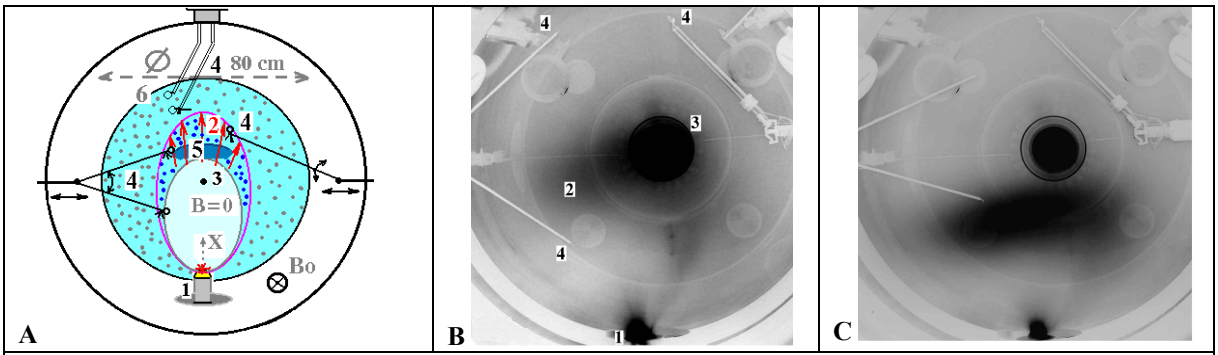

Fig. 1.**A**–Scheme of "BUW" experiment at KI-1 facility with a chamber ∅120 cm and CO_2-laser (~500 J/100ns): **1**-target at support, **2**-Laser Plasma front, **3**-central **Z**-axis of chamber and output of BP' source (θ-pinch) near it **4**-various probe' diagnostics, **5**-interaction region of two plasmas (**X**-target normal; B=0 in the magnetic cavity), **6**-boundary of Background Plasma (BP). **B**–time-integrated photo LPP in BP without magnetic field B_0. **C**–the same at presence B_0. All probes and target at **A** are placed in central **XY**-plane of KI-1 at Z=2,5 m from θ-pinch

At Fig. 2 the typical data of "BUW" experiment are presented for various conditions, in particular, for the cases of "free" LPP expansion without magnetic field B_0 both in vacuum (curve 1 at Fig. 2A) and unmagnetized BP (curve 2). The dynamics of current signal $J_{P0}(V)$ of thin cylindrical Langmuir probe (~ Debye radius) gives us near exact behaviour of total plasma density n via the relation for density of ion current $J_i(A/cm^2) = 80*J_{P0}(V) \propto j = eznV$. So, in comparison with rather smooth, "small" or with a little disturbances of curves 1,2 for given probe at distance X=75 cm, its signal 3 in magnetized BP (initial B_0=80 Gs) reveals a strong disturbances of n and B-field (curve 4), with their enough sharp fronts ($\tau \leq 500$ ns) and essential deceleration both of them during expansion across magnetic field.

A	B	C
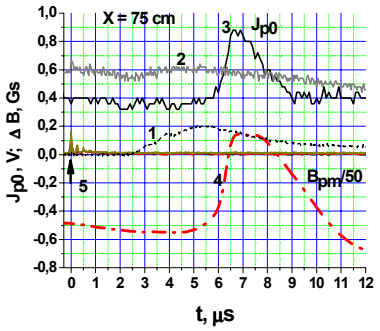	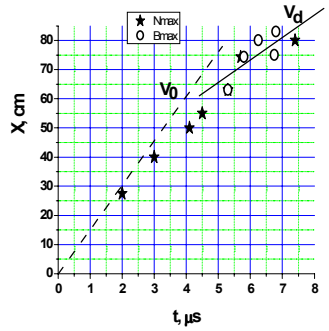	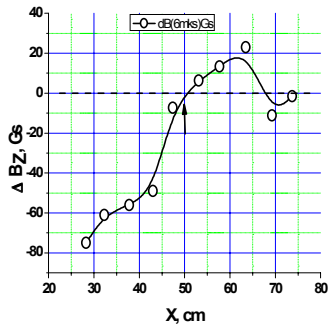
Fig. 1A. Dynamics of plasma ion current J_{P0} by Langmuir probe (ion flow j or its density n) and magnetic field B_{mp} at same point. 5–laser pulse.	Fig. 2A. Joint R-t diagram of the motion of maximums n and B: V_0 – initial velocity of LPP max; V_d–averaging disturbance velocity	Fig. 3A. Profile of LPP' magnetic cavity in magnetized plasma background with initial field B_0 = 80 Gs (t = 6 μs after laser).

The character of this deceleration is demonstrated at Fig. 2B for joint R-t diagram of the motion of maximums n and B, which clear shows that some deceleration process in a region X~50÷60 cm leads to formation of magnetosonic-type disturbance travelling beyond it with the velocity $V_d \approx 75$ km/s, which is large, than the velocity of fast magnetosonic wave (~ 50 km/s for initial electron temperature ~ 10 eV of BP). It corresponds to the own Alfven-Mach number of disturbance up to $M_{Ad} \sim 3$ and one could suggest, that is a case of non-stationary CSW, formed by LPP via MLM-interaction according to data of recent 2D/PIC-simulation [8]. Measured in the "BUW" experiment distribution of disturbed by LPP magnetic field (ΔB at Fig. 3C), with a magnetic cavity region ($B \leq B_0$) up to the record (for laboratory) value $X \approx 50$ cm ~ R_*, confirms our preliminary suggestion on CSW generation under given unique experimental conditions at KI-1 facility for LPP effective energy E_0 in a kJ-range.

This work was supported by the ILP Project II.10.1.4 of SB RAS on Basic Researches.

References

1. A.I. Golubev, A.A. Solov'ev, V.A. Terekhin, J. App. Mech. Tech. Phys., 19, 602 (1978).
2. V.P. Basurin, A.I. Golubev, V.A. Terekhin, Ibid, 24, 614 (1984).
3. V.M. Antonov, V.P. Bashurin, A.I. Golubev, Yu.P. Zakharov, et al., Ibid, 26, 757 (1986).
4. Yu.P. Zakharov, IEEE Trans.: Plasma Sc., 31, 1243 (2003).
5. Yu.P. Zakharov, A.G. Ponomarenko et al., Astroph. Space Sc., 322, 151 (2009).
6. C. Niemann, W. Gekelman, C.G. Constantin et al., Phys. Plasmas, 20, 012108 (2013).
7. D. Winske, S.P. Gary, J. Geophys. Res., 112, A10303 (2007).
8. D. Winske, M. Covee, Report LA-UR-12-22823, LANL (2012).
9. Yu.P. Zakharov, High Energy Density Phys., 8, 329 (2012).
10. Yu. P. Zakharov, V.M. Antonov, E.L. Boyarintsev, et al., *In Proc. V ALL-RUSS. CONF. LASERS & PLASMA TECH. (CLAPT–2013, Novosibirsk 26-29 March, ITAM SB RAS)* **1**, 126 (2013)-In Russ.
11. P. Mora, Phys. Fluids, 25, 1051 (1982).

Propagation of ultrahigh femtoseconds laser fields in glasses

V.P. Zhukov[1,2], N.M. Bulgakova[3,4]

[1] *Institute of Computational Technologies SB RAS, 6 Lavrentyev Ave., 630090 Novosibirsk, Russia*
[2] *Novosibirsk State Technical University, 20 Karl Marx ave., 630073, Novosibirsk, Russia*
[3] *Institute of Thermophysics SB RAS, 1 Lavrentyev Ave., 630090 Novosibirsk, Russia*
[4] *Optoelectronics Research Center, University of Southampton, SO17 1BJ, United Kingdom*
E-mail: zukov@ict.nsc.ru

In spite of impressive achievements in development of novel fs-laser-writing applications based on modification of optical glass properties, rich physics of the modification phenomenon is not fully understood. To get insight into modification processes, we have developed a 2D (axially-symmetric) model describing laser beam propagation through transparent solids, based on non-linear Maxwell's equations (NLME) [1]. The model accounts for the Kerr effect, photo-ionization, frequency dispersion of dielectric permittivity, and plasma hydrodynamics with laser-induced electron acceleration and avalanche. Material excitation dynamics has been studied numerically for the fused silica case in a wide range of irradiation parameters. Additionally, simulations based on the non-linear Schrödinger equation (NLSE) have been performed for the same irradiation conditions to investigate how accurately the unidirectional NLSE-based beam propagation approach [2,3], which does not take into account light scattering to large angles, can describe material excitation as compared to the higher-precision NLME approach.

The comparison of the NLME and NLSE approaches shows that, for the most interesting cases of short laser pulse durations (≤100 fs), large apertures (>0.3), and pulse energies (~1 μJ and higher), the results of the NLSE model differ dramatically from both the NLME results and available experimental data. The main reason of invalidity of the NLSE model for description of technologically important regimes of optical glass modification is generation of dense electron plasma with characteristic space scales comparable with the laser wavelength. Such plasma features are generated already by the front of the laser beam and strongly scatter the rest beam that may result in intricate interference patterns and cannot be taken into account in the truncated NLSE frame while is directly described by the NLME approach.

The simulations show that large-density free-electron plasma ($n_e \geq 3 \cdot 10^{20}$ cm^{-3}) is generated in the near-focal region of irradiated samples which remains however undercritical in respect to laser frequency that confirms the intensity clamping effect. Interesting is that the plasma density can have maxima out of the laser beam axis. The particularities of others process characteristics will be discussed in detail as a function of laser beam parameters.

Modeling reveals that, at large numerical apertures, relatively long laser pulse durations, and in a certain range of laser energies, laser energy absorption becomes unstable. It appears in the form of free electron density perturbations with a characteristic size of order of the laser wavelength. Although the observed absorption instability develops under the irradiation conditions when axial symmetry of the laser energy absorption is violated, it has been found that the instability is a physical phenomenon but not an artifact of axial symmetry breaking in our 2D model. This was verified by solving the exact 2D NLME problem of a "laser knife" geometry whose data also showed the absorption instability at the same range of irradiation parameters. Remarkable is that the volumetric nanomirror structures (nanogratings), which

were discovered by Shimotsuma et al. [4] and are employed now in numerous laser-writing technologies [5], are formed under the irradiation conditions characteristic for instability development.

The mechanisms of nanograting formation remain unclear and, based on the modeling results, we propose a most plausible explanation of imprinting these intriguing structures in fused silica glass. The absorption instability leads to free electron density perturbations with spatial dimension of laser wavelength and with a tendency to violate axial symmetry towards elongated cross-section geometry of the laser-excited zone. Due to the glass memory effects conditioned by defect formation, the subsequent laser pulses propagate in a modified medium, thus enhancing perturbation of the electron density distribution in the laser-affected region with further tendency of forming an elongated structure with 3D features. As a result of many pulses, the electron density perturbation transforms into a sliced (nanograting) structure. This mechanism is similar to a widely accepted mechanism of ripple formation on laser-irradiated surfaces [6,7] where the role of selvedge in laser light scattering is played by the plasma 3D features. We note that namely solving Maxwell's equations for the under-selvedge region has directly demonstrated periodic absorption of laser energy [8]. On the surface this leads to selective ablation and migration of matter from the absorption zones while in the bulk this results in enhanced bond-breaking, atomic oxygen release with formation of molecular oxygen, and thus in formation of periodic oxygen deficiency zones as observed experimentally as nanograting structures [4].

Acknowledgements: This work is supported by the Russian Foundation for Basic Research (project No. 12-01-00510-a). NMB acknowledges Marie Curie International Incoming Fellowship, No. 272919.

References

1. N.M. Bulgakova, V.P. Zhukov, Yu.P. Meshcheryakov, *Appl. Phys. B* (2013), in press.
2. A. Couairon, L. Sudrie, M. Franco, B. Prade, A. Mysyrowicz, *Phys. Rev. B* **71**, 125435 (2005).
3. I.M. Burakov, N.M. Bulgakova, R. Stoian, A. Mermillod-Blondin, E. Audouard, A. Rosenfeld, A. Husakou, I.V. Hertel, *J. Appl. Phys.* **101**, 043506 (2007)
4. Y. Shimotsuma, P.G. Kazansky, J.R. Qiu, K. Hirao, *Phys. Rev. Lett.* **91**, 247405 (2003).
5. M. Beresna, M. Gecevičius, P.G. Kazansky, *Opt. Mater. Express* **1**, 783 (2011).
6. J.E. Sipe, J.F. Young, J.S. Preston, H.M. van Driel, *Phys. Rev. B* **27**, 1141 (1983).
7. D. Dufft, A. Rosenfeld, S.K. Das, R. Grunwald, J. Bonse, *J. Appl. Phys*. **105**, 034908 (2009).
8. J.Z.P. Skolski, G.R.B.E. Römer, J.V. Obona, V. Ocelik, A.J. Huis in 't Veld, J.Th.M. De Hosson, *Phys. Rev. B* **85**, 075320 (2012).

Nonlinear photonic crystals of strontium tetraborate: properties and radiation conversion to the VUV

A.S. Aleksandrovsky[1,2], A.M. Vyunishev[1], A.I. Zaitsev[1,2], P. Trabs[3], F. Noack,[3] V. Petrov[3], V.V.Slabko[2], N.V.Radionov[1]

[1] *L. V. Kirensky Institute of Physics SB RAS, Akademgorodok, Krasnoyarsk, Russia*
[2] *Siberian Federal University, Pr. Svobodnii 79,Krasnoyarsk, 660041 Russia*
[3]*Max-Born-Institute for Nonlinear Optics and Ultrafast Spectroscopy, 2A Max-Born-Str., D-12489 Berlin, Germany*
E-mail: aleksandrovsky@kirensky.ru

Generation of vacuum ultraviolet (VUV) radiation from an all-solid-state laser source is of interest for numerous applications, including lithography [1], spectroscopy, ultrafast monitoring and control of chemical and biological processes. Strontium tetraborate (SBO) is a nonlinear optical crystal with the fundamental absorption edge around 120 nm, the value being the shortest one among all nonlinear crystals. It lacks angular phase matching as well as ferroelectric properties, the latter preventing the possibility of controllable production of quasi-phase-matching domain structures in it. Surprisingly, as-grown SBO crystals were found to contain alternating oppositely poled domains, a phenomenon not observed earlier in non-ferroelectric crystals. These domains form structures that relate to well-known quasi-phase-matching converters, however, they are highly randomized in thickness of individual domains. According to present-day terminology, these domain structures are classified as 1D nonlinear photonic crystals (NPC). Modulation of nonlinear susceptibility can be treated as formation of superlattice with the characteristic spectrum of reciprocal lattice vectors (RLV) that contribute to quasi-phase-matching of various nonlinear optical conversion processes. Two limiting cases of nonlinear processes can be phase matched in random 1D NPC. These are random quasi-phase-matching (RQPM), when fundamental radiation propagates normally to domain walls (along crystallographic axis *a* of SBO), and nonlinear diffraction (NLD), when fundamental propagates in the plane of domain walls (*bc* plane of SBO). NLD has been shown to be more efficient for matching the second harmonic of Nd:YAG laser in typical NPC structure of SBO, therefore it is suitable for detecting NPC structures within as-grown or unpolished samples of SBO. The RLV spectrum is tested via rotation of NPC around the *c* axis of SBO and shows preserving of NLD phase matching within external NLD angles up to 90 degrees. This indicates the existence of wide RLV spectrum in NPC SBO and implies the possibility to match SHG processes within wide wavelength range of fundamental radiation, in the particular, within the tuning range of Ti:Sapphire lasers. NLD of radiation from fs Ti:Sapphire oscillator resulted in SHG with an efficiency of 2.1%. The spectrum of fundamental radiation is almost completely converted to the spectrum of the second harmonic (SH), however, minor shift of the SH spectral maximum with respect to the doubled central frequency of the fundamental was detected. It is explained by the deviation of the NLD angle from Cherenkov relation due to the influence of partial fulfillment of Bragg NLD conditions. These experimental results are confirmed by calculations using Akhmanov's spectral amplitude approach modified by Chirkin for the case of NLD. Angular chirp and local spectrum of NLD-produced SH were measured in order to determine the limitation of pulse duration of generated radiation. This result was compared with direct measurements of SH pulse duration using cross-correlation third-harmonic generation process and found to be explainable by the concept of spatio-temporally coupled pulses.

RQPM in NPC SBO was investigated both for radiation of ns and fs pulse duration. Calculations of angular and spectral dependences for RQPM were performed using plane wave approximation. Calculated SH spectral dependence for typical random NPC SBO consists of large number of peaks with widths of the order of those for regular QPM

structures. These peaks cover the spectral range from near IR to near UV for the fundamental wavelength. Calculated angular dependence of RQPM shows irregular oscillations that can be treated as random Maker fringes. Their characteristic angular scale is increased compared to that of common Maker fringes in a single-domain sample of equal thickness. Angular dependence of SH measured with narrowband laser source for conversion from 532 to 266 nm was found to be in good agreement with calculations. The enhancement factor of SH power with respect to single domain reference sample was equal to 500, in excellent agreement with calculation, too. Combination of angular and spectral dependences results in the NPC band structure with the bands that are expected to experience red rotational shift, in contrast to linear photonic crystal. This prediction was experimentally proved in the process of RQPM generation of the fourth harmonic of fs Ti:Sapphire laser via frequency doubling of its SH in NPC SBO producing 1 μW of average power in the DUV. The spectrum of generated DUV radiation consists of individual peaks within the lineshape of doubled fundamental spectrum. This is explained by the fact that the shift of NPC band structure describing DUV generation due to summing of unequal frequencies within fundamental bandwidth is several times smaller than the width of individual spectral peaks. Rotation of NPC in the case of broadband fundamental wave spectrum does not show clear Maker fringes due to overlapping of random Maker fringes from various spectral components. Tuning of the central wavelength of the fundamental required no angular tuning of NPC and resulted in continuous tuning of DUV radiation over the range 232.5 - 187.5 nm. Short wavelength limit of DUV radiation was determined by air absorption in that experiment. In fact, converters based on NPC SBO exhibit super-noncritical spectral and angular behavior. No signs of decrease of contribution from NPC to the nonlinear optical generation due to finite thickness of domain walls were detected, in contrast to ferroelectric-based NPC. It is interesting to note that while for SHG of Ti:Sapphire lasers in NPC SBO NLD phase matching is more efficient than RQPM, for FHG the situation is opposite: RQPM is rather efficient, but NLD resulted in no observable signal. This is due to the fact that NLD requires thinner domains and larger RLV values for SHG at the same fundamental wavelength, and for NPC typical for SBO RLV spectra experience big drop in this region of values. NPC SBO exhibits large variation of properties for samples from different growth experiments. Recently obtained NPC structures showed higher efficiencies in the DUV, and the peaky structure of the spectrum is less pronounced than in the samples obtained via our earlier simplified technology.

NPC SBO was tested as nonlinear optical medium for diagnostics of fs pulses. Two geometries were investigated, namely, noncollinear RQPM and NLD from virtual beam. Both geometries showed that accuracy of pulse duration measurement with NPC SBO is as good as that obtained with a reference BBO crystal. NPC SBO enables measurement of Ti:Sapphire laser pulses throughout its tuning range with no tuning of the NPC crystal.

Generation of VUV radiation was realized using vacuum monochromator and tunable fs parametric generator. SH radiation was obtained in the range 170 - 121 nm, the lower limit being the shortest wavelength of coherent radiation ever obtained using solid state material. The conversion efficiency at 160 nm was 5×10^{-5}.

SHG of supercontinuum was investigated using a Newport Corp. source based on 2”-long photonic crystal fiber. This source generated up to 100 mW of average power throughout the spectrum with the maximum at 530 nm at coupled power of 150 mW. SH of the supercontinuum was generated in the range from 265 to 400 nm. Its spectrum consists of large number of peaks with widths typically determined by phase velocity mismatch. Broadening of most of these peaks is not evident, however, some peaks exhibit increased width connected with the complex multi-peak spectrum of the supercontinuum.

References

1. S. Kurimura, M. Harada, K. Muramatsu, M. Ueda, M. Adachi, T. Yamada, and T. Ueno, *Opt. Mat. Express* **1**, 1367 (2011).

Switching from normal to anomalous dispersion in photonic crystal with Raman gain defect

V.G. Arkhipkin, S.A. Myslivets

*L.V.Kirensky Institute of Physics, Krasnoyarsk, Russia*Type equation here.
avg@iph.krasn.ru

The search of efficient control of the group velocity of light in dispersive media has been the subject of extensive study both theoretical and experimental [1]. The group velocity $v_g = d\omega/dk$ depends on a dispersion relation [1]. One speaks of light being slow (subluminal propagation) under circumstances in which $v_g \ll c$ (c is the velocity light in vacuum). There are circumstances in which $v_g \gg c$ or even $v_g < 0$. This occurrence is referred to as fast light (superluminal propagation). The time group delay of pulse through media is defined as $t_d = t_0(n_g - 1)$), where t_0 is the time through the same vacuum distance, and, $n_g = c/v_g$ is the group index. There are two methods for controlling the group velocity of light [1]. One makes use of the dispersive properties associated with the resonance structure of a material medium - the material dispersion. The other makes use of structural resonances such as those that occur in photonic crystals - the structural dispersion. Both procedures have been proved useful in a variety of situations [1,3-5].

In this paper we give a method which can be used to changed the group velocity of a probe pulse from slower-than-*c* to faster-than-*c* by controlling the strength of a pump field in process of Raman interaction in medium placed in the defect of one-dimensional photonic crystal (PC). Let two plane waves (the pump and probe) with frequencies $\omega_{1,2}$ are normally incident on one-dimensional photonic crystal with a defect containing a Raman gain medium. The frequency difference $\omega_1-\omega_2$ is close to the Raman transition frequency ω_{20}. The parameters of the PC have been chosen such that a defect mode (DM) is located in the centre of a gap and its spectral width is broad enough for both waves to fall within this transmission band. The DM resonance frequency coincides with that of the probe wave under Raman resonance $\Omega_{20} = \omega_{20} - (\omega_1 - \omega_2) = \Omega_1 - \Omega_2 = 0$ ($\Omega_{1,2}$ is the one-photon detuning for a pump and probe field). For numerical simulation, we used sodium atomic parameters as a Raman medium. Wavelengths of the probe and pump fields were chosen close to the D1 line and $\omega_{20} = 1.8\ GHz$. By means of a pump field we can control the transmittance for the probe field of such PC structure [6,7].

Using the recurrence relations technique [7,8], we calculated transmission spectra of the probe field $T = |\mathrm{E}_{2t}|^2/|\mathrm{E}_{20}|^2$ (E_{20} , and E_{2t} denote, respectively, the electric vector amplitude of the incident probe wave and the transmitted wave) and considered the propagation of a probe pulse in presence of a monochromatic pump wave. Figure 1 shows typical PC transmission spectra for a probe field at different intensities of a pump field. Narrow structures (a peak or a dip) due to the Raman resonance can be observed in the center on the background of a broad transmission band. The transmittance can be larger or less than unity. In inset of Fig.1 transmittance maxima are plotted as functions of a Rabi frequency of an incident pump field. It is seen that the amplitude of the transmission peak enhances with the growing pump intensity until a Rabi frequency reaches the threshold, depending on the system parameters. Once this frequency goes beyond the threshold, the amplitude of a transmission peak decreases and the narrow peak is replaced with a dip.

Figure 2 illustrates a transmitted Gaussian probe pulse. From Fig.2 it follows that depending on a pump field intensity a transmitted probe pulse may either lag behind the reference pulse or lead the latter. In the first case a group velocity of the pulse is lower than the velocity of light in vacuum (subluminal propagation). In the second case a group velocity is larger than the velocity of light in vacuum (superluminal propagation). The same applies to the case of a reflection.

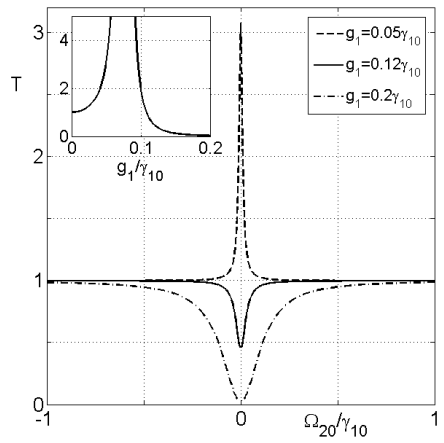

Fig.1. a) Transmission spectra T of PC with Raman gain defect as function of detuning from the Raman resonance (Ω_2 changes at $\Omega_1=30\gamma_{10}$) for various Rabi frequencies g_1. Inset: transmission coefficient for a probe field versus Rabi frequency of a pump g_1; $\Omega_{20}=\omega_{20}-(\omega_1-\omega_2)=0$; $\gamma_{10}=2\pi$ 10MHz.

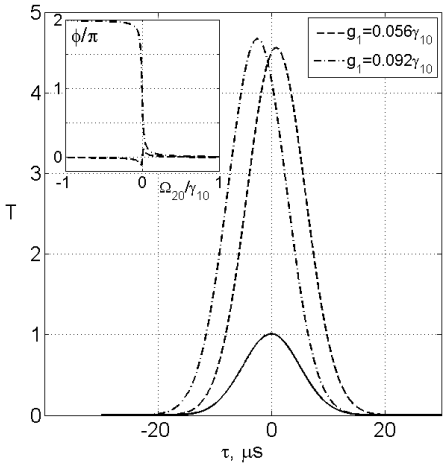

Fig.2. Time dependence of a probe pulse transmitted through PC with Raman gain medium for various Rabi frequencies g_1 of the incident pump field. The thin solid curve refers to the transmitted probe pulse when there is no Raman medium in the defect - the reference pulse. Insert: spectral dependencies of the phase of a transmitted probe wave.

The results obtained can be qualitatively explained in terms of the effective refractive index for PC $n(\omega) = \mathrm{c}\,\Phi(\omega)/\omega L$, where $\Phi(\omega)/$ is the phase of a probe wave passed through the PC, L is the PC length [8]. Obviously, $n(\omega)$ or $\Phi(\omega)/$ describe dispersion properties of the PC structure. In the inset of Fig.2 it is shown the spectral dependences of the phase $\Phi(\omega)$ of the transmitted probe wave for two values for two values of the Rabi frequency of pump field g_1 - below and above the threshold. In the first case dispersion is anomalous therefore we deal with superluminal propagation, i.e. the transmitted probe pulse leads the reference pulse, whereas in the second case dispersion is normal and results in subluminal propagation of the probe pulse as illustrated in Fig.2. Group delay for the transmitted pulses can be calculated as $t_d = \partial\Phi/\partial\omega|_{\omega=\omega_0}$ [9], where ω_0 is the carrier frequency of probe pulse. The calculated group delays are in good agreement to that shown in Fig. 2.

In conclusion, we investigate the subluminal and superluminal pulse propagation in PC with the Raman gain defect. The dispersion of the system can be controlled by a pump field. The mechanism of switching from normal to anomalous dispersion is associated with dispersion of photonic crystal (the structural dispersion) rather than with dispersion of the Raman medium (the material dispersion). The intensity required for these effects to be observed depends on a number of factors (one-photon pump frequency detuning, Raman resonance width, and quality factor of defect modes) and can be anything 10-100 μW/cm^2.

References

1. R.W. Boyd, *JOSA B*, **28**, A38 (2011).
2. P.W. Milonni, Fast Light, Slow Light and Left-Handed Light, Los Alamos, 2005 IOP Publishing Ltd.
3. A. Figotin, I. Vitebskiy, *Waves in Random and Complex Media*, **16**, 293 (2006).
4. A Akulshin, R.J. McLean, *J. Opt.*, **12**, 104001 (2010).
5. J.B. Khurgin, *Advances in Optics and Photonics*, **2**, 287–318 (2002)
6. V.G. Arkhipkin, S. A. Myslivets, *Phys.Rev.* A, **80**, 061802 (2009).
7. V.G. Arkhipkin, S. A. Myslivets, *JEThP*, **111**, 898 (2010)
8. N.L. Liu, S-Y. Zhu, H. Chen, et al, *Phys.Rev.* A, **65**, 046607 (2009).
9. V.S.C. Manga Rao, S.D. Gupta, G.S. Agarwal, *Opt. Lett.*, **29**, 307 (2004).

Adiabatic approach in the research of light pulses propagation in a medium of atoms with degenerate energy levels

M.Yu. Basalaev[1-3], D.V. Brazhnikov[1,3], A.V. Taichenachev[1,3,4], V.I. Yudin[1-4]

[1] *Institute of Laser Physics of SB RAS, Pr. Lavrentyeva 13/3, Novosibirsk, 630090 Russia*
[2] *Novosibirsk State Technical University, Pr. Karla Marksa 20, Novosibirsk, 630073 Russia*
[3] *Novosibirsk State University, ul. Pirogova 2, Novosibirsk, 630090 Russia*
[4] *Russian Quantum Center, Skolkovo, Moscow Reg., 143025, Russia*
E-mail: mbasalaev@gmail.com

In this work, we develop a common approach to the propagation of light pulses in resonant atomic media. Method is based on reduced Maxwell's equation for the vector electromagnetic field and the density matrix formalism. Consideration is performed beyond the perturbation theory on field amplitude. For the density matrix, using the adiabatic approximation, according to which the solution is found in form of the series of spatial and temporal derivatives of the slowly varying field envelope. This approach allows to derive the nonlinear reduced Maxwell's equation with the effects of temporal and spatial dispersion. As a concrete example we study the pulse advancing of elliptically polarized monochromatic light through the gas of resonant atoms in coherent population trapping.

Let us to consider the propagation of a plane resonant electromagnetic wave through the gas of atoms. The slowly varying amplitude of electric field vector $\tilde{\mathbf{E}}(t,z)$ satisfies the reduced wave

$$\left(\frac{\partial}{\partial z}+\frac{1}{c}\frac{\partial}{\partial t}\right)\tilde{\mathbf{E}}(t,z)=2\pi ik\tilde{\mathbf{P}}(t,z), \qquad (1)$$

where $k=\omega/c$ is the wave number, ω is the frequency of electromagnetic wave, c is the velocity of light in free space, $\tilde{\mathbf{P}}(t,z)$ is the slowly varying amplitude of polarization vector. The state of atoms interacting with light wave is described in electric dipole approximation by a quantum kinetic equation for one-atom density matrix $\hat{\rho}$

$$\left(\frac{\partial}{\partial t}+u_z\frac{\partial}{\partial z}\right)\hat{\rho}+\hat{\Gamma}\{\hat{\rho}\}=-\frac{i}{\hbar}\left[\hat{H}_0,\hat{\rho}\right]-\frac{i}{\hbar}\left[-\left(\hat{\mathbf{d}}\mathbf{E}\right),\hat{\rho}\right], \qquad Tr\{\hat{\rho}\}=1, \qquad (2)$$

where u_z is the projection of atomic speed in direction of the light wave propagation, $\hat{\Gamma}\{\hat{\rho}\}$ is the operator describing relaxation processes, $\hat{H}_0$ is the Hamiltonian of unperturbed atom, $\hat{\mathbf{d}}$ is the vector operator of dipole moment, $\hbar$ is the Planck constant.

Restriction on minimal pulse duration under which the field changes slightly at time of establishment the stationary state (adiabatic approximation of response of the medium) allows us to split the problem into two successive steps. At the first stage the elements of matrix density and the polarization vector $\tilde{\mathbf{P}}$ are calculated. Second stage is solution of the equation (1) considering obtained dependence of the polarization vector on field vector $\tilde{\mathbf{P}}(\tilde{\mathbf{E}})$.

We showed that polarization vector $\tilde{\mathbf{P}}$ can be represented in following form

$$\tilde{\mathbf{P}}(u_z)=\tilde{\mathbf{P}}^{(0)}(u_z)+\tilde{\mathbf{P}}^{(1)}(u_z)+\tilde{\mathbf{P}}^{(2)}(u_z)+\ldots, \qquad (3)$$

where

$$\tilde{\mathbf{P}}^{(0)}(u_z)=\hat{M}^{(0)}(u_z)\tilde{\mathbf{E}}\ , \qquad (4)$$

$$\tilde{\mathbf{P}}^{(1)}(u_z)=\hat{M}_1^{(1)}(u_z)\left(\frac{\partial\tilde{\mathbf{E}}}{\partial t}+u_z\frac{\partial\tilde{\mathbf{E}}}{\partial z}\right)+\hat{M}_2^{(1)}(u_z)\left(\frac{\partial\tilde{\mathbf{E}}^*}{\partial t}+u_z\frac{\partial\tilde{\mathbf{E}}^*}{\partial z}\right). \qquad (5)$$

In general case the matrixes $\hat{M}^{(0)}$, $\hat{M}_1^{(1)}$ and $\hat{M}_2^{(1)}$ depend on electric field vector $\tilde{\mathbf{E}}$ and complex conjugate vector $\tilde{\mathbf{E}}^*$. The first term $\tilde{\mathbf{P}}^{(0)}$ of the expansion (3) describes the absorption and reflection of light wave, the second term $\tilde{\mathbf{P}}^{(1)}$ takes into account the dispersion of the medium and determines velocity of pulses, the third term $\tilde{\mathbf{P}}^{(2)}$ is responsible for the dispersion of group velocity and distortion of the pulse shape. The polarization vector $\tilde{\mathbf{P}}(u_z)$ in equation (1) is necessary to average over all velocity groups of atoms.

The developed method allows to sequentially describe the propagation of arbitrarily polarized optical pulses in an arbitrary nonlinear regime (on the field amplitude) through atomic medium, where the atomic levels have an arbitrary Zeeman structure. This method enables the natural way to take into account both the effects of temporal dispersion associated with the inertia of medium and the effects of spatial dispersion due to the motion of atoms.

To demonstrate the efficiently of our method we consider the propagation of a plane resonance electromagnetic wave through the ensemble of two-level atoms with the transition $J_g \to J_e$, where J_g and J_e are the total angular momenta of the ground and excited state of an atom, respectively, degenerate in the projection of the angular momentum $\mu_j = -J_j,...,J_j$ ($j = g, e$).

In the case of dark transitions $J_g = J \to J_e = J$ (J is integer) and $J_g = J' \to J_e = J' - 1$ we find the full set of equation describing the space-time evolution of all real-value parameters of the field envelope

$$\left(\frac{\partial}{\partial z} + \frac{1}{c}\frac{\partial}{\partial t}\right) A = 0, \tag{6}$$

$$\left(\frac{\partial}{\partial z} + \frac{1+s}{c}\frac{\partial}{\partial t}\right) \varepsilon = 0, \tag{7}$$

$$\left(\frac{\partial}{\partial z} + \frac{1+s}{c}\frac{\partial}{\partial t}\right) \phi = 0, \tag{8}$$

$$\left(\frac{\partial}{\partial z} + \frac{1}{c}\frac{\partial}{\partial t}\right) \alpha = \sin(2\varepsilon)\left(\frac{\partial}{\partial z} + \frac{1}{c}\frac{\partial}{\partial t}\right) \phi, \tag{9}$$

where A is the real-value amplitude, ε is the ellipticity angle, ϕ is the azimuth angle of the light polarization ellipse and α is the general field phase. The parameter $s(A, \varepsilon)$ defines the speed of pulses and depends on the average atomic velocity. For $s(A, \varepsilon)$ we have obtained the analytical expressions.

The results of this work extend the knowledge of physics of the propagation of polarized pulses and can be applied in the area of optical communications.

The work is supported by the Ministry of Education and Science of the Russian Federation in the frame of the Program “Scientific and scientific-pedagogical personnel of innovative Russia” (the Contract no. 16.740.11.0466 and the Agreement no. 8387), by RFBR (grants nos. 12-02-00454, 12-02-00403, 11-02-00775, 11-02-01240), by the Russian Academy of Sciences, Presidium of Siberian Branch of Russian Academy of Sciences and the Russian Quantum Center. The young scientists D.V. Brazhnikov and M.Yu. Basalaev are also supported by the Presidential Grant MK-3372.2912.2 and the RFBR Grant 12-02-31208-“mol_a”.

Orientational imaging of single nanoemitters simulated by elliptical oscillators

S.V. Boichenko[1], S.A. Zilov[1]

[1] *Irkutsk Branch of Institute of Laser Physics SB RAS, Lermontov str., 130a, Irkutsk, 664033, Russia*
E-mail: ste89@yandex.ru

Fluorescent behavior of a single quantum fluorescent nanoemitter (single molecule, single quantum dot, single color center) is highly sensitive to the emitter local environment. For this reason, single nanoemitters can be used as nanosensors and vice versa their fluorescent properties can be controlled by local environment. This opportunity is beneficial for nanophotonics, medical sciences, biotechnology, quantum optics, material sciences, and some other applications. Observables of inhomogeneous local environment surrounded single nanoemitters are affected by their transition dipole orientation [1]. Hence, it is crucial to know the dipole orientation (or its behavior) to study an interaction of a single molecule with its local environment. Therefore, single molecule orientation determining is an important scientific task.

Many quantum systems absorb and emit light as classical electric dipole oscillators (transision dipole moment is a real vector), but in some cases they absorb and emit light as elliptical oscillators (transision dipole moment is a complex unit vector) [2]. It was shown in [2] that when a quantum system under investigation has nondegenerated excited state, its transition dipole moment is a real vector specified by the system. But when the system has doubly-degenerated due to orbital angular momentum projection excited state, its transition dipole moment is an elliptical oscillator specified by the system and exciting light field polarization. This situation can take place, for example, for color centers in crystals [3] and guess dye molecules in solids [4, 5], in which emitters are affected by a crystal electric field creating Stark effect.

In the present work we study an orientational visualization of elliptical-oscillator simulated arbitrary oriented single nanoemitter by means of laser-scanning confocal fluorescence single-molecule (LSCFSM) microscopy using cylindrical vector beams (CVBs). Previously, it has been shown that elliptical oscillator absorption cross section and emission intensity can be obtained by addition of right- and left-handed rotators cross sections and emission intensities [2]. The term "elliptical oscillator simulated nanoemitter orientation" implies the normal to the oscillator plane $\mathbf{n} = (\sin\theta\sin\varphi, \sin\theta\cos\varphi, \cos\theta)$ orientation, where θ and φ are polar and azimuthal angles. Note that if a nanoemiter is simulated by a classical dipole oscillator, the dipole orientation is called "nanoemitter orientation" [6, 7].

We calculate LSCFSM images according to

$$I(\mathbf{r},\mathbf{n}) \propto (1+\alpha\cos 2\theta)\left\{\left|\mathbf{E}(\mathbf{r})\boldsymbol{\sigma}^{+}(\mathbf{n})\right|^2 + \left|\mathbf{E}(\mathbf{r})\boldsymbol{\sigma}^{-}(\mathbf{n})\right|^2\right\}, \qquad (1)$$

where $\mathbf{r}$ is focal volume point vector, $\boldsymbol{\sigma}^{+}(\mathbf{n})$ and $\boldsymbol{\sigma}^{-}(\mathbf{n})$ are right- and left-handed rotator vectors, $\mathbf{E}(\mathbf{r})$ is focal volume light field vector, α is fluorescence collection efficiency dependent coefficient. According to calculation, for NA=1.2, sinus condition satisfying objective α=0.11. We carry out all calculations for this objective.

We compute focal volume light field distribution for complex CVB tight focusing by the microobjective [6]. Light field distribution in the beam cross section is

$$\mathbf{E}_0(\theta_0, \varphi_0; A, \Phi) = A\exp(i\Phi)\mathbf{E}_r(\varphi_0) + \mathbf{E}_\varphi(\varphi_0), \qquad (2)$$

where θ_0 and φ_0 are polar and azimuthal angels of the beam cross-section point; $\mathbf{E}_r(\varphi_0)$ and $\mathbf{E}_\varphi(\varphi_0)$ are electrical vectors of radially and azimuthally polarized beams; A and Φ are the

beam ellipticity parameters. We vary the ellipticity parameters and find their values providing optimal excitation of arbitrary oriented single nanoemitters.

The calculations showed that an optimal excitation of arbitrary oriented nanoemitters is provided by the beam with Φ=0 and A=1.2: intensity maximum of minimally excited molecule LSCFSM image is 96% of intensity maximum of maximally excited molecule one. For comparison, the same parameter is 12% for linearly-polarized excited beam and 40% for circularly-polarized one. Fig. 1 shows differently oriented nanoemitters LSCFSM images acquired using abovementioned complex CVB as excited. Angles (θ, φ) under pictures designate single nanoemitter orientation. We suppose that a nanoemitter is situated in microscopic system focal plane. One can see that image intensity maximums are approximately equal for different orientations. Image intensity distribution is a function of nanoemitter orientation. Hence, we can determine the nanoemitter orientation analyzing its image. Note that the images have a symmetry center (coinciding with geometrical focus).

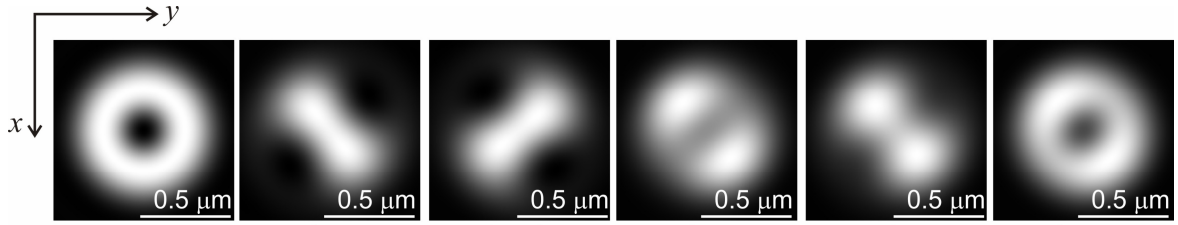

Fig. 1. Calculated LSCFSM images of differently oriented single nanoemitters.

In summary, we have shown using calculations that one can (I) effectively visualize single nanoemitters, whose transition dipole moment is an elliptical oscillator by means of LSCFSM microscopy using complex CVBs, (II) derive the nanoemitter orientation from its LSCFSM image.

This work was supported by the Division of Physical Sciences, Russian Academy of Sciences (project no. III.9.3), and jointly by the Siberian Branch, Russian Academy of Sciences, and the National Academy of Sciences of Belarus (project no. 13).

References

1. L. Novotny and B. Hecht, “Principles of nano-optics”, Cambridge University Press, (2006).
2. S.A. Zilov, E.F. Martynovich, Phys. of the Solid State **50**, (1692).
3. F. Jelezko and J. Wrachtrup, Phys. stat. sol. (a) **203**, 3207 (2006).
4. S.G. Lukishova, A.W. Schmid, R. Knox, et al., J. of Modern Opt. **54**, 417, (2007).
5. W.E. Moerner, New J. of Phys. **6**, 88 (2004).
6. S.V. Boichenko and E.F. Martynovich, JETP Letters **97**, 52 (2013).
7. B. Sick, B. Hecht, and L. Novotny, Phys. Rev. Lett. **85**, 4482 (2000).

CW Raman fiber laser generating below 1 μm at direct multi-mode laser diode pumping

S. I. Kablukov[1], E. I. Dontsova[1], E. A. Zlobina[1], I. N. Nemov[1], A. A. Vlasov[1]and S. A. Babin[1,2]
[1]*Institute of Automation and Electrometry, Siberian Branch of the Russian Academy of Sciences, 1 Ac. Koptyugave., Novosibirsk, 630090, Russia*
[2]*Novosibirsk State University, 2 Pirogova str., Novosibirsk, 630090, Russia*
E-mail: ekaterina.dontso@mail.ru

The main feature of Raman fiber lasers (RFL) is the opportunity for new wavelengths generation, that enables wide range of RFL applications. Wavelength of RFLs is shifted relative to the pump wavelength due to the Raman effect. Multistage RFLs allow one to obtain lasing in wide spectral range from 1.1 to 2 μm. A lot of works are devoted to RFLs, but in the most cases Raman lasers are pumped by rare-earth doped fiber lasers [1]. High power rare-earth doped (e.g. Yb or Er) fiber lasers are usually pumped by multimode laser diodes at 930 or 980 nm. Utilization of direct pumping of RFLs by high power laser diodes greatly simplifies the RFL scheme thus improving its parameters and offering generation at wavelengths RFL at 1 μm and even shorter wavelengths. In this paper we report on the first demonstration of RFL generation at wavelength below 1 μm under direct laser diode pumping.

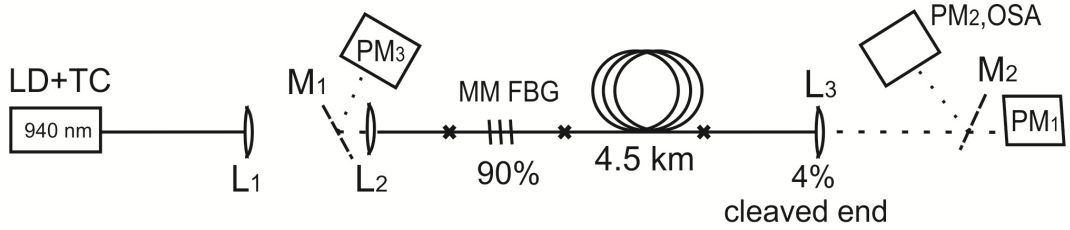

Fig.1. Experimental setup.

A scheme of the experimental setup is shown in the Figure 1. Multi-mode laser diode (LD) at ~938 nm (JENOPTIK Laser GmbH JOLD-75-FC-11) has fiber output. LD temperature is controlled by thermo controller (TC). Pump radiation is collimated by lens L_1 and focused by lens L_2 into a core of a multimode graded-index fiber (Corning 62.5/125 CPC7). The fiber length is 4.5 km. About ~ 46 W of pump power is coupled into the fiber. Home-made multi-mode fiber Bragg grating (MM FBG) with reflectivity of ~90% and cleaved fiber end with Fresnel reflection ~ 4% are used as the RFL cavity mirrors. Selective mirrors ($M_{1,2}$) are used for separation of the pump and the Stokes waves radiation. Generated RFL power in forward (P_1^{out}) and backward (P_1^{back}) directions are measured by power meters PM_2 and PM_3, correspondingly. Residual pump power (P_0^{out}) is transmitted through mirror M_2 and is measured by power meter PM_1. Output spectra are measured by Optical Spectrum Analyser (OSA) and one of them is shown in Figure 2.

The residual pump power and RFL output power versus the coupled pump power are plotted in Figure 3. One can see that about 3 W of RFL power is generated at wavelength of 980 nm overall for forward and backward waves. The 980 nm power is limited by the generation of the second Stokes wave (at 1025 nm) started at the maximum power. The residual pump power has maximum value of 4.5 W at the threshold and drops down to value of 3.5 W due to power transfer to the generated Stokes wave.

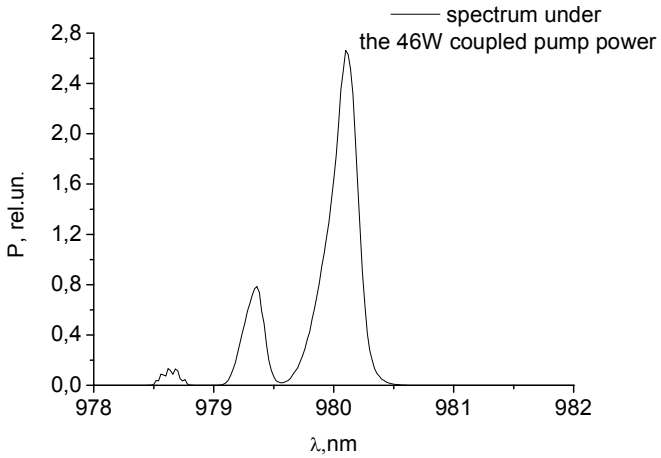

Fig.2. Output spectrum at maximal pump power.

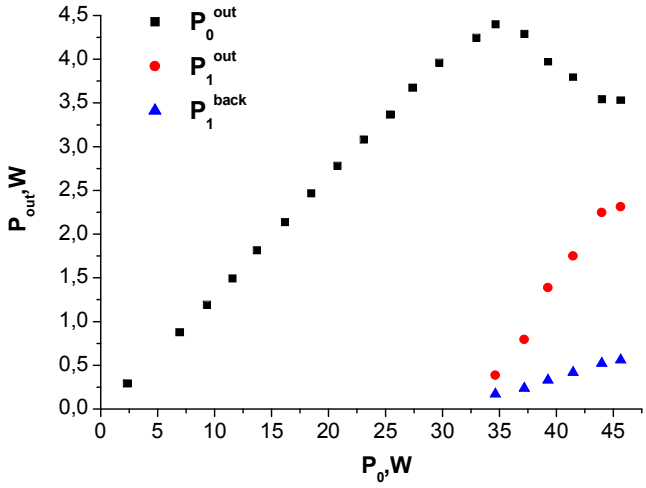

Fig.3. Stokes wave power in forward (circles) and backward (triangles) directions, and output residual pump power (squares) versus coupled pump power.

It is known that a beam cleanup is possible in a process of stimulated Raman scattering in graded-index multimode fibers [2,3]. We registered this effect by measuring output beam divergence in far field by Coherent Beam Master BM-7 profile meter. The measured beam divergence is reduced by ~3 times for the RFL output beam as compared with the residual pump beam. Details of the experiments will be presented at the conference.

References

1. A.S. Kurkov, E.M. Dianov, *Quant.Electron.***34**, 881-900 (2004).
2. S.H. Baek, W.B. Roh, *Opt. Lett*. **29,** 153-155 (2004).
3. N.B. Terry, K.T. Engel, T.G. Alley and T.H. Russell, *Opt. Express* **15**, 602-607 (2007).

Energy characteristics of a CuBr-laser operating in the single pulse mode

A.I. Fedorov[1], V.F. Fedorov[1], D.V. Shiyanov[1,2]

[1]V.E. Zuev Institute of Atmospheric Optics SB RAS, 1, Academician Zuev sq., Tomsk, 634021 Russia,
[2]NR Tomsk Polytechnic University, Lenin av. 30, Tomsk, 634050 Russia
E-mail: qel@iao.ru

A typical frequency range of the pulse-periodic lasers using the metal halide vapors is tens - hundreds kilohertz. In some instances the necessity appears of the operation of such lasers with the pulse repetition rate (PRR) of tens - hundreds hertz and high output energy. Such generation mode is provided with the excitation of laser active medium by double pulses. One of such pulses fulfils the dissociation function of a metal halide molecule, and another one fulfils the function of excitation of metal atoms.

In the present paper the investigations of the CuBr-laser characteristics are continued when excited by double pulses [1, 2]. The gas-discharge tube (GDT) being studied had the 1 cm diameter and 40 cm in length. When forming a dissociating pulse the thyristor power supply was used. The copper atom pumping was performed using the thyratron source with a pulse discharge of operating capacity. For a given laser we determined the effect of dissociation and pumping pulse energy on the laser energy characteristics at the cost of energy recording of one of pulses and energy variation of another pulse. This was achieved by varying the operating capacities and their voltage (to 15 kV and 6.8 nF in a pumping pulse). Besides, the limiting energies of dissociation and excitation pulses were determined, necessary for achieving a maximum of the specific radiation energy. The optimum delays were determined between the pulses of 40-120 ns in the frequency range from 10 to 100 Hz. Based on the obtained results it is suggested to make the scaling of the laser GDT volume to produce high generation energies.

References

1. A.I. Fedorov, V.F. Fedorov, D.V. Shiyanov. Pisma v ZhTF. 2013 (to be published) (in Rus).
2. F.A.Gubarev, V.F.Fedorov, K.V.Fedorov, G.S.Evtushenko. Atmosph. Ocean.Optics, 2012, V.25, No.12, p.1107-1111.

Plasmons between nanowires excited by evanescent wave

L.L. Frumin[1,2], S.V. Perminov[3], D.A. Shapiro[1,2]

[1] *Institute of Automation and Electrometry, SB RA S Academician Koptug ave. 1, Novosibirsk 630090, Russia*
[2] *Novosibirsk State University, Pirogov str. 2 , Novosibirsk 630090, Russia*
[3] *A.V. Rzhanov Institute of Semiconductor Physics, Siberian Branch, Russian Academy of Sciences, Academician Lavrentyev ave. 13, Novosibirsk 630090, Russia*
E-mail: lfrumin@iae.nsk.su

Study of plasmons excitation is of great interest for optics and photonics as a base of novel optical technologies, particularly, for metamaterials, optical antennas, plasmon-enhanced Raman scattering, broad-band solar cells and photonic crystals.

In this work, we consider two half-spaces where the first half-space has a greater dielectric permittivity than the second. When the incidence angle of the wave running from half-space 1 exceeds the angle of total internal reflection (TIR), an evanescent wave is generated in half-space 2. The plasmons are excited by this evanescent wave in two metallic cylinders (nanowires), placed in the half-space 2 near the flat interface. We studied this configuration by numerical simulation based on the boundary elements method. The special Green function [1, 2] of layered medium is used, that considerably simplifies the calculations.

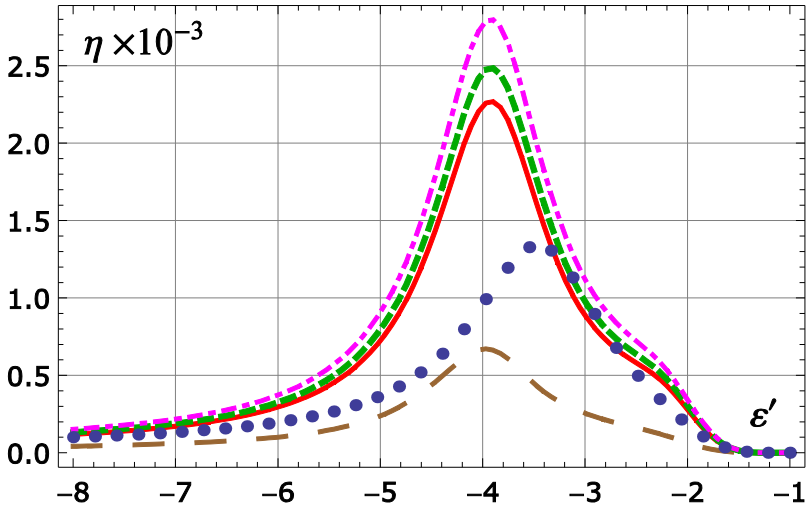

Fig.1. The field enhancement factor, $\eta = |E_C / E_0|^2$, as a function of the real part of metal's dielectric permittivity ε': for evanescent wave, the incidence angle $\theta = 0.7$ (long dashes); 0.78 (solid line), 0.8 (dashed), 0.9 (dot-dash), while $\varepsilon_1 = 2.25, \varepsilon_2 = 1$; for propagating wave, $\theta = \pi / 4$ (circles), with $\varepsilon_1 = \varepsilon_2 = 1$. In all cases, the imaginary part of the metal's permittivity $\varepsilon'' = 0.5$, the wavelength $\lambda = 2\mu m$.

The variation of the incidence angle near the TIR angle, strongly changes the amplitude of plasmons that gives a way to control the plasmon peak. The field strength E_C and its enhancement factor η are calculated in the central point of the narrow slit between two cylinders. The slit size and cylinders' diameter was 5 nm and 100 nm, accordingly. Fig.1 shows that in the narrow interval of angles for the case of evanescent wave the enhancement factor changes distinctly. In contrast, for the propagating wave the plasmon peak does not noticeably change its amplitude.

References

1. O.V. Belai, L.L. Frumin, S.V. Perminov, D.A. Shapiro, Opt. Lett., vol. 36, No. 6, pp. 954-956, 2011;
2. O.V. Belai, L.L. Frumin, S.V. Perminov, D.A. Shapiro, EPL, vol. 97, p. 10007, 2012.

Second harmonic generation of CO_2-laser radiation with self-mode-locking using GaSe and GaSeS crystals

D.E. Genin[1], D.V. Beloplotov[1], A.G. Sitnikov[1], A.N. Panchenko[1], S.Yu. Sarkisov[2]

[1] *Institute of High Current Electronics SB RAS, 2/3 Akademichesky Avenue, Tomsk, 634055 Russia*
[2] *Siberian Institute of Physics and Engineering, Novosobornaya square 1, Tomsk, 634050 Russia*
E-mail: dm_genin@vtomske.ru

Nowadays different research works connected with broadening of laser generation range are being conducted. Usually they deal with nonlinear crystals. Also recently a lot of crystals with new chemical compositions have been synthesized. They have unknown optical properties like nonlinear susceptibility. Second order nonlinear susceptibility can be calculated on the basis of the second harmonic generation (SHG) experiments.

GaSe crystals are rather widely used in middle IR and terahertz ranges [1]. They have wide transparency range (0.65-18 μm), low optical absorbtion (<0.1 cm^{-1}), high nonlinear susceptibility and damage threshold. On the other hand they have low hardness and their structure is layered. It is possible to increase hardness by doping crystals [2], for example by sulphur, but this process changes optical properties.

We made GaSeS crystal with 7% sulphur containing. We supposed it to be promising for being used in experiments with generation of THz radiation. That's why we decided to define its second order nonlinear susceptibility by experiments with SHG of CO_2-laser radiation.

On one hand we needed laser radiation pulses with high peak power. On the other hand this power must be limited by crystal damage threshold [3, 4]. That's why we tried to make laser pulse as short as possible. And we found two ways of solving the problem.

It is known that CO_2-laser is able to work in self-mode-locking regime (mode-locking without additional elements in the cavity, only by gain medium properties). The goal of our work was to obtain SHG in GaSe and GaSeS crystals with and without self-mode-locking. In the first case laser pulse had usual shape with powerful leading peak (up to 1.6 MW, 50 ns) and "nitrogen tail". In the second case leading peak was divided to multiple separate peaks (2-4 ns) because of self-mode-locking. In this case peak power was higher than 1.9 MW.

Both types of pulses were applied to obtain SHG on 6 mm length GaSe crystal.

In the first case laser pulse energy was 180 mJ. Total SHG efficiency was 0.38%, in peaks it was 0.51%.

In the second case laser pulse energy was much lower (70-80 mJ), but nevertheless SHG efficiency increased dramatically at about 5 times (to ≈2%).

We didn't manage to measure directly SHG energy with 3.7 mm length GaSeS crystal. We increased laser pulse energy a bit (to 100 mJ) and compared SHG signals with GaSe and GaSeS crystals registered by one and the same high-sensitivity detector. This way we found that peak SHG power with doped crystal is 200-250 times lower than with pure one. Assuming pulse shapes to be similar we can suppose that relation between efficiencies for this cases is equal to the relation between signal amplitudes. So the SHG efficiency with GaSeS crystals was about 0.015% and the energy was about 8 μJ.

Also we estimated the relation between nonlinear susceptibilities of these two crystals. It was about 10. It means that GaSeS crystal with 7% sulphur containing is not suitable for obtaining of nonlinear optical phenomena.

The main conclusion is that self-mode-locking regime is promising for the cases where high peak power is needed, like experiments in the field of nonlinear optics. Using this regime we increased SHG efficiency about 5 times.

References

1. Shi W. and Ding Y.J. // Appl. Phys. Lett. – 2004. – V. 84. – № 10. – P. 1635 – 1637.
2. Sarkisov S.Yu., Morozov A.N., Kazakov A.V. et al.// Proc. –Tomsk: The Tomsk IEEE Chapter & Student Branch. International Suberian Conference on control and communicztoins (SIBCON-2009). – Tomsk, March 27-28. – 2009. – P. 138 – 142.
3. Andreev Yu.M. et al.// Kvant. Electron. – 2001. – V. 31. – № 12. – P. 1075.
4. Березная С.А., Генин Д.Е., Коротченко З.В. и др. // Изв. вузов. Физика. − 2010. − № 9. − С. 65 – 70.

Metal-dielectric coatings for interferometry in reflected light

N.D. Goldina

Institute of Laser Physics of SB RAS, Pr. Lavrentyeva 13/3, Novosibirsk, 630090 Russia

E-mail: ngold@laser.nsc.ru

There are not a lot of calculation examples of multilayer metal-dielectric systems. In our forward studies such systems are used to create the narrow bright bands in reflected light likewise of transmission bands in Fabry-Perot interferometer [1]. Difficult step in this task is to design an asymmetrical front mirror which determines the contrast, width and asymmetry of the interference fringes. The reflection and absorption of asymmetric multilayer coating are different at the forward and reverse directions of incident light. In multibeam reflecting interferometers have found application the asymmetrical mirror which include the thin metal film of thickness $d<<\lambda$. The complex-conductive surface model is used in the computation of the optical properties of a thin absorbing film and is introduced the parameter $\xi = \xi' + i\xi''$.

Design of front mirror for the interferometer with a certain specified parameters is a difficult task. For example, the problem of obtaining a perfect symmetric bands together with ideal contrast. This problem was solved in [1, 2], which was first observed an experimental method of reception almost symmetric bands near zero reflection in the background. Modern calculation methods with the use of computers allow the search of more complex solutions to this problem presented in this paper. The multilayer structure is convenient to consider graphically using circle diagram for complex reflection coefficient. Graphical methods provide physical visibility of the design of resonant systems in interferometry and help to find the optimal solutions [3, 4].

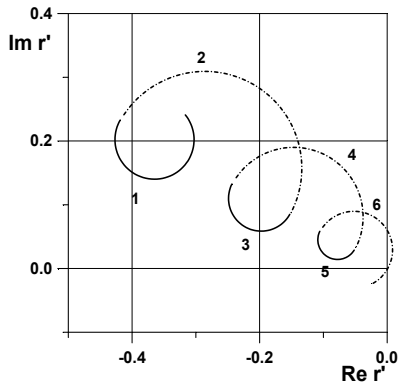

There are two version of dielectric multilayer deposition in the front mirror: before or after the absorbing film. Second variant of disposition of dielectric layers is realized easy practically. The evaporation of layer is stopped upon reaching the extreme R' (Fig.1). The case under consideration corresponds to the circle diagram for immersed layers when the layer is introduced between two thin-film systems. The first system is a thin metal film on the substrate. The second system is the dielectric multilayer. The thicknesses of introduced layers must be optimized for obtaining of desired view $\widetilde{R}(\varphi)$. The matching condition is ensured by choosing the parameter of the metal film $\xi' = n_0$, where n_0 – the refractive index of substrate.

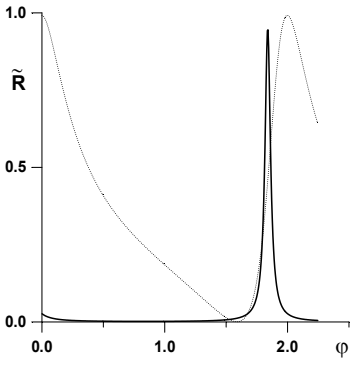

The interference fringes are substantially symmetrical form (Fig.2), where the solid line shows the dependency $\widetilde{R}(\varphi)$ with the synthesized front mirror and the dotted line – when the mirror comprises only a metal film.

1. Goldina N.D., Zakharov M.I., Troitski Ju.V. *Optoelectr. Instrum. and Data Process.,* no.10, p.107, 1975.
2. Kamenev N.N., Troitski Ju.V. *Opt. Spectrosc.,* **54** (4), p.725, 1983.
3. Apfel J.H. *Appl. Opt.,* **11**, no.6, p.1303, 1972.
4. Baumeister P. *Optical coating technology*. – Bellingham, SPIE Press, 2004. - 851 p.

Study of second order nonlinear optical properties of chromophore-containing polyimides in thin films

A.I. Gorkovenko[1], A.I. Plekhanov[1], A.E. Simanchuk[1], A.V. Yakimansky[2], G.I. Nosova[2], N.A. Solovskaya[2], N.N. Smirnov[2]

[1] *Institute of Automation and Electrometry of the Siberian Branch of the Russian Academy of Sciences, pr. Koptyuga 1, 630090 Novosibirsk, Russia*

[2] *Institute of Macromolecular Compounds of the Russian Academy of Sciences, Bolshoi pr. 31, 199004 St. Petersburg, Russia*

E-mail: fractal@iae.nsk.su

In latest decades, chromophore-containing polymers attract a careful attention of researchers as perspective materials for applications in electro-optical and photonic devices such as optical switches, light modulators, optical logics and memory, etc [1]. Films of chromophore-containing polymers, polarized by external electric field, demonstrate macroscopic second order nonlinearities that are by an order of magnitude higher than those of analogous solid state crystalline structures, and half-wave voltage about 1 V. For practical applications, it is rather important that the molecular structure of chromophore-containing polymers can be widely varied in order to increase the temporal and thermal stability of the nonlinear response.

In the present work new synthesized polyimides with covalently attached dye Disperse Red 13 (DR13) were investigated. Films were prepared by spin-coating of polyimides solutions onto glass substrates (1 mm thickness) and then poled by corona poling method. Films heated during the poling process up to 190 °C (their glass transition temperature). Applied voltage was 6.5 kV and distance between electrode and film surface was 1 cm. Optical constants (refraction indexes and extinction coefficients) in the range of 400-800 nm were observed on the spectral ellipsometer 'Spectroscan'. Films thicknesses were measured by two methods: spectral ellipsometry and interferometry method (on the interference microscope WLI Lab). Observed values are 250-400 nm and in good agreement. Second order nonlinear optical susceptibility was measured by the Maker fringes method and used theory taking absorption into account [2]. As a light source, we used Solar OPO 601 (with 15 ns pulses). Measurements were made in the range of 850-1450 nm for fundamental wavelength (SHG wavelength was changed from 425 to 725 nm) with 50 nm step. As reference for getting absolute nonlinear coefficient values was used quartz 1mm thickness plate (nonlinear coefficient value is 0.5 pm/V). Samples measurements were made in p-p (p-polarized signal and p-polarized excitation) scheme with fixed incident angle of 55□.

Our third structure demonstrate higher magnitude of nonlinearity d_{33}=125 pm/V (under the same preparation and poling conditions) than other structures which points to the great promise of this structure for the practical application. In comparison with the previous results, new samples demonstrate increase an order of magnitude, which can be result of more optimal poling conditions. Red shift of nonlinear coefficient maxima with respect to absorption maxima can be caused by wide-developed vibration structure of chromophore molecules electronic levels.

Also we should underline high beam resistance of samples on fundamental wavelength: their nonlinear properties remain unchanged after the action of 104 pulses.

References

1. Larry R. Dalton, Philip A. Sullivan, and Denise H. Bale, Chem. Rev., 110, 25–55 (2010).
2. W. N. Herman, L. M. Hayden, J. Opt. Soc. Am. B, Vol. 12, No. 3 (March 1995)

Controlled synthesis of novel lanthanide-doped nanocrystals and upconversion fine-tuning

Xue Teng, Ling Huang[a,b]

[a]*Institute of Advanced Materials, Nanjing University of Technology, Nanjing 210009*
[b]*School of Chemical and Biomedical Engineering, Nanyang Technological University, Singapore 637457*
E-mail: iamlhuang@njut.edu.cn

Rare earth-based nanomaterials have recently drawn impressive attention due to their unique energy upconversion (UC) capabilities. However, studies on Sc^{3+}-based nanomaterials are still absent. Herein, we report the synthesis and fine-control of $NaScF_x$ nanocrystals by tuning the ratio of oleic acid (OA, polar surfactant) to 1-octadecene (OD, nonpolar solvent). When the OA:OD ratio increases from low (3:17) to high (3:7), the nanocrystals change from pure monoclinic (Na_3ScF_6) to pure hexagonal phase ($NaScF_4$), via a transition stage at intermediate OA:OD ratio (3:9) where not only the mixture of nanocrystals in monoclinic and hexagonal phases was obtained, the co-existence of both phases inside individual nanocrystals was also observed. More significantly, due to the small radius of Sc^{3+}, $NaScF_x$:Yb/Er nanocrystals show different UC emission from that of $NaYF_4$:Yb/Er nanocrystals, which further widens the applications of rare earth-based nanomaterials ranging from optical communications to disease diagnosis [1,2].

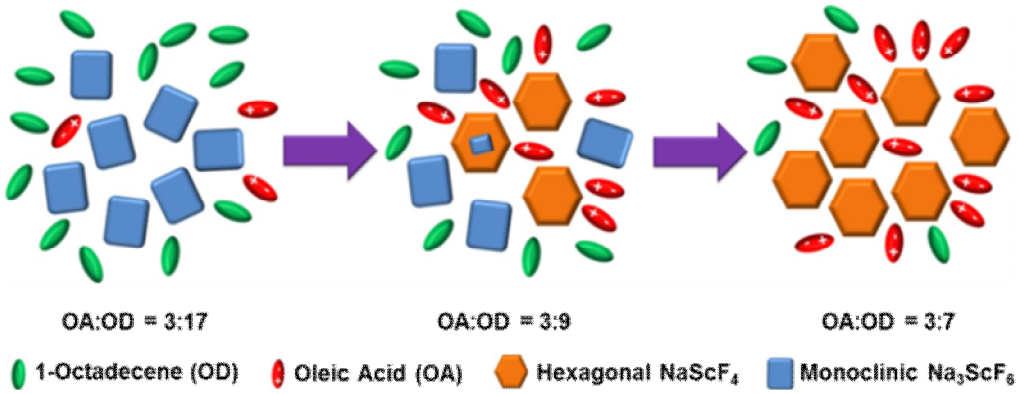

Fig. 1. Schematic illustration of the crystal structure evolution at varying polarities of the reaction medium, i.e., OA:OD ratios.

References

1. Teng, X.; Zhu, Y.; Wei, W.; Wang, S.; Huang, J.; Naccache, R.; Hu, W.; Tok, A.; Han, Y.; Zhang, Q.; Fan, Q.; Huang, W.; Capobianco, J. A.; Huang, L. *J. Am. Chem. Soc.* **2012**, *134*, 8039-8043.
2. Ding, Y.; Teng, X.; Zhu, J.; Huang, L. *Nanoscale*, submitted.

Regenerative mode locking of fiber lasers with the use of a tracking generator

B.N. Nyushkov[1,2], A.V. Ivanenko[3], S.A. Farnosov[1], V.S. Pivtsov[1,2], V.I. Denisov[1], S.M. Kobtsev[3]

[1] *Institute of Laser Physics of SB RAS, 13/3 Lavrentyev Str., Novosibirsk, 630090 Russia;*
[2] *Novosibirsk State Technical University, 20 Karl Marx Str., Novosibirsk, 630073 Russia;*
[3] *Novosibirsk State University, 2 Pirogov Street, Novosibirsk, 630090, Russia;*
E-mail: nyushkov@laser.nsc.ru

Actively mode-locked (AML) fiber lasers are an attractive source for a regular train of ultra-short pulses. Such lasers normally consist of a fiber-based cavity and an intensity modulator. The modulator is driven by an external RF generator at a frequency f_{mod}, which is set equal to an integer multiple of the fundamental pulse repetition frequency f_{rep} governed by the cavity length. Despite high stability of the used RF generator an AML laser itself requires stabilization for long-term performance. The motivation for stabilizing an AML laser is to ensure that the detuning between the laser repetition frequency at nf_{rep} and the modulation frequency f_{mod} is kept within a tolerance, which is typically less than 0.1% [1]. This is required to maintain mode locking in the presence of mechanical relaxation, thermal drift, and other environmental perturbations that affect the cavity length. Traditional approach is stabilizing the laser cavity via piezo-electric control, while the external modulation function f_{mod} is kept constant. Thus, the oscillation frequency f_{rep} remains constant. The regenerative approach allows f_{rep}, in principal, to drift freely and force the modulation frequency to follow f_{rep}. However a typical regenerative feedback, which has a clock extraction circuit based on a high-Q dielectric filter and a high-gain electrical amplifier, is designed to operate only at a selected harmonic of the fundamental repetition rate f_{rep} [2]. The frequency tuning range is very limited due to the narrow band filtration. Another problem is the coupling of the amplitude noise back to the cavity through such a regenerative feedback.

In this paper we propose and preliminary explore a novel technique of AML with a regenerative feedback which is based on the concept of a tracking generator. Such an approach ensures permanent mode locking, allows on-the-run continuous tuning of the pulse repetition rate as well as changing of the order of harmonic mode locking. Basically the developed regenerative scheme employs a simple phase lock loop (PLL) to control a widely-tunable RF oscillator used as a clock for the laser intensity modulator.

A simplified schematic diagram of the developed regeneratively mode-locked fiber laser system is shown in Fig. 1. The laser has a unidirectional ring cavity composed of an erbium-doped fiber amplifier (EDFA), a Mach-Zehnder intensity modulator (MZIM), and supplementary components. All the fiber components are polarization maintaining (PM) that enhance environmental stability of the laser. The regenerative feedback circuit employs a voltage-controlled oscillator (VCO) which can be tuned in a wide frequency range (exceeding manifold f_{rep}) by varying the reference voltage (V_{REF}). A digital phase-frequency detector (PFD) detects detuning between the VCO and a signal at the laser repetition rate frequency, which is extracted by means of a fast photodiode (PD) and a tunable band pass filter (TBP). The error signal yielded by PFD is used to control the VCO via PLL. Thus, in the closed-loop conditions the VCO frequency, which is actually $f_{mod,}$, remains tightly locked to a selected harmonic of the instantaneous repetition rate frequency (f_{rep}) of the laser, even if the cavity optical length changes with time. This enables permanent maintenance of AML even in an unstabilized laser despite environmental perturbations. This feature allows also continuous tuning of the pulse repetition rate in a wide range (by adjusting the cavity length) without interruption of mode locking.

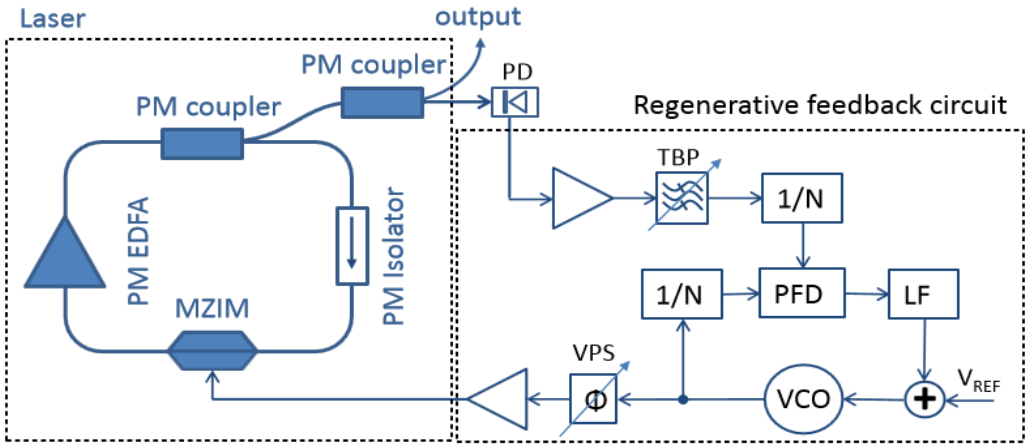

Fig.1. Schematic of the regeneratively mode-locked fiber laser system: MZIM – Mach-Zehnder intensity modulator; EDFA – erbium doped fiber amplifier; PD –photodiode; TBP – tunable band pass filter; 1/N – prescaler; PFD – phase-frequency detector; VCO – voltage-controlled oscillator; VPS – variable phase shifter.

For preliminary experiments we built a laser cavity with a fundamental repetition frequency of approximately 13 MHz. Using a single sample of a wide-range VCO based on commercial integrated circuit, we managed to obtain regenerative mode-locking alternatively at the 1st, 2nd, and 3rd harmonics of the fundamental frequency. To trigger mode-locking it was necessary to set roughly the VCO frequency in the vicinity of the selected harmonic of the frequency f_{rep} and close the PLL. The system tolerates an initial detuning between f_{mod} and f_{rep} as large as few MHz (in excess of 10%). In the closed loop conditions the residual phase error does not exceed 30 mrad (in the band 0,1 Hz to 60 kHz). The mode locking can be maintained permanently without any attendance. The generated pulses have duration of order of 100 ps. The highest per-pulse energy was achieved in a single-pulse mode-locking regime (at the fundamental repetition rate) and reached approximately 2 nJ. The Fig. 2 demonstrates optical spectra of the laser, while Fig.3 represents a radio-frequency spectrum of the laser intermode beats upon mode locking at the fundamental frequency.

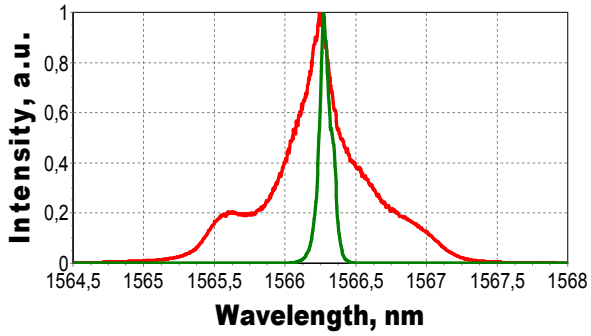

Fig.2. Optical spectra: the green trace – free-running cw lasing; the red – mode-locked lasing.

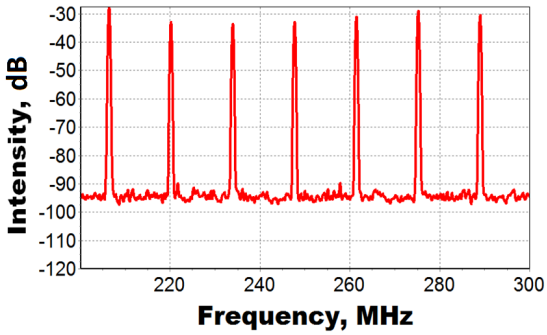

Fig.3. RF spectrum of intermode beat notes upon mode locking.

Thus, we have preliminary tested a novel technique of regenerative mode locking in a fiber laser. The technique employs a concept of a tracking generator for feedback circuit. It features a simple design, permanent maintenance of mode locking despite environmental perturbations, and possibility of on-the-run continuous tuning of the pulse repetition rate. It also allows switching the order of harmonic mode-locking. Such a regenerative technique may greatly facilitate developing of mobile and unattended pulsed laser systems.

References

1. N.A. Koliada et al., *Quantum electronics* **43,** 95-98 (2013).
2. Masato Yoshida et al., *Optics Letters* **32**, 1827-1829 (2007).

Spatial characteristics of filaments generated during focusing of femtosecond pulses of different diameters at two harmonics of Ti:Sapphire-laser

D.V. Apeksimov[1], O.A. Bukin[2], E.E. Bykova[1], Yu.E. Geints[1], S.S. Golik[3], A.A. Zemlyanov[1], A.M. Kabanov[1], G.G. Matvienko[1]

[1] *V.E. Zuev Institute of Atmospheric Optics SB RAS, 1 Academician Zuev Square, Tomsk, 634021 Russia*
[2] *Institute of Automation and Control Processes FEB RAS, 5 ul. Radio, Vladivostok, 690041 Russia*
[3] *Far-Eastern Federal University, 8 ul. Sukhanova, Vladivostok, 690950 Russia*
E-mail: kam@iao.ru

Propagation of femtosecond laser pulses of gigawatt power in air is accompanied by filamentation of a light beam. The unique properties of filamentation open new possibilities for using of femtosecond laser techniques in different fields of activity [1, 2]. Investigations of peculiarities of filamentation of sharply focused laser beams are of special interest from the viewpoint of determination of the effect of geometrical focusing and Kerr self-focusing on the spatial characteristics of the filaments [3, 4]. The experiments on light filamentation were performed in IACP FEB RAS jointly with IAO SB RAS. At the experiments we used Ti:Sapphire-laser radiation of gigawatt power with pulse duration of 45 fs (FWHM) at the main (800 nm) and second (400 nm) harmonics during focusing to the air by a lens with focal length of 200 mm. The technique of measurement of the plasma filaments is similar to those used in [5]. In the experiments performed, the laser beams with diameters of $d_0 = 2.5$; 4.5; 7; 9; and 18 mm were used. The plasma filaments were recorded during the same energy and power of the laser pulses for different beam diameters. The main task of the experiments was obtaining the quantitative information about dependence of length and position of filamentation zone of the sharply focused femtosecond radiation on initial beam size. For this purpose, side-photorecording of the filamentation zone being as luminous string-like or spindle-like area near the geometrical focus of the lens was made by a CCD-camera. The results of the experimental measurements of filamentation length depending on radiation power are presented in Fig. 1.

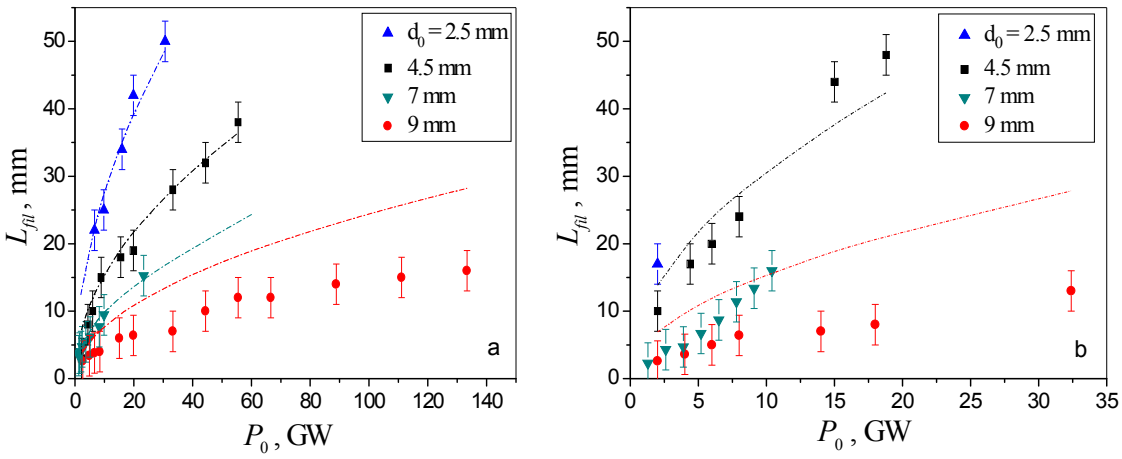

Fig. 1. Filamentation area length as a function of radiation power for λ_0 = 800 (a) and 400 nm (b).

It is seen that the filamentation area length increases monotonously with increase of laser pulse power. The angle of slope of the dependence decreases with growth of light beam size. The dependence of the filamentation area length on laser pulse intensity for different beam diameters presented in Fig. 2 differs considerably from the power dependence. Almost for all diameters, the experimental values of filament length concentrate near a curve, which is well determined by linear dependence of length of the optical breakdown area in the vicinity of the

geometrical focus without considering nonlinear self-focusing of the beam. The same trend is observed for the dependence of distance from the focusing lens to filament start presented in Fig. 2b.

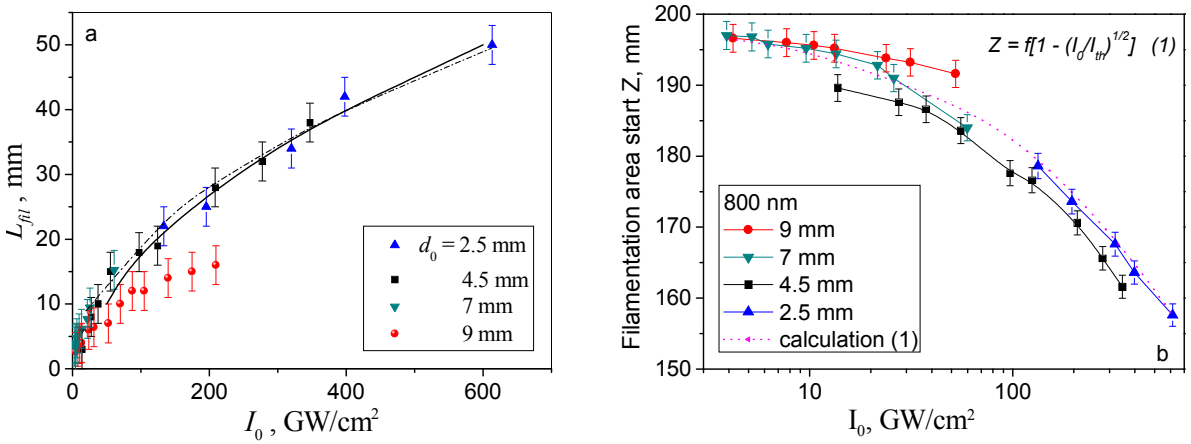

Fig. 2. Dependence of filamentation area length (a) and position of filament start (b) at different peal pulse intensity (λ_0 = 800 nm); dashed line is approximation, solid line is calculation [4].

The presented experimental results on filamentation area length of gigawatt femtosecond laser radiation with millimeter-size diameters propagating in air under sharp external focusing indicate finding of qualitatively new regularity, at least at two wavelengths, does not referred earlier in publications, i.e., invariance of length of the observed emission area (filamentation) related to beam diameter under the condition of the same peak intensity. The stated regularity does not result from the equations of the stationary theory of self-focusing of collimated or weakly focused radiation and is described mainly by linear character of transverse compression of the light beam before the nonlinear focus.

References

1. Yu.E. Geints, A.A. Zemlyanov, A.M. Kabanov, G.G. Matvienko. *Nonlinear Femtosecond Atmospheric Optics*. 212 pp. (2010).
2. V.P. Kandidov, S.A. Shlenov, O.G. Kosareva, *Quant. Electron.* **39**, 205 (2009).
3. Yu.E. Geints, A.A. Zemlyanov, *Atmos. Ocean Opt.* **26**, 11 (2013).
4. D.V. Apeksimov, O.A. Bukin, E.E. Bykova et al., *Atmos. Ocean Opt.* **26**, 247 (2013).
5. O.A. Bukin, E.E. Bykova, Yu.E. Geints, *Atmos. Ocean Opt.* **24**, 351 (2011).

Continuous wave fiber optical parametric oscillator tunable from 923 to 1005 nm

E.A. Zlobina[1], S.I. Kablukov[1], S.A. Babin[1, 2]

[1] *Institute of Automation and Electrometry of SB RAS, Ac. Koptug ave. 1, Novosibirsk, 630090 Russia*
[2] *Novosibirsk State University, Pirogova str. 2, Novosibirsk, 63009, Russia*
E-mail: kab@iae.nsk.su

Fiber optical parametric oscillators (FOPOs) based on a four wave mixing (FWM) process offer an opportunity to generate tunable laser radiation in new spectral ranges, where conventional fiber lasers are not effective or not available. Low power of available CW pump lasers and dispersion fluctuations along the fiber limit the conversion efficiency of CW parametric process resulting in a few number of the CW FOPOs realizations to date [1-3], in spite of a great demand for CW tunable fiber sources in various applications.

The developed oscillators are usually pumped near 1.55 μm and use highly nonlinear dispersion shifted fibers with length of >100 meters. The widest tuning range and the highest Stokes output power obtained for 1.55-μm pumped FOPOs amount to 250 nm (1480–1730 nm) [2] and 1W [3], respectively. However, the anti-Stokes power did not exceed 100 mW [3]. As for 1-μm spectral range, the parametric process has been studied only in single-pass scheme with conversion efficiency as low as 0.3% [4].

Recently, we have demonstrated CW all-fiber optical parametric oscillator with 9.7% slope efficiency and 460 mW output power at 972 nm [5]. It is based on 18-m long birefringent photonic crystal fiber LMA5-PM (produced by NKT Photonics) pumped near zero dispersion wavelength (~1052 nm) by a tunable ring cavity CW Ytterbium-doped fiber laser (YDFL). In the developed FOPO the Stokes wave is generated in a parametric ring cavity formed by WDM couplers, which had low losses for the Stokes wave at 1140 nm and high output coupling for the anti-Stokes wave at 975 nm. Tuning range of the anti-Stokes wave in this scheme is limited by spectral range of the used WDM couplers amounting to 950 - 1050 nm.

In the present paper we describe a CW all-fiber optical parametric oscillator operating near 930 nm. This spectral range has been obtained by using proper WDMs to form a ring cavity, which had low losses for the Stokes wave at 1205 nm and high output coupling for the anti-Stokes wave at 930 nm. The PM MOPA source used for the FOPO pumping consists of tunable YDFL with randomly polarized radiation and a polarizer at the YDFL output and two PM amplifier stages. Application of polarized pump radiation results in reduction of the threshold pump power and in growth of parametric conversion efficiency in the scalar phase matching scheme requiring the same polarization for all the involved waves. Figure 1a shows the FOPO spectra at tuning of the pump wavelength around 1050 nm. Tuning range of the anti-Stokes wave in this configuration amounts to 923 – 1005 nm. Spectral linewidth (FWHM) of the FOPO changes from 0.7 nm at short-wavelengths to 5 nm at long wavelength according to variations of the parametric bandwidth.

Figure 1b presents experimental FOPO output power versus pump power at the input of LMA photonic crystal fiber taking into account 10% splicing losses of the LMA fiber with the input pigtail. Triangles and circles correspond to parametric wavelength of 931 and 942 nm, respectively. One can see that the FOPO slope efficiency is almost the same for two wavelengths and reach value of ≈ 19% while the pump power threshold increases with the

parametric shifts since dispersion fluctuations along the fiber decrease the parametric gain. The FOPO output power at 931 and 942 nm is 120 and 230 mW, respectively. One should note that the obtained slope efficiency value is two times higher than that for FOPO at 970 nm owing to utilization of the linearly polarized pump radiation.

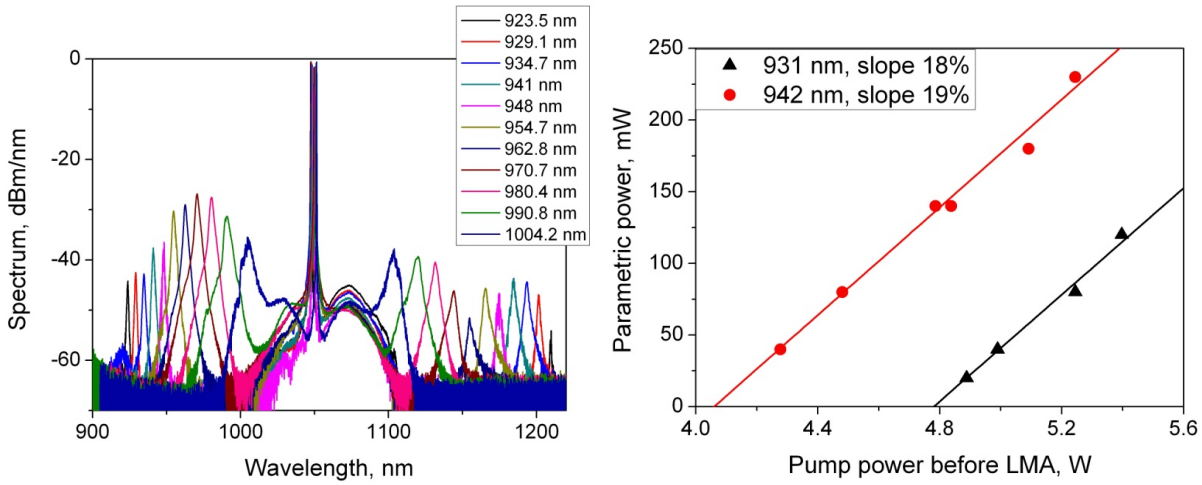

Fig.1. (a) The FOPO spectra at tuning of the pump wavelength. (b) The experimental parametric power vs. pump power coupled into LMA fiber at parametric wavelength of 931 (triangles) and 942 (circles) nm.

References

1. J. E. Sharping, *J. Lightwave Tech* **26**, 2184 (2008).
2. R. Malik and M. E. Marhic, *LAOP conference 2010*, OSA Technical Digest (CD), paper MD1.
3. R. Malik and M. E. Marhic, *OFC conference 2010*, OSA Technical Digest (CD), paper JWA18.
4. T.V. Andersen, K.M. Hilligsoe, C.K. Nielsen, J. Thogersen, K.P. Hansen, S.R. Keiding and J.J. Larsen, *Opt. Express* **12**, 4113 (2004).
5. E. A. Zlobina, S. I. Kablukov and S. A. Babin, *Opt. Express* **21**, 6777 (2013).

Influence of the Raman effect on formation and scaling of dissipative solitons in a fiber laser cavity

D. S. Kharenko[1,2], S. A. Babin[1,2], E. V. Podivilov[1,2], A. E. Bednyakova[2,3], M. P. Fedoruk[2,3], V. L. Kalashnikov[4], A. A. Apolonski[1,5]

[1] *Institute of Automation and Electrometry SB RAS, 1 Ac. Koptyug Ave., 630090 Novosibirsk, Russia*

[2] *Novosibirsk State University, 2 Pirogova Street, 630090 Novosibirsk, Russia*

[3] *Institute of Computational Technologies SB RAS, 6 Ac. Lavrentiev Ave., 630090 Novosibirsk, Russia*

[4] *Institut fuer Photonik, TU Wien, A-1040Vienna, Austria*

[5] *Ludwig-Maximilians-Universitaet, 85748 Garching, Germany*

E-mail: kharenko@iae.nsk.su

One of the problems trends of modern laser physics is scaling the energy of femtosecond pulses in laser oscillators. The great achievement in this direction consisted in the discovery of the chirped dissipative soliton (DS) regime that can be realised in fiber lasers [1] featured by their high stability, especially in the all-fiber scheme [2]. However, scaling the energy of the DS pulses with the laser cavity length is limited by an onset of stimulated Raman scattering (SRS) converting part of the DS energy to the Stokes-shifted wavelengths above the SRS threshold [3]. It is a fundamental limitation that one cannot exclude and the remaining question is how the DS evolves in the presence of SRS.

In the presentation we report, in continuation of our previous work [3], on the comprehensive experimental study and numerical simulation of the DS formation and evolution under influence of strong Raman scattering. We experimentally demonstrated generation of stable chirped pulses under this condition and performed numerical analysis clarifying laser operation in this regime based on the generalized nonlinear Schrödinger equation (NLSE) which is usually used for simulation of broadband pulse evolution in optical fibers [4].

Fig. 1a represents output spectra obtained in the experiment, and simulation demonstrating their good agreement. The DS part of the spectrum (centered at 1015 nm) is ~15-nm wide and has steep edges characterizing its high chirp. The Stokes-shifted Raman peak (centered at 1060 nm) is wider than the DS and not so steep. Measured auto-correlation function (ACF) of the chirped DS and Stokes-shifted Raman pulse together with ACFs of the compressed pulses are presented in Fig.1b. The generated DS pulse acquires large chirp due to propagation in the long PM fiber reaching duration 30-70 ps (for cavity variations between 30 and 120 m) before and 200-300 fs after the compression, accordingly. Nearly triangular ACF corresponds to rectangular DS shape.

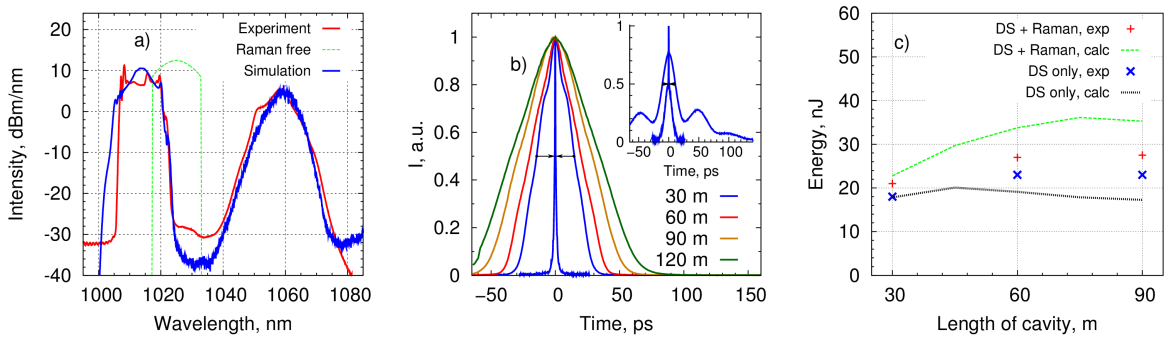

Fig.1. a) Experimental and simulated spectra with the Raman scattering and without it. b) ACF of the DS pulse at cavity lengthening together with ACF of the compressed DS (arrows), and ACF of the Raman pulse after compression (inset). c) Experimental and simulated output pulse energy for different cavities.

The generated DS and Raman pulses are separated both in spectral and time domains having comparable energies (~10 nJ for 5.5 μm core) inside the cavity and different ones at the output (~20 and ~5 nJ, correspondingly). The dependence of the output pulse energy as a function of the cavity length is presented in Fig.1c. The DS energy slightly increases in the range of the cavity lengths between 30 and 60 m, with saturation at a level of 24 nJ (for 90 m). Stable DS pulses with slightly smaller energy (~20 nJ) have also been obtained in the 120-m cavity, but at this length we had to decrease the pump power in order to get stable mode-locking. So, the DS energy practically does not grow at the cavity lengthening (both in the experiment and simulation). However, the total energy (of the DS and Raman pulses) can be sufficiently higher. The generated Raman pulse has partial coherence and can be externally compressed by a factor of 4 (see inset in Fig.1b).

Thus, a possibility to generate stable DS pulses in the fiber laser cavity in the presence of strong SRS effect has been demonstrated. A detailed analysis of the experimental and numerical results clarifying mechanisms of the stable complex formation consisting of the dissipative soliton and the Raman pulse will be presented at the conference. A possibility to generate chirped Raman dissipative soliton thus scaling the energy of the chirped soliton complex will also be discussed.

References

1. W. H. Renninger, F. W. Wise, “Dissipative soliton fiber laser,” in Fiber Lasers, O. G. Okhotnikov, ed., Wiley, 2012.

2. D. Mortag, D. Wandt, U. Morgner, D. Kracht, J. Neumann, *Optics Express* **19**, 546 (2011).

3. D. S. Kharenko, E. V. Podivilov, A. A. Apolonski, and S. A. Babin, *Optics Letters* **37**, 4104 (2012).

4. G. P. Agrawal, Nonlinear Fiber Optics, Academic Press, San Diego, California, 2001.

High-energy pulse fiber laser based on synchronous pumping

A. Komarov[1,2], A. Dmitriev[2]

[1] Institute of Automation and Electrometry, Russian Academy of Sciences, Acad. Koptyug Pr. 1, 630090 Novosibirsk, Russia
[2] Novosibirsk State Technical University, K. Marx Pr. 20, 630092 Novosibirsk, Russia
E-mail address: komarov@iae.nsk.su

At the present time the development of lasers of high-energy ultrashort light pulses has major scientific impact. These lasers are widely used in various areas of science, technology, and engineering. We put forward a way to realize such pulse sources based on fiber lasers with synchronous pumping. We present results of a numerical simulation of a formation of high-energy pulses in these lasers. The investigated laser is schematically represented in figure. It contains a source periodic pulse pumping 1, a coupler for input of pumping 2, the active fiber activated by ions of rare-earth elements serving as the amplifier 3, the passive fiber 4 serving for increase of length of the fiber resonator, a coupler for output of generated radiation from the fiber resonator 5, an additional coupler 6 for output from the resonator of a part of generated radiation in the form of a sequence of generated pulses with the purpose of their further use for management of a source of periodic pulse pumping, the photodetector 7, a time-delay line 8, the block for management of a source of pump pulses 9. In this scheme we control the time period between neighbor pump-pulses and their repetition frequency. For effective formation of the laser pulses it is necessary that the pump-pulse repetition period equals to a resonator round-trip period.

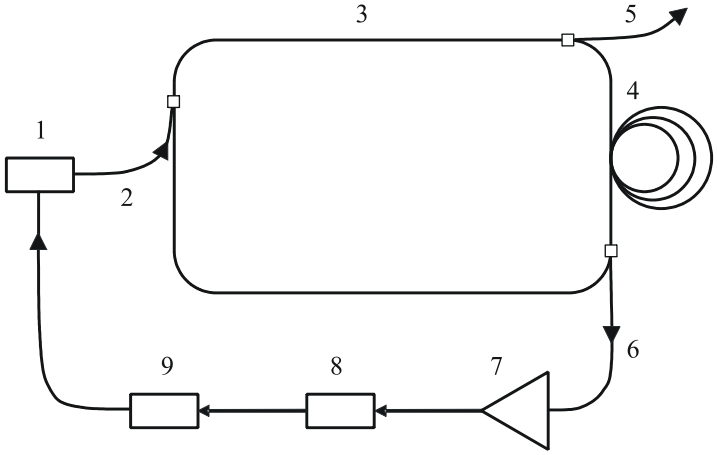

Fig. Schematic representation of laser setup.

For our analysis we use the following equations [1,2]

$$\frac{\partial E}{\partial \zeta} = (D_r + iD_i)\frac{\partial^2 E}{\partial \tau^2} + \left(G - \sigma_0 + iq|E|^2\right)E, \tag{1}$$

$$\frac{\partial G}{\partial \tau} + \gamma\left(G - P^l\right) = -BG|E|^2. \tag{2}$$

The first equation describes field evolution in fiber laser. The second determines an inertial amplification in the active fiber which is changed because of an interaction with a generated

pulse and a pump pulse. The parameters E, ζ, τ are the dimensionless field amplitude, the coordinate, and the time, respectively; D_r and D_i are the gain-loss and refractive index dispersions, σ_0 is associated to the linear losses, q is the Kerr nonlinearity, B is a stimulated emission constant, a value P^l is a periodic synchronous pulse pump, which is determined by a duration of pumping pulses and their repetition frequency. The periodic pulse pump is taken in the form of a sequence of equidistant Gaussian pulses. We have used a model with normal dispersion and a focusing nonlinearity of refractive index of a fiber medium (i.e. $D_i < 0$, $q > 0$).

Our numerical simulation is based on the split-step Fourier method. That is for each temporal step the total action of intracavity elements to the field is split into nonlinear and dispersion components. The performed numerical simulation has shown the following advantage of the suggested technique of mode-locking of fiber lasers. The use of the suggested scheme for laser mode-locking with a feedback loop for a control of parameters of pulse pumping results in a creation of amplification in a volume of a single generated pulse in the laser cavity and in an absence of amplification outside of this volume. As a result, an occurrence of new pulses in the laser resonator is suppressed, that is, the single pulse operation is stabilized. Thanks to suppression of multipulse operation, all energy of pump goes on formation of a single pulse in the laser resonator that creates opportunities of generation of pulses with essentially higher energy. Furthermore, the quality of a lasing field related to suppression of generation of radiation outside of volume of the generated pulse and to suppression of a pulse structurization is also improved. The important role in a formation and a decrease of duration of a generated pulse is played with a saturation of amplification. In the steady-state operation a time of increase of amplification in the active fiber 3 is determined by duration of a pump pulse. A time of its decrease is determined by duration of a generated pulse. The analyzed scheme of laser mode-locking works most effectively when a time of a relaxation of inversion in a gain medium is less or of the order of the resonator round-trip period. This condition is realized at a use of an enough long passive fiber 4. At work with an active fiber on a basis of rare-earth elements having a relaxation time ~ 0,1 ms, at length of an additional passive fiber ~ 1 ÷ 10 km and more, the condition for mode-locking is favorable. We have investigated a change of properties of a steady-state operation with a variation of a relaxation time of amplification, a length of the fiber resonator, a pump powerful, a detuning of a resonator round-trip period from an interpulse period of pumping. We have compared the results obtained for a laser with synchronous pump with the results obtained for laser with an active mode-locking. In case of an active mode-locking the above-mentioned requirements for a fiber resonator length and for a saturation of amplification become less rigid. However, in this case there exists an additional loss caused by spontaneous emission of atoms of a gain medium outside of volume of the generated pulse that results in an additional noise radiation. It is necessary to note, that in the suggested scheme of a laser mode-locking the set of synchronously pumped amplifiers equidistantly distributed along the ring resonator can be also used. The additional amplification results in an increase of an energy of the generated pulse and in its additional stabilization.

The suggested scheme of a laser mode-locking opens up fresh opportunities to design high-energy pulse lasers.

References

1. A. Komarov, F. Armani, A. Dmitriev, K. Komarov, D. Meshcheriakov, F. Sanchez, *Phys. Rev. A* **85**, 013802 (2012).
2. A. Komarov, F. Armani, A. Dmitriev, K. Komarov, F. Sanchez, *Phys. Rev. A* **87,** 023838 (2013).

Passive mode-locked fiber lasers: multipulse regimes and operation of high-energy pulses

A. Komarov[1,2], A. Dmitriev[2], K. Komarov[1], F. Sanchez[3]

[1] Institute of Automation and Electrometry, Russian Academy of Sciences, Acad. Koptyug Pr. 1, 630090 Novosibirsk, Russia
[2] Novosibirsk State Technical University, K. Marx Pr. 20, 630092 Novosibirsk, Russia
[3] Laboratoire de Photonique d'Angers EA 4644, Universitŭ d'Angers, 2 Bd Lavoisier, 49000 Angers, France
E-mail address: komarov@iae.nsk.su

We present results of a numerical simulation of multipulse passive mode locking and also a single pulse operation for the purpose of a creation of high-energy pulses in the laser cavity. Our results on the multipulse regimes include the multihysteresis dependences of a number of pulses in the laser cavity, of pulse peak intensities and an intracavity radiation energy on a pump power. The analysis of mechanisms of an interpulse interaction in the laser cavity has been performed. It is shown, that the strongest interaction is realized through the dispersive waves which are emitted by solitons because of the impact of intracavity lumped elements. The properties of the bound steady-states of various soliton structures have been investigated. The opportunity of the coding of information with the use of bound soliton sequences has been demonstrated. Various mechanisms for a realization of intersoliton repulsion in the laser resonator are proposed. As consequence of pulse repulsion a harmonic passive mode-locking is realized. We put forward a way to realize harmonic passive mode-locking in fiber lasers with an ultrahigh-repetition-rate pulse train. In this case, the equidistant distribution of ultrashort pulses filling the total laser cavity is due to bound-soliton mechanism. For large bound energy such long soliton train is very stable and has the ideal periodic structure as a soliton crystal. Such ultrashort optical pulse sources with a high repetition rate are a key element in high-speed optical communications and are also of primary importance in a number of other applications.

Another object of our investigation is the generation of high-energy pulses in the laser cavity. The key obstacle for the generation of such pulses is a multipulse operation due to the quantization of radiation into identical solitons. In consequence of this phenomenon, an increase of pumping results in an increase of the number of intracavity pulses, thus their energy remains the same. We have found how to suppress a multipulse operation and to realize a lasing regime with single high-energy pulse.

For our analysis we use the following master equation [1,2]

$$\frac{\partial E}{\partial \zeta} = (D_r + iD_i)\frac{\partial^2 E}{\partial \tau^2} + \left(\frac{a}{1 + b\int I d\tau} - \sigma_0 + (p + iq)I - (p_2 + iq_2)I^2 \right) E, \qquad (1)$$

where E, ζ, τ are the dimensionless field amplitude, the coordinate, and the time, respectively; D_r, D_i are the gain-loss and group velocity dispersions; a is the pump power, b is the gain saturation parameter, $I = |E|^2$, σ_0 is associated to the linear losses, p and p_2 are nonlinearities of losses, q and q_2 are the Kerr nonlinearities.

Figure 1 shows the dependences of a number of identical intracavity pulses in a steady state operation on a pump power a for the focusing nonlinearity q and various values of the normal dispersion D_i. In the case of the dissipative soliton resonance (see Fig. 1(c)), the number of pulses depends on initial conditions, but it does not change with increasing pump power. The generation is multistable. All pulses have identical parameters (a form, a peak intensity, a spectrum, and so on).

In the case of the dissipative soliton resonance, the peak intensity of the individual steady-state pulse initially increases with increasing intensity, then it does not vary, while its

bell-shaped form transforms into a rectangle one (Fig. 2(a)). The further increase of pumping a results in a monotonous increase in width of the rectangle pulse. Such transformation of a stationary pulse is connected with the stabilizing quadratic nonlinearity of losses p_2 in Eq. (1). The pulse energy also monotonously increases.

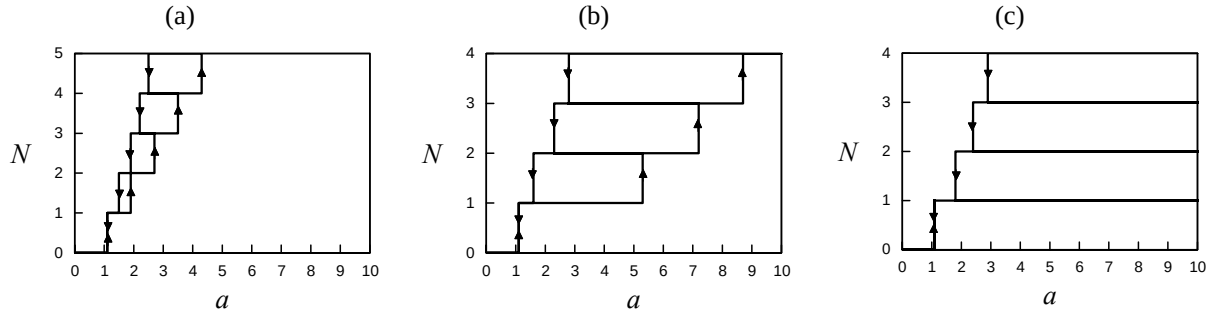

Fig. 1. Dependences of the number of pulses N on the pump power a. (a, b) Dissipative soliton resonance is absent, $D_i = -20$ and -25. (c) Dissipative soliton resonance, $D_i = -28$. In both cases $D_r = 1$, $p = 1$, $q = 18$, $\sigma_0 = 1$, $p_2 = 3$, $q_2 = 0$, $b = 0{,}01$.

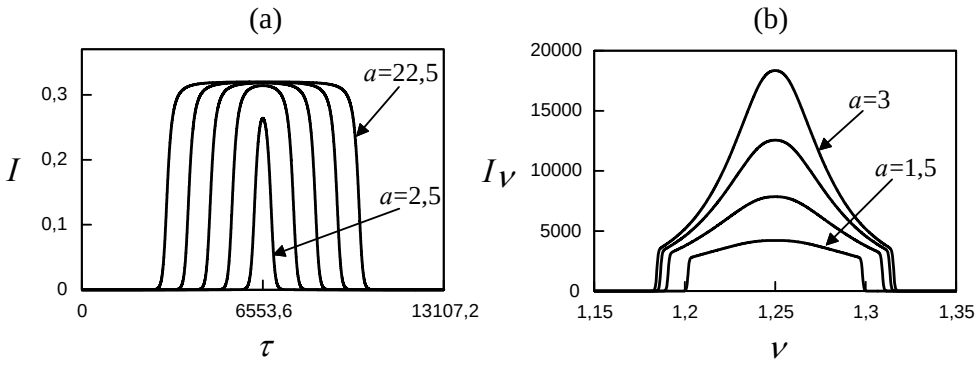

Fig. 2. Dependences of the temporal (a) and spectral (b) profiles of a steady-state pulse on the pump power a. The laser parameters are the same as in Fig. 1(b).

The increase of a pump power results in transformation of the rectangle spectral profile into the bell-shaped one (Fig. 2 (b)). The rectangle part of spectrum is due to soliton wings with strong gradients of intensity resulting in a great frequency chirp. While in the central part of a rectangle pulse the gradient of intensity is small; consequently, the frequency variation is also small. Therefore, this part of the pulse forms a narrow-band bell-shaped fraction in spectrum. As a result, the central part of the pulse interacts resonantly with a gain medium and effectively depletes the gain. In this case the amplification outside of a pulse volume is negative, that prevents an appearance of new pulses from spontaneous laser radiation with increasing pump power**.** As a result, with increasing pumping the number of pulses is kept, and the energy of an individual pulse can be arbitrarily large under a corresponding level of pumping. The smaller nonlinearities of refractive index and the greater values of a normal dispersion promote a realization of a dissipative soliton resonance. This phenomenon opens up fresh opportunities to design high-energy pulse lasers.

References

1. A. Komarov, F. Armani, A. Dmitriev, K. Komarov, D. Meshcheriakov, F. Sanchez, *Phys. Rev. A* **85**, 013802 (2012).
2. A. Komarov, F. Armani, A. Dmitriev, K. Komarov, F. Sanchez, *Phys. Rev. A* **87,** 023838 (2013).

Hybrid highly-nonlinear fiber for spectral supercontinuum generation

I.I. Korel[1,2], B.N. Nyushkov[1,2], V.I. Denisov[1], V.S. Pivtsov[1,2], N.A. Koliada[1], A.A. Sysolyatin[3]

[1] *Institute of Laser Physics of SB RAS, Lavrentyev Str. 13/3, Novosibirsk, 630090 Russia*
[2] *Novosibirsk State Technical University, Karl Marx Str., 20, Novosibirsk, 630073 Russia*
[3] *Prokhorov General Physics Institute of RAS, Vavilov Str., 38, Moscow, 119991 Russia*
E-mail: ikorel@gmail.com

Spectral supercontinuum (SC) generation in highly-nonlinear fibers (HNLF) is a well-studied subject that underlies an effective approach to obtaining ultra-wide femtosecond optical frequency combs [1]. However, there are still some problems to adopt such a method for special femtosecond laser systems with restricted performance capabilities. It concerns, for instance, mobile versions of femtosecond optical clocks [2], when the requirements of miniaturization and low power consumption along with a short HNLF length impede octave-spanning SC generation. In particular, it is hardly possible to obtain a coherent SC, spanning the range from 1000 nm (or less) to 2000 nm (or more), in a conventional HNLF with a short length (≤1 m) when pumping the fiber directly by a low-power femtosecond erbium fiber laser at 1560 nm. Such a compact laser, when used as a master oscillator in a femtosecond clock, unfortunately has to be assisted by a low-noise high-gain erbium-doped fiber amplifier (EDFA) in order to enable octave SC generation in a relatively short piece of HNLF. The HNLF length restriction arises from the requirement of high coherence and low phase noise along the edges of the generated SC.

Another issue is obtaining of SC with a high signal-to-noise ratio at a selected wavelength which matches with an optical standard of particular interest. For instance, the mobile erbium-fiber-based femtosecond clocks, that are under construction in the Institute of laser physics (Novosibirsk), require alternative locking of the femtosecond frequency comb to an optical standard at 1064 nm (Nd:YAG/I_2), or 1030 nm (Yb:YAG/I_2), or 934 nm (Yb^+). These wavelengths are on the very edge of achievable SC.

In this paper we present a further elaboration of the recent concept of hybrid HNLFs [3] that shall allow fulfilling the above tasks and meeting the specific requirements. It is known that lengthwise management of HNLF parameters (mainly of chromatic dispersion) allows fine control and optimization of SC generation (i.e. profiling of energy distribution in the SC). However well-known dispersion decreasing fibers (DDFs) of that sort [4] have a longitudinal gradient, which is too low to provide reasonable dispersion variation on the scale of less than 1 meter. Therefore we propose and consider a special case, when the required SC is generated in a hybrid dispersion-managed HNLF. This fiber is composed of four spliced 25-cm-long fiber segments with sufficiently different dispersion parameters.

Calculations were performed by use of nonlinear Shrodinger equation that was integrated consequently for each of the fiber samples. Numerical model shows a number of interesting SC generation regimes. Thus, if hybrid HNLF is consisted of few pieces with zero dispersion wavelength shifted in short-wave region, we managed (at least numerically) to obtain an octave SC from 900 to 2200 nm (Fig. 1), while spectral broadening in HNLF of the same length, but with stable dispersion gives SC up to 2 times narrower. This regime is especially interesting since there is a need for a stable signal in the range of 1000 nm.

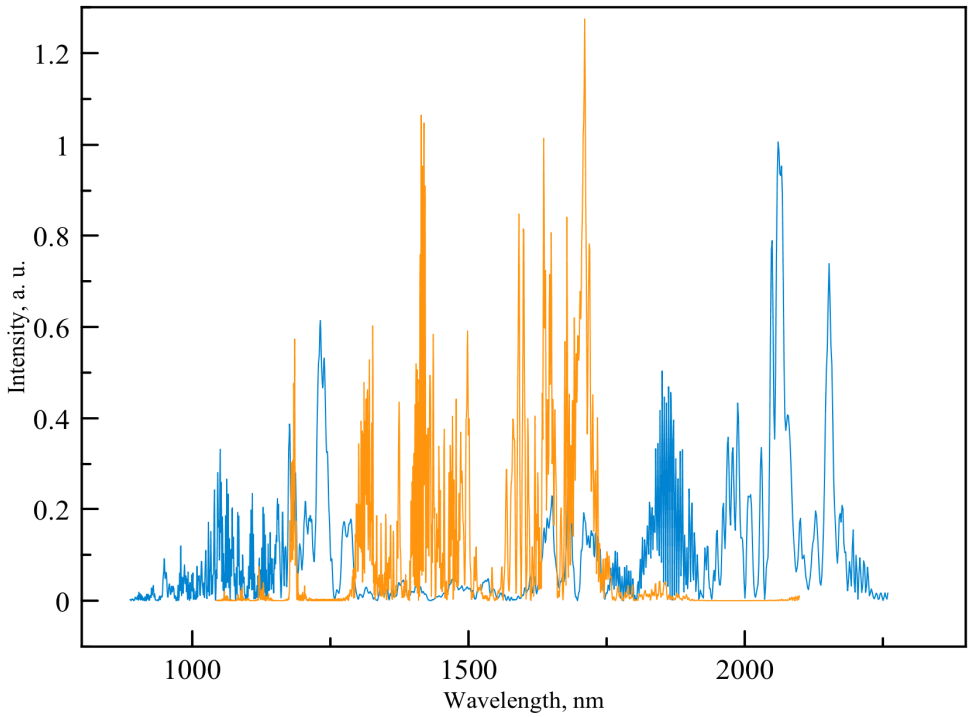

Fig.1. Numerical calculation of spectral supercontinuum, generated in hybrid HNLF with shifted zero dispersion wavelength. Central wavelength 1560 nm, P=100 mW. Blue curve corresponds to the SC calculated in hybrid HNLF, yellow curve – to SC in a straight HNLF.

SC shown on Figure 1 (blue curve) was calculated for a hybrid fiber consisted of four fibers welded one after another. Each fragment was 25 cm long, first sample had a zero dispersion wavelength close to the central wavelength – 1560 nm, the next sample had two zero dispersion points: 1350 and 1750 nm, two last samples had zero dispersion on 1150 nm and 1900 nm. For a comparison, the yellow curve shows spectral broadening in a straight 1 meter long HNLF with parameters close to the ones of the first fragment. Simple explanation of this efficient spectral broadening can be done by a model with separated nonlinear and dispersion effects. The strongest spectral broadening occurs if intensity (nonlinearity) is high and dispersion is small. That is why we can profile the SC generation efficiency by use of HNLF with certain dispersion parameters on the certain places of the hybrid fiber.

Thus, we have proposed and examined a novel design of a short-length dispersion-managed hybrid HNLF, which is intended for low-noise wideband supercontinuum generation with controlled energy distribution over the range 1÷2 microns. Such a HNLF may greatly facilitate developing of mobile femtosecond optical clocks.

The work was supported by the Russian Foundation for Basic Research (grant No 11-02-00771-a) and grant of the President of Russia (NSh-1549.2012.2).

References

1. S.N. Bagaev, V.I. Denisov, I.I. Korel', S.A. Kuznetsov, V.S. Pivtsov, S.V. Chepurov, E.M. Dianov., A.K. Senatorov, A.A. Sysolyatin, A.Yu. Plotskiĭ, *Journal of Experimental and Theoretical Physics* **105**, 881-885 (2007).
2. S.N. Bagayev, V.I. Denisov, V.M. Klementyev, I.I. Korel, S.A. Kuznetsov, V.S. Pivtsov, V.F. Zakharyash, *Laser Physics* **14**, 1-8 (2004).
3. Takashi Hori, Jun Takayanagi, Norihiko Nishizawa, and Toshio Goto, *Opt. Express* **12**, 317-324 (2004).
4. A.A. Sysoliatin, U.G. Achmetshin, S.V. Muraviev, A.V. Kirsanov, *Laser Physics* **15**, 1288-1291 (2005).

Laser-induced formation of semiconductor nanoparticles and structures

A. Antipov[a], S. Arakelian[a], V. Emelianov[b], S. Zimin[c], S. Kutrovskaya[a], A. Kucherik[a], A. Makarov, A. Osipov[a]

[a]Russia, Vladimir State University named after Alexander Grigorievich and Nikolai Grigorievich Stoletovs", Vladimir, Gorkii st. 87, 600000

[b] Russia, Lomonosov's Moscow State University, Moscow

[c] Russia, Yaroslavl State University named after P.G.Demidov

E-mail: kucherik@vlsu.ru

A nanostructured state of the narrow-gap semiconductors PbSe (band gap Eg=0.29 eV), PbTe (0.32 eV) and PbS (0.41 eV) is of interest for gaining insight into quantum size effects in relatively large systems, tens of nanometres in dimensions [1]. Nanostructures based on PbTe, PbSe, PbS and their solid solutions can be produced by a variety of techniques [1 - 3], including laser and laser-plasma deposition processes, which are of practical importance. Both below-band-gap ($\hbar\omega < Eg$) and above-band-gap ($\hbar\omega > Eg$) laser radiation, in different modes (e.g., laser ablation and/or heating), effectively changes the structural and electrical properties of the lead chalcogenides, producing micro- and nanostructures.

Laser exposure of semiconductor and metal surfaces is a promising technique for producing nanoparticle ensembles with tailored geometric characteristics (characteristic size and size distribution of the nanoparticles). To this end, a metallic or semiconductor target is typically ablated by high-power femto- (Si) [4], pico- (Ta) [5] or nanosecond (CdTe) [6] laser pulses.

In the first series of experiment we used the PbSe(Te)/CaF2/Si(111). The thickness of the PbSe(Te) film was varied from 0.3 to 4 mkm.

A Nd : YAG laser beam (CW-laser, 5 to 15 W output power, $\lambda = 1.06$ mm) was focused to a spot diameter of 30 mm on the sample surface. The incident power density was thus 10^4 to 10^5 Wcm^{-2}. During the laser exposure, the sample was scanned with the laser beam on a positioning stage, which was translated at 80 mm s^{-1}. The laser-exposed zone on the sample surface was examined in real time using a laser monitor, which allowed us to directly control the exposure conditions.

We studied solid-state laser modification of the surface of PbX semiconductor films and identified surface self-organization at photon energies above the band gap of the semiconductor [7,8]. Experimental data were used to construct a model for defect-deformation instability developing on the surface of an epitaxial film through strain-induced drift of laser-induced point defects. The model is capable of qualitatively describing the observed surface morphology and predicting the surface profile in laser modification experiments.

In the second series of experiments the method of producing semiconductor nanoparticles of lead chalcogenides with an average size of 5 -50nm by continuous laser radiation of a moderate intensity near-by infrared range (up to $10^6 W/cm^2$) has been proposed [9]. The method of laser ablation in liquids has been used for obtaining colloid systems; ethanol (C2H5OH) and glycerin (C3H5(OH)3) having been used as solvents.

The sizes of the particles obtained were determined by means of the particle size analyzer Horiba LB-550; the principle of its operation relying on the phenomenon of dynamic light scattering. The analyzer is designed for measuring particles in the range from 3nm to 6 micrometers. Table 1 gives average values of a middle-size semiconductor particle calculated on the basis of six successive measurements with the time difference of one minute. There was no shift of the histogram of the particle size distribution which is the evidence of the colloid solution stability and of a spherical shape of nanoparticles being formed.

The results of Table 1 indicate that in all cases the size of nanoparticles obtained in glycerin is less than of those obtained in ethanol. Thus, solvent viscosity has a great effect on the kinetic processes of nanocrystal formation.

Table 1. Average size of colloidal particles obtained from the targets in solutions

Solution	Target	Intensity W/cm^2	Average size of colloidal particles, R_0, nm
C3H5(OH)3	PbS	10^4-10^6	6-26
C2H5OH	PbS	10^4-10^6	5-18
C3H5(OH)3	PbTe	10^4-10^6	6-30
C2H5OH	PbTe	10^4-10^6	4-13

The paper represents the results of laser synthesis of semiconductor nanoparticles of lead chalcogenides. The method of laser evaporation in liquid was used for obtaining nanoparticles. The way proposed for obtaining nanoparticles under the action of continuous laser radiation has shown that nanoparticles can be quantum dots by their geometric properties. The method of drop deposition used for shaping a deposited layer consisting of quantum dots has been considered. It has been demonstrated that the given method enables to obtain structures with various morphology which depends on the substrate temperature. Later, optical and electro-physical properties of the obtained structures will be studied which is very important for their use in the devices of optoelectronics and photonics.

1. Mukherjee S., Li D., Kar A.G.J., Shi Z. Transworld Research Network (Kerala, India, 2010) p. 88.
2. Abtin L., Springholz G., Holy V. Phys. Rev. Lett., 97, 266103 (2006).
3. Zimin S.P., Gorlachev E.S., Amirov I.I., Zogg H. J. Phys. D:Appl. Phys., 42, 165205 (2009).
4. Shen M.Y., Crouch C.H., Carey J.E., Mazur E. Appl. Phys. Lett., 85, 5694 (2004).
5. Barmina E.V., Barberoglu M., Zorba V., Simakin A.V., Stratakis E., Fotakis C., Shafeev G.A. Kvantovaya Elektron., 39, 89 (2009) [Quantum Electron., 39, 89 (2009)].
6. Baidullaeva A., Vlasenko A.I., Kuzan L.F., Litvin O.S., Mozol' P.E. Fiz. Tekh. Poluprovodn., 39, 1064 (2005).
7. A.A.Antipov, S.M.Arakelyan, V.I.Emel'yanov, S.P.Zimin, S.V.Kutrovskaya, A.O.Kucherik, V.G.Prokoshev. Quantum Electronics, 41, 735 (2011).
8. A.A.Antipov, S.M.Arakelyan, V.I.Emel'yanov, S.P.Zimin, S.V. Kutrovskaya, A.O. Kucherik, V.G.Prokoshev. Quantum Electronics, 41, 441 (2011).
9. Antipov A.A., Arakelian S.M., Zimin S.P., Kutrovskaya S.V., Kucherik A.O., Osipov A.V., Prokoshev V.G. Laser formation of semiconductor coatings using droplet technology. // Physics Procedia 39 (2012) 401-408

Anisotropic deformation of the photonic crystal lattice as a base of a highly sensitive selective optical chemosensor

A.S. Kuchyanov[1], A.I. Plekhanov[1], H. Spisser[2], P.A. Chubakov[1]

[1]Institute of Automation and Electrometry of SB RAS,Pr. Acad. Koptyug, 1, Novosibirsk, 630090 Russia
[2] Institut d'Optique Graduate School, Campus Polytechnique, 2 Avenue Augustin Fresnel, 91127 Palaiseau cedex, France

Photonic crystals (PhCs) are the subject of the interest both from a fundamental point of view, and for practical applications. Silica PhCs provide a new opportunity for the methods of optical detection of liquid and gaseous substances in a wide range of applications due to its properties: high internal surface, small size, high sensitivity and resistance to aggressive environments.

The numerous applications of sensors based on the PhC for measurement of the spectral position of the photonic band gap as a function of pore filling various substances. These changes are caused either by changing the effective refractive index of PhC or change of the lattice constant due to its deformation.

The angular spectrum of light reflected from the interface between glass and PhC is made up of several components: the diffraction spectrum by reflection from the boundary layer of the monodisperse spherical silica particles (MSSPs), and the spectrum of the Bragg reflection from the crystal planes $(\bar{1}11), (1\bar{1}1), (11\bar{1})$ at an angle of 60^0 to the substrate plane (band gap). We have observed the peak of spectral-angular distribution of reflection from the glass-PhC interface.

It should be noted that if a light is arrived at the PhC from an air even at an incidence angle close to 90^0, the reflected light from these surfaces does not observed because total internal reflection. Obviously, this is one of the reasons that the effect described in this paper has not been observed.

When PhC pores are filled of polar molecules (ammonia or water), this peak is shifted by 5^0 (i.e. 10 nm wavelength range). This effect we have observed for the first time, as far as we know. Importantly, this shift can be easily observed without resorting to a spectral instrument.

In our opinion, the explanation for this effect is as follows. An adsorption of the polar molecules on the surface of MSSPs leads to a capillary condensation. It leads to the change a distance between the MSSPs. We have experimentally found that such a change occurs only across the film PhC. We have carried out experimental verification of the anisotropy changes in the distance between MSSPs constituting PhC due to capillary condensation.

We propose to use this effect for the development of relatively low-cost tech optical sensor of such gases as ammonia and water.

A film of opal-like PhC has been grown on one of the faces of a glass prism. The glass prism was used to provide a wide range of angles of incidence on the glass – PhC interface. The PhC films have been prepared by a convective self-assembly technology in a suspension of MSSPs with a diameter of 260 nm. The film thickness was determined to be 30 layers of MSSP. The PhC film grown by this method has a minimum number of defects in a large area. The film size is 15x25 mm. The response signal to the ammonia formed in the following manner. The white light diffracted at the glass-PhC interface arrives on two photodetectors placed at the angles corresponding to the rise and fall of the curve of spectral - angular distribution. The signals from them change in opposition because of the curve shift during analyte vapor condensation.

The sensitivity of the device reaches a few ppm (fig.1).

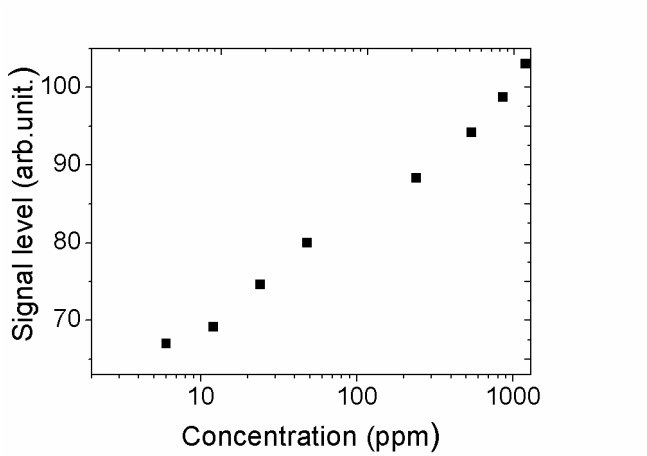

Fig. 1. The dependence of the signal on the concentration of ammonia vapor.

With a laser with a narrow spectrum this approach leads to an angular width of the curve of 1.5^0 what is a sharp steepness for the slopes, and the sensitivity of the sensor can be improved by nearly two orders of magnitude.

Low cost and ease of fabrication of sensors, the response of which can be easily observed without resorting to the spectral instrument it is very attractive.

Components of femtosecond laser system based on diode pumped Yb-doped media

A.V. Laptev, V.V. Petrov, G.V. Kuptsov, V.A. Petrov, E.V. Pestryakov

Institute of Laser Physics of SB RAS, Pr. Lavrentyeva 13/3, Novosibirsk, 630090 Russia
E-mail: alaptev@laser.nsc.ru

In the recent years many researchers are devoted to the development of femtosecond solid-state lasers systems based on chirped-pulse amplification technique and as consequence to generation of high-peak-power ultrashort pulses. Among known laser media ones of promising media for high power operation are crystals and ceramics doped with ytterbium ions. These media have simple schemes of energy levels, free of up-conversion, excited state absorption and concentration quenching, and due to their low quantum defects, they have low thermal loading.

It is known that for amplification of laser pulses with duration near 100 fs to the terawatt peak power level it is necessary to minimize nonlinear effects and the risk of amplifier damage by use of the technique of chirped pulse amplification (CPA). The principle of CPA systems is amplification of stretched input pulses to high energy and then to compress pulse to initial duration, with a minimum of residual pedestal. For achievement it is necessary to compensate phase deviation up to forth order of group velocity dispersion introduced during the stretching and amplification processes by using a matched pulse compressor. The uncompensated chirp results in a decrease of the achievable pulse contrast and imperfect recompression of the pulse [1].

Laser system is being developed in our laboratory is based on diode pumped Yb^{3+}-doped ceramics and crystals ($Yb:Y_2O_3$, Yb:KYW and others) [2]. The system consists of pump channel and amplification channel which are optically synchronized. Master oscillator (λ = 1030 nm) is based on diode-pumped $Yb:Y_2O_3$ ceramics with repetition rate about 100 MHz and pulse duration 160-180 fs, then radiation is divided to two channels. In pump channel stretcher, regenerative amplifier, cryogenic multicascade amplifier system, compressor, nonlinear crystal LBO are arranged. Passing after pump channel radiation enters to parametric amplifier of amplification channel for pumping of nonlinear crystal. Amplification channel consists of high non-linear photonic crystal fiber for broadening of a gain bandwidth to ~ 400 nm (which corresponds to pulse duration 7 fs), stretcher, parametric amplifier based on LBO crystal and compressor. The planned parameters in the output of the amplification channel are pulse duration 5-7 fs, pulse energy 5-7 mJ, repetition rate 1 kHz and output power 1 TW.

In our researches the system of stretcher-compressor base on diffraction gratings for pump and amplification channel were calculated and designed. Determined the conditions of phase compensation up to forth order of group velocity dispersion. Experimental data of broadening of gain spectrum of master oscillator were presented. Obtain results are used in creation of terawatt femtosecond laser system with high pulse repetition rate.

This work is supported by RAS Program “Extreme light fields” and by The Ministry of education and science of Russian Federation, project 8387.

References

1. G. Cheriaux, P. Rousseau, F. Salin, and J.P. Chambaret, *Optics Letters*, **21**, 414, (1996)
2. V.V.Petrov, E.V.Pestryakov, V.I. Trunov, A.V. Kirpichnikov, M.A. Merzliakov, A.V.Laptev, *Atmospheric and Oceanic Optics*, **25**, 285 (2012)

Laser fluorescence spectroscopy of radiation defects in sapphire crystals irradiated with fast neutrons

N.L. Lazareva[1,2], A.L. Rakevich[1], E.F. Martynovich[1,2]

[1]Irkutsk Branch of Institute of Laser Physics SB RAS,
130a Lermontov Str., Irkutsk, 664033 Russia,
[2]Irkutsk State University, 20, Gagarin Blvd, Irkutsk, 664003 Russia
filial@ilph.irk.ru

A single-crystal sapphire (leucosapphire, corundum, α-Al_2O_3) is a high-tech material of a wide range of scientific and industrial applications.

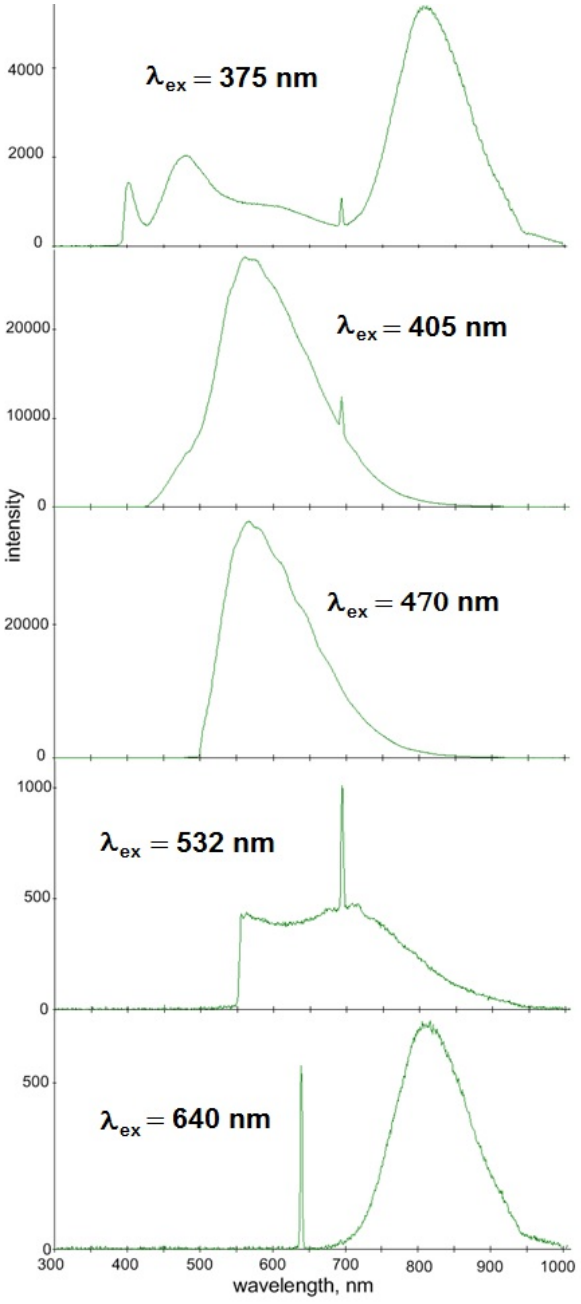

Fig. 1. The luminescence spectra of one of the sapphire samples, which has been investigated.

Radiation-induced defects in it are the working centers of luminescent materials, laser media, saturable absorbing optical materials, radiation detectors, optical storage media [1-3]. In this work we investigated the spectral and temporal characteristics of luminescence of color centers created by neutron irradiation. The investigated samples were grown by horizontal directional crystallization and irradiated in the active zone of the research nuclear reactor IR-8 of NRC "Kurchatov Institute". Fluence of fast neutron varied in the range 10^{16} - 10^{19} neutron/cm^2. Studies of the kinetics and luminescence spectra performed with a laser scanning confocal fluorescence microscope MicroTime 200 (Picoquant Gmbh), staffed by fluorescent spectrometer Ocean Optics 65000. Picosecond lasers with a wavelength of 375, 405, 470, 532 and 640 nm were used for luminescence excitation. The spectra were recorded through interference filters with a special spectral response for suppression or attenuation of the exciting radiation scattered by the sample. Luminescence kinetics was studied by time-correlated single photon counting method. Experimental data on the number of fluorescent photons and the time of their arrival after the excitation processed by SymPhoTime 64 software package for the separation of total emission into separate time components. Next found time components of luminescence compared with the registered spectral bands and with luminescence quantum transitions responsible for them in color centers created

by neutron irradiation.

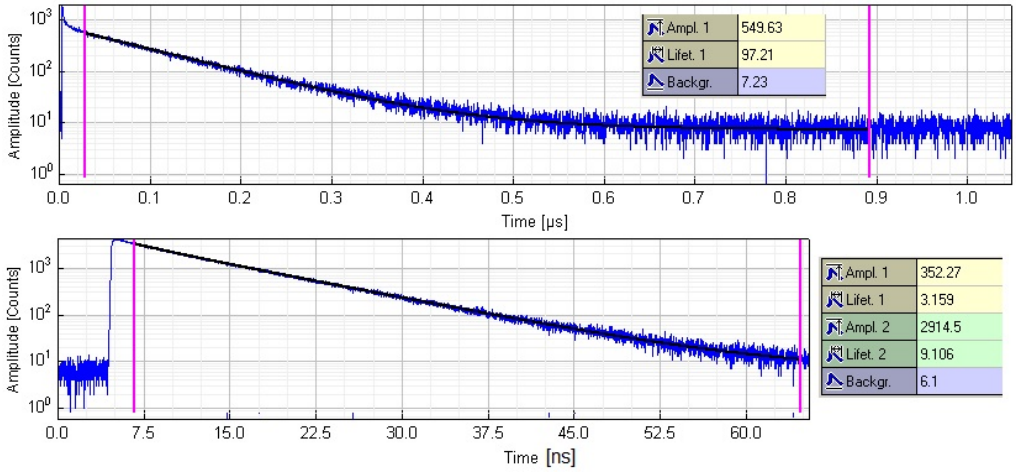

Fig. 2. The kinetics of rise and decay of luminescence intensity with the picosecond excitation, λ_{ex}= 640 и 470 nm

Tab. 1. The maxima of spectral bands and the decay time constants of the sapphire color centers luminescence

$\lambda_Л$, нм	τ, нс, 300 K	Источ-ник
1180	43	[1]
990	60	[1]
830	94	[1]
830	97	
750	80	[4]
710	1,0	
600	5,7	
560	9,1	
550	9	[1]
520	9	[4]
480	17	
386	0,4	
330	5	[4]

Fig. 1 shows one example of the luminescence spectra of the samples excited by a picosecond laser light with the above wavelengths. In addition to the spectral emission bands of color centers in the spectra exhibit a narrow line luminescence of impurity chromium ions Cr^{3+}, $\lambda = 694$ nm. The samples were measured of kinetic curves of rise and decay of the integral intensity shown in Fig. 2. The results of the decomposition of the integral intensity in the individual time components are shown in the insets in the same place. The values of the decay time constant and numbers of photons belonging to the individual components of the temporary shows.

Table 1 summarizes the data on the values of the wavelengths of spectral maxima of the luminescence bands of sapphire color centers and luminescence decay time constants in these bands. The results obtained in this study are compared with the results of previous studies noted in the table the bibliographic references. The relationship between spectral bands and temporal components of the luminescence was analyzed. Energy levels and the quantum transitions schemes are built for the color centers that fluoresce in spectral range of 300-1300 nm.

The research was supported by the Presidium of RAS (Programme No. 13, project № 4.12) and by the Siberian Branch of RAS (Programme No. II.8.1, project № 6).

References

1. E.F. Martynovich. Color Centers in Laser Crystals. Irkutsk: Publishing House of the ISU, 2004, 227 p. (in Russian).
2. Mark S. Akselrod, Frank J. Bruni. Modern trends in crystal growth and new applications of sapphire. Journal of Crystal Growth, Volume 360, 1 December 2012, p. 134–145.
3. E.F. Martynovich, A.V.Kuznetsov, D.V.Baliunov, S.N.Bagayev. Optical storage media. Patent RU 85027 U1, 24.11.2008 (in Russian).
4. Mark S. Akselrod. Patent US 6846434. Aluminum oxide material for optical data storage. January 25, 2005.

Organic nanocrystal semiconductors towards luminescent devices and organic lasers

Z.-Q. Lin, S.-H. Yang, L.-H. Xie, W. Huang

Center for Molecular Systems and Organic Devices (CMSOD), Key Laboratory for Organic Electronics & Information Displays (KLOEID) and Institute of Advanced Materials (IAM), Nanjing University of Posts & Telecommunications, 9 Wenyuan Road, Nanjing 210046, China

The cruciform spirocyclic aromatic hydrocarbons (SAHs) is a promising candidate to form various uniform nanodisk and polyhedral organic semiconductive micro/nano-crystal through manipulating the supramolecular interactions in slefassembly. The clean cut of crystal surface and well-defined morphology provides an unexplored opportunity in constructing the organic electroluminescence and laser devices.

Principles of generation of laser radiation on the prepared magnetomultipolar transition

V.P. Lopasov

[1] *V.E. Zuev Institute of Atmospheric Optics SB RAS 1, Academician Zuev square Tomsk 634021 Russia*
E-mail: lopas@iao.ru

Principles of self-organization in the molecular gas of an ensemble of diamagnetic optically active electron-ion nanoparticles on the prepared magnetomultipolar transition are substantiated. It is shown how self-generation of radiation with anomalous magnetooptical properties is excited at the frequency of magnetotomultipolar transition.

The probability of electric dipole transitions of molecules is by six orders of magnitude higher than the probability of magnetic dipole transitions [1]. Within the framework of the electric dipole approximation, it is impossible to obtain lasing on the magnetic dipole and magnetic multipole transitions. Haken in 1980 proposed an approach that allows space-time ordering of elements to be implemented in the open system of many elements due to their coordinated interaction among themselves and with the control field.

This approach can radically increase the probability of the magnetic multipole transition of molecules in the molecular gas if the conditions for the implementation of Fermat's principle, "coherent superposition," and two-dimensional (in time and space) feedback between the Stark and Zeeman energies by the V-scheme of vibrational-rotational transitions have been created in the control field of the biharmonic light wave. The feedback mechanism changes resonantly the polarizability and diamagnetic susceptibility of molecules during their elastic collisions with particles in the coherence volume occupied by photons of the biharmonic light wave absorbing molecules and broadening particles.

In the region of the magnetic multipole transition of molecules, the magnetomultipolar transition is being prepared on which the ensemble of optically active electron-ion nanoparticles is self-organized. The ensemble of nanoparticles is ordered in the space-time coordinates and takes the shape of an "optical resonator coil" and diamagnetic properties of the photonic crystal.

At the frequency of the prepared magnetomultipole transition of the ensemble of nanoparticles, the spin-flip self-generation with high-order coherence, screw wave front, and large orbital angular momentum is excited [2].

References

1. El'yashevich M.A. Atomic and Molecular Spectroscopy. Moscow, 892 pp. (1962)
2. Lopasov V.P., Applied Physics, No. 4, 24 (2012)

Selective enhancement of photoluminescence due to exciton-plasmon interaction in the hybrid system quantum dot – metal droplet grown by MBE

A.A. Lyamkina, S.P. Moshchenko

Rzhanov Institute of Semiconductor Physics, Novosibirsk 630090, Russia
Email: lyamkina@isp.nsc.ru

Efficiency increase and control of optical properties of quantum emitters is a challenge in modern nanotechnology. Quantum dots (QDs) have received much attention because they are key elements for diverse advanced devices such as single photon source etc. An efficient approach is to use metal nanoparticles as nanoantennas for QDs. It is well known that under the effect of light the oscillations of the electron density near the metal-dielectric interface can be excited in the form of localized surface plasmons. The local enhancement of the plasmon electrical field near the particle increases the rate of spontaneous recombination in the QD due to the Purcell effect [1]. Therefore, the coupling of the QD with a metal particle increases the efficiency of the emitter.

To realize the coupling we propose to use the ensemble of metal droplets that are the initial stage of the droplet epitaxy. It is a promising technique of QD fabrication based on preliminary formation of metal droplets on the substrate [2] and thus its initial stage can be used for metal particle fabrication. It is known that QDs layers grown close enough tend to align vertically and form stacks due to the distribution of elastic tension in the matrix [3]. The substitution of an upper layer of QDs with droplets should lead to the same self-alignment i.e. the formation of a droplet just over a QD. Despite of a random position of the pair, such approach fixes the distance between QD and droplet and therefore allows controlling their interaction precisely by adjusting the buffer layer thickness. The important advantage of this method is the full compatibility with the MBE technique used for QD growth.

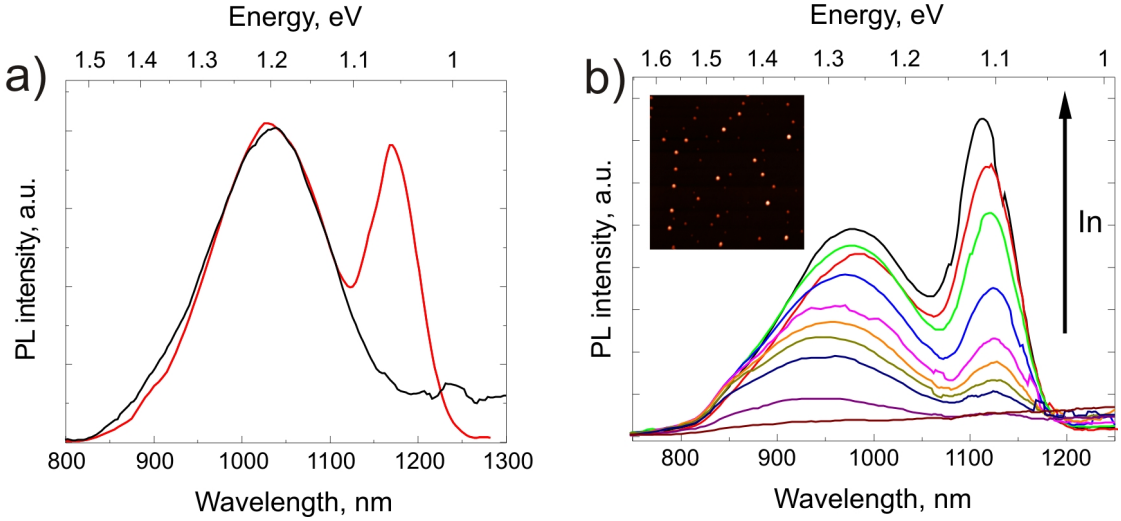

Fig.1 a) Spectra of QD and MD structures shown in black and red respectively; b) spectra of MD2 structure for increasing QD sizes. Inset is an AFM image 10x10 μm

To investigate the interaction of plasmons in the droplet with excitons of QDs, we grew a structure containing a layer of buried InAs/AlGaAs QDs with indium droplets on top (the MD structure). A reference sample with the same structure but QDs on top was grown (the QD structure). PL spectrum of the QD structure demonstrates only the wide peak corresponding to QDs (Fig. 1a). In the spectrum of MD structure this peak is accompanied by

an additional narrow one which we attribute to the interaction of QD excitons with the plasmon mode of the droplet. Perfect agreement in QD peak positions of both structures additionally confirms the identity of the growth conditions.

The presence of the additional peak can be explained with the resonant interaction of QD excitons with the plasmon mode of the droplet. A long-wavelength part of the wide size distribution of QDs that located under the droplets is in resonance with the surface plasmons in droplets. Due to Purcell effect the spontaneous recombination rate increases, especially in the largest QD being the closest to the plasmon particle. Via plasmon-mediated mechanism [4] the excitation can be efficiently transmitted nonradiatively from QDs surrounding to the QD with the lowest radiative life time. This would result in the enhanced PL for a QD subensemble as shown in Fig. 1a.

To study this interaction more thoroughly a structure with varying QD sizes was grown. No rotation was applied during the QD growth, resulting in an increasing In amount and thus QD size along one axis. Uniform indium droplets were formed on the top of this structure (MD2). A typical 10x10 μm AFM image is presented in the inset in Fig. 1b revealing the droplet density of $5 \cdot 10^7$ cm^{-2}. The spectra taken along the gradient with the increase of QD sizes are shown in Fig.1b. The QD band redshifts and its intensity increases significantly, corresponding to the increase of QD size and density. Meanwhile the enhanced (plasmon) band is independent of the QD band position. It indicates that the interaction between QDs and plasmons is highly selective and the enhancement takes place when the emission of QDs is in resonance with LSP. Therefore the demonstrated exciton-plasmon interaction could be tuned with the position of localized plasmon resonance presenting an important instrument for the control of QD properties.

The work was supported by the RFBR (13-02-00959). AAL acknowledges the financial support via RF president scholarship (SP-805.2013.3).

References

1. E.M. Purcell, *Phys. Rev*. **69**, 681 (1946).
2. N. Koguchi, S. Takahashi and T. Chikyow*, J. Cryst. Growth* **111**, 688 (1991).
3. V.A. Shchukin, D. Bimberg, V.G. Malyshkin, N.N. Ledentsov, *Phys. Rev. B* **57**, 19 (1998).
4. V.N. Pustovit and T.V. Shahbazyan, *Phys. Rev. B* **83**, 085427 (2011).

Color centers creation in LiF crystals under the action of VUV radiation of barrier discharge

E.V Milyutina[1,2], A.F. Petrovskiy[1], A.L. Rakevich[1], E.F. Martynovich[1,2]

[1] Irkutsk Branch of Institute of Laser Physics SB RAS, Lermontov str., 130a, Irkutsk, 664033, Russia
[2]Irkutsky State University, 664003, Irkutsk, Gagarin Blvd, 20
E-mail: filial@ilph.irk.ru

A number of laser technology using color centers in thin layers or films of lithium fluoride is described in literature. Thin-film records the information by various methods, for example by laser spectral hole burning in the inhomogeneously broadened spectral loop [1]. Direct recording micro text on a thin layer of single crystal by using extremely short wave ultraviolet (13.5 nm) of the laser-induced plasma, focused by a Schwarzschild objective was implemented [2]. There are other applications associated with color centers [3].

In the present paper, for the best of our knowledge, the possibility of creating color centers in thin layers on the surface of a single crystal of lithium fluoride under the influence of VUV radiation barrier discharge is investigated for the first time. The barrier discharge involves the implementation simplicity [4, 5] and the possibility of obtaining a vacuum ultraviolet without using vacuum technology, i.e. directly at atmospheric gas pressure.

In the experiment a barrier discharge between planar electrodes at 10-15 kV pulse voltage with a frequency of 1 kHz is used. The irradiated sample in the form of a plane-parallel plate 2 mm thickness was directly used as a barrier. The discharging occurs in air at atmospheric pressure. The irradiated samples were examined to determine the types of color centers induced by radiation barrier discharge. For this the spectra of the formed centers and their luminescence kinetics investigated. The centers were excited by picosecond laser excitation. The studies were conducted using the time-correlated photon counting. The spectral and kinetic characteristics of the centers were compared with those of known color centers in lithium fluoride obtained under intense femtosecond laser irradiation or gamma irradiation. The studies were performed using a laser scanning confocal fluorescence microscope with a time resolution MicroTime 200 (Picoquant GmbH) equipped by spectrometer Ocean Optics QE65000. Fig. 1 shows the spectral data: 1 - crystal irradiated by focused femtosecond pulses; 2 - crystal irradiated by unfocused light femtosecond pulses in the filamentation mode; 3 - crystal irradiated by radiation barrier discharge.

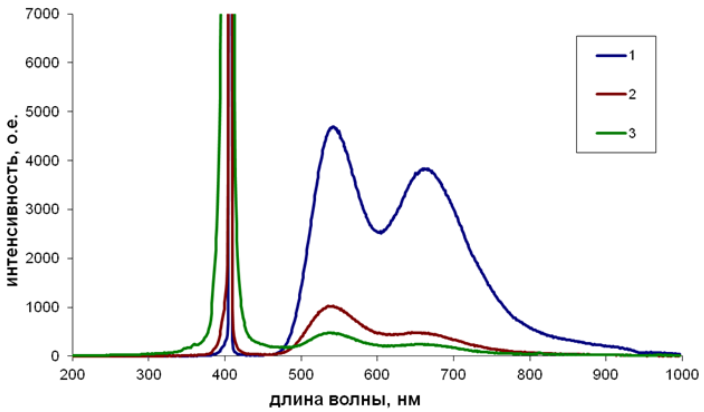

Fig. 1. The luminescence spectra of the crystal LiF and of the reference samples, the excitation is 405 nm.

As follows from this data, during the barrier discharge irradiation as well as during intense femtosecond irradiation two main types of luminescent center are formed: F_3^+ and F_2 color centers having emission bands with maxima at about 530 and 680 nm, respectively. This is confirmed by the data on the kinetics of luminescence shown in Fig. 2. The two main components of

luminescence kinetics, registered in the experiment (Table in Fig. 2 right), decaying with time constants of 18 and 8 ns (error ~ 10%) belong to the above-mentioned centers.

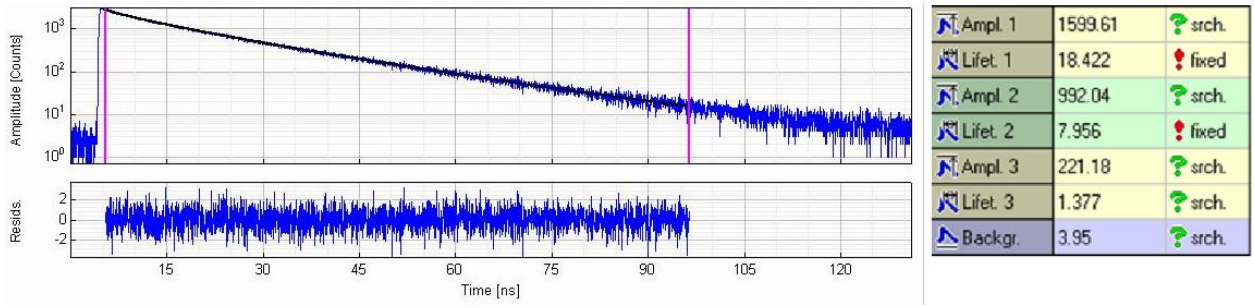

Fig. 2. The kinetics of the luminescence of color centers with the picosecond laser excitation

Registered color centers in lithium fluoride crystals are formed due to charge exchange and aggregation of primary Frenkel defects, which are created by nonradiative decay of excitons anion arising from the recombination of electrons and holes. Electrons and holes in the crystal of lithium fluoride can be formed either by electron impact ionization of the interband barrier discharge, or as a result of photon absorption spectral lines of nitrogen and oxygen, falling within the scope of the fundamental absorption in the vacuum ultraviolet.

When scanning a thick colored layer on a confocal fluorescence microscope, we have a value of 12 microns. Evaluation of the discharge electrons crystal penetration depth according to Kanayo-Okayama formula shows that it is repeatedly smaller. Therefore, the dominant mechanism for the electron-hole pair formation is the photon mechanism.

Thus under experimental conditions in the surface layer of lithium fluoride crystals are formed color centers due to the radiation barrier discharge. It is shown by the decay kinetics and the luminescence spectra analyzing that these centers are F_3^+ and F_2 ones. The main mechanism of electron-hole pair generation is the photon mechanism. The barrier discharge in different gases can be successfully used to generate on the surface of transparent dielectric thin layers containing color centers for various scientific and technological applications.

References

1. Carmen Ortiz, Carmen N. Afonso, Peter Pokrowsky, and Gary C. Bjorklund. Appl. Phys. Lett. **43**, 1102 (1983)
2. Frank Barkusky, Christian Peth, and Klaus Mann. Review of Scientific Instruments 76, 105102, 2005.
3. Мартынович Е.Ф. Центры окраски в лазерных кристаллах. Иркутск: Изд-во ИГУ, 2004, 227 с.
4. Самойлович В.Г., Гибалов В.И., Козлов К.В. Физическая химия барьерного разряда. М.: Изд-во МГУ, 1989,176 с.
5. Дж. Мик, Дж. Крегс. Электрический пробой в газах.-М: Изд. ИЛ, 1960, 605 с.

Fluorescence of a degenerate two-level atom near nanoparticle: polarization and temporal anomalies

G. N. Nikolaev

Institute of Automation and Electrometry of SB RAS, pr. Koptyuga 1, Novosibirsk, 630090 Russia
Novosibirsk State University, Pirogova str. 2, Novosibirsk, 630090 Russia
E-mail: nikolaev@iae.nsk.su

It has been known for a long time that radiation processes in the vicinity of a material body can differ significantly from those in free space. A large number of theoretical and experimental works performed so far studied the relaxation of excited atomic and molecular states in the vicinity of material bodies with particular geometries. In this respect, nanometer bodies are of special interest. However, theoretical calculations of the relaxation and fluorescence of an atom (molecule) in the vicinity of a nanoparticle were so far based on the models of either a classical oscillating dipole or a generalized ("vector") two-level system, where the matrix elements of the Cartesian components of the dipole moment operator, exactly like the components of the classical oscillating dipole, are attributed to the polarization direction of the light field acting on the atom (see [1–4] with extended bibliography, including earlier works). However the atomic or molecule decay rate is measured by the fluorescence detection after light pulse excitation of the atom or molecule. So, fluorescence is two-step process, and hence, orientation of the oscillating atomic dipole in general is not the same as exciting light polarization.

To rigorous description of the vector nature of the atomic dipole moment it is necessary to take into account the atomic angular degrees of freedom that is degeneracy of atomic levels.

This work is aimed at calculating the relaxation rate and fluorescence of an atom in the vicinity of a nanoparticle on the basis of accurate quantum-mechanical inclusion of rotational degrees of freedom (degeneracy of atomic energy levels with respect to the direction of the angular momentum).

We start with quantum mechanical expression for the atomic deexcitation probability expressed in terms of the normal correlation function of the atomic dipole moment operator and the antinormal correlation function of the electric field strength operator. Then the antinormal correlation function is expressed in terms of the field susceptibility by use of the fluctuation-dissipation theorem. The atomic dipole moment operator as well as the atomic density matrix operator is expressed in terms of irreducible tensor operators. In order to simplify the deexcitation probability expression, orthogonality and completeness of the irreducible tensor operators are used. Finally, it is shown that the atomic deexcitation rate is proportional to the reduced matrix element squared of the atomic dipole moment and a linear combination of the products of the so-called atomic polarization moments, population and alignment, and they relaxation rates. The population relaxation rate is proportional to the field susceptibility tensor trace. The alignment relaxation rate is proportional to the difference between the radial and tangential parts of the field susceptibility tensor.

It is shown that relaxation rate of an atom excited by linearly polarized light coincides with the predictions of the models of classical oscillating dipole and a generalized two-level system only for the atom with angular momenta $J_m = 1$ and $J_n = 0$ of the upper and lower atomic level, respectively. In the case of isotropic excitation, the relaxation rate does not at all depend on the polarization of light and the type of optical transition. Relaxation rate is also independent on the excitation light polarization for the atom with the angular momenta $J_m = 1/2$ and $J_n = 1/2$ or $J_n = 3/2$ of the coupled levels. In all other cases, the relaxation rate and its relation to the polarization of the excitation light field turn out to depend on the angular momenta of the coupled atomic levels (Fig. 1).

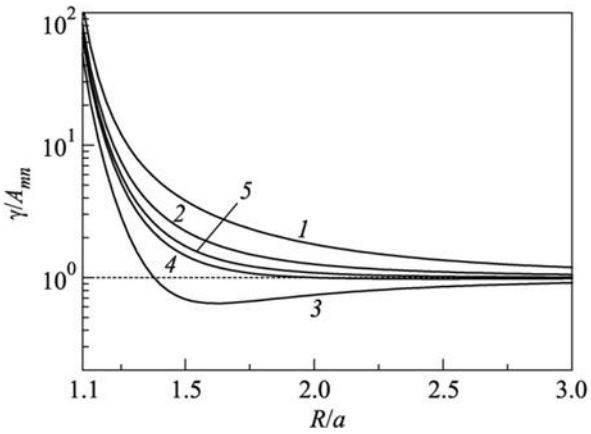

Fig.1. Dimensionless relaxation rate of an excited atom with (curves 1, 3) $J_m = 1, J_n = 0$ and (curves 2, 4) $J_m = 1, J_n = 1$ versus the distance between the atom and a silver nanoparticle (λ = 632.8 nm). The excitation field acting on the the atom is linearly polarized (curves 1 and 2) along or (curves 3 and 4) perpendicular to the symmetry axis. Curve 5 corresponds to isotropic excitation of the atom.

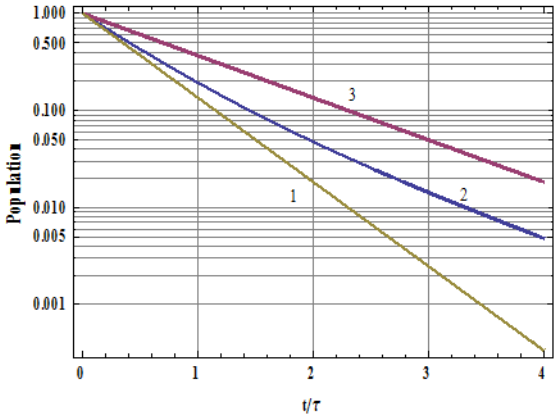

Fig.2. Temporary dynamics of the upper level population (fluorescence) of an atom with $J_m = 1$, $J_n = 0$. The excitation field acting on the atom is linearly polarized at an angle (curve 1) 0^0, (curve 2) 30^0, and (curve 3) 90^0 to the atom-nanoparticle axis. Curves (1) and (3) are proportional to $\exp(-2t/\tau)$ and $\exp(-t/\tau)$, correspondently.

Such a single exponential excitation decay and fluorescence decrease holds only at the initial times after the excitation when difference between changes in the population and alignment can be neglected [5]. To find out general deexcitation dynamics, a master equation for atomic density matrix is derived from an evolution equation for the total density matrix describing both atom and field. A consistent system of linear first-order ordinary differential equations for the atomic polarization moments is obtained from the master equation [6]. Components of the anisotropic relaxation matrix describing the consistent system are expressed in terms of the field susceptibility tensor. Symmetries of the anisotropic relaxation matrix are found. It is shown that atomic deexcitation in general is multi-exponential. The simple exponential decay of the excited energy level takes place in general only if its total angular momentum is less than one. Deexcitation dynamics and fluorescence is considered in more detail for the case when the total angular momenta of the upper and lower levels are equal to 1 and 0 respectively. It is shown that in this case deexitation dynamics also may be exponential under the two linear polarizations of the excitation light (Fig.2) and also under the circular polarization of the excitation light propagating along the symmetry axis. In all other cases fluorescence dynamics is more complicated.

References

1. V. V. Klimov, M. Dyuklua, and V. S. Letokhov, *Quantum Electron.* **31**, 569 (2001).
2. L. Novotny and B. Hecht, *Principles of Nano-Optics* (Cambridge Univ. Press, New York, 2012).
3. V. V. Klimov, *Nanoplasmonics* (Fizmatlit, Moscow, 2009; Pan Stanford, Singapore, 2011).
4. S. A. Maier, *Plasmonics: Fundamentals and Applications* (Springer, New York, 2007; Regulyar. Khaotich. Dinamika, Moscow, Izhevsk, 2011).
5. G. N. Nikolaev, *JETP Lett.* **97**, 383 (2013).
6. G. Nikolaev, *Deexcitation Dynamics of a Degenerate Two-Level Atom Near (Inside) a Body*, in: Abbass Hashim (Ed.), *Smart Nanoparticles Technology* (InTech, 2012); http://www.intechopen.com/books/smart-nanoparticles-technology/deexcitation-dynamics-of-a-degenerate-two-level-atom-near-inside-a-body.

Supercontinuum generation in hybrid nanocomposite materials with the inclusion of Na-hyaluronate and measurement of nonlinear refractive index by Z-scan

S.S. Golik[1,2], A.A. Chekhlenok[1,4], I.V. Postnova[2,3], D.Yu. Proschenko[1,4], Yu.A. Shchipunov[3], O.A. Bukin[1,4] and Yu.N. Kulchin[1]

[1]Institute of Automation and Control Processes of FEB RAS, 5 Radio St., Vladivostok, 690041 Russia
[2]Far Eastern Federal University, Vladivostok, 690950, Russia
[3]Institute of Chemistry of FEB RAS, prospect 100-letiya Vladivostoka 159, Vladivostok, 690022, Russia
[4]Maritime State University named after G.I. Nevelskoi, 50a Verkhneportovaya St., Vladivostok, 690059, Russia
E-mail: dima.prsk@mail.ru

Nowadays creation of the new nonlinear optical elements is highly important and demanded direction for modern optical problems. Materials with high nonlinear-optical susceptibilities are widely used in such practical applications as optical switching, two-photon laser scanning microscopy, microfabrication, three-dimensional optical data storage. In view of these circumstances necessity of constant searching of new mediums with certain physical and optical properties is observed to increase the effectiveness of various optical devices. In turn, highly promising direction is to create a non-linear materials which let to generate stable coherent wideband radiation as result of interaction ultra short laser pulses with medium. Such radiation is called supercontinuum [1]. This phenomena has found wide application due to its unique properties [2,3]. Despite the fact that for efficient generation of of supercontinuum mainly photonic-crystal fibers are used (PCF) [4] for problem of formation of specified spatial profile of result radiation condensed medium are applied [5]. Highly promising direction of synthesis of new mediums which satisfy the above criteria is creation of the hybrid materials based on zol-gel technology. It lets to create samples with good mechanical and perfect optical properties [6].The nanocomposite structure of such samples gives opportunities to develop and to prepare many different types of photonic material having engineered linear and nonlinear optical properties. Moreover, important advantage of these materials over the photonic crystal fibers in their robustness, excellent optical properties and low cost [7].

We have synthesized transparent monolithic nanocomposite materials based on silica with the inclusion of polysaccharide of hyaluronate of Na synthesized by zol-gel process (Fig.1a). During the synthesis using completely watersoluble precursor tetrakis (2-hydroxyethyl) orthosilicate (Si-precursor THEOS) with linear refractive index n = 1.517

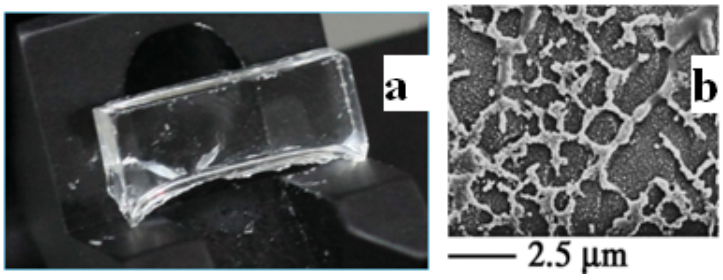

Fig.1. a) Photo of the synthesized sample; b) SEM photo of synthesized hybrid nanocomposite, which was prepared by adding 10% wt of silica precursor into the solution with concentration of Na-hyaluronate of 0.5 wt %.

nanocomosite hybrid materials are formed at low temperatures. At the same time excluding a denaturating effect on biopolymers, so macromolecules of polysaccharides, proteins and even DNA may not be decomposed due to biocompatibility of the precursor with them. The small concentrations of the molecules play role of skeleton and can radically change the structure of

the hybrid organic–inorganic material. Particularly, natural polysaccharides are the main morphological element of the complex cross-linked fibrils. They are made up of silica that cover polysaccharide macromolecules. The rest volume of the material is spherical silicate particles (Fig. 1b). The density of fibrils network, thickness of fibers, mechanical properties of synthesized materials depend on the polysaccharide type and charged degree of the macromolecules. Thus small concentrations of polysacharides' macromolecules can strongly influence on optical properties.

For investigation of the nonlinear properties and spatio-temporal features of transformation of the USP in presented materials we used Laser complex Spitfire Pro 40F (Spectra Physics, USA). The duration of generated pulses was 40 fs, pulse energy was about 1 mJ, repetition rate of USP was 100 Hz with carrier frequency corresponding to light wavelength 800 nm. Full width of USP at half maximum was 35 nm, diameter of laser beam was 7 mm. Significant broadening of spectrum of transmitted USP was observed both in Stokes and anti-Stokes spectral regions (Fig.2a). As result the supercontinuum generation took place.

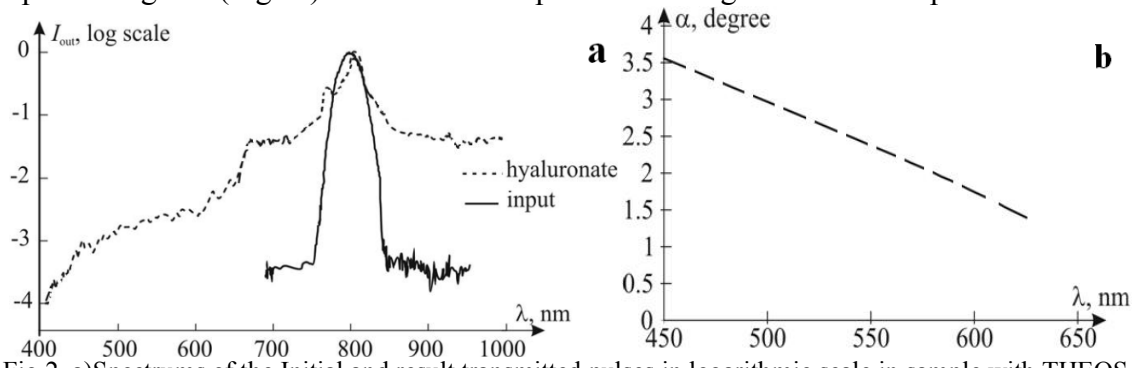

Fig.2. a)Spectrums of the Initial and result transmitted pulses in logarithmic scale in sample with THEOS-50% and Na-hyaluronate- 0.25 wt %; length of interaction 15 mm;
b) The spectral dependence of conical emission α(λ).

Along with the broadening of the spectrum of the initial pulse stable picture of the conical emission of the well-defined colored rings was observed. At the Fig.2b dependence of the angle of divergence of the spectral components of the transmitted radiation is presented.

For determination of the nonlinear refractive index n_2 of the investigated media Z-scan technique has been used as an accurate and sensitive tool. According to the study hybrid nanocomposite materials based on silica with the inclusion of Na-Hyaluronate possess n_2 more than an order of magnitude superior to the similar parameter for quartz.

Conducted researches have shown that monolithic nanocomposite biomaterials based on silica with the inclusion of polysaccharide of Na-hyaluronate synthesized by zol-gel technology possess good nonlinear optical properties. A manifestation of this fact is a stable pattern of conical emission of the supercontinuum generation in the interaction of ultrashort laser pulses with the test materials. Thus given materials are favorable medium for supercontinium generation and represent interest for creation new optical elements and further investigation.

References

1. R. R. Alfano, S. L. Shapiro, *Phys. Rev. Lett.* **24**, 592-594 (1970).
2. V.P. Kandidov , S.A. Shlenov , O.G. Kosareva, *Kvantovaya Elektron*. **39**, 205 (2009).
3. P. Li, K. Shi, Z. Liu, *Opt. Lett*. **30**, 156 (2005).
4. R. Buczynski, I. Kujawa, R. Kasztelanic, D. Pysz, etc., *Laser Phys*. **22**, 784 (2012).
5. D. Neshev, A. Dreischuh, G. Maleshkov, M. Samoc, Yu. Kivshar, *Optics Express* **18**, 18368 (2010).
6. H. Liu, W. Tan, J. Si, X. Liu, X. Hou, *Opt. Express* **16**, 13486 (2008).
7. J. Clark, G. Lanzani, *Nat. Photon*. **4**, 438-446 (2010).

Potassium nitrate as optical crystal: temperature and composition dependence of nonlinear susceptibility

B.I. Kidyarov[1], I.A. Kartashov[1], V.I. Kovalevskii[2], V.K. Malinovsky[2], A.M. Pugachev[2], A.F. Rozhkov[3], A.V. Shishaev[1]

[1] *A.V. Rzhanov Institute of Semiconductor Physics of SB RAS, Pr. Lavrentyeva 13, Novosibirsk, 630090, Russia*
[2] *Institute of Automation and Electrometry of SB RAS, Novosibirsk, Pr. Koptyuga 1, 630090 Russia*
[3] *V.S. Sobolev Institute of Geology and Mineralogy of SB RAS, Novosibirsk, Pr. Koptyuga 3, 630090 Russia*
E-mail: avis@isp.nsc.ru

The rhombic crystals (*mmm, D_{2h}*) of potassium nitrate (KNO_3), are basic polymorphous modification of natural mineral (niter). Nevertheless, there are some other trigonal (D_{3d}, C_{3v}) and rhombic (C_{2v}) crystal modification of potassium nitrate, among which ferroelectric phase R_{3m} is stable in very narrow temperature range 115 - 123 ^{o}C [1]. The crystals of non-centrosymmetric (NCS) structure posesses a nonlinear optic properties (NLO). They can be widely used in optoelectronics, particularly for creating stimulated Raman scattering lasers [2]. The goal of this work is to grow up perfect NCS KNO_3 crystals having their size more than 1-3 cm, which are stable at normal pressures and room temperature. The growth of perfect KNO_3-crystal from aqueous solution is very difficult and labour -consuming. It is possible only at very precise temperature control and stabilization with accuracy ± 0.01…0.001^{o}C and also at addition into solution of some specific components. Particularly, it was demonstrated that the growing of small ferroelectric crystals is possible at temperature 20÷50 ^{o}C from aqua system $Ba(NO_3)_2$ - KNO_3- H_2O [3]. Formation of small NCS pseudo-cubic crystals from binary compound $Ba(NO_3)_2 \cdot 2KNO_3$ was also shown in [3].

In our experiments we used crystals grown from water-salt solution with various ingredients, as well as basic reagents (KNO_3, $Ba(NO_3)_2$) and a precipitate from solutions. Crystals under investigation milled in a mortar and sieved through a sieve with mesh size of 50 microns.

For registration of the NCS phase, the method of second-harmonic generation (SHG) of laser radiation was used. The method is based on the fact that in the centrosymmetric phase the SHG signal is zero while nonlinear response proportional to the square of the spontaneous polarization should be registered when the NCS phase appears [4]. In order that phase matching conditions didn't influence a total signal, the powder method described in [6] was applied for registration of the SHG signal.

Figure 1 shows the results of measurements of the SHG signal of the powders obtained from crystals. The crystals were heated to the temperature of 160° C and then cooled to the room temperature. When heated, the SHG signal is virtually absent in all samples, indicating the absence of the ferroelectric phases. Upon cooling, the SHG signal increases sharply at temperatures from 130° C to the temperature which depends on the sample. This experimental fact indicates the phase transition from centrosimetric trigonal D_{3d} phase to the polar trigonal ferroelectric phase C_{3v}. [1]. Reducing of SHG signal (and hence the spontaneous polarization) under a further cooling indicates that trigonal ferroelectric phase C_{3v} disappears, wherein the temperature dependence of the SHG and the temperature range in which the ferroelectric phase exist depend on the type of the sample.

Studies on the effect of growth conditions to nonlinear optical response of potassium nitrate in the range of 25 - 160° C showed that the temperature interval of ferroelectric phases depends on the content of impurities in the solution in an aqueous-salt system KNO_3 - $Ba(NO_3)_2$ - H_2O. When heating above 130°C reconstructive phase transition $D_{2h} \rightarrow D_{3d}$ occures. Subsequent cooling leads to a transition from the central symmetric D_{3d} trigonal phase to the ferroelectric phase C_{3v}. The exception is precipitate consisting of a binary compound crystals $2KNO_3 \cdot Ba(NO_3)_2$, in which the ferroelectric phase is presented at room temperature. Currently, high quality single crystals of crystallites $2KNO_3 \cdot Ba(NO_3)_2$ was unable for grown. From the data shown in Figure 1 b, it follows that the highest temperature range wherein the ferroelectric phase exists is in the crystal KNO_3, obtained for the sample, grown from a solution of KNO_3 with 0.1 wt. % $Ba(Cl_2)_2 \cdot 2H_2O$ and 0.2 wt. % $Ba(NO_3)_2$.

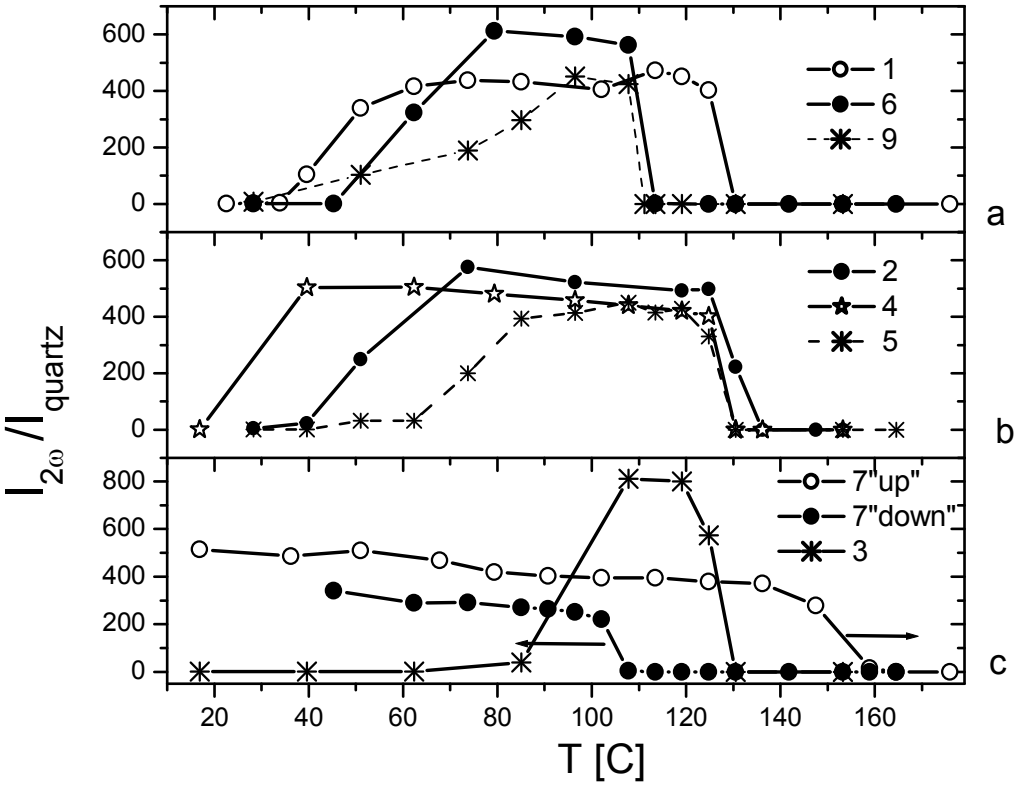

Fig.1. The arbitrary temperature dependence of nonlinear-optical susceptibility for KNO_3 different phases: 1- pure KNO_3 crystal, 2- KNO_3 crystal, grown from solution with addition 0.1% $Ba(Cl_2)_2 \cdot 2H_2O$, 3- KNO_3 crystal, from solution with addition 0.1% $Ba(Cl_2)_2 \cdot 2H_2O$ and 0.1% $Ba(NO_3)_2$, 4 - KNO_3 crystal, from solution with addition 0.1% $Ba(Cl_2)_2 \cdot 2H_2O$ and 0.2% $Ba(NO_3)_2$, 5 - KNO_3 crystal, grown from solution with addition 0.1% $Ba(NO_3)_2$, 6 KNO_3, 7- eutonic phase, 8- initial $Ba(NO_3)_2$ reagent, 9- defect KNO_3 crystal from pure solution,

References

1. Parsonage N.G., Staveley L.A.K. Disorder in crystals. V.1. Oxford: Clarendon Press. 1978. - 434 p.
2. Zverev P.G., Basiev T.T., Osiko V.V., Kulkov A.M. Physical, chemical and optical properties of the barium nitrate Raman crystal. Optical material. **11**. № 4, 315-318 (1999).
3. Kidyarov B.I. Mechanism, kinetics of crystals growth, and formation for optoelectronics. Thesis for a Doctor's degree. Novosibirsk. 2011. (In Russian).
4. M. E. Lines and A. M. Glass, Principles and Application of Ferroelectrics and Related Materials. Clarendon Press, Oxford (1977).
5. Vogt H. Study of Structural Phase Transitions by Techniques of Nonlinear Optics, Appl. Phys. 1974. **5**, P.85 - 96.
6. Kutrz S. K., Perry T. T. A Powder Technique for the Evaluation of Nonlinear Optical Materials, Journ. of Appl. Phys. 1968. **39**, P. 3798 – 3813.

New generation regimes of fiber lasers mode-locked due to nonlinear polarization evolution effect and their applications

S.M. Kobtsev[1], S.V. Smirnov[1], S.V. Kukarin[1], A.V. Ivanenko[1], S.K. Turitsyn[1,2]

[1] *Department of Laser Physics and Innovative Technologies, Novosibirsk State University, Pirogova 2, Novosibirsk, 630090 Russia*
[2] *Aston Institute of Photonic Technologies, Aston University, Birmingham, B4 7ET,UK*
E-mail: smirnov@lab.nsu.ru

Fiber lasers mode-locked due to non-linear polarization evolution (NPE) are relatively simple and efficient tool for ultra-short pulse generation what makes them an object of intensive study last years. Compared to lasers mode-locked with the use of saturable absorbers NPE-lasers have simpler and robust design due to absence of a "weak" elements with respect to radiation power. All-normal dispersion NPE-mode-locked lasers allow producing relatively high-energy pulses without wave-breaking in contrast to soliton lasers. Moreover, one can further increase pulse energy by elongating cavity of the lasers. Since pulse repetition rate of passively mode-locked lasers is inverse proportional to cavity length, the pulse energy grows linearly with cavity length at fixed average pump power. Thus for example pulses with energy as high as 3.9 uJ was achieved in 3.8-km-long passively mode-locked master oscillator [1].

The unique feature of NPE-mode-locked lasers is an exceptionally wide set of generation regimes what makes them an ideal platform for investigations in non-linear dynamics [2]. Thus, NPE-based ultra-fast oscillators are capable to produce pulse train at fundamental repetition frequency as well as its harmonics. The lasers can generate pulses of different temporal and spectral shape and, as it was found recently, with different pulse-to-pulse stability [3,4]. Pulse stability can vary in a wide range – from conventional stable pulse generation regimes (with negligible fluctuations of $10^{-6}..10^{-4}$) via slight phase and intensity fluctuations toward strong pulse disorder and noise-bursts formation. Since both pump power increase and laser cavity elongation impedes stable pulse generation [5] one can expect mainly partial coherence pulse generation in ultra-long NPE-based lasers, what makes such pulses particularly interesting due to its higher energy level compared to conventional fully-coherent bell-shaped laser pulses with smooth shape profile. However to the best of our knowledge practical applicability of such pulses has not been studied yet. In this work we investigate novel partially coherent generation regimes of fiber lasers passively mode-locked due to NPE and compare their practical applicability with conventional fully-coherent ultra-short laser pulses.

In our work we use all-normal dispersion NPE-mode-locked ring fiber laser shown in Fig 1a. The laser consisted of 4-m long active ytterbium fiber, two fiber-based polarisation controllers PC1 and PC2 and a 6-m-long stretch of passive SMF-28 fiber used for cavity elongation and boosting of the output pulse energy. To improve convergence of the solution to the limiting cycle, the numerical model includes also a spectral filter with a 30-nm band-width what exceeds considerably the typical band-width of generated laser pulses. In experiments implicit spectral filtering is performed by wavelength-dependent gain of the active fiber as well as effective Lyot filter action of optical fiber and FPBS. Our numerical simulation based on a set of generalized Schrödinger equations yields a large variety of single-pulse lasing regimes with different settings of PC1 and PC2. According to pulse-to-pulse fluctuations all these regimes can be divided into three groups: conventional stable pulse trains, noise-like bursts and intermediate regimes. Figure 1 b shows typical examples of simulated ACF and spectrograms for three different generation regimes similar to [4] obtained for analogous laser of another cavity length within the same numerical model.

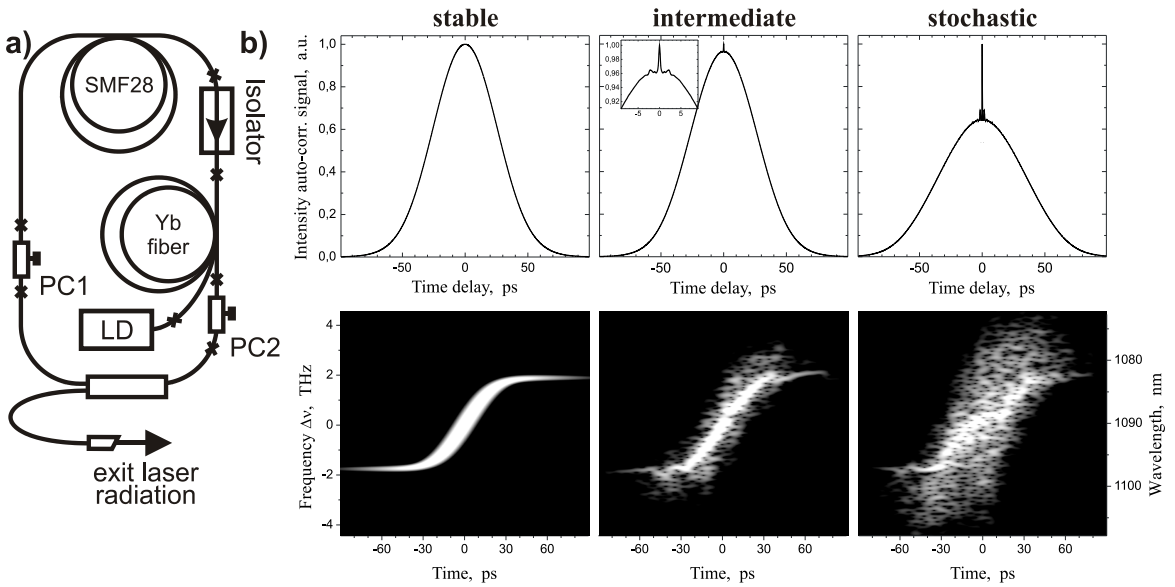

Fig.1. (a) Laser scheme, (b) ACF and spectrogram for different generation regimes.

In particular, in stochastic generation regime the laser produces a train of wave-packets consisted of random sub-pulses. The optical phase of such wave-packets strongly fluctuate what impedes pulse compression via chirp compensation. Transient lasing regime exhibits much smaller phase and intensity fluctuations what makes possible up to tenfold optical pulse compression in a linear dispersive medium, however compressed partially coherent pulses are still far from being spectral limited. In stable regime laser pulses have virtually no fluctuations in intensity and phase and thus can be compressed almost to Fourier limit.

Conventional ultra-short laser pulses generated in stable regime have a vast area of applications, including optical combs and metrology, medical imaging, femtochemistry, micro-machining, super-continuum generation, parametric frequency conversion, T-rays generation and detection and many others. Partial coherence of laser pulses produced in other regimes may impose some limitations on their applicability which are considered in this work. In particular, phase fluctuations prevent using such pulses for optical frequency metrology and frequency comb generation. However partially coherent picosecond pulses may be attractive for medical imaging, micromachining and super-continuum generation. Using numerical simulations we show for the first time that second-harmonic generation efficiency of partially coherent pulses may be comparable to or just a dozen per cents less than for conventional stable pulses generated by the same laser. Since the energy of partially coherent pulses and their long-time stability are potentially higher than for stable lasing regimes, and stochastic pulses are much easier to obtain in long and ultra-long cavities, they may constitue an attractive alternative to conventional laser pulses.

This work was partially supported by the Russian President grant MK-4683.2013.2; grant of Ministry of Education and Science of the Russian Federation for Leading Scientists (agreement N 14.B25.31.0003); President Council of the Russian Federation for the Support of Leading Research Groups of Russia, project No. NSh-2979.2012.2; Grant of Ministry of Education and Science of the Russian Federation (agreement No. 14.B37.21.0452).

References

1. S. Kobtsev, S. Kukarin and Yu. Fedotov, *Opt. Express* **16**, 21936 (2008).
2. P. Grelu and N. Akhmediev, *Nat. Photonics* **6**, 84 (2012).
3. S. Kobtsev, S. Kukarin, S. Smirnov, S. Turitsyn and A. Latkin, *Opt. Express* **17**, 20707 (2009).
4. S. Smirnov, S. Kobtsev, S. Kukarin and A. Ivanenko, *Opt. Express* **20**, 27447 (2012).
5. S.M. Kobtsev and S.V. Smirnov, *Las. Physics* **21**, 272 (2011).

The potential ability of a basically new method for exciting gas lasers: fast heavy particles beams of glow discharge

A.R. Sorokin

A.V. Rzhanov Institute of Semiconductor Physics of SB RAS, Pr. Lavrentyeva 13, Novosibirsk, 630090 Russia
E-mail: ars@isp.nsc.ru

In all gas-discharge lasers, which form the base of laser engineering, the basic processes are originally associated with electrons interaction with heavy atomic particles.

A fundamentally new way of gas lasers excitation by fast heavy particles beams (atoms and molecules) [1, 2] of glow discharge is offered.

According to the Messi criterion in the collision of heavy particles, cross section σ excitation reaches its maximum at energy *w* of the incident particles in tens or more *keV*.

Messi criterion does not account for the molecular complexes formed by approaching particles. Transitions between potential curves of complexes are possible at low kinetic energy *w* of the incident particles where the curves close together. Maximum cross section $\sigma \sim 10^{-17} cm^2$ and more was achieved for kinetic energy *w* at tens or hundreds of *eV*. In a discharge with a cathode potential fall of a few *kV's*, the energy of fast atoms generated by charge exchange is accounted for with tens and hundreds of *eV*.

The experiments were carried out in a discharge cell with a duralumin ring 4 mm thick (hole – 22 *mm*) separated by a dielectric ring of 2.4 mm thick (hole – 22 *mm*) from net cathode *C* with geometry transparency $\tau = 0.67$ and with 0.16 *mm* of holes. The connection of the duralumin ring to the cathode provides an additional ionization by fast electrons from the interior surface of the ring hole. A net anode *A* with $\tau = 0.56$ and 0.5 *mm* of holes was placed at the distance of $d = 15$ *mm* from the cathode for electron beam (*EB*) extraction into the drift region at the distance of 24 mm. The drift region for the atomic beam was limited by electrode *E* at the distance of 40 mm. Comparative characteristics of spontaneous emission power integrated over spectrum *P* were studied under the following conditions: gas discharge excitation when applying voltage to interval *C–E* (radiation power P_d), excitation by fast atoms (power P_a), and by electron beam (P_{EB}) when applying voltage to interval *A-C*. The discharge diameter was 22 *mm*. At 3.3 *Torr* of *He*, and at additional ionization, the relationship between the corresponding radiation power was as follows: P_d: P_{EB}: P_a = 3:7:35 at the identical amplitude of the initial pulse $U = 4.9$ *kV* applied to the cell (additional ionization interrupted when *U* was applied to *C-E*). When disconnecting the duralumin ring, the ratio between radiation powers was P_{EB}: P_a = 2:5, discharge burning voltage U_b increased from 2.4 to 4.2 *kV*, current density *j* decreased from 4 to 0.17 A/cm^2. For a discharge between *C-E,* the parameters were $U_b = 3.9$ *kV*, $j = 0.3$ A/cm^2.

Qualitatively the same pattern was observed in experiments with air, *Ar*, and a mixture of *He* plus 1% of O_2. The difference in emission spectrum for different conditions of gas excitation (by fast atoms, or by discharge, or *EB*) is shown in color discharge photography. It was also found how to increase the output power of He-Xe laser with a coaxial cell nine fold by changing only the polarity of power supply.

The research opens a perspective for further development of such a kind of laser pumping source, including new wavelengths generation.

References

1. A.R. Sorokin. *Russia patent* № 2450398, *Bul*. №13 (10.05.2012).
2. A.R. Sorokin. *Russia patent* № 2452056, *Bul*. №15 (27.05.2012).

Nanoroughness measurements of high quality optical surfaces

E.V. Sysoev[1], R.V. Kulikov[1], A.V. Latyshev[2], I.A. Vykhristuk[1]

[1] *Technological Design Institute of Scientific Instrument Engineering, Siberian Branch of the Russian Academy of Sciences (TDI SIE SB RAS), 41, Russkaya str., Novosibirsk, 630058, Russia*
[2] *A.V. Rzhanov Institute of Semiconductor Physics, Siberian Branch of the Russian Academy of Sciences (ISP SB RAS), 13, Academician Lavrentiev prosp., Novosibirsk, 630090, Russia*
E-mail: evsml@mail.ru

Inspection of roughness in the subnanometer range is to be performed under the monitoring of high-quality optical surfaces, for example, during the manufacture of mirrors of laser gyroscopes [1]. The noncontact methods are most suitable to carry out such measurements.

Using the low coherence interference for nanorelief measurements surfaces is well-known technique [2]. The principle of phase shifting in interferometry (PSI) is based on shifting a phase of one beam in an interferometer [3]. Michelson, Linnik or Mirau interferometers are commonly used in PSI measurement systems [4, 5].

Measurement in subnanometer range requires taking into account phase instrument function of interferometer optical channel. Aberration of waves in interferometer optical scheme, the nonuniformity of refractive index of optical materials and the reference mirror nonflatness of interferometer determine the main phase distortions.

To increase the resolution ability of measurements of nanorelief it was proposed to use the method of partial correlogram scan [6] and atomic-smooth surface in the reference arm of the interferometer. The measurement of nanorelief is performed by displacement of the reference mirror along the axis. Using a CCD camera at each step of scanning the interferograms are registered and then the digitized data are transferred for further processing in the PC. The correlogram (fig. 1) after the scan for each point of the measured surface is formed.

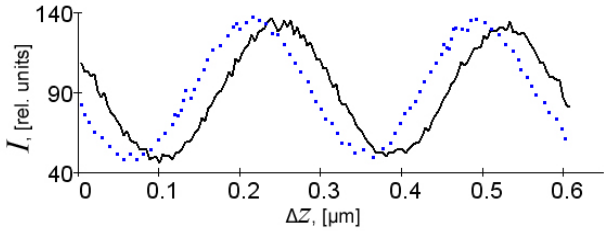

Fig. 1 Correlograms for two different points of the surface: I – light intensity, Δz – light path difference in reference and measuring arms.

To reconstruct the relief the phase difference between the correlograms corresponding to the different points of measured surface is calculated at minimisation root mean square difference between them. In order to increase the resolution ability by height it is used a specially prepared sample of silicon which contains extremely smooth surface. It is placed in the reference arm of the interferometer as a reference mirror.

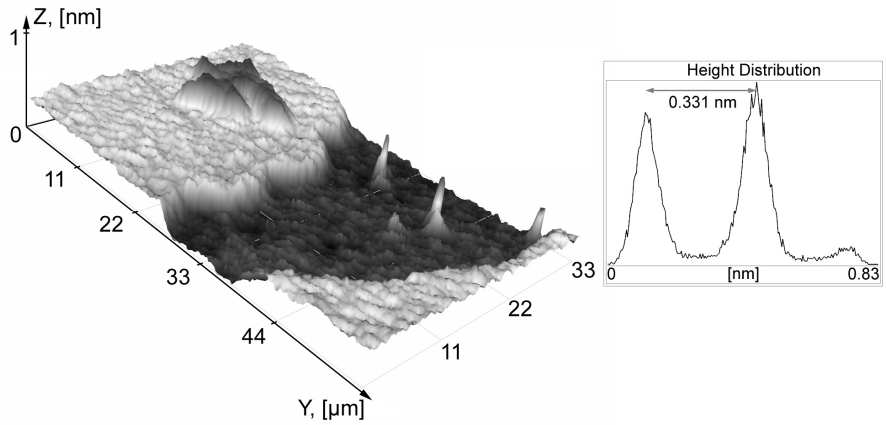

Fig. 2. 3D surface relief reconstruction of Si (111) sample with plot of height distributions.

The resolution ability by height of the interferential system is determined by measurement of monatomic steps with height 0.31 nm by means of method described above. Measurements are shown that resolution ability by height is no worse than 0.025 nm.

References

1. V.V. Azarova, Yu.D. Golyaev, V.G. Dmitriev, "Ring gas lasers with magneto-optical control for laser gyroscopy", QUANTUM ELECTRONICS, 2000, 30 (2), 96–104.
2. De Groot, P., “Coherence Scanning Interferometry,” Optical Measurement of Surface Topography, pp. 187-208, 2011.
3. Hariharan P., Malakara D., “Interference, Interferometry, and Interferometric metrology,” SPIE Optical Engineering Press, Bellingham, Wa., 1995.
4. Niehues, J., Lehmann, P. and Xie, W., “Low coherent Linnik interferometer optimized for use in nano-measuring machines,” Measurement Science and Technology, Vol. 23, No. 12, pp. 125002, 2012.
5. Windecker, R., Fleischer, M., Körner, K., Tiziani, H. J., “Testing micro devices with fringe projection and white-light interferometry,” Optics and Lasers in Engineering, Vol. 36, Issue 2, pp. 141-154, 2001.
6. Sysoev, E. V., “White-Light Interferometer with Partial Correlogram Scanning,” Optoelectronics, Instrumentation and Data Processing, Vol. 43, No. 1, pp. 83-89, 2007.

The oscillation performance of 0.8% Nd:YAG ceramics

S. Vatnik[1], I. Vedin[1], V. Kravchenko[2], Yu. Kopylov[2], P. Tverdokhleb[3], I. Steinberg[3]

[1] *Institute of Laser Physics, av Lavrentjeva 13/3, Novosibirsk 630090 Russia*
[2] *Institute of Radio-engineering and Electronics, Mokhovaya 11/7, Moscow, 125009, Russia*
[3] *Institute of Automation and Electrometry, Academician Koptug ave. 1, Novosibirsk, 630090, Russia*

The lasing and spectroscopic properties of oxide laser ceramics have been studied since 1990s. Lasing in 1%Nd:YAG ceramics was obtained for the first time in 1995, and already in 2001 the lasing efficiency of Nd:YAG ceramics was almost as high as of single crystals. Laser ceramics has some important advantages compared to single crystals, among which are the relatively simple synthesis of large-size samples, the possibility of producing multilayer (composite) ceramic structures, and a comparatively low production cost [1]. All this makes the highly transparent ceramics very promising for wide application in multikilowatt solid-state laser systems. In this work, we present the results of investigation of the lasing characteristics of 0.8%Nd:YAG ceramics synthesized at the Institute of Radio-engineering and Electronics by the high-pressure colloidal slip casting (HPCSC) method [2].

We report on the oscillation performance of 0.8%Nd:YAG ceramics laser pumped by a laser diode bars with a maximum average QCW optical power up to 6.5W at a wavelength of 808 nm. The YAG ceramic samples #08, #10 used in our experiment were disks with dimensions ∅16×3.0 mm. All surfaces of the samples were polished flat to high optical quality required for coating. One of the polished surfaces was covered with a dielectric coating with a high reflectivity (R > 99.8%) at lasing (λ_g = 1064 nm) and pumping (808 nm) wavelengths. Then a metallic coating was added for mounting active element to the copper heat sink. The front surface was AR-coated for these wavelengths, and the residual reflection was less 0.2%. The pump beam from two laser diode bars was focused on the sample using two-mirror collimator [2] and some lens optics, the beam waist was ∅0.95 mm. The laser cavity with a length of L = 33 mm was formed by a spherical output coupler (curvature radius r = 40 mm, transmittance T = 2.2% at λ_g = 1064 nm) and a rear mirror deposited on the end-face of ceramic samples. Figure 1 shows the input-output characteristics of the Nd-doped YAG ceramics lasers with a duty cycle of 14%, i.e. 7 ms pump pulses at a repetition rate of 20 Hz. According to the measured data (Fig. 1), the slope efficiency of 20.8% and the optical efficiency of 18.8% with respect to absorbed pump power were obtained for a sample #10. We compared the slope efficiencies samples of 0.8%Nd:YAG ceramics and 1%Nd:YAG ceramics (see Fig. 1, sample #R10097) produced in BAIKOWSKI, LTD. In the latter case, the slope efficiency and optical efficiency were 44.7% and 43.2%, respectively. A trend toward higher slope efficiencies is clearly visible with increasing optical transparency and homogeneity of the samples (see Fig.2).

The study of the optical inhomogeneity distribution on depth in the laser ceramics was carried out using the method of heterodyne detection [3].This method was developed in IA&E SB RAS. It gives unique opportunity to reconstruct the optical inhomogeneity distribution for one cycle of scanning on depth with resolution of 6.5 μm. The resolution in the transverse direction is 1.5 μm. The pictures of two-dimensional distributions of the reading signal (topograms) received as a result of 31 cycle of scanning on depth and consecutive shifting in the transverse direction for three samples of ceramics is shown in fig. 2.

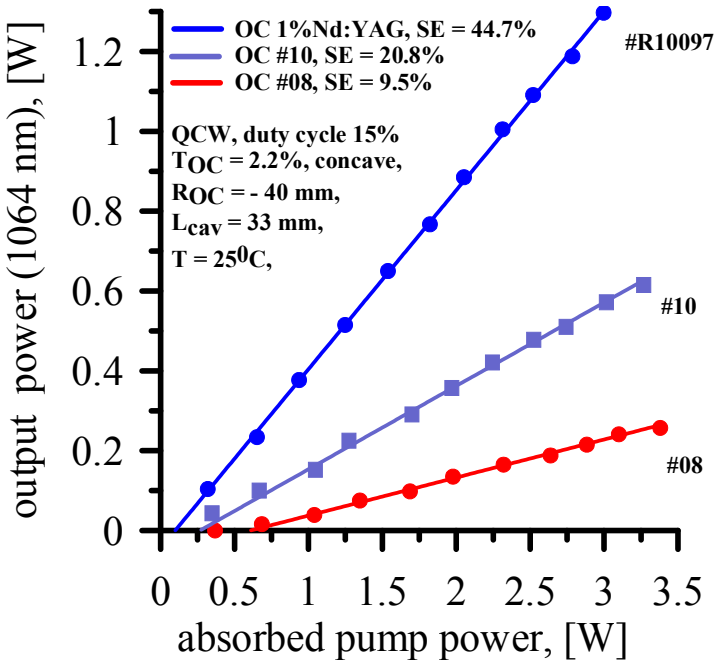

Fig.1 The quasi-CW laser performance of the Nd:YAG ceramic disk lasers versus absorbed pump power at 808 nm

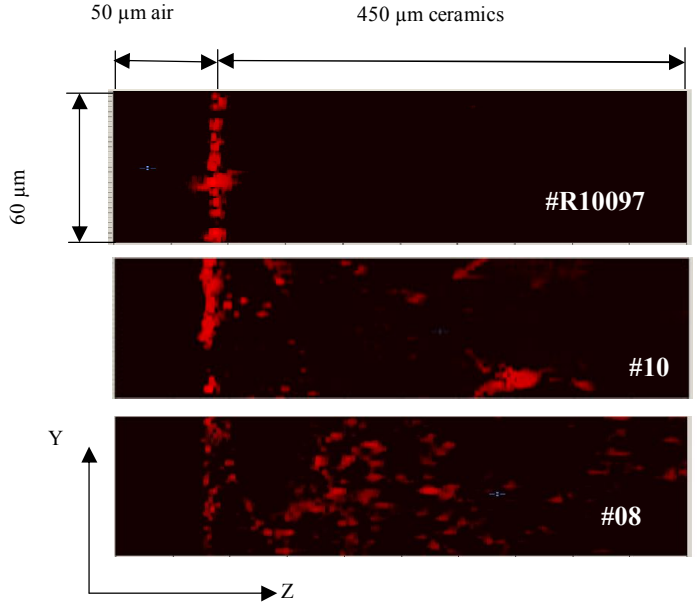

Fig. 2. The topograms of the reading signal of the area Y×Z = 60×450 µm^2 for three laser ceramics samples.

References

1. Sanghera J., Kim W., Villalobos G., et al. Materials, 5, 258 (2012)
2. Kaminskii A., Kravchenko V., Kopylov Yu., et al. Phys. Stat. Sol. (a), 7, 2411 (2007)
3. Clarkson W., Hanna D., et al. Opt. Lett., 21, 375 (1996)
4. Steinberg I. Sh., and Shepetkin Yu. A. App. Opt. **47** 9 (2008)

Control of exciton spin statistics through spin polarization in organic optoelectronic devices

J. Wang[1,2], A. Chepelianskii[1], F. Gao[1], N. C. Greenham[1]

[1]*Cavendish Laboratory, J.J. Thomson Avenue, Cambridge CB3 0HE, United Kingdom*
[2]*Institute of Advanced Materials, Nanjing University of Technology, Nanjing, China*
E-mail: Jw479@cam.ac.uk, iamjpwang@njut.edu.cn

Spintronics based on organic semiconductor materials is attractive because of its rich fundamental physics and potential for device applications. Manipulating spins is obviously important for spintronics, and is usually achieved by using magnetic electrodes. Here we show a new approach where spin populations can be controlled primarily by energetics rather than kinetics. We find that exciton spin statistics can be substantially controlled by spin-polarizing carriers after injection using high magnetic fields and low temperatures, where the Zeeman energy is comparable with the thermal energy. Using this method, we demonstrate that singlet exciton formation can be suppressed by up to 53% in organic light-emitting diodes (OLEDs) (Fig. 1), and the dark conductance of organic photovoltaic (OPV) devices can be increased by up to 45% due to enhanced formation of triplet charge-transfer states (Fig. 2), leading to less recombination to the ground state. The role of spin-dependent recombination in organic devices is still controversial, and our technique allows models for device operation to be tested by achieving direct control of spin populations in a manner that is energeticly controlled. These effects are unique to organic semiconductors, since they are free from the Pauli paramagnetism effects, high doping densities, and strong spin-orbit coupling typically present in inorganic semiconductor devices.

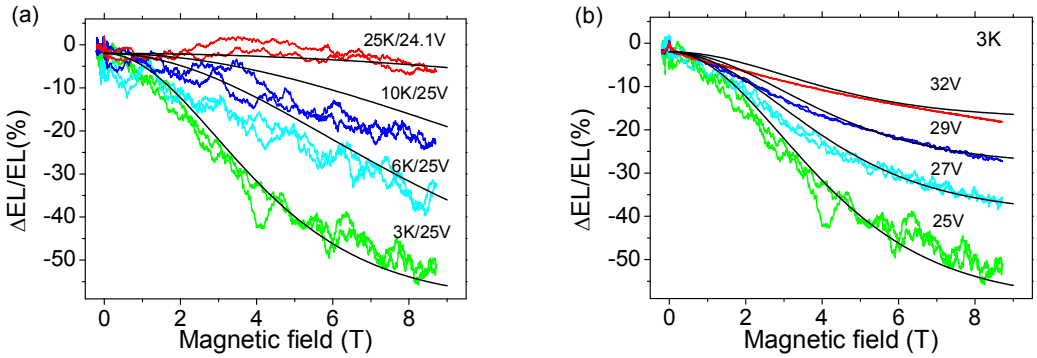

Fig. 1. Magnetic field effects in an TFB:F8BT LED. (a) Fractional change in EL as a function of magnetic field under constant biases at various temperatures. (b) Fractional change in EL as a function of magnetic field at 3K under various bias voltages. The black curves are fits to the model described in the text.

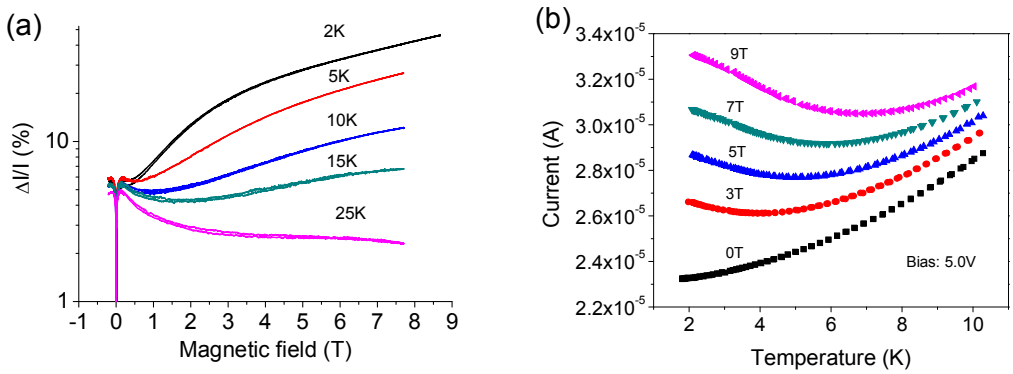

Fig. 2. Magnetic field effects in an P3HT:PCBM OPV device. (a) Fractional change in current as a function of magnetic field under constant bias at various temperatures. (b) Device current under constant bias as a function of temperature in various magnetic field.

References

1. J. Wang, A. Chepelianskii, F. Gao and N. C. Greenham, *Nature Communications* 3 1191 (2012).

UV laser from ZnO whispering gallery microcavity

C.X. Xu, J. Dai, G. Zhu

State Key Laboratory of Bioelectronics, Southeast University, Nanjing 210096, China
E-mail: xcxseu@seu.edu.cn

As a wide gap semiconductor material with large exciton binding energy, ZnO is considered an ideal material for UV optoelectronics. Recently the whispering gallery mode (WGM) lasing Iin ZnO micro/nanostructure attracts researchers' attention for its ultrahigh quality factor, low lasing threshold and distinct modes. Based on ourselves systematical investigation on ZnO WGM microlaser, we review the WGM lasing in the ZnO microcavity. The microphotolumescence resonances from ZnO WGM microstructures have been presented. The single photon pumped WGM excitonic lasing, electron-hole plasma lasing and exciton-polariton lasing are deeply discussed, and the mode modulation due to surface decoration on ZnO microstructure have been explored. Furtherly, the multiphoton absorption induce nonlinear optical effects in the ZnO WGM microstructures, such as multiphoton photoluminescence, lasing and second harmonic genereation, have been demonstrated. Finally the electrically pumped WGM lasing from a heterostructured n-ZnO microrod/p-GaN microlaser diode has been obtained.

This work was supported by "973" Program (2011CB302004), NSFC (61275054), RFDP (20110092130006) and MOE (20110092130006).

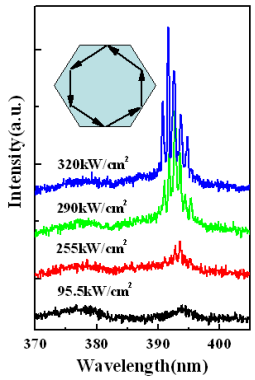

Figure 1

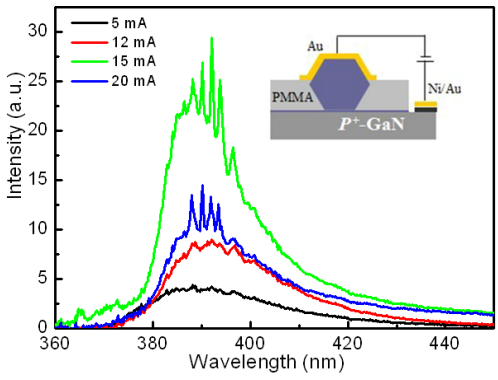

Figure 2

Fig. 1. The PL spectra from the single ZnO microrod under different excited power densities, the inset shows the WGM lasing resonance mechanism.

Fig. 2. The EL spectra form the ZnO microrod/GaN heterostructured laser under different applied currents, the inset presents the schematic diagram of the ZnO microrod/GaN heterostructured laser

References

1. Zhu G P, Xu C X, Zhu J, et al., Appl Phys Lett, 2009, 94, 051106.
2. Dai J, Xu C X, Zheng K, et al., Appl Phys Lett, 2009, 95, 241110.
3. Dai J, Xu C X, Ding R, et al., Appl Phys Lett, 2009, 95,191117.
4. Dai J, Xu C X, Wu P, et al., Appl Phys Lett, 2010, 97: 011101.
5. Dai J, Xu C X, Sun X W, Opt Commun. 2011, 284, 4018.
6. Dai J, Xu C X, Shi Z L, et al., Opt Mater. 2011, 33, 288.
7. Dai J, Xu C X, Sun L X, et al., J Phys D: Appl Phys, 2011, 44, 025404.
8. Dai J, Xu C X, Sun X W, et al., Appl Phys Lett, 2011, 98, 161110.
9. Zhu G Y, Xu C X, Cai L S, etal., ACS Appl. Materi. Interf., 2012, 4, 6195.
10. Dai J, Xu C X, Sun X W, Adv. Mater., 2011, 2, 4115.

Generation of two-dimensional lasers-optical angular momentum

H. Yu, H. Zhang

State Key Laboratory of Crystal Materials and Institute of Crystal Materials, Shandong University, Jinan 250100, China
E-mail: haohaiyu@sdu.edu.cn

Angular momentum of photons is a subject attracting much interest over the past few decades. For the photons, the orbital and spin angular momenta corresponds the distribution of the intensity and polarization direction, respectively. Previous studies have identified that the orbital and spin angular momenta of photons are quantized. Recently, the optical spin transfer torque, predicated theoretically several years before, has been experimentally observed. For light with orbital angular momentum, its generation, collapse, propagation dynamics, generation of atomic rotational states, knots and entanglement etc., have been investigated. The orbital angular momentum of photons would generate optical vortex and phase singularity. The Laguerre-Gaussian ($LG_{p,l}$) laser modes are important and most widely studied optical vortices with orbital angular momentum equal to $l\hbar$ per photon, where l denotes the azimuthal mode index or topological charge.

In this manuscript, the continuous-wave and pulsed lasers with optical vortex and periodical structure are generated with different methods. The generating mechanism is discussed and the promising application is proposed.

Using a compact cavity, the cw and pulsed lasers with vortex were obtained. In order to confirm the order of the LG modes, the mode converter shown in Fig.1 (I) composed by two cylindrical lenses was used to transform the $LG_{p,l}$ to $HG_{m,n}$ modes. The laser output beam was focused into the mode converter. The distance between the two cylindrical lenses of the converter was precisely adjusted to be $\sqrt{2}f$, where f is the focal length of the cylindrical lens. By second-harmonic generation, the orbital angular momentum per photon can be doubled and the laser emission can be made visible. For the $LG_{0,l}$ mode, the second harmonic generation presents a $LG_{0,2l}$ mode, and by mode-conversion, the frequency-doubled mode should be $HG_{0,2l}$. With a $KTiOPO_4$ (KTP) crystal cut along the type II phase-matching direction, second harmonic generation of optical vortex pulses was also studied. The transverse patterns of the frequency doubled optical vortex pulses, converted from $LG_{0,l}$ to $HG_{0,2l}$ modes by the mode converter, were also recorded and can be seen in Fig. 1 (II)). From this figure, it can be concluded that the fundamental laser modes are $LG_{0,l}$ modes, the second-harmonic laser modes are $LG_{0,2l}$ modes (l=0, 1, 2), and the transformed HG mode is $HG_{0,l}$ or $HG_{0,2l}$, respectively. The transformation from $LG_{0,2l}$ to $HG_{0,2l}$ mode also indicates that the directly generated optical vortex pulses possess a single transverse mode structure.

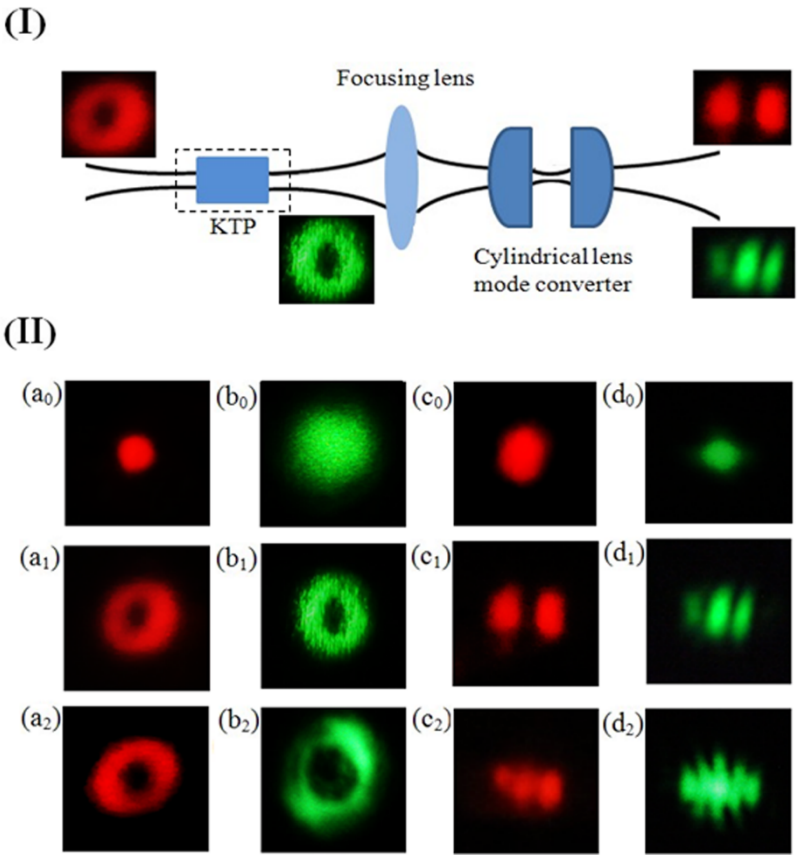

Fig.1 (I) Experimental configuration of the mode converter. (II) The transverse pattern of the laser beam, (a_n) shows the fundamental $LG_{0,l}$ modes; (b_n) shows the $LG_{0,2l}$ produced after second-harmonic generation; (c_n) shows the fundamental Hermite-Gaussian ($HG_{0,l}$) modes after the mode converter; and (d_n) shows the second-harmonic $HG_{0,2l}$ modes after the mode converter.

In summary, the generated two-dimensional laser physics were achieved. The generating mechanism is discussed and the promising application is proposed.

Oxyfluoride glass ceramics

Hua Yu

The MOE Key Laboratory of Weak Light Nonlinear Photonics and School of Physics, Nankai University, Tianjin 300191, China

Er^{3+}/Yb^{3+} ions co-doped transparent oxyfluoride glass were prepared and subsequently heat-treated with different time and temperatures. In the crystallization process, the heat-treated temperature promotes the growing size of fluoride NCs, while the heat-treated time increases the quantity of them. Moreover, fluorescence measurements exhibit an obviously stronger red emission in GCs with the increasing of heat-treated time and temperature.

High efficient luminescent intensity, adjustable size, narrow size distribution, and unique optical properties are helpful to practical applications of up-conversion materials, especially RE-ion-doped inorganic nano-particles after heat-treatment, in the fields of flat-panel display, light-emitting diodes, temperature sensors, biolabels, DNA detection, photodynamic therapy, etc. Fluoride nano-particles in aqueous solution were prepared by means of thermal induction to produce nano-particles in glass matrix and corroding the glass host by hydrofluoric acid. The fluoride nano-particles in aqueous solution have the same structure and luminescent properties as fluoride nano-particles existing in glass matrix.

In GCs, rare earth ions are selectively incorporated into the fluoride NCs embedded among the oxide glassy matrix. The crystal field environment influences the optical properties such as the absorption and emission spectra of the RE ions intensively. However, neither the formulas (chemical composition) nor the structures of the NCs based on different hypotheses can reach a unified understanding. A tetragonal phase model with the chemical formula as $PbREF_5$ proved by quantitative energy dispersive X-ray spectroscopy and X-ray diffraction analyses has been proposed in this paper for the first time. Two specific crystalline phases with the same space group have been observed at 460 ^{o}C–500 ^{o}C and 520 ^{o}C–560 ^{o}C, respectively. Moreover, a super ‘‘pseudo-cubic’’ cell based on our tetragonal model may give a good explanation to the probable previous cubic-symmetry misunderstanding by researchers. Additionally, the thermodynamic mechanism of phase transition and the thermal stability related to the structure of nanocrystals in GCs have been studied and supported by ab initio calculations and experimental methods.

Microsun company was founded in 2000 as a logistic company supplying radio-electronic industrial enterprises with electronic components and devices. The staff of the company consists of professionals in the field of logistics.

The company specializes in supply of large sets of electronic components from producers (from factories directly), express supply of small lots as well as unique components of little known producers. We maintain official distribution principles in the field of electronic components delivery.

One of the main principles of successful work of our company is fair and open policy with respect to our partners. Microsun company is one of few companies in Novosibirsk which offers a whole complex of service in delivery of electronic components. The company cooperates with electronic components producers in Southeast Asia, Korea, North America and Western Europe.

We will do our best to be of service for You.

Respectfully Yours,
OOO “Microsun company” director,
Vitaly Gellert

630091, Россия, Новосибирск
Красный проспект, 54 офис 426-428
тел.: (383) 209-01-48, 217-05-31
e-mail: box@microsun.ru

Офис в Академгородке:
Россия, Новосибирск
пр-т Академика Лаврентьева, 6/1 - 34
тел.: (383) 363-1390, сот. 8-960-787-5610
e-mail: academ@mkmail.ru
skype: academ.microsun